UNIVERSITÉ DE MONTRÉAL

RHEOLOGY, PROPERTIES AND MICROSTRUCTURE DEVELOPMENT OF POLYMER/CARBON NANOTUBE COMPOSITES IN MICROINJECTION MOLDING PROCESS

SAMANEH ABBASI

DÉPARTEMENT DE GÉNIE CHIMIQUE

ÉCOLE POLYTECHNIQUE DE MONTRÉAL

THÈSE PRÉSENTÉE EN VUE DE L'OBTENTION

DU DIPLÔME DE PHILOSOPHIAE DOCTOR (Ph.D.)

(GÉNIE CHIMIQUE)

Décembre 2009

UNIVERSITÉ DE MONTRÉAL

ÉCOLE POLYTECHNIQUE DE MONTRÉAL

Cette thèse intitulée:

RHEOLOGY, PROPERTIES AND MICROSTRUCTURE DEVELOPMENT OF POLYMER/CARBON NANOTUBE COMPOSITES IN MICROINJECTION MOLDING PROCESS

présentée par : ABBASI Samaneh

en vue de l'obtention du diplôme de : Philosophiae Doctor

a été dûment acceptée par le jury d'examen constitué de :

M. LAFLEUR Pierre, Ph.D., président

M. CARREAU Pierre, Ph.D., membre et directeur de recherche

M. DERDOURI Abdessalem, Ph.D., membre et codirecteur de recherche

M. AJJI Abdellah, Ph.D., membre

Mme KONTOPOULOU Marianna, Ph.D., membre

To:

My Parents

Their constant support and encouragement made this possible

The important thing in science is not so much to obtain new facts as to discover new ways of thinking about them.

Sir William Bragg

ACKNOWLEDGEMENTS

This dissertation would not have been possible without the help and support of a great number of people.

First and foremost, I would like to express my sincere gratitude and thanks to my supervisors *Prof. Pierre J. Carreau* and *Dr. Salim Derdouri* for their extensive support throughout the program. I am always encouraged and inspired by their enthusiasm toward scientific research, their insightful suggestions and their attitude to life.

I would like to convey my heartfelt thanks to my colleagues and friends during this work. My especial thanks are dedicated to my best friends who have been a great source of strength all through this work during the time far from home.

A sincere appreciation goes to all the staff and technicians of école polytechnique de montreal, chemical engineering department and Industrial Material Institute (IMI) for their help and meaningful contribution to this thesis. Specifically, I must acknowledge *Ms. Mélina Hamdine* and *Ms. Weawkamol Leelapornpisit* for their sympathies, supports and great helps in rheological and morphological studies in this thesis.

And finally, my special gratitude to my parents and my brothers for their unwavering supports and their loves.

RÉSUMÉ

Dans le cadre de cette thèse des concepts nouveaux pour l'alignement des nanotubes de carbone multi-couche (MWCNT) induit par le cisaillement, la caractérisation de MWCNT / polymères nanocomposites et la fabrication par microinjection de pièces à base de nanocomposites optimisés sont présentés. Les effets des microstructures et des morphologies développées dans diverses conditions, de mise en oeuvre par le procédé de micromoulage sur les propriétés rhéologiques, électriques et mécaniques de nanocomposites à base de CNT sont étudiés.

Le développement dans la technologie des microsystèmes et la demande constante de dispositifs fonctionnels à des échelles de longueur de plus en plus petites a imposé l'application du procédé de moulage par microinjection comme une technologie clé dans ce domaine. Le moulage par microinjection est un procédé relativement nouveau avec un grand potentiel de production en série de microdispositifs comprenant des détails d'un niveau de complexité élevé qu'il n'est pas possible de fabriquer par les techniques de moulage par injection classique. Il s'agit d'un nouveau domaine de recherche et on s'attend à une croissance continue au cours des dix prochaines années, étant donné la tendance croissante à la miniaturisation des composants et l'augmentation de la demande de microdispositifs.

Les nanotubes de carbone sont des matériaux de grande utilité dans ce contexte avec des conductivités électrique et thermique supérieures et des propriétés mécaniques extrêmement importantes, essentiellement dues à leur structure et à leur facteur de forme élevé. Par conséquent, les nanocomposites à base de CNT dans une matrice de polymère sont des matériaux prometteurs pour la fabrication de micropièces multifonctionnelles ayant des propriétés uniques pour une large gamme d'applications.

L'étude des propriétés rhéologiques des matériaux composites, notamment leur comportement viscoélastique a non seulement une importance pratique, liée à leur mise en oeuvre, mais a aussi un intérêt scientifique, car elle peut être utilisée comme une sonde de la microstructure des composites investigués. Par conséquent, une recherche fondamentale est nécessaire pour établir la relation entre le comportement rhéologique, les conditions de mise en œuvre et les propriétés finales des pièces en composites à base de nanotubes de carbone / polymère par le procédé de microinjection.

Dans cette thèse, nous avons l'intention de développer une connaissance intuitive du couplage entre le procédé de moulage par microinjection et le développement des propriétés de performance de composites à base de CNT / polymère, en se concentrant sur la rhéologie, la microstructure et les propriétés de micropièces moulées.

Pour explorer la fonction des CNT et permettre leur transformation, nous avons optimisé la préparation de nanocomposites par un ensemble de mesures rhéologiques et la caractérisation de la microstructure.

Le procédé de moulage par microinjection a été notre procédé de choix dans cette étude car il nécessite une quantité minimale de matériaux et il permet d'investiguer l'effet de taux de cisaillement élevés. Par conséquent, après le micromoulage dans des conditions différentes, nous avons utilisé différentes méthodes de caractérisation afin de d'étudier l'effet de ces conditions sur la structure et les propriétés des CNT / polymère composites. Une étude rhéologique novatrice et une analyse microstructure ont été utilisées pour trouver une corrélation appropriée entre la rhéologie, la morphologie et les propriétés des micropièces. En outre, l'effet de la structure cristalline a été analysé en comparant les résultats obtenus avec un polymère amorphe (PC) et un polymère semi-cristallin (PP). Nos connaissances dans cette partie peuvent être utilisées pour optimiser les conditions du procédé dans le but de fabriquer des micropièces avec des propriétés physiques supérieures.

L'optimisation, la caractérisation et une amélioration importante des propriétés finales des pièces microinjectées à base de CNT conduisent à une compréhension fondamentale du moulage par microinjection de composites CNT / polymères et à un progrès significatif dans le domaine des nanocomposites multifonctionnels et de la technologie de la miniaturisation.

ABSTRACT

Carbon nanotubes (CNTs) are great materials with superior electrical and thermal conductivity, mechanical properties and high aspect ratio. Consequently, CNT/polymer nanocomposites are promising materials for making multifunctional microscale components with unique properties and a wide range of applications. If considerable research has been conducted regarding the physical properties of carbon nanotube filled nanocomposites, including mechanical properties, electrical conductivity and rheological properties, only a few investigations have focused on the practical applications of nanocomposites in various industrial fields.

In this dissertation, we intended to create a predictive understanding of the coupling of microinjection molding process to the development of the performance properties of carbon nanotube/polymer composites, focusing on the rheology, microstructure and properties of microparts. To explore the CNTs feature and to enable their processing, the nanocomposite preparation was optimized through a set of rheological measurements and microstructure characterization.

We first examined the rheological behavior of polycarbonate (PC)/ MWCNT nanocomposites in light of interactions between CNTs and polymer chains or between CNTs themselves. To understand the percolated structure, the nanocomposites were characterized via a set of rheological, electrical and thermal conductivity measurements. The rheological measurements revealed that the structure and properties were temperature dependent; the percolation threshold was significantly lower at higher temperature suggesting stronger nanotube interactions. However, when the measurement temperature was high enough the percolation threshold tend to reach a plateau (0.3 wt%) The nanotube networks were also sensitive to the steady shear deformation particularly at high temperature. Following preshearing, the elastic modulus decreased markedly indicating that the nanotubes were aligned in the flow direction. Consequently, they interconnected minimally leading to a remarkable increase in the percolation threshold. The effect is more pronounced at higher temperature suggesting that nanotubes became more rigid. As expected, it was found that the rheological threshold (0.3-0.8 wt%) was smaller than the thermal (1-2 wt%) and electrical threshold (2-3 wt%).

At the next step we investigated the effect of flow field and deformation rate on the nanotube alignment and on the properties of PC/MWCNT nanocomposites. The obtained results of SEM, TEM and Raman spectroscopy revealed that the nanotubes are preferentially aligned in the flow direction, particularly at large injection rates. Rheological measurements corresponding to high shear rate conditions showed drastic changes in the viscoelastic behavior. The complex viscosity significantly decreased and percolation threshold notably rose. High degrees of nanotube alignment also resulted in a significant increase in the electrical percolation threshold. For compression molded samples the percolation threshold is found to be about 3 wt% nanotube content as the electrical conductivity rises suddenly by more than 10 decades. However, the longitudinal flow in the dog-bone shaped cavity resulted in a very high value for the percolation threshold, about 9 wt% of nanotube loading.

The mechanical properties of the nanocomposites for different nanotube loadings were also shown to depend on the processing conditions, and somehow improved when the material was processed at higher rates.

The electrical conductivity and percolation behavior of PC (polar amorphous polymer)/MWCNT nanocomposites and iPP (non-polar semi-crystalline)/MWCNT were analyzed and compared. In spite of the different levels of dispersion, the nanotubes in both nanocomposites were connected and a percolated network was formed. The crystallinity of the PP/MWCNT nanocomposites as a function of nanotube content was found to go through a maximum at 2 wt% loading while the overall rate of crystallization increased. We observed for the highly sheared microinjected PP/MWCNT samples the formation of well oriented crystals; however, the overall crystallinity was only slightly affected by strain. The electrical conductivity of the nanocomposites was improved by the presence of the crystalline structure even in high sheared samples. The percolation threshold for compression molded (non-processed) samples was found to be around 1 wt% for PP nanocomposites. Similarly, the conductivity values after percolation were about one order of magnitude higher in the case of PP nanocomposite. Although a high degree of nanotube alignment in the microparts resulted in a significant increase in the electrical percolation threshold, the level of alignment was less in the crystalline polymer. In the crystalline material the orientation of crystalline phase also decreased with the incorporation of nanotubes.

It was also shown that the PP nanocomposites exhibited mechanical properties significantly enhanced by nanotube loading; this effect was small in the case of the PC nanocomposites.

Finally the effect of carbon nanotube on the morphology and electrical conductivity of nanocomposites of MWCNT and PP/CBT blend were investigated and it was found that a double percolation threshold is the basic mechanism for the conductivity of such nanocomposites. It was also shown that the nanotubes affected the morphology of the blends by increasing the viscosity of the filler-rich phase. Consequently the CBT domains became smaller and more elongated changing from droplets into strips, which are more favorable to form a continuous phase.

CONDENSÉ EN FRANÇAIS

Suite aux progrès récents survenus dans le domaine de la microtechnologie, le développement de nouveaux matériaux prometteurs et l'optimisation des conditions de leur transformation pour fabriquer en série des produits d'excellente qualité et à haute valeur ajoutée, à faibles coûts et en gros volumes, constituent des défis majeurs.

Bien que la plupart des microdispositifs sont actuellement basés sur le silicium, le verre ou le quartz, ces matériaux et leurs procédés de fabrication correspondants sont compliqués et coûteux. Le remplacement de ces matériaux avec des matériaux composites de polymères de haute performance connait une attention croissante en raison de leur polyvalence et la facilité de leur production en série.

L'expansion rapide et récente des microtechnologies a ouvert la voie à de nouvelles applications pour les composites de polymères ayant des propriétés supérieures ne pouvant être fournies par des polymères purs ou même additionnés de renforts conventionnels tels que les fibres de carbone et les fibres de verre. Le développement de divers nanocomposites est un nouveau domaine de croissance qui a le potentiel pour répondre à la forte demande de matériaux polymériques plus forts et plus légers. Dans ce contexte, les nanotubes de carbone sont des nanomatériaux novateurs possédant une combinaison unique de dimensions nanométriques, structure électronique et composition chimique qui se traduisent par des propriétés thermiques, électriques, mécaniques et optiques exceptionnelles; grâce à leurs propriétés physiques les nanotubes de carbone permettent d'élaborer des nanocomposites multifonctionnels.

Une variété de méthodes de fabrication à l'échelle micro a été explorée ces dernières années pour les matériaux polymères. Parmi eux, le moulage par microinjection est un procédé de microfabrication relativement nouveau avec un grand potentiel de production de microdispositifs en série utilisant des matériaux comme les polymères et leurs composites. Les composites à base de polymère et de CNT sont des candidats appropriés pour la microfabrication de composants à forte valeur ajoutée où seulement quelques grammes de matériaux par pièce sont nécessaires. Il s'agit d'un nouveau domaine de la technologie, qui est encore à ses débuts, et même s'il y a eu une croissance importante récemment, il y a peu d'études de compréhension de l'effet de la dynamique de ce nouveau procédé sur les propriétés finales des produits fabriqués, en particulier dans le cas où des nanocomposites sont utilisées. L'examen des travaux de recherche précédents

montre que le domaine de la mise en œuvre des nanocomposites par le procédé de moulage par microinjection n'a pas été exploré.

Dans ce procédé, contrairement aux procédés conventionnels, la rhéologie de volume (bulk) ne suffira pas pour une caractérisation rhéologique adéquate en raison de conditions de mise en œuvre sévères et leurs effets sur le comportement du matériau. Le développement d'une microstructure spécifique est un autre aspect dont il faut tenir compte, à cause des propriétés structurelles exceptionnelles des matériaux nanocomposites et des conditions de mise en œuvre particulières imposées par le procédé de moulage par microinjection.

Compte tenu de ce contexte et à la lumière de l'état actuel de la technique, il est nécessaire de faire des études fondamentales afin d'améliorer la compréhension de moulage par microinjection de composites de CNT / polymère, pour découvrir l'effet des conditions de mise en oeuvre sur les propriétés de micropièces et de trouver une corrélation appropriée entre les propriétés rhéologiques et les résultats de la mise en oeuvre.

Dans ce projet, nous avons cherché à produire et à caractériser des pièces microinjectées, utilisant des nanocomposites polymères à base de nanotubes de carbone et de développer des méthodes rhéologiques innovantes afin d'estimer et de prévoir l'effet des conditions spécifiques de la microinjection, soit un taux de déformation très élevé et l'effet de confinement exercé par les parois en présence de nanoparticules. Le polycarbonate, un polymère de haute performance a été choisi comme la matrice polymérique principale. En outre, pour étudier l'effet de la cristallinité sur les propriétés des nanocomposites, le polypropylène a aussi été utilisé. Des nanocomposites PP/MWCNT ont été préparés et ont été caractérisés. Pour les nanocomposites PC / MWCNT, nous nous sommes principalement concentrés sur l'étude des propriétés rhéologiques et des conductivités thermique et électrique. Différentes techniques de microscopie et spectroscopie ont été employées pour étudier l'effet du cisaillement élevé sur l'alignement des nanotubes et par conséquent sur les propriétés des micropièces. Pour les nanocomposites PP / MWCNT, les propriétés finales ont été étudiées par différents méthodes de cristallographie et de spectroscopie. Enfin, sur la base des résultats obtenus dans les parties précédentes et afin d'améliorer la conductivité électrique, le principal point d'attention dans ce travail, des nanocomposites MWCNT / mélange de polymères ont été produits et caractérisés.

Les résultats principaux obtenus lors de cette thèse sont résumés comme suit :

1) Le comportement rhéologique des nanocomposites de polycarbonate (PC/ MWCNT) a été examiné à la lumière des interactions entre les nanotubes de carbone et les chaînes de polymère ou entre les nanotubes de carbone eux-mêmes. Plus précisément, l'effet du niveau de chargement des nanotubes, de leur alignement et de la température sur le comportement rhéologique des nanocomposites a été étudié. Les nanocomposites ont été préparés par dilution d'un lot commercial de polycarbonate contenant initialement 15% en poids de nanotubes. La dilution a été réalisée à l'état fondu en ajoutant la quantité nécessaire d'un polycarbonate pur dans une extrudeuse bi-vis dans des conditions auparavant optimisées. Une dispersion raisonnablement bonne des nanotubes et la formation de réseaux de nanotubes dans la matrice polymère a été analysée par microscopie électronique à balayage (MEB), microscopie électronique à transmission (MET) et microscopie à force atomique (MFA). Le seuil de percolation, i.e. la concentration critique de nanotubes permettant d'observer une augmentation soudaine des propriétés rhéologiques, des conductivités électrique et/ou thermique a aussi été caractérisé par un ensemble de mesures rhéologiques et de conductivité électriques et thermiques. Les mesures rhéologiques ont révélé que la structure et les propriétés dépendent de la température ; aussi, le seuil de percolation est significativement plus faible à température plus élevée suggérant une forte interaction entre des nanotubes. Cependant, à température suffisamment élevée, le seuil de percolation atteint un plateau (0.3% en poids de nanotubes). Les réseaux de nanotubes ont également été sensibles au cisaillement continu, particulièrement à haute température. À la suite d'essais de pré-cisaillement, le module d'élasticité a largement diminué suggérant que les nanotubes sont devenus plus rigides et orientés dans la direction de l'écoulement. En conséquence, les nanotubes sont moins connectés les uns aux autres, et une augmentation remarquable du seuil de percolation en résulte. Ces résultats ont été analysés à l'aide de modèles simples pour les suspensions de bâtonnets. Enfin, les seuils de percolation rhéologique, de conductivité électrique et thermique ont été comparés. Comme prévu, le seuil rhéologique (0.3-0.8%) a été plus faible que les seuils thermique (1-2%) et électrique (2-3%).

2) L'effet du champ d'écoulement et de la vitesse de déformation sur l'alignement des nanotubes et sur les propriétés des nanocomposites PC / MWCNT a été étudié. Des conditions de mise en œuvre différentes ont été utilisées pour changer systématiquement le degré d'alignement des nanotubes. L'étude morphologique par microscopie MEB et MET ainsi que l'analyse par

spectroscopie Raman ont révélé que les nanotubes sont préférentiellement alignés dans le sens de l'écoulement, notamment dans le cas de l'injection à des taux élevés. Les résultats correspondant aux taux de cisaillement élevés ont montré des changements drastiques dans le comportement viscoélastique. La viscosité complexe a diminué de façon significative et le seuil de percolation rhéologique a notablement augmenté. Le degré élevé d'alignement des nanotubes ont également entraîné une augmentation considérable du seuil de percolation électrique. Dans le cas de barres de tension injectées par micromoulage où l'écoulement est essentiellement longitudinal le seuil de percolation électrique a atteint une valeur élevée, de l'ordre de 9% en poids de nanotubes de carbone. Dans le cas du moulage par compression où le taux de cisaillement est beaucoup moindre, le seuil de percolation électrique obtenu est d'environ 3% : à ce niveau de charge la conductivité électrique a augmenté soudainement de 10 décades. Enfin, nous avons utilisé une équation de type loi de puissance pour corréler le comportement de percolation et l'alignement des nanotubes. Le seuil de percolation estimé et l'indice q de la loi de puissance augmentent de manière significative avec le degré d'alignement des nanotubes tel que déterminé par l'analyse Raman. Finalement, il a aussi été démontré que les propriétés mécaniques des nanocomposites dépendent du taux de chargement de nanotubes et des conditions de mise en œuvre : elles ont été quelque peu améliorées par des taux d'injection plus élevés.

3) Les effets de la structure cristalline et des conditions de mise en œuvre sur la morphologie et les propriétés des nanocomposites PP / MWCNT ont été étudiés. Des échantillons à taux de chargement différents en MWCNT ont été préparés par dilution d'un lot commercial de polypropylène contenant initialement 20% en poids de nanotubes. La dilution a été réalisée à l'état fondu en ajoutant la quantité nécessaire d'un polypropylène pur dans une extrudeuse bi-vis dans des conditions auparavant optimisées. L'observation par microscopie électronique à balayage et à transmission a révélé que la dispersion des nanotubes de carbone a été généralement confinée entre les zones cristallines, où ils ont formés des réseaux de connexion. La cristallinité et l'orientation cristalline des échantillons fabriqués par les procédés de moulage par compression et de microinjection ont été étudiés par les méthodes de DSC et de diffraction des rayons X et il a été constaté que la cristallinité passe par un maximum lorsqu'on augmente la teneur en nanotubes. Le degré de cristallinité global a également diminué. Dans les échantillons obtenus par microinjection les cristaux formés ont été bien orientées alors que la

cristallinité globale n'a que lentement changé. La conductivité électrique des nanocomposites de polypropylène a été améliorée par la présence de réseaux de nanotubes situés entre les structures cristallines, mais le degré élevé d'alignement des nanotubes dans les pièces microinjectées a entraîné une augmentation significative du seuil de percolation électrique. Pour les nanocomposites à base de PP, les propriétés mécaniques ont été sensiblement affectées par le chargement de nanotubes; cet effet a été faible dans le cas des nanocomposites à base de PC

4) Finalement, la spectroscopie Raman et la diffraction de rayons X (XRD) ont été utilisées pour confirmer les résultats observés lors de l'étude morphologique et examiner avec plus de précision le comportement de percolation des composites de PP / MWCNT et PC / MWCNT précédemment mentionnés. Les résultats de spectroscopie Raman ont montré que les nanotubes sont bien alignés dans les échantillons ayant subi un taux de cisaillement élevé ; cependant le niveau d'alignement est moindre pour le polymère semi-cristallin. Les résultats de diffraction XRD ont révélé que l'orientation de la phase cristalline a diminué avec l'ajout de nanotubes dans la matrice PP. Ces résultats ont clairement montré que l'incorporation de nanotubes ou la présence d'une phase cristalline réduit l'effet du taux de cisaillement élevé du micromoulage. Par conséquent, bien que les propriétés de conductivité aient été significativement modifiées par l'alignement des nanotubes, la présence d'une phase cristalline peut améliorer la conductivité électrique malgré le cisaillement élevé grâce à l'existence d'un double seuil de percolation : l'un est dû au taux de charge des nanotubes de carbone et l'autre à l'importance de la phase cristalline. L'introduction d'un oligomère très peu visqueux, le butylène terephthalate cyclique (CBT), dans les nanocomposites polypropylène / MWCNT a été examinée. La conductivité électrique des mélanges polymères PP / CBT additionnés de nanotubes de carbone a été améliorée grâce à au phénomène de la percolation double qui contrôle la conductivité électrique dans un mélange de deux polymères en présence de nanoparticules conductrices.

TABLE OF CONTENTS

List of Tables

List of Figures

xxiv

List of Symbols

C_h	Nanotube chiral vector
T_g	Glass transition temperature
Ω	Ohm (resistivity unit)
V	Volt (voltage unit)
ρ_v	Volume resistivity
σ	Electrical conductivity
k	Thermal conductivity
$\eta*$	Complex viscosity
G'	Storage modulus
G''	Loss modulus
ω	Frequency
$tan\delta$	Loss tangent
δ	phase angle
m	Nanotube loading
m_{cG}	Rheological percolation threshold (wt%)
$m_{c,\sigma}$	Electrical percolation threshold (wt%)
E_C	Cohesive energy per volume unit
γ_C	Critical deformation amplitude for the limit of the linear domain
λ	Characteristic elastic time
ϕ	Volume fraction
$[\eta]$	Intrinsic viscosity $[\eta]$
η_r	Ratio of the suspension viscosity to the medium viscosity
η_{sp}	Specific viscosity
P	Aspect ratio
P_{eff}	Effective aspect ratio
N_B	Number of particles
V_η	Particle hydrodynamic volume

V	Total volume
E_a	Flow activation energy
R	Universal gas constant
η	Steady state viscosity
η_∞	Limiting viscosity at high shear rate
v_r	Radial velocity
v_y	Longitudinal velocity
η_e	Effective viscosity
p	Pressure
Δp	Pressure difference
$\dot{\gamma}$	Rate of deformation
$D_\Pi \, \& \, G_\Pi$	Raman intensity ratios parallel to the flow direction
$D_\perp \, \& \, G_\perp$	Raman intensity ratios perpendicular to the flow direction
X_c	Degree of crystallinity
ΔH_f	Enthalpy of fusion of the samples
ΔH_f^0	Enthalpy of fusion of the 100% crystalline polymer
T_c	Crystallization temperature
T_m	Melt temperature
$t_{1/2}$	Half crystallization time
X_r	Relative crystallinity
Q	Heat flow
T_0	Initiation crystallization temperature
T_∞	Termination crystallization temperature
ΔG	Free energy
ΔS	Entropy of crystallization
ΔH	Enthalpy of crystallization
A_Π	FTIR absorption parallel reference axis
$A_\perp$	FTIR absorption perpendicular reference axis
f	Herman orientation function

f_{c} Orientation of the crystalline phase

f_{am} Orientation of the amorphous phase

f_{av} Average orientation function

Chapter 1

Introduction

The recent advances occurring in the field of microfabrication and related methods entails the development of new and promising materials, modifying the current technologies and optimizing the processing conditions to achieve low-cost, high-speed and high quality mass production. All these requirements constitute major challenges which need careful consideration and research.

Although most of microdevices are currently based on silicon, glass, or quartz, these materials and their related fabrication methods are too complicated and expensive. Replacing these materials with high performance polymer composites has gained increasing attention because of their versatility and ease of mass fabrication.

The recent explosion in microfabrication has opened up new applications for polymer composites with superior properties which could not be supplied by pure polymers or even composites using conventional reinforcements such as carbon and glass fibers. Polymer nanocomposites are a growing and new field of technology, which has the potential to meet the need for stronger and lighter polymeric materials. In this context, carbon nanotubes are novel nanomaterials with a unique combination of nanometric dimensions, electronic structure and chemical composition that results in exceptional thermal, electrical, mechanical and optical properties; these properties make them promising fillers for multifunctional nanocomposites.

A variety of microscale fabrication methods have been explored in recent years for polymeric materials. Among them, microinjection molding is a relatively new microfabrication process with a great potential of mass production of miniaturized devices using materials such as polymers and composites. The polymer-based composites of CNT are suitable candidates to fabricate microscale components where only grams of materials are necessary to manufacture high-valued products. This is a new field of technology, which is still in its infancy, and although there has been significant growth in the technology, there is little understanding of the effect of the process dynamics on product properties, particularly in the case of nanocomposites. Review of the previous works shows only few investigations have focused on the processing of nanocomposites using microinjection molding.

In investigating and modeling microinjection molding, contrary to conventional processes, the bulk rheology will not suffice for adequate rheological characterization because of the process space and time scales and their effects. Microstructure development is another aspect which needs to be researched, particularly regarding the exceptional structural properties of nanocomposite materials and the special process conditions imposed by the microinjection molding process.

In view of this context and in light of current state-of-the-art, it is required to do fundamental research to enhance the understanding of microinjection molding of CNT/polymer composites, to elucidate the effect of processing conditions on the micropart properties and to find a suitable correlation between rheological properties and processing outcome.

In this project, we aim to produce and characterize carbon nanotube and polymer based microinjected parts and to develop innovative rheological methods to estimate and predict the effect of specific conditions of microinjection, i.e. high temperature, very high rates of deformation and wall effects due to the presence of nanoparticles. Polycarbonate, a commonly used high performance polymer, is chosen as the main polymeric matrix. Moreover, to investigate the effect of crystallinity on the nanocomposite properties, polypropylene based nanocomposites are produced and are characterized. In PC/MWCNT nanocomposites, we mainly concentrate on the rheological properties, thermal and electrical conductivity. Different microscopy and spectroscopy techniques are employed to investigate the effect of high shear conditions on the nanotube alignment and consequently on the microparts properties. In PP/MWCNT nanocomposites, the final properties of microinjected parts are investigated by different crystallography and spectroscopy methods. Finally, based on the results obtained in the previous parts and in order to improve the electrical conductivity, which is the main point of attention in this work, MWCNT/polymer blend nanocomposites are produced and characterized. This thesis is comprised by the following sections:

1.   Literature review which is mainly the scientific background and literatures on the theoretical and experimental properties of nanotubes and nanotube-reinforced polymers, characterization techniques used for measuring the nanocomposite properties, microinjection molding and production of composite based microparts.

2.   Materials, processing and characterization part which explains the adopted methodology, the materials and the experimental methods used in this work.

3.   The main achievements of the thesis given in the format of four scientific papers as follows:

   ✓ First paper: "*Rheological properties and percolation in suspensions of multiwalled carbon nanotubes in polycarbonate*"; characterization of rheological, electrical and thermal conductivity of PC/MWCNT nanocomposites; investigation of the dependency of nanotube networks on temperature and steady shear deformation.

   ✓ Second paper: "*Flow induced orientation of multiwalled carbon nanotubes in polycarbonate nanocomposites: rheology, conductivity and mechanical properties*"; investigation the effect of flow field and deformation rate on the nanotube alignment and on the properties of nanocomposites.

   ✓ Third paper: "*Properties of microinjection moldings of polymer multiwalled carbon nanotube conducting composites*"; studying the effects of crystalline structure and polymer processing conditions on the morphology and properties of nanocomposites.

   ✓ Forth paper: "*Carbon nanotube conductive network in crystalline and amorphous polymers and polymer blends*"; investigation and comparing the electrical conductivity and percolation behavior of binary composites of PP/MWCNT and PC/MWCNT and ternary composites of PP/CBT/MWCNT.

4.   Finally, a general discussion including a brief review of the final achievements and the summary of the results obtained in this project followed by conclusions and recommendations.

Chapter 2

Literature Review

2.1. Nanotechnology and Nanocomposites

If technology is defined as "the application of science and scientific knowledge for industrial or commercial objectives", then nanotechnology might be specifically defined in its most simplistic form as "the application of science and scientific knowledge, at the nanoscale, for industrial or commercial objectives." For better understanding of the size of matter at the nanoscale level, it is necessary to trace down the units of measurement, starting , as an illustration, with an ant (at the milliscale) and ending at the very bottom, at the nanoscale. Eventually the nanoscale is far from being the smallest unit of measurement; it is however, the smallest scale at which matter can be manipulated. Figure 2.1 illustrates the nanoscale comparing to other scales.

Recently, outstanding advances in producing nanostructured materials with novel properties have driven research to develop multi-functional macroscopic engineering materials by designing structure at the nanometer scale. Owing to this aim, nanotechnology became a significant part of science and technology and attracted a huge amount of interest and investment.
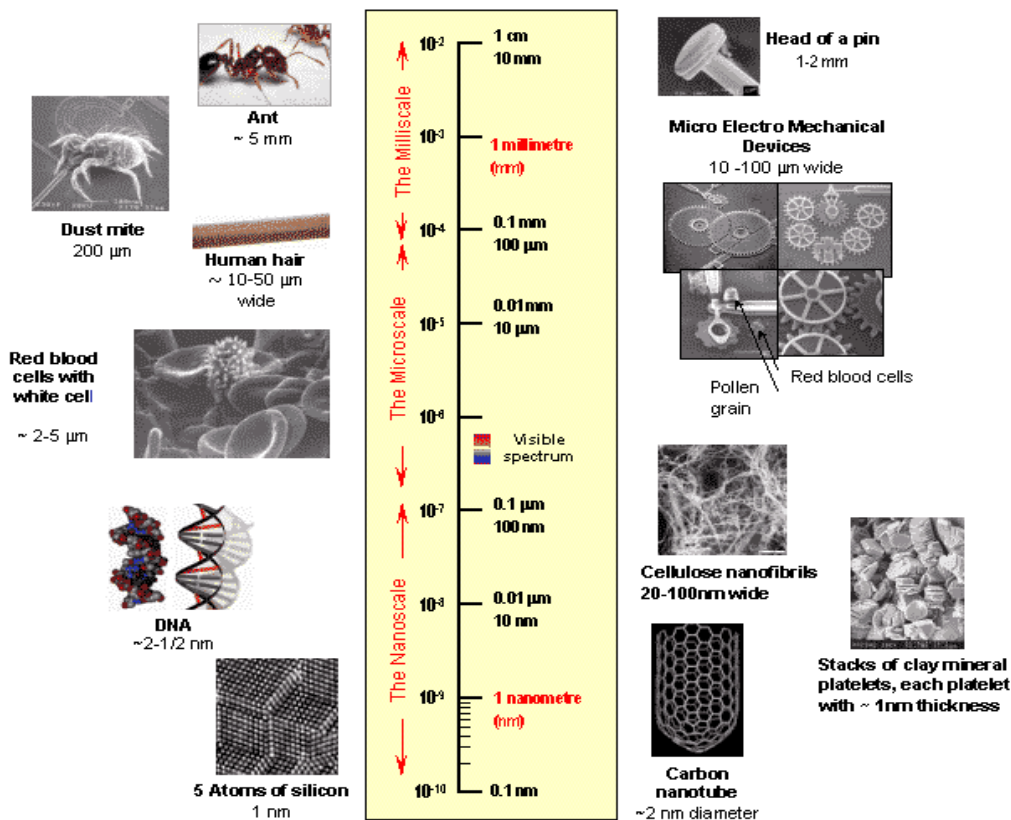
Figure 2.1: The size of nanotechnology(www.nano.gov/html/facts/whatIsNano.html)

Today, real world applications of nanotechnology exist in commercial business. Wide variety of applications of nanomaterials and process have been fielded ranging from non-scuff floor tile to high strength brackets for running boards on vehicles or high temperature protective materials for spacecraft. While nanomaterials are a significant portion of today's nanotechnology focus, several other areas are equally as promising (Fig. 2.2).

Figure 2.2: Nanotechnology industry focus (www.directionsmag.com/article.php?article_id=375)

2.2. Carbon nanotubes

During the progressive advances in nonoscience and nanotechnology of the last two decades, most of scientists have been attracted to the field of novel solid state nanomaterials, called carbon nanotubes (CNT). Since their discovery in 1991 by Iijima (Iijima, 1991, Iijima and Ichihashi 1993) CNTs became attractive candidates for fundamental investigations and an extensive research effort has been devoted to their fabrication, characterization and development of applications due to their unique electronic structure and extraordinary properties (Meyyappan 2005). Intrinsic structure, size scale and aspect ratio of CNTs suggest a variety of applications such as nanoelectronic, sensors and field emission as well as high performance nanocomposites with ultra light structure and enhanced mechanical, electrical, thermal and optical characteristics. It has been predicted that nanotechnology, largely fueled by the remarkable properties of carbon nanotubes, may ultimately transform technology to a wider extent than does the considerable advances of silicon revolution.

2.2.1. Structure and morphology

A carbon nanotube is a hollow cylinder of graphite sheet with a diameter in the range of nanometer and with a length from a few nanometers to several microns. Unlike the 3-D structure of diamond in which each carbon atom has four nearest neighbors, carbon nanotubes are made of 2-D sheets of graphene where carbon atoms are arranged in a hexagonal pattern. In this structure, each carbon atom has three neighbors. Therefore, unlike the sp^3 electronic structure of diamond, carbon nanotubes are based on a sp^2 electronic structure with Van der Waals bonding between carbon atoms. In such structure, the in-plane bonds, referred to as s-bonds or σ-bonds are strong covalent bonds between atoms. On the other hand, interlayer interaction in this structure is due to out-of-plane, delocalized bonds referred to p-bonds or π-bonds (Fig. 2.3). These bonds interact with the p-bonds on the neighboring layer; however, this interlayer interaction is much weaker than s-bonds (Meyyappan 2005). According to experimental measurements, the shear strength between the outermost shell and the neighboring inner shell is of the order of 0.3 Mpa (Qian, Wagner et al. 2002).
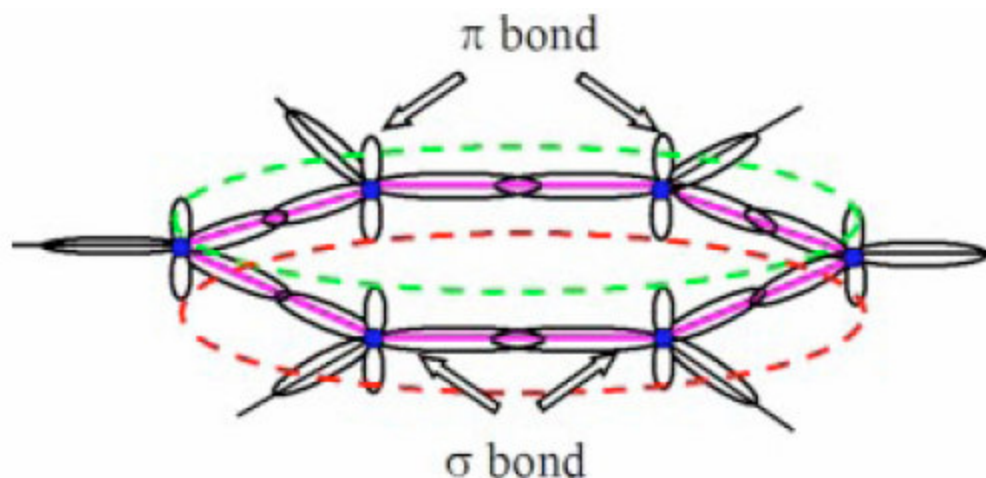
Figure 2.3: Basic hexagonal bonding structure for a graphite sheet; carbon nuclei shown as filled circles, out-of plane p-bonds represented as delocalized ~ dotted line, and s-bonds connect the C nuclei in-plane (Qian, Wagner et al. 2002)

A tube made of a single tubular shell of graphene sheet rolled up into a hollow cylinder is called single-wall- carbon nanotube (SWCNT). Another type of nanotube is multi-wall-carbon nanotube (MWCNT) that is made up of a tube comprising several concentrically arranged cylinders.

Two terms are usually employed to describe the microstructure of a carbon nanotube. Tube chirality or helicity, which is defined by the chiral vector, c_h and the chiral angle θ (Thostenson, Ren et al. 2001).
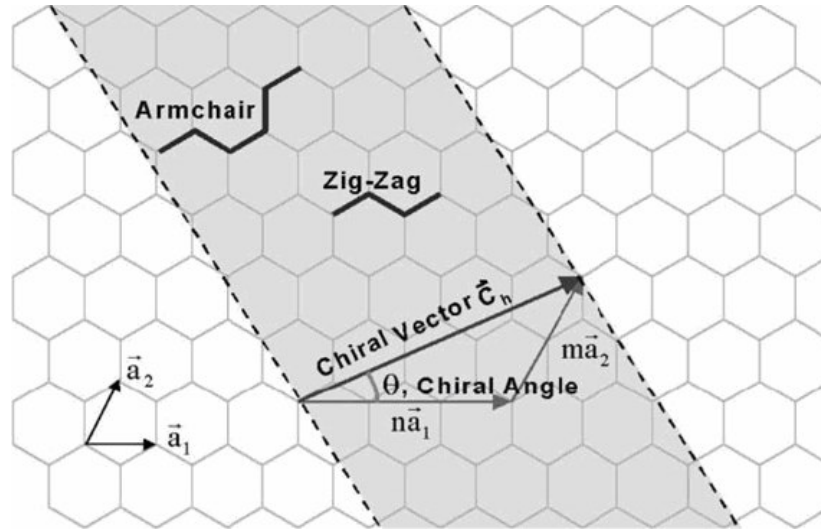
Figure 2.4: Graphene honeycomb lattice with the lattice vectors a_1 and a_2 (Thostenson, Ren et al. 2001)

In the graphene honeycomb lattice, the unit cell is spanned by two vectors a_1 and a_2 and contains two carbon atoms at the position $1/3(a_1+ a_2)$ and $2/3(a_1+ a_2)$, where the basic vectors of length $|a_1| = |a_2| = a_0 = 2.461$Å form an angle of 60°. In carbon nanotube the graphene sheet is rolled up in such a way that a graphene lattice vector $c_h= na_1 + ma_2$ becomes the circumference of the tube. This circumference vector c, which is usually denoted by the pair of integers (n,m), is called the chiral vector and uniquely defines a particular tube (Reich 2004). The amount of "twist" in the tube is determined by the chiral angle. Two limiting cases in this field are referred to as zigzag $((n,0)$ structure with chiral angle of 0°) and armchair $((n,n)$ structure with chiral angle of 30°) structures. Other possibilities are referred to as chiral structure.
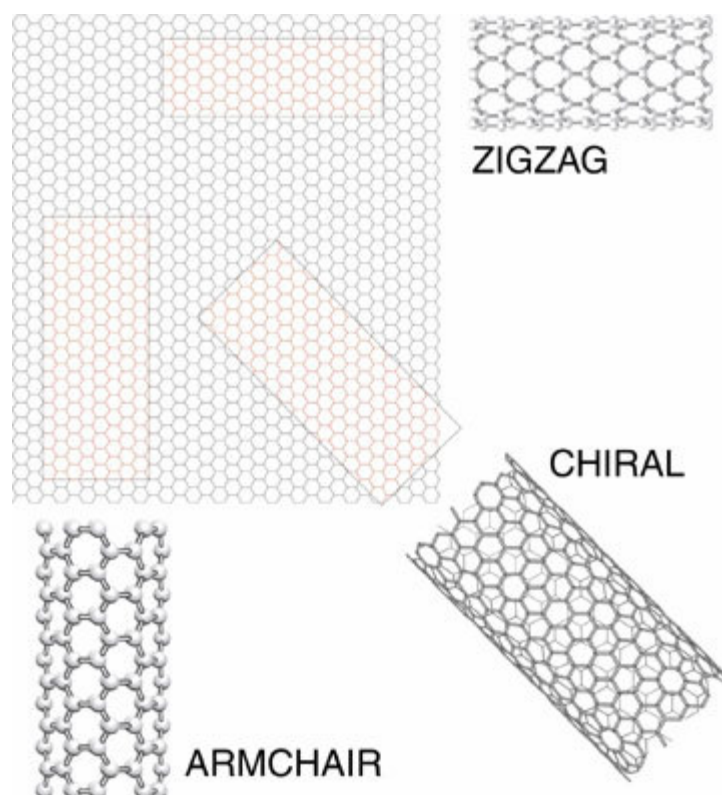
Figure 2.5: Atomic structure of zigzag, chiral and armchair carbon nanotube
(www.seas.upenn.edu/mse/research/nanotubes.html)

Many of the CNT's properties such as symmetry and electronic structure may vary dramatically when changing the chirality.

2.2.2. Fabrication methods

There are various methods to synthesize carbon nanotubes. CNTs can be fabricated in carbon arcs, through laser vaporization, catalytic combustion, chemical vapor deposition and ion bombardment. The type of produced nanotubes strongly depends upon the presence or absence of catalysts. Noncatalytic methods usually result in multi-wall nanotubes, while single-wall nanotubes are usually produced under catalytic conditions (Bernholc, Roland et al. 1997).

2.2.3. Properties

Mechanical properties

Carbon nanotubes have been recognized as among the strongest materials in the world, both in terms of tensile strength and elastic modulus because of the covalent sp^2 bonds formed

between the individual carbon atoms. The mechanical properties of CNTs have been extensively studied both analytically and experimentally (Thostenson, Ren et al. 2001; Breuer and Sundararaj 2004; Thostenson, Li et al. 2005; Xie, Mai et al. 2005; Lau, Gu et al. 2006). Large values of tensile strength, for instance a tensile strength of 63 GPa for a MWCNT (Yu, Lourie et al. 2000), and also extremely high elastic modulus, in the order of 1 TPa, have been proven by both simulation and experimental measurements (Salvetat, Bonard et al. 1999). These reported strengths are 10 to 100 times higher than the strongest carbon steel with the tensile strength of approximately 1.2 GPa. Considering the low density of carbon nanotubes, which is in the range of 1.3-1.4 g/cm^3, their specific strength is the best of known materials. Experimental observations indicate that CNTs are not nearly as strong under compression. Because of their hollow structure, they tend to undergo buckling when placed under compressive, torsional or bending stress (Bernholc, Roland et al. 1997; Qian, Wagner et al. 2002; Lau, Gu et al. 2006).

Electrical properties

Although carbon nanotubes generally have exceptional properties, a wide range of their special applications are related to their unique electrical behaviors. CNTs have large band gap electrical properties depending on the symmetry and electronic structure of graphene and resulting nanotubes. Carbon nanotubes are high-conductive metallic materials if in their (n,m) structure, $2n + m = 3q$ (where q is an integer), otherwise the nanotubes are semiconductors. For instance CNTs with an armchair structure ($n=m$) are metallic, and nanotubes (7,0), (8,4), (9,1), etc. are semiconducting. Based on theoretical calculations, electrical current density of an individual carbon nanotube can be more than several times greater than metals such as silver and copper (Breuer and Sundararaj 2004; Xie, Mai et al. 2005).

Thermal Properties

Theoretical predictions have indicated that carbon nanotubes are very good thermal conductors along the tube axis but good insulators in the transverse direction (Hone, Llaguno et al. 2002; Breuer and Sundararaj 2004). CNTs also have extremely high thermal stability (higher than 700 ^{o}C in air and than 2800 ^{o}C in vacuum) and negligible thermal expansion (Xie, Mai et al. 2005).

Defects

Besides the basic properties of carbon nanotubes, their behavior is largely affected by the existence of defects such as atomic vacancies and Stone Wales defect (creation of a pentagon and heptagon pair by rearrangement of the bonds). These defects, in high level, can decrease tensile strength up to 85% as well as electrical and thermal conductivity (Sammalkorpi, Krasheninnikov et al. 2004). Some defect formation can also change the electrical nature of tubes in the region surrounding those defects. For instance, the armchair-type tubes (which are metallic) can be semiconducting in this region.

2.3. Carbon nanotube / polymer composites

The exceptional mechanical, electrical, optical and thermal properties of CNTs, combined with their low density and superior high aspect ratio, offer the exciting opportunity for material composite reinforcement. Particularly, considerable attention has been given to carbon nanotube / polymer composites owing to their extraordinary properties from both processing and application points of view.

2.3.1. Composite preparation

In spite of the remarkable properties of CNTs, in many cases, carbon nanotube composites can not demonstrate their theoretical potential. A major challenge in this field is to disperse CNTs individually and uniformly within the polymer matrix without destroying their integrity or reducing their high aspect ratio. Without proper pre-treatment, CNTs usually aggregate when introduced into the polymeric matrix. That is because of strong Van der Waals interactions resulting from large surface area, inter-particle fusing by impurities such as amorphous carbon, and tube entanglement. Therefore, to enhance dispersion of CNT, surface treatment, purification and disentanglement are essentially required (Breuer and Sundararaj 2004; Lin, Cheng et al. 2005; Sung, Kum et al. 2005). It should be noticed that, this pre-treatment process usually reduce the properties of individual tubes (Wu, He et al. 2006). Moreover, obtaining good dispersion with high level of properties generally requires optimized pre-treatment process as well as proper processing technique.

Several processing techniques are presented for preparing CNT/polymer nanocomposites, all of which try to address the critical processing issues that directly affect the composite

properties: deagglomeration of bundles and ropes, CNT dispersion, nanotube/matrix wetting and adhesion, alignment and interfacial bonding (Breuer and Sundararaj 2004). The efficiency of each technique directly depends on its ability to better resolve these issues in order to provide an effective utilization of CNTs in composite application.

Solution processing

Perhaps, solution-based methods are the most common way for preparing polymer/nanotube composites providing easy mixing and dispersion of CNTs through low viscosity solvents (Breuer and Sundararaj 2004; Coleman, Khan et al. 2006). A large number of researchers have used solution methods to prepare polymer/CNT composites (Ding, Eitan et al. 2003; Du, Fischer et al. 2003; Velasco-Santos, Martinez-Hernandez et al. 2003; Fisher, Eitan et al. 2004; Lin, Cheng et al. 2005; Xinfeng, Hudson et al. 2005; Kymakis and Amaratunga 2006; Chen, Yu et al. 2006; Wu, Ma et al. 2006; Zhang, Kandadai et al. 2006; Zhang, Zhang et al. 2006). Most of these methods have tried to improve the CNT dispersion and the interaction between CNT and polymer through high-energy ultrasonication , surfactant-assisted mixing via the formation of colloidal intermediate, noncovalent polymer wrapping and covalent functionalization of nanotube with the polymer matrix (Thostenson, Li et al. 2005). However, the possibility of damaging the surface properties of CNT by utrasonication and the utilization of exclusively toxic and/or volatile solvents and acids, constitute weak points in solution techniques.

Melt-mixing

CNTs can be incorporated into thermoplastic polymers through melt processing techniques. The speed, simplicity, and availability of these techniques in plastic industry have made them the preferred methods of composite formation in many cases (Potschke, Fornes et al. 2002; Breuer and Sundararaj 2004; Coleman, Khan et al. 2006).

Unlike the solution processing and in-situ polymerization, melt-mixing methods are free of solvents and contaminants. In addition, high temperature and high shear mixing which is different from those in solution techniques may enhance the dispersion of CNTs and minimize their tendency to form aggregate in composites; also, aligned nanotubes are obtained when these conditions are coupled with elongational flow.

Melt processing of CNT composites can be realized in two ways:

i. Direct addition of CNT to polymer during melt mixing

ii. Using commercially available masterbatches of CNT/polymer composites and diluting them with pure polymers

While using a direct incorporation method makes it possible to use a variety of materials and tailor their properties (Anand, Agarwal et al. 2006; Dondero and Gorga 2006; Kim and Kim 2006; Kim and Kim 2006; Li, Luo et al. 2006; Wu, He et al. 2006; Zhang, Zhang et al. 2006), it is difficult to disperse the individual nanotubes in polymeric matrixes.

The masterbatch dilution technique is a preferred method in many cases (Potschke, Fornes et al. 2002; Potschke, Bhattacharyya et al. 2004; Abdel-Goad and Potschke 2005; Sung, Kum et al. 2005; Lin 2006) and is more convenient because of the ability to use existing technology without big changes.

In situ polymerization

For improving dispersion and integration between the phases, polymer grafted nanotubes are introduced in the corresponding matrix via in situ polymerization method. In this method functionalized carbon nanotubes are introduced together with monomers and catalysts in the polymerization reactor. During in-situ polymerization, polymer macromolecules are grafted onto the walls of carbon nanotubes and reinforcement is obtained at a molecular scale (Breuer and Sundararaj 2004; Coleman, Khan et al. 2006). In situ polymerization is also beneficial because of the possibility to achieve high loading and very good miscibility with almost any polymer type (Jia, Wang et al. 1999; Kuan, Ma et al. 2005; Lee, Oh et al. 2005; Blond, Barron et al. 2006; Kwiatkowska, Broza et al. 2006; Li, Huang et al. 2006; Li, Huang et al. 2006; Lu, Chao et al. 2006; Shin, Yoon et al. 2006; Zeng, Gao et al. 2006). This technique is usually a proper selection in the case of insoluble and thermally unstable polymers, which are impossible to be processed by solution or melt mixing.

2.3.2. Properties

A great deal of experimental and theoretical works has been presented in the literature regarding the effective properties of carbon nanotube-polymer composites. These results are seldom the same and it is difficult to generalize them because of many effective parameters including the size, form and fabrication method of CNT, characteristic of polymer chemistry,

processing conditions, nanotube loading, dispersion and alignment in polymer matrix and CNT-polymer interaction.

However, most of the relevant works have shown significant improvements in the properties of the resulted composites with respect to the pure polymer.

Mechanical properties

The superior structure of carbon nanotubes and their high aspect ratio, low density and extraordinary mechanical properties provide an outstanding potential for reinforcement in composite materials. To date, characterization of the mechanical properties of nanotube - reinforced polymers has been considered in many studies for different applications. However, the common theme has been the significant enhancement of the most important mechanical properties such as Young modulus and tensile strength, with a relatively small amount of carbon nanotube loading. By adding 1 wt% MWCNT to polystyrene, 25% improvement in tensile strength is achieved (Breuer and Sundararaj 2004). Dendero et al. (Dondero and Gorga 2006) employed melt mixing method followed by melt drawing and their results showed a 32% increase in toughness and 138% increase in modulus with a 0.25 wt% MWCNT in polypropylene (PP). Inversely, in many cases, the elongation at break, an indicator of material toughness and flexibility, decreases when CNTs are incorporated in a polymer (Zeng, Gao et al. 2006). Meincke et al. (Meincke, Kaempfer et al. 2004) studied the mechanical properties of MWCNT/polyamide-6. In their study, tensile tests of the CNT-composites showed a significant increase of 27% in the Young's modulus, however the elongation at break of these materials decreased dramatically.

The tensile modulus and strength of nanotube-polymer composites are strongly affected by nanotube loading, dispersion and alignment. Therefore, when employing proper processing techniques, extremely high modulus and strength can be achieved without large changes in elongation at break (Moniruzzaman and Winey 2006). Blond and his colleagues (Blond, Barron et al. 2006) prepared poly (methyl methacrylate)(PMMA)-functionalized MWCNTs by in situ polymerization methods. In this study, increases in Young's modulus, breaking strength, ultimate tensile strength, and toughness by factors of 1.9, 4.7, 4.6 and 13.7 respectively were observed with the addition of less than 0.5 wt% of nanotube. They also observed that effective reinforcement is only obtained at a level of nanotube content of up to approximately 0.1 vol%; above this amount all the mechanical tend to decrease, probably due to nanotube aggregation.

Eventually, it seems that the processing method is the most important parameter in this area. The following table shows typical results of mechanical properties related to different processing methods.

Table 2.1. Mechanical properties of CNTs/polymer composites

Nanotube type	Polymer	Y_{Poly} (GPa)	Y_{Max} (GPa)	Max CNT content	Processing method	Reference
CVD-MCWNT	PS	1.53	3.4	2.5 vol%	Solution processing	(Safadi, Andrews et al. 2002)
CVD-MCWNT	HDPE	0.98	1.35	1 wt%	Solution processing	(Ruan, Gao et al. 2003)
Arc-MCWNT	MEMA	0.71	2.34	1 wt%	Solution processing	(Velasco-Santos, Martinez-Hernandez et al. 2003)
CVD-MWCNT	PVA	1.9	7.04	0.6 vol%	Solution processing	(Coleman, Cadek et al. 2004)
Arc-MWCNT	PMMA	0.73	1.63	17 wt%	Melt-mixing	(Coleman, Khan et al. 2006)
CVD-MWCNT	PS	2	4.5	25 vol%	Melt-mixing	(Coleman, Khan et al. 2006)
CVD-MWCNT	PC	0.8	1.04	15 wt%	Melt-mixing	(Potschke, Bhattacharyya et al. 2003)
CVD-MWCNT	PMMA	2.7	3.7	10 wt%	Melt-mixing	(Gorga and Cohen 2004)
CVD-MWCNT	Nylon	0.4	1.24	2 wt%	Melt-mixing	(Liu, Phang et al. 2004)
Arc-SWCNT	PP	0.85	1.19	0.75 wt%	Melt-mixing	(López Manchado, Valentini et al. 2005)
Arc-MWCNT	PMMA	1.5	2.5	1 wt%	In situ polymerization	(Coleman, Khan et al. 2006)
SWCNT	PMMA	o.3	0.38	0.01 wt%	In situ polymerization	(Putz, Mitchell et al. 2004)

Coleman et al. (Coleman, Khan et al. 2006) used Young's modulus reinforcement, dY/dV_f , as a yardstick to compare different studies. Their results are summarized in Table 2.4.

Table 2.2. Summary/comparison of reinforcement of SWCNT and MWCNT/composites fabricated by various processes (Coleman, Khan et al. 2006)

	Solution	Melt	In situ poly	Functionalization
Mean dY/dV_f (GPa)	309	23	430	157
Median dY/dV_f (GPa)	128	11	60-150	115
Max dY/dV_f (GPa) SWCNT	112	68	960	305
Max dY/dV_f (GPa) MWCNT	1244	64	150	380

Electrical Properties

The first achieved major commercial application of carbon nanotubes is their use as electrically conducting components in polymer composites (Xie, Mai et al. 2005).

High electrical resistivity is a common characteristic of polymers, which causes insulating behavior of these materials. While this feature is highly desirable for many applications, accumulation of static charges on the polymer surface may induce explosion or fire in some special sites such as oil field, mine, chemical factory and some special storage facilities. On the other hand, the constant growth of the electronic industry results in more and more usage of polymers to produce special parts such as fuel cells, shells for electronic devices, circuit board, and so on (Li, Luo et al. 2006). These applications need conductive or anti-static polymer materials. Currently the common method to enhance electrical conductivity in a polymer is to compound the polymer with conductive carbonaceous fillers. However, in spite of widely used fillers such as carbon fiber and carbon black, high loadings of such conductive fillers are often needed to obtain conductive materials. Hence, not only the final cost of the material is increased due to the high cost of the filler, but also often other properties of the material are impaired.

Generally, conductive materials can be achieved when the filler content exceeds a critical value, known as the percolation threshold. At the percolation threshold, formation of a three-dimensional conductive network of the fillers within the matrix, contributes to a sharp jump in

the conductivity by many orders of magnitude. The well established method to determine the percolation threshold is to plot the electrical conductivity as a function of reduced mass fraction of fillers and to fit the results with power law function (Meincke, Kaempfer et al. 2004; Dalmas, Dendievel et al. 2006; Hu, Zhao et al. 2006; Li, Luo et al. 2006)

Recently, a considerable attention has focused on the use of carbon nanotubes as conductive fillers in functional polymer composites. The combination of superior electrical conductivity, one-dimensional structure and high aspect ratio of CNTs, results in a very low percolation threshold in nanotube/polymer composite (Fig. 2.6 & 2.7). Consequently, it is possible to achieve several orders of magnitude enhancements in electrical conductivity with a very small loading of CNTs while the other performance aspects of the polymers such as mechanical properties and low melt flow viscosity can be maintained constant.
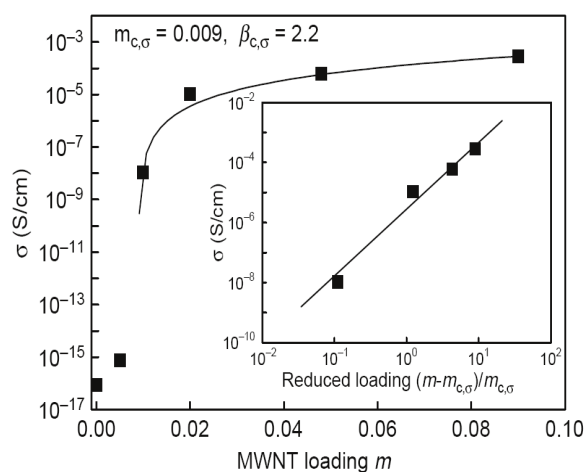
Figure 2.6: Electrical conductivity (σ) of the PET/MWCNT nanocomposites as a function of MWCNT loading. Inset: a log–log plot of electrical conductivity versus reduced MWCNT loading. The solid lines are fits with a power law dependence of electrical conductivity on the reduced MWCNT loading (Hu, Zhao et al. 2006)
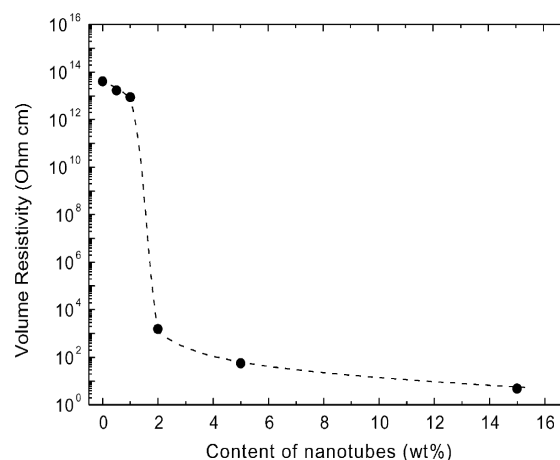
Figure 2.7: Effect of CNT content on volume resistivity of PC/MWCNT nanocomposites (Potschke, Fornes et al. 2002)

The wide range of conductivity of these nanocomposites introduces a variety of applications in electronic industries and related branches: electrostatic dissipation, electrostatic painting, electromagnetic interface (EMI) shielding, printable circuit writing, and transparent conductive coating, to name a few. Figure 2.8 shows the electrical conductivity of solution processes SWCNT/polystyrene (PS) composites as a function of loading (Ramasubramaniam, Chen et al. 2003).
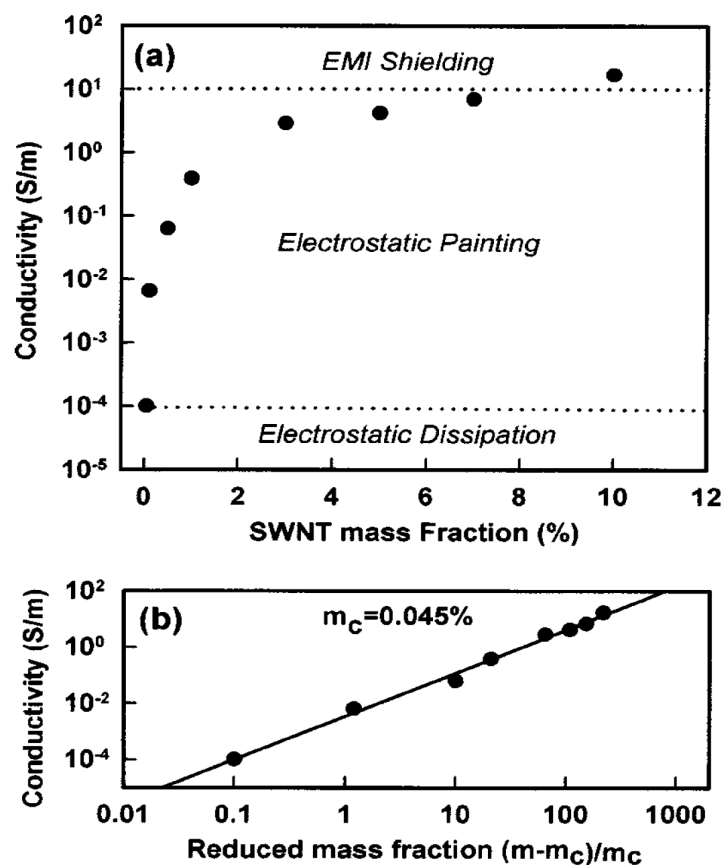
Figure 2.8: (a) Room temperature electrical conductivity of PPE-SWCNT/PS composite vs. the SWCNT weight loading. Dashed lines represent the approximate conductivity lower bound required for several electrical applications. (b) Room temperature conductivity of the PPE-SWCNT/PS composite as a function of the reduced mass fraction of SWCNTs (Ramasubramaniam, Chen et al. 2003)

The percolation threshold is influenced by several nanotube characteristics including its aspect ratio, dispersion and alignment. CNTs with higher aspect ratio generally result in a smaller percolation threshold (Moniruzzaman and Winey 2006). Better dispersion decreases the percolation threshold as a result of high aspect ratio of well-dispersed nanotube rather than

nanotube aggregates (Du, Fischer et al. 2003; Moniruzzaman and Winey 2006). In a system containing highly aligned nanotubes, fewer contacts between tubes give a reduction in electrical conductivity and result in a higher percolation threshold compared to that obtained in a composite of randomly oriented nanotubes (Du, Fischer et al. 2003; Fangming, Fischer et al. 2005; Moniruzzaman and Winey 2006). This effect has been studied in detail using of SWCNT/PMMA composite where melt fiber spinning was employed to control the alignment (Du, Fischer et al. 2003; Fangming, Fischer et al. 2005). The results showed that at a fixed SWCNT concentration (2 wt%), the electrical conductivity parallel to the alignment direction increased sharply with decreasing alignment. In a recent study, S. H. Yao and his colleague (Dang, Yao et al. 2007) have studied the dielectric property of MWCNT/PVDF nanocomposites prepared by solution mixing method. Their results showed that the dielectric constant and conductivity after stretching were always lower than those before stretching.

Finally, the percolation points are different in various types of polymers, as morphological differences such as the degree of crystallinity and the presence of multiple polymer phases can affect the amount of filler needed to reach the percolation point. Using amorphous polymeric matrices, loading levels to achieve comparable resistivity, typically run a few percentage points higher than in the case of semi-crystalline polymers. In semi-crystalline thermoplastics, as crystallites grow, all additives including nanotubes are occluded (pushed out of the way) due to the rigid spacing requirements which characterize crystalline regions of polymers (Sharples 1966). The polymeric matrix is an electrical insulator and electrons move from one nanotube to another. Therefore, the higher the crystalline structure of a resin, the lower the volume of nanotubes will be required to complete the conductive array.

The results of the most important studies done so far about electrical properties of CNT/polymer composites are summarized in Table 2.3.

Table 2.3. Summary of conductivity results for CNT/polymer composites

System under study	Processing method	Percolation threshold	Resistivity (R) or conductivity(C)	Reference
MWCNT/PMMA	Spin coating	0.5 wt%	**R:** $10^3 \Omega$ cm	(Breuer and Sundararaj 2004)
SWCNT/PA	Powder technology methods	3 vol%	**R:** 10^{-1}-$10^0 \Omega$ cm at 6 vol%	(Breuer and Sundararaj 2004)
MWCNT/PP	Melt-mixing in internal mixer	0.05 vol %	**R:** 10^5-$10^{12} \Omega$/square (surface resistivity)	(Breuer and Sundararaj 2004)
MWCNT/PS	Melt-mixing in internal mixer	0.25 vol%	**R:** $10^5 \Omega$/square (surface resistivity)	(Breuer and Sundararaj 2004)
MWCNT/PS	Film casting and spin casting	2.49 vol%	**R:** $10^3 \Omega$ cm	(Safadi, Andrews et al. 2002)
MWCNT/PC	Diluting a masterbatch of 15 %wt NT (Melt-mixing in twin screw extruder)	1-2 wt %	**R:** $10^3 \Omega$ cm	(Potschke, Fornes et al. 2002)
SWCNT/PMMA	Spin coating	0.4 wt%	**R:** $10^3 \Omega$ cm	(Breuer and Sundararaj 2004)
SWCNT/PS	Nano-covalant functionalization - Solution processing	0.02-0.05 wt% (0.045 wt%)	**C:** $9*10^{-3}$ S/m	(Ramasubramaniam, Chen et al. 2003)
SWCNT/PMMA	Coagulation method	2-4 wt%	**C:** 10^{-4} S/m	(Du, Fischer et al. 2003; Du, Scogna et al. 2004)
MWCNT/PA6	Melt-mixing in co-rotating twin screw extruder	2-4 wt%	**R:** $10^3 \Omega$.cm	(Meincke, Kaempfer et al. 2004)
SWCNT/PMMA	Coagulation method	0.365 wt%	**C:** 10^{-7} S/m	(Fangming, Fischer et al. 2005)
MWCNT/PET	Coagulation method	0.5-1 wt%	**C:** 10^{-8} S/m	(Hu, Zhao et al. 2006)
FMWCNT/PC	Solution processing	NT: 5 wt% FNT: 2-3 wt%	**C:** 10^{-4} S/m 10^{-2} S/m	(Sung, Han et al. 2006)
MWCNT/PET	Melt-mixing in a compounder	0.3-0.4 wt%	**C:** 10^{-4} S/m	(Li, Luo et al. 2006)
MWCNT/PS	Solution processing/ electrospining	4 wt%	**C:** 10^{-4} S/m	(Mazinani, Ajji et al. 2009)

Rheological properties

Rheological properties of nanotube/polymer composites including effective viscoelastic (time or frequency-and temperature–dependent) behavior have both practical importance related to composite processing and scientific interest as a probe of the composite microstructure and dynamics. In other words, while low frequency behavior is sensitive to the structure of the composite, the processing properties are estimated using rheological behavior at high frequencies. Probing the effective viscoelastic response typically shows that in such composite systems interconnected structures of anisometric fillers at low frequencies, result in an apparent yield stress, which is visible in dynamic measurements by a plateau in the rheological properties.
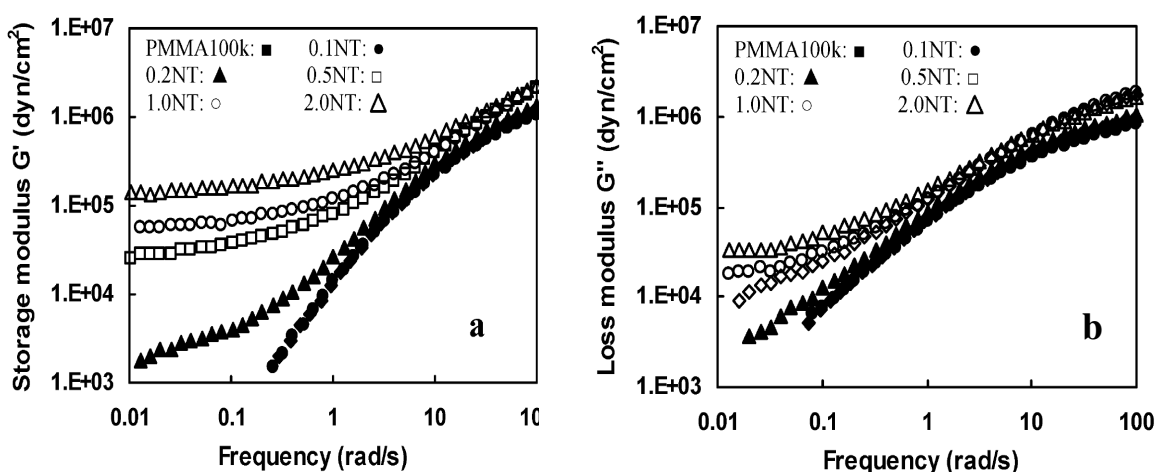
Figure 2.9: (a) Storage modulus and (b) loss modulus of SWCNT/ PMMA nanocomposites with various nanotube loadings. Rheology performed at 200 °C and 0.5% strain (Du, Scogna et al. 2004)

In the CNT/polymer composite system, as the nanotube content increases viscoelastic behavior at low frequency progresses from liquid-like response ($G' \propto \omega^2$ & $G'' \propto \omega$) to a solid-like response (G' and G'' independent of ω) (Fig. 2.9). The onset of solid-like behavior corresponds to the rheological percolation threshold and can be determined by applying a power law function to G' versus nanotube loading (Du, Scogna et al. 2004; Moniruzzaman and Winey 2006) (Fig. 2.10).
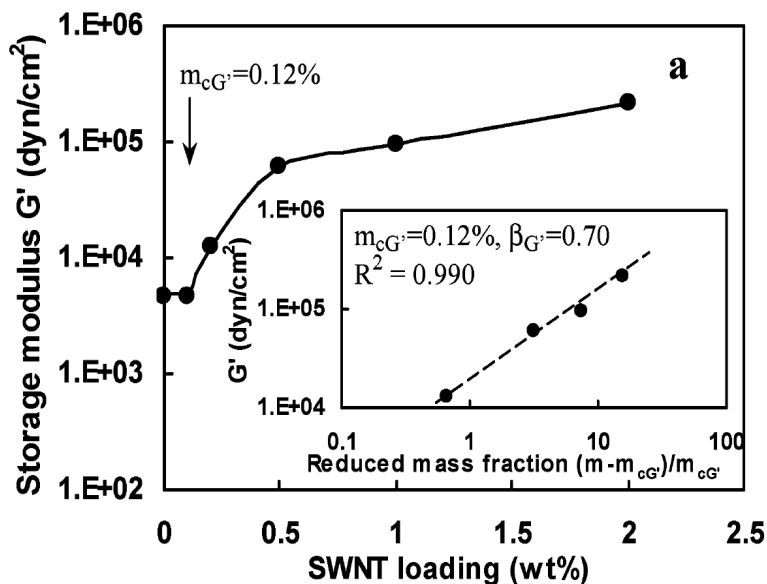
Figure 2.10: Storage modulus, G', of the SWCNT/PMMA nanocomposites as a function of the nanotube loading at a fixed frequency of 0.5 rad/s. Inset: a log-log plot of G' vs reduced mass fraction (Du, Scogna et al. 2004)

Plotting the phase angle δ versus the absolute value of the complex modulus ($|G^*|$) is another sensitive tool to investigate the percolation of filler in a viscoelastic fluid (Fig. 2.11). In this plot, called "Van Gurp Palmen" plot, the percolation threshold corresponds to a plateau at low complex modulus (Meincke, Kaempfer et al. 2004).
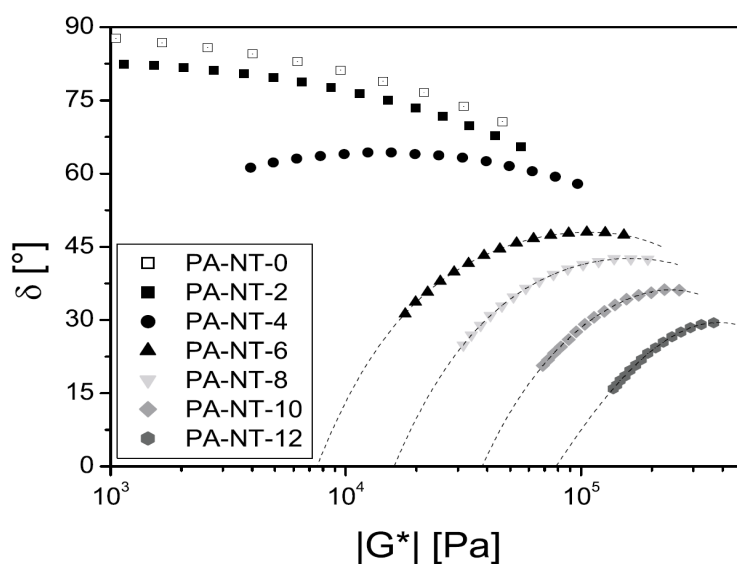
Figure 2.11: Van Gurp plot of the PA-NT-x composites (Meincke, Kaempfer et al. 2004)

As another criterion, *tanδ*, where *δ* is the phase angle, is very sensitive to the structural change of the materials and decreases with CNT loading, as shown in Figure 2.12a. In this figure peak occurs at the frequency of about 1 rad/s and disappears with increasing the CNT content, showing that the material becomes more elastic (Xiao, Zhang et al. 2007). This is also characteristic of a viscoelastic fluid experiencing a fluid–solid transition. At the transition point, *tanδ* is expected to be independent of frequency. With this composite, a similar fluid–solid transition is observed, which occurs at a CNT content between 3 and 5 wt%. After the transition, *tanδ* increases with frequency, indicating a dominating elastic response of the material.

The CNT content at the transition point can be estimated more accurately from a multifrequency plot, as shown in Figure 2.12b for the same system described above (Xiao, Zhang et al. 2007). All curves intersect at nearly a single point where *tanδ* becomes frequency-independent. Thus the fluid–solid transition composition of the present composites, C_t, is estimated to be 4.8 wt%.
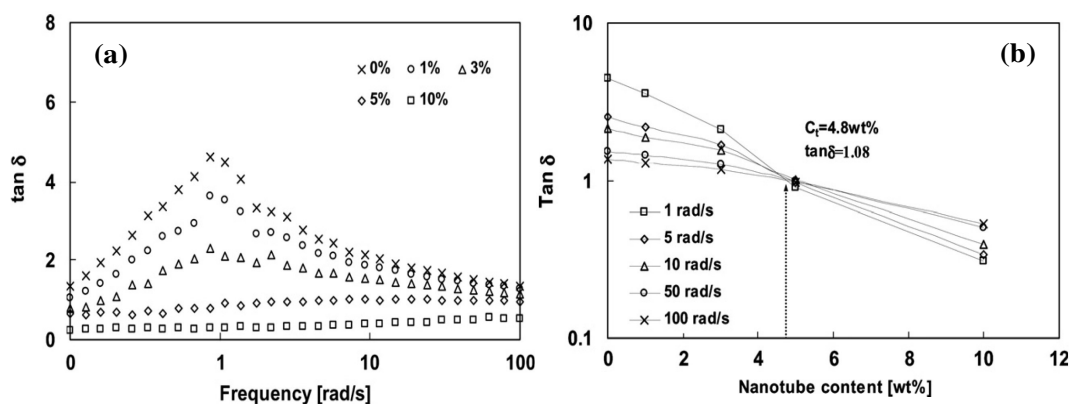
Figure 2.12: (a) *tanδ* of the MWCNT/LDPE composites as a function of sweep frequencies (b) *tanδ* versus nanotube content at different frequencies (Xiao, Zhang et al. 2007)

All the methods for investigating the rheological percolation threshold are summarized in Table 2.4.

Table 2.4. Available methods for investigating the rheological percolation threshold

Method	Criteria	Reference
Applying a power law function to the G' versus nanotube loading	Onset of solidlike behavior (G' and G'' independent of ω)	(Du, Scogna et al. 2004) (Moniruzzaman and Winey 2006)
Plotting the phase angle δ versus the absolute value of the complex viscosity $\left| G^* \right|$ (Van Grup Palmen plot)	A plateau at low complex modulus	(Meincke, Kaempfer et al. 2004)
Plotting $tan\delta$ versus sweep frequencies at different nanotube loadings	Disappearing of the peak at nearly low frequency	(Xiao, Zhang et al. 2007)
Plotting $tan\delta$ versus nanotube loading at a complete range of frequency (from low frequencies to high frequencies)	A single point at which all curves intersects and where $tan\delta$ becomes frequency-independent	(Xiao, Zhang et al. 2007)

The low frequency behavior of CNT/polymer nanocomposites was reported the first time in 2002 (Potschke, Fornes et al. 2002). In this study, the rheological behavior of compression molded nanocomposites of polycarbonate containing 0.5-15 wt % MWCNT was investigated using oscillatory rheometry at 260 °C. The viscosity curves are shown in Figure 2.13.
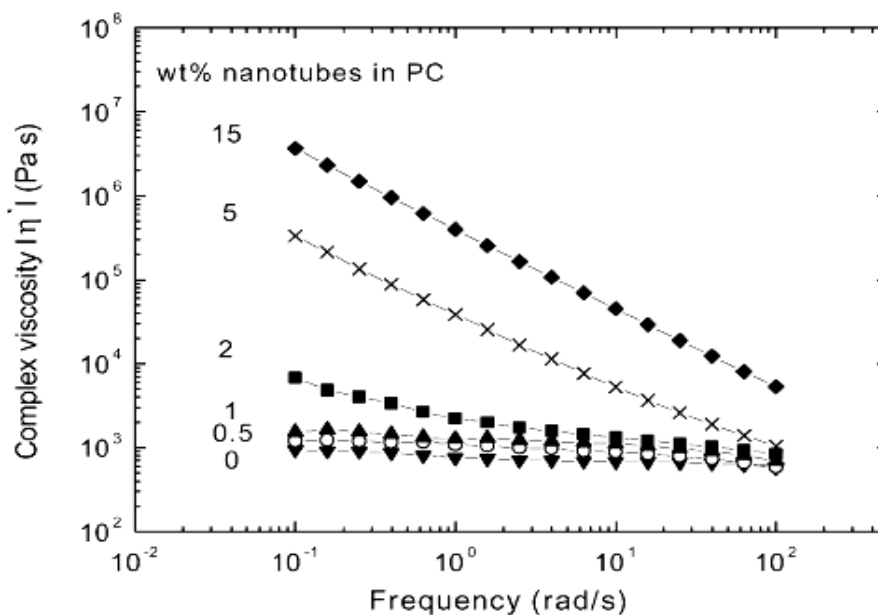
Figure 2.13: Complex viscosity of nanotube filled polycarbonate at 260 °C (Potschke, Fornes et al. 2002)

These composites were obtained by diluting a masterbatch containing 15 wt% nanotubes using a twin-screw extruder. The results showed that the increase in viscosity associated with the addition of nanotubes is much higher than viscosity changes reported for carbon nanofibers having larger diameter. The viscosity increase was accompanied by an increase in elastic melt properties, represented by the storage modulus G', which was much higher than the increase in the loss modulus G''. The viscosity curves above 2 wt% nanotubes exhibited non-Newtonian behavior at lower frequencies. A step increase at approximately 2 wt% nanotubes observed in the viscosity-composition curves at low frequencies was considered as the rheological threshold. Ultimately, the rheological threshold coincided with the electrical conductivity percolation threshold, which was found to be between 1 and 2 wt% nanotubes.

Since then, more attention has been paid to the rheological properties of CNTs/polymer nanocomposites with the main focus on the percolation threshold as one of the most important factors affecting the material properties or as a factor determining the dispersion quality.

O. Meincke and his colleagues (Meincke, Kaempfer et al. 2004) found that in composites of polyamide-6 and carbon nanotubes, prepared in a corotating twin screw extruder, the experimentally determined percolation threshold from van Gurp Palmen plot lied between 2 and 4 wt%. However, according to theoretical studies, the percolation threshold for solid rods with an aspect ratio of 100 amounts to approximately 1.1 wt% (Winslow, Cohen et al. 1994). They explained the discrepancy between theory and experiment with two experimental findings. First, despite the fine dispersion of carbon nanotubes in the polymer matrix TEM experiments still showed larger clusters of nanotubes. Secondly, it was found from TEM micrograph that nanotubes, cannot be assumed to be solid rods, but must be described as flexible and intertwined fibers. Both of these effects shift the percolation threshold to higher filler contents.

Polycarbonate/multiwalled carbon nanotube composites produced by diluting a masterbatch, have been rheologically characterized (Abdel-Goad and Potschke 2005). The results showed that the dynamic modulus and the viscosity increased with increasing MWCNT content. At a concentration of 0.5 wt% MWCNT, a significant change in the frequency dependence of the modulus was observed which indicates a transition from a liquid-like to a solid-like behavior of the nanocomposites. They concluded that this transition could be related to the formation of a combined network between the nanotubes and the polymer chains.

Y.T. Sung and his colleagues (Sung, Han et al. 2006) have studied the rheological and electrical properties of the polycarbonate (PC)/functionalized MWCNT. They suggested that the electrical and rheological properties of the PC/MWNT composites are affected by the nanotube-nanotube network structure, which is related to the MWCNT morphologies such as the degree of aggregation and aspect ratio of the MWCNT.

In nanocomposites of MWCNT and poly (ethylene terephthalate) (PET), prepared by coagulation method, both electrical conductivity and rheological properties have been well characterized (Hu, Zhao et al. 2006). They found that with MWCNT loading, the nanocomposites undergo transition from electrically insulating to conductive at room temperature, while the melts show transition from liquid-like to solid-like viscoelasticity. The percolation threshold of 0.6 wt %(based on viscosity) for rheological property and 0.9 wt% for electrical conductivity was found.

Poly (ethylene terephthalate) (PET)/ MWCNT composites prepared through melt compounding in a twin-screw extruder were also studied (Kim, Park et al. 2007). They obtained the shear-thinning and relaxation exponents of the nanocomposites by fitting the experimental data in a low frequency region to power-law equations, such as $\eta^* \approx \omega^n$ (where ω is the frequency and n is the shear-thinning exponent) and $G' \approx \omega^n$ (where ω is the frequency and n is the relaxation exponent) (Fig. 2.14). A significant dependence of the rheological properties of the PET/MWCNT nanocomposites on the MWCNT content was also observed. The MWCNT loading increased the shear-thinning nature of the nanocomposite melt. The storage and loss modulii of the PET/MWCNT nanocomposites increased with nanotube loading, and this increment effect was more pronounced at lower frequencies.
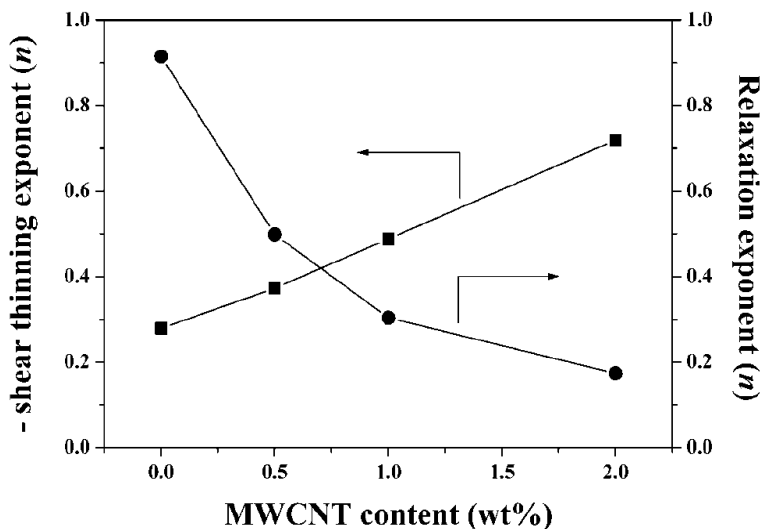
Figure 2.14: Variation of the shear-thinning exponent and relaxation exponent of the PET/MWCNT nanocomposites with the MWCNT content (Kim, Park et al. 2007)

Rheological properties of low density polyethylene (LDPE) composites reinforced by MWCNTs have been investigated by Xiao et al. (Xiao, Zhang et al. 2007). They found that the materials experienced a fluid–solid transition at the composition of 4.8 wt%, beyond which a continuous MWCNT network was formed throughout the matrix.

At high frequencies, the influence of nanotube loading on the viscoelastic response is relatively weak indicating that CNTs do not significantly influence the short–range dynamic of polymer chains particularly in the length scale comparable to the entanglement lengths (Du, Scogna et al. 2004).

It is widely accepted that the rheological percolation threshold is smaller than the electrical one (Du, Scogna et al. 2004; Hu, Zhao et al. 2006; Moniruzzaman and Winey 2006). This difference can be described in terms of the smaller tube–tube distance required for electrical conductivity as compared to that required to impede polymer mobility, so that more nanotubes are required to reach the electrical percolation threshold. Furthermore, the nonmetallic tubes do not have significant contribution in electrical conductivity, although they can restrict polymer motion (Fig. 2.15).
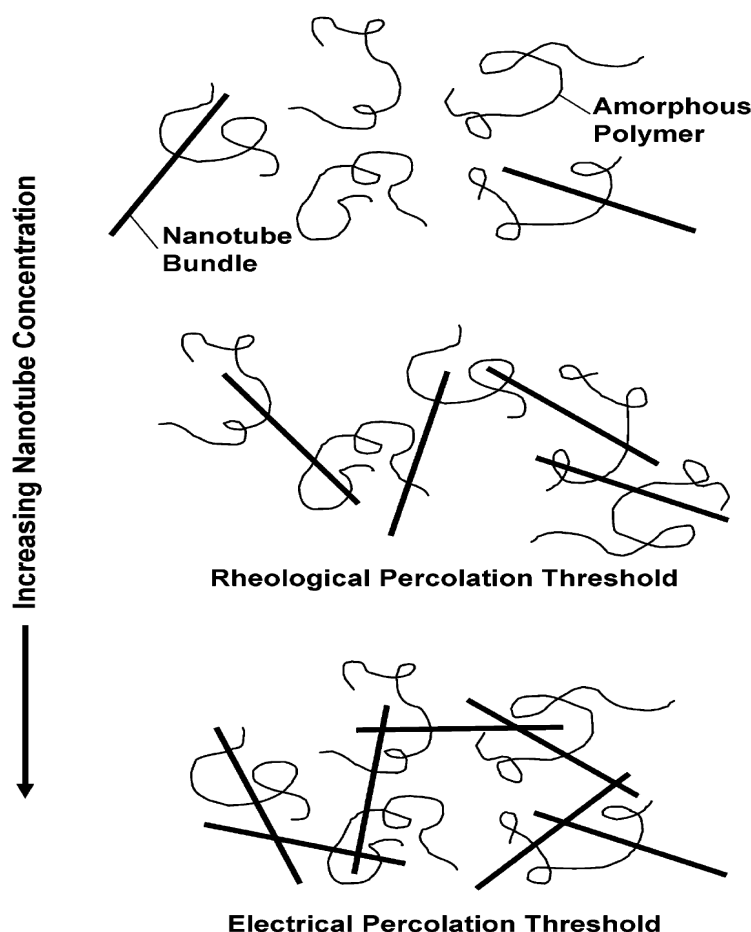
Figure 2.15: Schematic of SWCNT/polymer nanocomposites in which the nanotube bundles have isotropic orientation .At low nanotube concentrations, the rheological and electrical properties of the composite are comparable to those of the host polymer (top). The onset of solid-like viscoelastic behavior occurs when the size of the polymer chain is somewhat large to the separation between the nanotube bundles (middle). The onset of electrical conductivity is observed when the nanotube bundles are sufficiently close to one another to form a percolating conductive path along the nanotubes (bottom) (Du, Scogna et al. 2004)

CNTs also affect the temperature-dependant behavior of the polymer matrix. Although the viscoelastic material response increases at low temperature (below the polymer glass transition), significant increases are shown at high temperature (above T_g). Slight shifting of the effective glass transition usually to higher temperatures than that of the neat polymer and broadening of the loss modulus and loss tangent peaks on the high temperature side are other effects of addition of nanotube into a polymer matrix (Fisher, Eitan et al. 2004). In a recent work, Satapathy and his colleagues (Satapathy, Weidisch et al. 2007) analyzed the temperature dependency of viscoelastic behavior of a set of PC/MWCNT composites prepared by diluting a commercially available

masterbatch. Their DMA analysis showed an increase in the T_g and broadening of the *tan* δ peaks when increasing the MWCNT content suggesting confinement of the PC chain mobility.

It is largely found that the rheological properties also depend on nanotube dispersion, aspect ratio and alignment. Nanocomposites with better nanotube dispersion have smaller low-frequency slope of storage modulus G' versus frequency ω and higher G' at low frequency (Du, Scogna et al. 2004). Also the rheological percolation threshold drops when the quality of dispersion is improved (Moniruzzaman and Winey 2006). Using the effect of nanotube dispersion on the rheological properties, many researchers tried to determine the quality of dispersion and the efficiency of the technique used to improve the dispersion. Bin Lin et al. (Lin 2006) used this criterion to compare the quality of dispersion of MWCNT/PC composites prepared in three different miniature mixers by the masterbatch dilution method. Such studies have been also done on nanotube composites based on poly (methyl methacrylate) (PMMA) (Du, Scogna et al. 2004), poly (propylene fumarate)(PPF) (Xinfeng, Hudson et al. 2005; Shi, Hudson et al. 2006), polycarbonate(PC) (Lin 2006; Sung, Han et al. 2006) and poly(ethylene terephthalate) (PET) (Shin, Yoon et al. 2006) as the polymeric matrices. It is also revealed that when nanotubes are aligned in the polymer matrix the probability of tube-tube contacts decreases and the nanotube network is less effective at impeding the polymer motion (Du et al. 2004; Wu et al. 2007). Therefore, the nanocomposite storage modulus G' decreases with alignment of carbon nanotubes. In fact, alignment decreases the elastic response of nanocomposites (Du, Scogna et al. 2004). It is also found that the percolated nanotube network is very sensitive to the temperature (Potschke et al. 2004; Wu et al. 2007).

The steady shear viscosity is another important rheological parameter, especially when processing the composite. Steady shear viscosity is often estimated from the composite's complex viscosity using the Cox-Merz rule. This rule, which is based on empirical observation, states that the steady shear viscosity and complex viscosity are closely super-imposable for numerically equivalent values of shear rate and frequency. However, the rule only holds for isotropic polymeric solutions and polymer melts (i.e. not to liquid crystals or flocculated systems) (Kinloch, Roberts et al. 2002). Kinloch et al. (Kinloch, Roberts et al. 2002) investigated steady shear properties of aqueous MWCNT dispersions and found that the Cox-Merz rule is no longer valid for these dispersions and the steady shear viscosity is a few orders of magnitude lower than the complex one. A similar phenomenon was also reported in other composite systems (Shenoy,

Saini et al. 1983). Xiao et al. (Xiao, Zhang et al. 2007) found that in low density polyethylene (LDPE) composites reinforced by MWCNT by melt mixing, the Cox-Merz rule holds when the CNT content is low, but becomes inaccurate when the CNT concentration is high and the composite is more solid-like (Fig. 2.16).
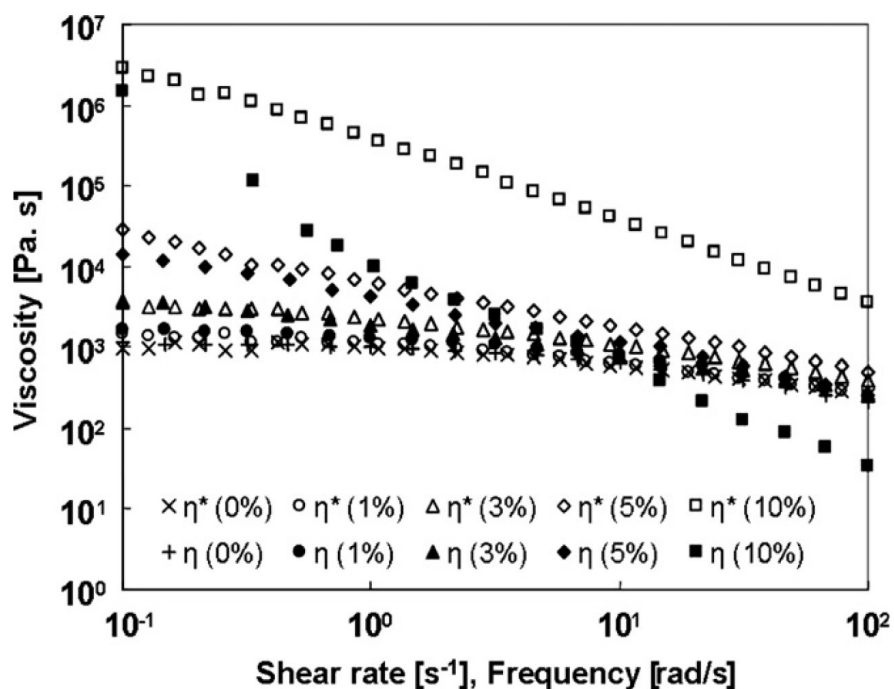
Figure 2.16: A comparison of complex and steady shear viscosities (Xiao, Zhang et al. 2007)

Other aspects of rheological studies can be found in the literature. In 2005, Kuan et al. (Kuan, Ma et al. 2005) showed that carbon nanotubes can increase the melt viscosity and reduce the variation of processing viscosity in CNT/ waterbone polyurethane composites. In 2006, rheological behavior of CNT/ poly (ethylene terephthalate) has been considered by Li et al. (Li, Luo et al. 2006) and their study indicated that the viscosity of composites containing high nanotube loadings exhibited a large decrease with increasing shear frequency. Finally, a few investigations on the modeling of the rheological behavior of carbon nanotubes suspended in low molecular weight polymeric resins have been recently carried out (Rahatekar et al. 2006; Fan and Advani 2007; Hong and Kim 2007; Ma et al. 2008).

A brief report of the most important papers in the field of rheology of CNT/polymer nanocomposites is given in the following table.

Table 2.5. Summary of rheological studies of CNT/polymer composites

System under study	Processing method	Percolation threshold	Parameters under study	Reference
Aqueous dispersed oxidized MWCNT	–		G', G'', G'/G'', $\lvert\eta^*\rvert$, η (steady shear viscosity), σ (shear stress) at 25 °C	(Kinloch, Roberts et al. 2002)
MWCNT/PC	Diluting a masterbatch of 15 %wt NT (Melt- mixing in twin screw extruder)	2 wt%	$\lvert\eta^*\rvert$, G', G'' at 260 °C	(Potschke, Fornes et al. 2002)
MWCNT/PA6	Melt-mixing in co-rotating twin screw extruder	2-4 wt%	δ, $\lvert G^*\rvert$, G_e at extrusion temp. 260 °C	(Meincke, Kaempfer et al. 2004)
SWCNT/PMMA	Coagulation method	0.12 wt%	G', G'' at 200 °C	(Du, Scogna et al. 2004)
MWCNT/PC	Solution mixing	–	G', G'', G'/G'', $H(\tau)$(relaxation spectra) at 150 °C and vs. temperature	(Fisher, Eitan et al. 2004)
MWCNT/PC	Diluting a masterbatch of 15 %wt NT (Melt-mixing in twin screw extruder)	0.5 wt%	$\lvert\eta^*\rvert$, $\lvert G^*\rvert$, G', G'', $tan\ \delta$, n (shear thining exponent) at 280 °C	(Abdel-Goad, Potschke et al. 2004; Abdel-Goad and Potschke 2005)
MWCNT/WPU	Solution mixing	–	Viscosity vs time & temp.	(Kuan, Ma et al. 2005)
SWCNT/PPF	Solution mixing	0.05 wt%	$\lvert\eta^*\rvert$, G', G'' at 25 °C	(Xinfeng, Hudson et al. 2005; Shi, Hudson et al. 2006)
MWCNT/PC	Solution mixing	NT:2 wt% FNT:1 wt%	G', G'', $tan\delta$ at 260 °C	(Sung, Han et al. 2006)
MWCNT/PET	Coagulation method	0.6 wt%	η, G', G'' at 265 °C	(Hu, Zhao et al. 2006)

MWCNT/PC	Diluting a masterbatch of 15 %wt NT (Melt-mixing in three mixers: DACA, APAM, MBM)	MBM & APAM : 0.38 wt% DACA: 0.5 wt%	$\left|\eta^{*}\right|, \delta$ at 265 ºC	(Lin 2006)
MWCNT/PET	Melt-mixing in a compounder	_	Shear viscosity at 280ºC	(Li, Luo et al. 2006)
MWCNT/PET	Melt-mixing in twin screw extruder	2 wt%	$\left|\eta^{*}\right|, \left|G^{*}\right|, G', G'', \tan \delta$, n(shear thining exponent) at temperature processing window (270 -290 ºC)	(Kim, Park et al. 2007)
MWCNT/LDPE	Melt-mixing in a mechanical mixer	4.8 wt%	$\left|\eta^{*}\right|, \eta$(steady shear viscosity) and $tan\delta$ at 125 ºC	(Xiao, Zhang et al. 2007)
MWCNT/PC	Diluting a masterbatch of 15 %wt NT (Melt- mixing in twin screw extruder)	2 wt%	G' and $\left|\eta^{*}\right|$ at 260 ºC and vs. temperature	(Satapathy, Weidisch et al. 2007)

Thermal properties, crystallinity and flammability

Incorporation of CNTs in a polymer matrix could increase the glass transition, melting and thermal decomposition temperatures of the polymer matrix due to their effect on the polymer segments and chains. As it was mentioned in the rheological properties section, increasing of the effective glass transition temperature (T_g) is usually observed in the CNTs/polymer composites. With 1wt% well-dispersed SWCNTs in PMMA, T_g is increased by ~ 40 ° C (Xie, Mai et al. 2005). Similarly, Fisher et al. (Fisher, Eitan et al. 2004) observed a slight increase in T_g of PC by adding 2 wt% of MWCNT.

Understanding the effect of carbon nanotubes on crystallization of semi-crystalline polymers is also of great importance because of the large impact of the crystalline structure on almost all the physical and mechanical properties. CNTs act as nucleation sites in the matrix, which enhance polymer crystallization and increase melting temperature. Zhifei et al. (Li, Luo et al. 2006) found that incorporation of CNTs in PET increases the initial and average crystallization temperatures of molten polymer composite and accelerates crystallization. Anand and his colleagues (Anand, Agarwal et al. 2006) showed that SWCNT has the same effect on PET. Similarly, in PET/MWCNT nanocomposites prepared through melt compounding in a twin-screw extruder, MWCNTs acted as good nucleating agents and enhanced the crystallization of PET through heterogeneous nucleation (Kim, Park et al. 2007). Interestingly, even in the amorphous polymers, like polycarbonate, addition of MWCNT results in a partially crystalline structure in MWCNT/ PC composites after annealing the samples at 190 ^{o}C for 8h (Sung, Kum et al. 2005).

The amount of increase in the thermal conductivity is obtained by the atomic vibration. The CNTs show excellent potential for thermal conductivity improvement, and the same trend is expected for the CNT/polymer nanocomposites. However, the results achieved by employing CNTs in thermal conductivity improvement do not fulfill the expectations since the phonons entering the nanotube/polymer system move through the matrix rather than the electrons. The low amount of thermal transfer in polymer nanocomposites comes from the high thermal resistance to heat transfer between the nanotubes in the matrix due to the inherent structure of CNTs. The introduction of covalent bonds between the nanotubes results in a reduction in the amount of high thermal interfacial resistance of the nanotubes and the thermal conductivity development of nanocomposite (Moniruzzaman and Winey 2006). There are some works in the area of CNTs application for thermal properties modification; however, no considerable results have been obtained in this matter compared to the use of CNTs for electrical properties improvements. Surprisingly, there is no significant percolation threshold in thermal transport measurement (Shenogina, Shenogin et al. 2005). Similar to other properties, thermal conductivity of these composites is affected by nanotube characteristics such as aspect ratio, dispersion and alignment (Xie, Mai et al. 2005; Moniruzzaman and Winey 2006). Thermal conductivity also strongly depends on the temperature. Increasing the temperature results in higher level of thermal

conductivity in CNT/polymer composites as it is found by Kim et al. (Kim, Kim et al. 2006) in MWCNT/PP composites.

CNTs also increase the thermal stability of polymer nanocomposites. Particularly the onset decomposition temperature and the temperature of maximum weight loss are increased in thermogravimetric analysis (TGA) (Moniruzzaman and Winey 2006). It was found that the incorporation of a small quantity of MWCNTs improved the thermal stability of the PET/MWCNT nanocomposites (Kim, Park et al. 2007). This improvement hints that carbon nanotubes could be efficient as fire-retardant additives in polymer composites which can introduce new application of CNT-polymer composites in a wide range of applications including aircraft, building/construction, public transport, and electrical/electronics equipment. For example, MWCNTs have significant effect in increasing the thermal stability and reducing the heat release rate in polypropylene composites (Kashiwagi, Grulke et al. 2002). As flame-retardant materials, these nanocomposites are found to be at least as effective as clay/polypropylene nanocomposites.

Microstructure and morphology

The major challenge in research on nanocomposites can be categorized in terms of structures from nano to micro to macro levels. In fact, there is still considerable uncertainty in theoretical modeling and experimental characterization of the nano-scale reinforcement materials, particularly nanotubes. In this regard, morphological characteristic is of fundamental importance in understanding the structure-property relationship of nanocomposites. Consequently, in order to determine the factors that contribute to, or inhibit nanocomposite efficiency, aid in the synthesis and design of the next generation of nanocomposites and to optimize nanocomposite processes, it is important to develop techniques, methodologies and tools to characterize nanostructure and morphology of the nanocomposites.

In carbon nanotube composites, transition of the nano-physical properties to macro scale composites is the most important issue, which is directly dependant on the quality of dispersion. Therefore, investigating the microstructure and the morphological properties of CNTs composites is commonly the starting point of all studies in this field. There are numerous amounts of techniques to characterize the level of dispersion each with different scale of characterization.

Microscopy techniques are the most widely used methods to demonstrate qualitatively nanotube dispersion and investigate nanocomposite morphology. However, combination of the

various microscopy techniques generally provides the best insight into the morphology of CNT/polymer composites. Resolution and contrast are the key parameters in microscopy studies. The increased use of optical microscopy, scanning electron microscopy (SEM) and transmission electron microscopy (TEM) in polymer research has been the result of widespread acceptance of the techniques and larger demands placed on the properties of these composites (Ajayan, Schadler et al. 2000; Meincke, Kaempfer et al. 2004; Potschke, Bhattacharyya et al. 2004; Coleman, Khan et al. 2006). Optical microscopy is sufficient to characterize dispersion on a >1 mm scale, "Optically Dispersed". Scanning electron microscopy (SEM) is able to map the electric field in CNT composites to assess dispersion from few mm down to tens of nm. Using SEM, the quality of dispersion and homogeneity can be observed in the length scale of micrometer range. Transmission electron microscopy (TEM) can directly visualize single tubes, bundles and catalyst particles. Therefore, in order to assess the bundle size, presence of agglomerates, local concentration gradients and to fully characterize dispersion, TEM is generally employed. Combination of SEM and TEM can also provide a general view of the orientation of nanotubes in the system (Dondero and Gorga 2006). Atomic force microscopy (AFM) is another important microscopy technique, employed to determine the length of nanotube in polymeric matrix and to characterize the deformation mechanisms of composite as well as failure mechanisms of nanotubes. AFM is also a suitable method to investigate the surface properties of nanocomposites (Barber, Cohen et al. 2004; Lin 2006)

Spectroscopy techniques are alternative methods of characterization to evaluate nanotube dispersion quantitatively. Raman spectroscopy (Ajayan, Schadler et al. 2000; Du, Scogna et al. 2004; Kuan, Ma et al. 2005; Eitan, Fisher et al. 2006) and Fourier transform infrared spectroscopy (FTIR) (Kuan, Ma et al. 2005; Moniruzzaman, Du et al. 2006) are suitable techniques to investigate nanotube/matrix interactions and to determine the load transfer between CNT and polymer matrix as well as the structural properties of individual nanotubes. Particularly when using functionalization, these techniques are preferred methods to characterize the side groups created on the CNTs (Du, Scogna et al. 2004).

Crystalline structure and orientation are other issues of interests in the field of CNTs/polymer composites. X-ray diffraction (XRD) and differential scanning calorimetry (DSC) are the most important techniques for this aim. The former is used to quantitatively study crystal morphology and orientation; while the later can qualitatively reveal the changes in overall

crystallinity (Leelapornpisit, Ton-That et al. 2005; Dondero and Gorga 2006). Wide angle X-ray scattering (WAXS) experiments provide opportunity to simultaneously analyze the crystalline structure, the extent of the crystallization, as well as the crystalline orientation (Konishi and Cakmak 2005; Anand, Agarwal et al. 2006; Phang, Ma et al. 2006; Zeng, Gao et al. 2006), while small angle X-ray scattering (SAXS) is a suitable method to characterize alignment of nanotube in the system (Du, Fischer et al. 2003; Du, Scogna et al. 2004; Fangming, Fischer et al. 2005). In differential scanning calorimetry (DSC) experiments, the recorded thermograms are used to determine the onset melting temperature, peak melting temperature and enthalpy of melting (ΔH); the shape of the curves are evaluated qualitatively to determine changes in crystal structure; finally the overall percentage of increase in crystallinity is calculated by dividing the enthalpy of melting for the sample by the enthalpy of melting of pure matrix (Dondero and Gorga 2006).

2.3.3. CNTs/polymer composites in processing

It is well known that the microstructure of plastic parts is the result of complex changes imposed to the base polymer by the special processing conditions. Typical thermoplastic processing involves pellet melting, plastication, melt flow and pressurization and finally solidification from the molten state, either by crystallization or vitrification. (Garcia-Gutierrez, Nogales et al. 2006). The complex thermo-mechanical history imposed on the polymer during processing leads to substantial spatial variations of chain orientation under shear and elongational flows and to the formation of a superstructure controlled by the local dynamics of the process. These effects result in a large anisotropy of the final physical properties particularly if the polymer is filled with solid particles of various shapes (glass or carbon fibers, clay or mica platelets, and carbon nanotubes or nanofibrils, etc.) (Konishi and Cakmak 2005). Use of carbon nanotube based nanocomposites for commercial applications, thus, needs an understanding of how the processing conditions influence the nanotube networks and subsequently the nanocomposites properties.

It was reported that both electrical conductivity and viscosity of polypropylene/MWCNT nanocomposites decreased strongly with shear rate, and these nanocomposites exhibited large and negative normal stress (Kharchenko, Douglas et al. 2004). Andrews et al.(Rich, Collins 2002) showed that an increase of mixing energy, achieved by increased mixing time (up to 25 min) at a given screw speed, enhances dispersion (as characterized by light microscopy). At the same time, they found a reduction of the MWCNT length up to 25%. Potschke et al. (Potschke,

Bhattacharyya et al. 2004) found that in the MWCNT/polycarbonate composites prepared by dilution a masterbatch of PC with 15 wt% MWCNT using melt mixing method in a DACA-Micro Compounder, increasing the mixing time and screw speed below the percolation concentration (between 0.5 and 1 wt% of MWCNT) reduces electrical resistivity. Their results showed that appropriate mixing conditions (in this case enhanced mixing time) could transform the system from a non-percolated structure into a percolated one. The effect of mixing time can be explained by the time necessary for diffusion of the polymer chains between the nanotube aggregates of the masterbatch. Finally, they concluded that better dispersion by an increase in mixing time and use of higher screw speed prevails over the reduction of nanotube length. A reduction of nanotube length is expected to shift the percolation threshold to higher compositions, since the aspect ratio of MWCNT is decreased.

Considering the flow field effect, polymer-nanocomposites have been studied by assessing Raman spectra obtained from embedded SWCNTs subjected to strain and pressure (Garcia-Gutierrez, Nogales et al. 2006). It is demonstrated that flow fields similar to those used in industrial processing, have a strong impact on the bundle structure of SWCNT within polymer nanocomposites and on the structure of the polymer matrix.

Similarly, the effect of pressure on the structural distortion of SWCNT bundles has been revealed by X-ray scattering and modeling has been reported (Garcia-Gutierrez, Nogales et al. 2006). However, in spite of the crucial influence of processing induced flow fields on the microstructure and properties of CNT / polymer composites, this effect remains almost untreated until now.

2.4. Microfabrication of polymeric materials

2.4.1. Microtechnology

Since the 1980s, microsystem technology has been progressing rapidly and it is predicted to become one of the main technologies of the 21st century (Zhao, Mayes et al. 2003). Consequently, miniaturization of components and producing functional devices in even-smaller length scales have gained considerable attention in recent years, due to the exceptional development of the microsystems technology. Miniature devices such as fiber-optic connectors, fuel cells, micro-optics, gears and transmissions, mechanisms and biomedical devices, sensors

and Micro-Electro-Mechanical Systems (µMEMS), have been applied widely in the microelectronics, optoelectronics, biotechnology and microchemical systems.

2.4.2. Microinjection molding process

Microinjection molding is a relatively new microfabrication process with a great potential of mass production of microdevices using materials such as polymers and their composites as well as ceramic and metallic powder (polymer based) feedstocks.

Kukla et al. (Kukla, Loibl et al. 1998) defined microinjection molded parts as (1) parts with a weight grams down to milligrams, (2) parts with microstructured regions, and (3) parts with microprecision dimensions. The first category of parts have with masses of a few milligrams, but their dimensions are not necessarily on the micron scale. Parts of the second category are characterized by local micro features on the micron order, such as microholes and slots. The third category includes parts of any dimension that have tolerances in the micron range.

 Microinjection molding process is fundamentally similar to the conventional injection one. The mold cavity equipped with a microstructured mold insert is first injected with heated materials, for example polymer melts heated above the melt temperature (T_m). To compensate subsequent melt shrinkage, the injection is followed by a packing step (additional melt squeeze). Finally, the part is cooled down below its glass transition temperature, T_g and ejected from the mold.

As in the case of the conventional injection molding, in the microinjection molding product properties are strongly affected by process parameters. However, because of the exceptional features of microinjection molding, these parameters and even their effects are not necessarily the same.

In the conventional injection molding, process parameters that affect the quality of injection molding products include cooling time and rate, injection pressure, injection speed, injection time, filling time, melt temperature, ejection pressure, mold temperature, mold geometry shape and material properties of the melt. Nevertheless, in the case of microinjection molding the conditions are somehow more drastic. Because of the process scale, microinjection molding features extreme injection pressures, shear rates and cooling rates as well as very short cycle times. These exceptional conditions combined with a large surface area to volume ratio may have a much greater influence over the resultant properties of micromolded parts. In addition, as

dimensions are in the order of microns, surface effects are expected to play a major role on flow behavior during injection, which occurs at very high deformation rates.

A great deal of studies has been conducted to investigate the effect of processing conditions on microinjected parts. In a more recent study Sha et al. (Sha, Dimov et al. 2006) found that the effective process factors are dependent on the materials, for example their study revealed that the barrel temperature and the injection speed are the key factors affecting the aspect ratios of micro features replicated in PP and ABS. In the case of POM, in addition to these two factors, the mould temperature is also an important factor to improve the replication capabilities of the microinjection molding process. All the parameters considered so far as the effective microinjection parameters are summarized in Table 2.8.

Table 2.6. Different influential parameters of microinjection molding process

Parameters	Reference
Metering size Holding pressure time	(Zhao, Mayes et al. 2003)
Injection time Mold temperature, injection Temperature injection Pressure	(Shen, Chien et al. 2004)
Injection pressure Mold temperature Injection velocity	(Su, Shah et al. 2004)
Melt temperature Mold temperature Injection speed Packing pressure	(Wu and Liang 2005; Chien 2006)
Mold temperature Packing pressure	(Chen, Chang et al. 2005)
Effective process factors are dependent on the materials	(Sha, Dimov et al. 2006)

In the microinjection molding process, because of the small size of the products, it is very difficult to see them clearly without the aid of microscopic techniques. Therefore, the conventional testing methods cannot be applied to such small geometries and so product property measurement would be one of the main challenges associated with this process.

Various experimental and simulation studies have been reported about microinjection molding process. For instant, Whiteside et al. (Whiteside, Martyn et al. 2004) studied the effects

of micromolding processing conditions on component surface topography, morphology and mechanical properties. The microstructure was evaluated using scanning electron microscopy (SEM), atomic force microscopy (AFM) and nano-indentation techniques. Zhao (Zhao, Mayes et al. 2003) used the design of experiments (DOE) technique to evaluate weight and tip diameter of a miniature gear, as quality indexes of injection molded components for a 1 mm diameter microgear. There are also similar studies in this field with the aim of finding the effect of process conditions on different characteristics such as achievable aspect ratio of micro and sub-micron structures (Sha, Dimov et al. 2006; Liou and Chen 2006), replication accuracy (Chien 2006), weld-line strength (Wu and Liang 2005), etc.

A number of researchers carried out processing and simulation studies of the microinjection molding process and flow behavior of polymer melts in micro mold-cavity (Shen, Chien et al. 2004; Su, Shah et al. 2004; Yao and Kim 2004; Xu, Yu et al. 2005). However, generally, simulation predictions were not in good agreement with experimental results. This discrepancy may be attributed to the lack of constitutive models describing the features of fluid flow and heat transfer in confined flows at the micro-scale, including the roles of very high shear rates/stresses and rapid cooling rates in a confined geometry with a large surface area to volume ratio.

In fact, significant reports of the research in microinjection molding started only during this decade mostly considering the pure polymers. A number of pure polymers such as LCP (liquid crystal polymer), PC (polycarbonate), PS (polystyrene), PP (polypropylene), HDPE (high-density polyethylene), PMMA (polymethylmethacrylate), ABS (acrylonitril-butadiene-styrene) and POM (polyoxymethylene or acetal) have been successfully processed through micromolding (Zhao, Mayes et al. 2003; Su, Shah et al. 2004; Whiteside, Martyn et al. 2004; Wu and Liang 2005; Sha, Dimov et al. 2006; Chien 2006; Liou and Chen 2006; Yang 2006). However, in many applications, it is necessary to enhance one or several physical properties (strength, barrier properties, thermal stability, electrical conductivity, among others), as pure polymers cannot satisfy these requirements. Micro parts with enhanced properties can be produced with inclusion of suitable fillers in polymers. Reducing the cost is another aim of using fillers for commercial application. In this regards, polymer nanocomposites, polymer reinforced by nano sized particles (nanocaly, carbon nanotube, etc.), can be employed to fabricate high-valued products using microinjection molding. One main reason of using nanofillers in this process is that conventional fillers have dimensions comparable to those of the small cavities of the mold (Huang and Chiu

2005; Huang 2006). Only in few research investigations by Huang et al. (Huang, Chen et al. 2005; Huang and Chiu 2005; Huang 2006) polymer compounds containing fillers such as short glass fiber, glass particles and nanoceramic materials (SiO_2, TiO_2 and ZnO) have been studied in microinjection process.

Rheological measurement is another missing part of studies in this field. Although the rheological properties extensively affect the processing, structure and properties of microparts, there have been a few published studies on the rheological properties in relation to micromolding, especially in the case of polymer nanocomposites. In fact, in most simulation works, the viscosity data used was obtained by conventional techniques for macroscopic applications and scaled down to the sub-millimeter range. However, because of different conditions in microinjection molding compared to conventional molding, this scaling might be a serious cause of inaccuracy. It is expected that the increase of viscosity would not be a hindrance in micromolding of CNT-based nanocomposites because of the high shear rate encountered. Such high shear rates can result in the alignment of the CNTs within the matrix, which will further have an effect on the rheology during processing. In the final product, this will also result in enhancement of both the mechanical properties and the thermal and electrical conductivities.

2.5. Originality of the work

If considerable research has been conducted regarding the physical properties of carbon nanotube filled composites, including mechanical, electrical and rheological properties, only a few investigations have focused on the practical applications of nanocomposites in various industrial fields. In the microinjection molding process, especially in the case of nanocomposites, experimental progress has been slow, due to the difficulties in micromachining and the absence of a clear strategy for characterization of microstructure and its development. To our knowledge, there is no report in the literature considering the effect of high shear rates of polymer processing on the properties of the nanocomposites. The rheological properties of such systems in relation to the conditions featured in microinjection have not been studied so far. Finally, crystalline structure and orientation and the consequence effect of crystalline phase on the nanocomposite properties have not been reported for microinjected products. The knowledge and experience obtained in conventional injection molding may be applied to the understanding of orientation in microinjection molding parts. However, rapid cooling experienced by micromolded components

may restrict crystal growth and therefore cause the product to exhibit mechanical properties different from those normally listed by the resin manufacturer. Consequently, in order to understand the relationship between the nanocomposite rheology, microinjection conditions and resulting properties, it is essential to characterize the rheological properties and microstructure of composites as well as the dispersion and alignment of nanotubes in the parts. In addition, understanding of crystallization phenomena is of great importance because of considerable impact of the crystalline structure on most physical and mechanical properties of semi-crystalline polymers.

2.6. Objective

The main objective of this project is "*to improve the properties of MWCNT/polymer composite based microinjected parts*"; investigation of the influence of high shear conditions on the properties of MWCNT/polymer nanocomposites will guide this work, with a special focus on the rheological properties, electrical conductivity and structural changes in the nanotube networks.

The sub-objectives of the current work can be summarized as follows:

➢ To investigate the effect of nanotube loading, nanotube alignment and temperature on the rheological behavior of the nanocomposites.

➢ To discover the influence of high shear conditions on the properties of the nanocomposites with a special focus on the electrical conductivity and structural changes in the nanotube networks.

➢ To explore the effect of crystalline structure on the shear induced properties of the nanocomposites.

➢ To investigate the effect of selective location of carbon nanotube and the double percolation phenomenon on the electrical conductivity of the nanocomposites.

Chapter 3

Materials, Processing and Characterization

3.1. Methodology

Taking into account the aim of this work, the adopted methodology is described in this part. Different tasks were carried out to achieve the mentioned objectives through this work as summarized in Figure 3.1.
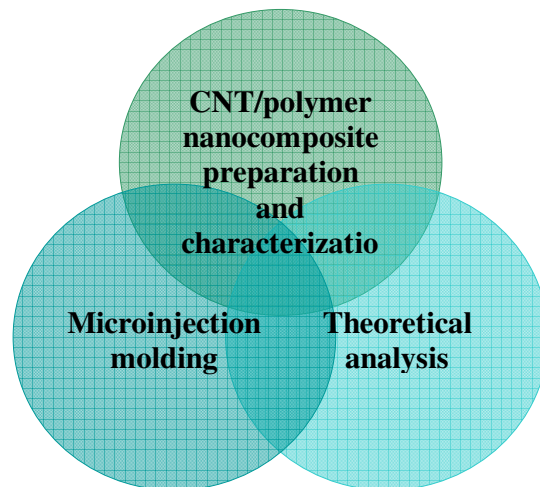
Figure 3.1: Project general scheme

The experiments were designed and carried out in two phases (Fig. 3.2):

♦ Initial material preparation (carbon nanotube/polymer composite preparation and characterization)

♦ Final processing (microinjection molding process and product characterization)

Our main target was to establish a relationship between these two phases to provide a whole image of polymer CNT nanocomposite behavior in the microinjection molding process.
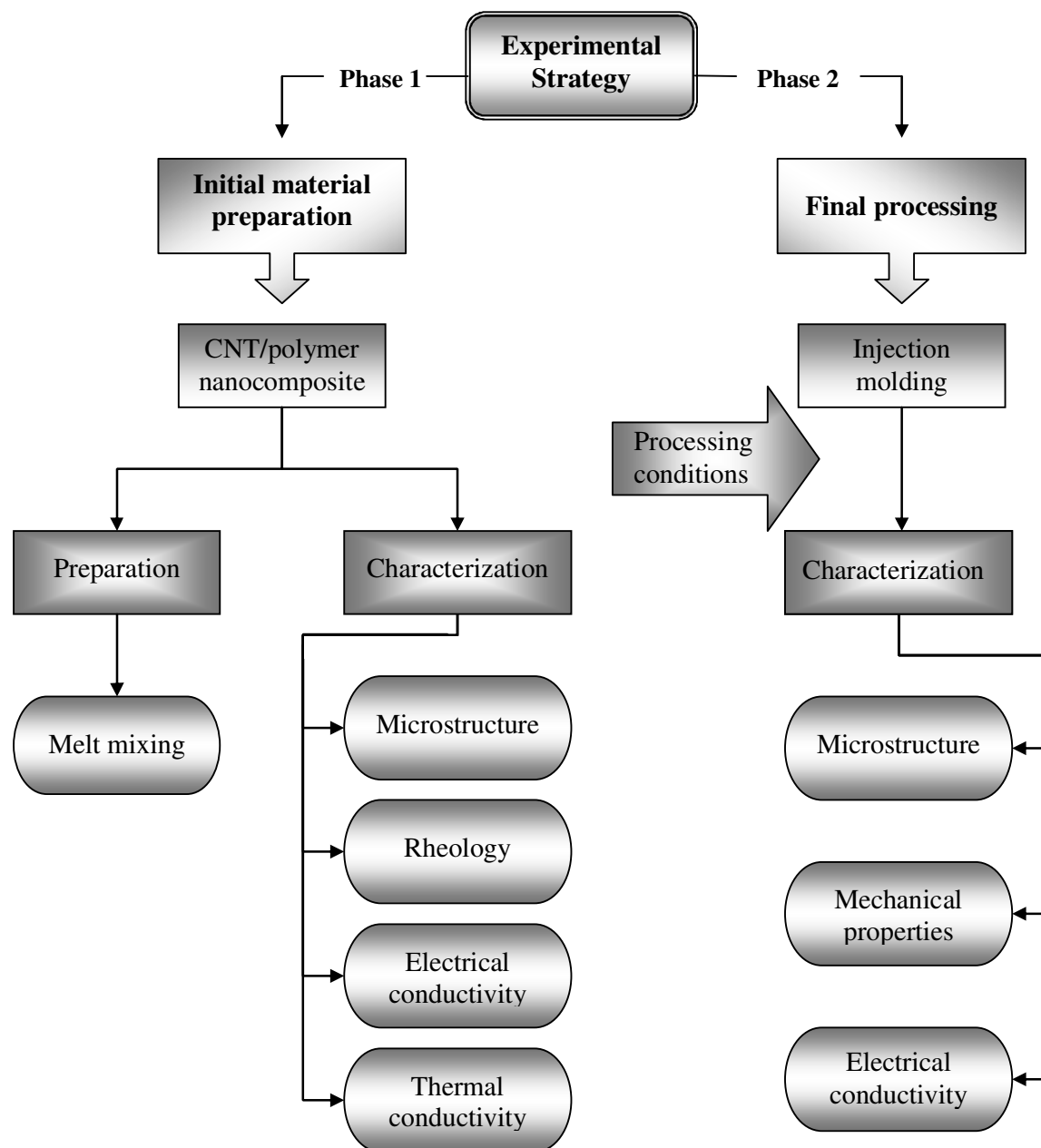
Figure 3.2: Experimental strategy

As-made nanotubes intertwine into agglomerates that are difficult to disperse; therefore in order to insure consistent and high quality performance as well as versatility and ease of handling, instead of mixing pure CNT with a given polymer we used premixed polymer/carbon nanotube masterbatches and diluted them to the required concentrations by adding the base polymer.

In light of the objectives of this work, the availability of commercially available masterbatches determined our choices of materials and methods. Regarding the materials, we exclusively focused on two kinds of polymer: polycarbonate (PC) as a polar amorphous polymer and isotactic polypropylene (iPP) as a non-polar semi-crystalline polymer. Furthermore, cyclic butylene terephthalate (CBT), a very low viscosity oligomer, was used in the final stage of this project to prepare MWCNT-filled PP/CBT blend.

In addition, melt-mixing was the preferred method in this project to prepare the CNT/polymer composites through dilution of masterbatches with the corresponding polymers. The prepared nanocomposites in phase 1 were then employed in phase 2 as initial feeding materials for the microinjection molding process.

In order to enhance our understanding of microinjection molding process and its effect on the nanocomposites structure and properties and to obtain optimized operating conditions, it is important to well define the system and evaluate the degree of achievement of final properties. Therefore, material characterization was one of the most important steps in both phases of the experimental strategy. It was essential for the following main reasons:

➢ To evaluate the properties and dispersion quality of CNTs/polymer nanocomposites prepared through dilution of the masterbatches.

➢ To recognize the most important parameters in microinjection and to optimize the microinjection conditions considering the effect of these parameters on target properties.

➢ Finally, to assess the effect of microinjection process on the structure and properties of CNT/polymer composite by comparing the results of the previous steps.

In the remaining sections of this part, the materials and experimental methods used in this work are described. In section 3.2 a brief description of the materials will be given. In section 3.3 the sample preparation and processing will be described. The characterization methods will be mentioned and described in section 3.4.

3.2. Materials

Masterbatches: Two kinds of masterbatch were used in this project: a masterbatch of 15wt% MWCNT in polycarbonate (PC/MWCNT) and a masterbatch of 20wt% MWCNT in polypropylene (PP/MWCNT). Masterbatches were supplied by Hyperion Catalysis International, Cambridge, MA. The carbon nanotubes are vapor grown with purity more than 90% and typically consist of 8-15 graphitic layers wrapped around a hollow 5 nm core. Typical diameters range from 10 to 15 nm while lengths are between 1 and 10 µm (Potschke, Fornes et al. 2002).

Polycarbonate (PC): Polycarbonate, a clear amorphous polymer, is the most popular polymer material for microfabrication via injection molding due to its special properties in both application and processing. In addition, it is a widely used material in CNT/polymer composite industry since its special mechanical properties offer a good opportunity to produce multi functional nanocomposites. Therefore, polycarbonate was the main point of our attention.

In this project, PC Calibre1080 (injection grade), supplied by Dow Chemical, was used for the dilution of the masterbach. PC has a density of 1200 kg/m^3 according to ASTM D792, with a melt flow rate of 11 g/10min at 250 ^{o}C and a water absorption of 0.20% after 24 h at 23 ^{o}C according to ASTM D570. Therefore, it was necessary to dry this material for a minimum of 3-4 h at 120 $^\circ$C. The suggested maximum allowable moisture for PC grade is 0.0100 %.

Polypropylene (PP), a very easily working semi-crystalline polymer, was selected to investigate the effect of crystallinity on nanotube distribution and how this would affect the final properties investigated.

In this work, the high crystallinity isotactic polypropylene (iPP HD120) used was supplied by Borealis Co. This PP grade has a density of 908 kg/m^3 according to ASTM D792, with a melt flow rate of 8 g/10min at 230 ^{o}C.

PP-g-MA: Polypropylene grafted maleic anhydride (PP-g-MA Polybond PB3150 with 0.5 wt% MA and with a melt flow rate of 20 g/10min at 190 ^{o}C) was used as a compatibilizer in an attempt to improve nanotubes dispersion in PP/MWCNT nanocomposites. Various kinds of PP-g-MA with broad range of MA content and molecular weight were previously used in the preliminary steps to find the most efficient one in the dispersion modification.

CBT (cyclic butylene terephthalate): CBT is an oligomer of poly butylene terephthalate (PBT) and was used in this study to try to improve the electrical conductivity of the nanocomposite through formation of iPP/CBT blend. CBT was supplied by Cyclics Co.

3.3. Sample preparation and processing

Phase I: CNT/ polymer nanocomposites preparation

The composites were produced by melt mixing the masterbatches with the neat polymers. Polycarbonate and PC/MWCNT masterbatch were dried for a minimum of 4h at 120°C prior to mixing. Polypropylene, PP/MWCNT and PP-g-MA were dried for 1hr at 90°C.

To prepare the samples for rheological measurements, six different composites of PC with MWCNT contents between 0.2 and 5 wt% MWCNT were prepared using a Brabender internal mixer. Different conditions were investigated and the final dispersion was checked to obtain the optimum condition for CNT dispersion. The best condition was obtained at 50 rpm during 16 min. To compare the nanotube dispersion at low and high temperature, samples were produced at two different temperatures, 210 $^{\circ}$C and 250 $^{\circ}$C.

To carry out the micromolding experiments nanocomposites of PC/MWCNT and PP/MWCNT were produced using a twin screw extruder. The materials were dried under the conditions previously described. Eight different composites with MWCNT contents between 0.5 and 15 wt% MWCNT were prepared using a lab-twin screw extruder, Leistritz ZSE 18HP (with 1.78 mm diameter and length of 40D). Different temperature profiles and rotation speeds were investigated and the final dispersion at each condition was checked to obtain the optimum condition for CNT dispersion.

For PC nanocomposites, the best condition for CNT dispersion was obtained at 100 rpm screw speed using a temperature profile along the extruder screw started from 205 $^{\circ}$C (first zone after hopper) to 215 $^{\circ}$C (Die). The twin-screw included 8 thermal zones starting from hopper and ending at the die. The temperature profile used was:

Zone 1 (Hopper): 205 $^{\circ}$C;   Zone 2: 205 $^{\circ}$C;   Zone 3: 210°C;   Zone 4: 210 $^{\circ}$C;   Zone 5: 210 $^{\circ}$C;   Zone 6: 215 $^{\circ}$C;   Zone 7: 215 $^{\circ}$C;   Zone 8 (Die): 215 $^{\circ}$C

For PP nanocomposites, a two step procedure was used to prepare the nanocomposites:

- **Step1**: The masterbatch of 20wt% MWCNT in polypropylene was diluted with PP-g-MA to prepare a new masterbatch of 15wt% MWCNT. The dilution was done using the twin screw extruder operating at 200 rpm with the following temperature profile:

  Zone 1: 205 ^{o}C;   Zone 2: 210 ^{o}C;   Zone 3: 220°C;   Zone 4: 230 ^{o}C;   Zone 5: 240 ^{o}C; Zone 6: 250 ^{o}C;   Zone 7: 250 ^{o}C;   Zone 8 : 235 ^{o}C

- **Step2**: The prepared masterbatch of step 1 was then diluted to the desired MWCNT contents by mixing with neat PP in the twin screw extruder. Mixing was done at 250 rpm while the temperature profile was set as follows:

  Zone 1: 180 ^{o}C;   Zone 2: 185 ^{o}C;   Zone 3: 190°C;   Zone 4: 190 ^{o}C;   Zone 5: 195 ^{o}C; Zone 6: 205 ^{o}C;   Zone 7: 200 ^{o}C;   Zone 8 : 195 ^{o}C

Finally, ternary nanocomposites of PP/CBT/MWCNT were produced by diluting the PP/MWCNT masterbatch with proper amount of PP and CBT. Thirty six composites with six different CBT contents between 0 and 40wt% and six nanotube loadings between 0.2-5 wt% were prepared using the same twin screw operating at 250 rpm and the following temperature profile:

Zone 1 : 185 ^{o}C;   Zone 2: 185 ^{o}C;   Zone 3: 170 ^{o}C;   Zone 4: 170 ^{o}C;   Zone 5: 160 ^{o}C;   Zone 6: 150 ^{o}C;   Zone 7: 185 ^{o}C;   Zone 8 : 185 ^{o}C

These conditions were used to minimize residence time to avoid CBT polymerization which occurs ideally at 185°C. Separate rheological measurements at 185°C showed that polymerization time of CBT into PBT is about 300s.

Phase II: Molding processes

Compression molding, conventional injection molding, microinjection molding and microinjection-compression molding were employed in this project to produce final parts under different levels of shear or deformation rate. Prior to each processing, the materials were dried under the conditions previously mentioned.

Compression molding of dried nanocomposites were done using a Carver laboratory press, model 3912, operated manually at 270 ^{o}C and 230 ^{o}C for PC and PP nanocomposites respectively. The disk shaped molded samples of 60mm diameter and 1.5 mm thickness were then cooled down to room temperature.

For the conventional injection molding we used a Sumitomo SE50S electrical 50 ton injection molding machine to mold standard dog-bone shaped tensile test specimens of 150 mm in total length, with a gage section 10 mm wide by 4 mm thick by 80 mm long. Only PC/MWCNT nanocomposites were processed in conventional injection molding. Injection was done at an average barrel temperature of 300 $^{\circ}$C under a pressure of approximately 100 MPa while injection speed was constant at 400 mm/s. The mold temperature was kept constant at 80 $^{\circ}$C and cooling time was set to 10 s.

Microinjection molding was done using a Battenfeld Microsystem 50 micromolding machine (Fig.3.3).
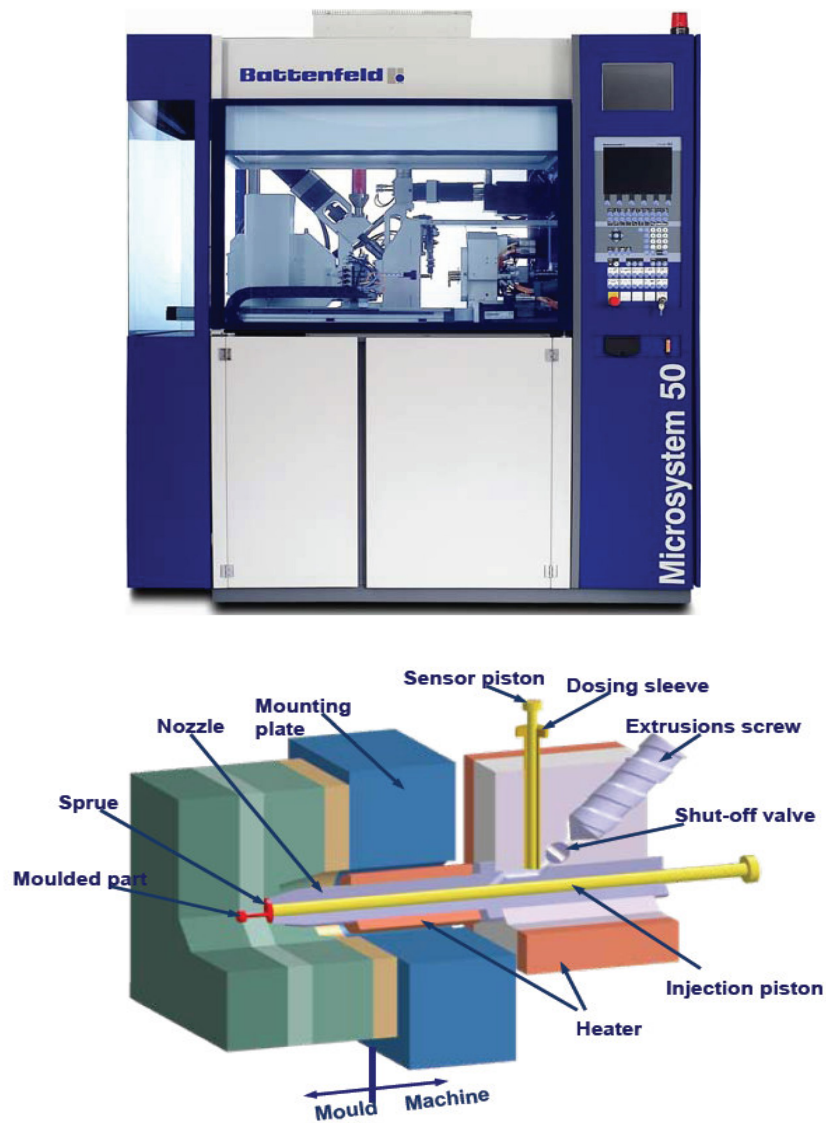
Figure 3.3: Battenfeld microsystem 50 injection machine

In the case of PC/MWCNT nanocomposites, microinjection was done at the same processing conditions as the conventional one. For PP/MWCNT nanocomposites, an average barrel temperature of 260°C, a constant injection speed of 400 mm/s and a holding pressure of approximately 100 MPa were used. In crystalline material, shrinkage is often observed in the final parts. To reduce the shrinkage percentage the mold temperature was optimized and was kept constant at 20 ^{o}C while the cooling time was set to 10 s. To investigate the effect of mold geometry, two different mold cavities were used: one having a dog-bone shape of 15 mm long, with the gage section of 1 mm wide by 0.78 mm thick by 4.3 mm long, gated at one end, and the other a disk shape of 25 mm in diameter and 1mm thick, gated at the centre. To examine the effect of the injection speed two additional injection speeds were also used in the case of the dog-bone samples: 200 and 800 mm/s.

Finally, microinjection-compression molding was employed to evaluate the effect of applying a compression step at the end of the injection phase on the part properties, using the centrally gated disk cavity with the same dimensions as described before. The process consisted of injecting the melt into the cavity, while the mold was not totally closed. This leads to an initial cavity filling under a lower pressure than if the mold was closed, as in conventional injection molding. After the injection stage, the mold was closed to compress the melt and to completely fill the cavity. The operating conditions in this case are the same as microinjection molding using only 400 mm/s for the injection speed. The closing gap between the mold plates was about 1.2 mm and the mold closing speed used in this experiment was 1.5 mm/s.

3.4. Characterization

Characterization before and after microinjection is one of the main important concerns of this work. Different characterization methods, their applications and purposes are given in the following table. The parameters and procedures of each of these experiments are given in the following chapters, including the results related to each of the associated tests.

Table 3.1. Characterization methods and their application in this study

Method	Application
SEM (Scanning Electron Microscopy)	• Morphological analysis • CNT dispersion and distribution analysis • Aggregates formation and localization • CNT alignment analysis • Blend morphology analysis and CNT localization in the blend
AFM (Atomic Force Microscopy)	• Morphological analysis • CNT dispersion and distribution analysis • CNT alignment analysis • CNT dimensions analysis
TEM (Transmission Electron Microscopy)	• Morphological analysis • CNT dispersion analysis • CNT alignment analysis • CNT dimensions analysis
Rheological measurements	• Microstructure analysis • Nanotube networks behavior analysis (dependency on the temperature & steady shear rate) • Nanotube alignments study • Correlation between rheology and microparts properties • Investigation the shear rate dependency of the viscosity
Raman spectroscopy	• Nanotube structure & alignments analysis
DSC &XRD	• Crystallinity measurements and orientation detection
FTIR	• Polymer chains and crystalline phase orientation
Conductivity measurements	• Electrical conductivity analysis • Thermal conductivity analysis
Mechanical properties measurements	• Stress-strain behavior analysis

Chapter 4

Organization of Articles and Thesis Structure

The main achievements of this thesis will be given in chapters 5 to 8. Each of these chapters includes the main findings in a scientific journal paper format. The organization of these chapters is as follows:

- *Chapter 5* explains the rheological behavior of PC/MWCNT nanocomposites. In this chapter percolated structure of nanotubes is studied via a set of rheological, electrical and thermal conductivity measurements. The dependency of percolation threshold on the temperature and steady shear deformation is explored in detail. This paper was published at journal "Rhelogica Acta" (Abbasi, Carreau, Derdouri, et al. 2009).

- *Chapter 6* covers the results of processing of PC/MWCNT at different processing conditions used to systematically change the degree of nanotube alignment, from random orientation to highly aligned. Investigation of the effect of flow field and deformation rate on the nanotube alignment and on the properties of nanocomposites is thoroughly given in this chapter. This paper was submitted to the journal "Polymer".

- *Chapter 7* studies the final properties of microinjected nanocomposites of PC/MWCNT and PP/MWCNT prepared at various conditions. Effects of the crystalline structure and polymer processing conditions on the morphology and properties of nanocomposites are analyzed in this paper. This paper was submitted to the journal "Polymer Engineering and Science".

- *Chapter 8* investigates and compares the electrical conductivity and percolation behavior of binary composites of PP/MWCNT and PC/MWCNT and ternary composites of PP/CBT/MWCNT. The effects of nanotube incorporation and the presence of crystalline phase on the properties of the nanocomposites in high shear conditions are covered in details. The double percolation concept, the main focus in this study, was used to improve the electrical conductivity. This chapter is in preparation as a paper to be submitted to the journal "Polymer".

Chapter 9 is a general discussion and it covers a summary and comparison of the results obtained in this study. Finally, a brief conclusion of this thesis and the recommendations for future works will be given in chapter 10.

Chapter 5

Rheological Properties and Percolation in Suspensions of Multiwalled Carbon Nanotubes in Polycarbonate[*]

5.1.   Presentation of the article

The objective of the first paper was to examine the rheological behavior of polycarbonate (PC)/ MWCNT nanocomposites in light of interactions between CNTs and polymer chains or between CNTs themselves. We used PC as an amorphous polymer to make a good dispersion of nanotubes and to avoid complexities arisen from crystalline structure. Moreover, since these nanocomposites were further used as the feeding materials of micromolding, in this work we intended to discover the effect of conditions featured in the microinjection molding on the rheological properties and microstructure of the nanocomposites. More specifically, the investigation of the effect of nanotube loading, nanotube alignment and temperature on the rheological behavior of the nanocomposites was the main objective of this study. The results revealed that the nanotube networks were strongly temperature dependent; the percolation threshold was significantly lower at higher temperature suggesting stronger nanotube interactions. The structure was also sensitive to the steady shear deformation particularly at high temperature. These results were analyzed using simple models for suspensions of rod-like particles. The relationship between the rheological properties and the microstructure is also discussed in light of electrical and thermal conductivity of the nanocomposites.

Rheological Properties and Percolation in Suspensions of Multiwalled Carbon Nanotubes in Polycarbonate

Samaneh Abbasi [1], *Pierre J. Carreau* [1], *Abdessalem Derdouri* [2], *Michel Moan* [3]

1) CREPEC, Department of Chemical Engineering, Ecole Polytechnique Montreal, P.O.Box 6079, Station Centre-Ville Montreal QC, Canada

2) CREPEC, Industrial Materials Institute, National Research Council Canada, 75 de Mortagne, Boucherville, QC, Canada

3) Université de Bretagne Occidentale, 3 rue des Archives-CS 93837-F29238 Brest cedex3, France

5.2.   Abstract

This paper is concerned with several issues related to the rheological behavior of polycarbonate/ multiwalled carbon nanotube nanocomposites. The composites were prepared by diluting a masterbatch of 15 wt.% nanotubes using melt-mixing method, and the dispersion was analyzed by SEM, TEM, and AFM techniques. To understand the percolated structure, the nanocomposites were characterized via a set of rheological, electrical, and thermal conductivity measurements. The rheological measurements revealed that the structure and properties were temperature dependent; the percolation threshold was significantly lower at higher temperature suggesting stronger nanotube interactions. The nanotube networks were also sensitive to the steady shear deformation particularly at high temperature. Following preshearing, the elastic modulus decreased markedly suggesting that the nanotubes became more rigid. These results were analyzed using simple models for suspensions of rod-like particles. Finally, the rheological, electrical, and thermal conductivity percolation thresholds were compared. As expected, the rheological threshold was smaller than the thermal and electrical threshold.

Keywords: Multiwalled carbon nanotube**,** Polycarbonate, Suspension**,** Rheological percolation, Electrical percolation**,** Thermal conductivity percolation, Filled polymer**,** Storage modulus

5.3. Introduction

During the progressive advances in nonoscience and nanotechnology of the last two decades, many scientists have developed a strong interest in the unique properties of novel solid state nanomaterials, called carbon nanotubes (CNT). Since their discovery in 1991 by Iijima (Iijima, 1991, Iijima and Ichihashi 1993) CNTs became attractive candidates for fundamental investigations and an extensive research effort has been devoted to their fabrication, characterization and development of applications due to their unique electronic structure and extraordinary properties (Meyyappan 2005). Their intrinsic structure, size scale and aspect ratio suggest a variety of applications such as nanoelectronics, sensors and field emission as well as high performance nanocomposites. They exist as single wall nanotubes (SWNT) or multi wall nanotubes (MWNT). A SWNT is made by wrapping a graphene layer into a cylinder. Each tube is represented by its chiral vector, C_h, which is a pair of indices (n,m) with values depending on the way the graphene sheet is wrapped (Meyyappan 2005). Carbon nanotubes have been recognized among the strongest known materials. For instance measured values of tensile strength were found to be as high as 63 GPa for a MWCNT (Yu et al. 2000) and extremely high elastic modulus, on the order of 1 TPa, have been proven by both simulation and experimental measurements (Salvetat et al. 1999; Yu et al. 2000). These reported strengths are 10 to 100 times higher than the strongest carbon steel with a tensile strength of approximately 1.2 GPa. Considering the low density of carbon nanotubes, which is in the range of 1.3-1.4 g/mL, their specific strength is the best of known materials. Although carbon nanotubes generally have exceptional properties, the wide ranges of their special applications are mainly related to their unique electrical properties. For a given nanotube, if its chiral vector is represented with $n = m$, the nanotube is metallic; the tube is semi-conducting if $n - m$ is a multiple of 3, otherwise it is a moderate semiconductor (Meyyappan 2005). Based on theoretical calculations, the electrical current density of an individual carbon nanotube can be more than several times greater than that of metals such as silver and copper (Breuer and Sundararaj 2004; Xie et al. 2005). CNTs also have excellent thermal conductivity in the range of 3000W/m.K for individual MWCNTs (Hone 2004).

Recently, considerable attention has been devoted to carbon nanotube / polymer composites owing to their extraordinary properties from both processing and application points of view. Besides the individual properties of carbon nanotubes, a number of potential benefits are

expected when they are employed as reinforcing agents in nanocomposites. However, the efficiency of nanotubes to live up to their theoretical potential depends on a good dispersion within the host polymer. At the moment, three methods are commonly used to incorporate nanotubes into a polymer: solution mixing and film casting of suspensions of nanotubes in dissolved polymers, in-situ polymerization of nanotube-polymer monomer mixture and mixing of nanotubes in molten polymers. Melt mixing is the industrially preferred method in many cases because of its environmentally benign character, its versatility and its compatibility with current polymer processing techniques.

Polycarbonate (PC), a typical amorphous polymer, is an important commercially available engineering thermoplastic for injection molding applications because of its excellent process ability and mechanical properties. Recently, carbon nanotubes have been used as special filler to be incorporated into PC for stiffness reinforcement as well as thermal and electrical conductivities enhancement purposes (Ding et al. 2003; Singh et al. 2003; Potschke et al. 2004; Pham et al. 2008).

The rheological properties of polymer nanocomposites including viscoelastic (time or frequency-and temperature–dependent) behavior are of practical importance in relation to processing and characterizing the composite microstructure. The rheological behavior depends on the material microstructure, the state of the nanotubes dispersion, the aspect ratio and orientation of the nanotubes, the interaction between nanotubes and polymer chains as well as nanotube-nanotube interactions. The temperature influences the rheological properties of the matrix, but it also can affect the state of dispersion of the nanocomposites via changes in the particle-particle interactions and in the wettability of the nanotubes with the matrix.

If considerable research has been conducted regarding the physical properties of nanocomposites, including mechanical properties and electrical conductivity, only a few investigations have focused on the rheological behavior of polymer/carbon nanotube nanocomposites. Most of the rheological studies have concentrated on the typical linear viscoelastic response and on the non terminal character at low frequencies, which is attributed to the formation of a filler network (Kharchenko et al. 2004; Meincke et al. 2004; Abdel-Goad and Potschke 2005; Xinfeng et al. 2005; Hu et al. 2006; Moniruzzaman and Winey 2006; Sung et al. 2006; Wu et al. 2007). To our knowledge this low frequency behavior was reported first by Potschke et al. in 2002. Since then, more attention has been paid to rheological properties of

CNTs/polymer nanocomposites with focus on the percolation threshold as one of the most important factors affecting the material properties or as a characterization parameter of the dispersion quality. Such a percolated system was studied using polyamide-6 /MWCNT nanocomposites (Meincke et al. 2004), polycarbonate/MWCNT composites (Abdel-Goad and Potschke 2005), polycarbonate /functionalized MWCNT nanocomposites (Sung et al. 2006), and poly (ethylene terephthalate) (PET)/ MWCNT (Hu et al. 2006). Finally, a few investigations on the modeling of the rheological behavior of carbon nanotubes suspended in low molecular weight polymeric resins have been recently carried out (Rahatekar et al. 2006; Fan and Advani 2007; Hong and Kim 2007; Ma et al. 2008).

The rheological behavior of nanocomposites strongly depends on the carbon nanotube alignment as well. For example, it was found that the storage modulus G' that describes the elastic response decreases with the alignment of nanotubes. When nanotubes are aligned in the polymer matrix the probability of tube-tube contacts decreases and the nanotube network is less effective at impeding the polymer motion (Du et al. 2004; Wu et al. 2007). It is also found that the percolated nanotube network is very sensitive to the temperature (Potschke et al. 2004; Wu et al. 2007).

In this work we examined the rheological behavior of polycarbonate (PC)/ MWCNT nanocomposites in light of interactions between CNTs and polymer chains or between CNTs themselves. This is a quite complex and difficult system to study since the typical behavior of polymeric systems almost vanishes in the presence of a nanotube network. For example, as soon as the nanotube network is formed the low frequency terminal zone observed for the neat polymer disappears. Furthermore, the high temperature behavior adds another complexity to this difficult system. Therefore, typical analysis methods used for conventional polymeric systems are not useful in this context and a more innovative investigation is required to establish the relationship between the rheological behavior and microstructure of such a system. More specifically, the investigation of the effect of nanotube loading, nanotube alignment and temperature on the rheological behavior of the nanocomposites was the main objective of this study. The nanocomposite preparation was optimized using various characterization methods. As nanotubes intertwine into agglomerates that are difficult to disperse we used premixed polymer/carbon nanotube masterbatches and diluted them to the required concentrations by adding the base polymer. This insured consistent and reproducible results. The relationship

between the rheological properties and the microstructure is also discussed in light of electrical and thermal conductivity of the nanocomposites.

5.4. Experimental

5.4.1. Materials

A masterbatch of 15 wt% MWCNT in PC was purchased from Hyperion Catalysis International, Cambridge, MA. According to the supplier, the carbon nanotubes are vapor grown and typically consist of 8-15 graphite layers wrapped around a hollow 5 nm core (Potschke et al. 2002). The diameter range was stated to vary from 15 to 50 nm and the length range between 1-10 μm as was confirmed by TEM characterization. The masterbatch was diluted with polycarbonate (Calibre 1080) supplied by Dow Chemical to prepare nanocomposite samples of various loadings. Its glass transition temperature (T_g) was determined by DSC measurements and found to be equal to about $145^{\circ}C$.

5.4.2. Nanocomposite preparation

The composites were produced by melt mixing the masterbatch with the neat PC. Prior to mixing, all materials were dried for a minimum of 4h at $120^{\circ}C$. Six different suspensions with MWCNT contents between 0.2 and 5 wt% MWCNT were prepared using a Brabender internal mixer at 50 rpm during 16 min and for two different temperatures, $210^{\circ}C$ and $250^{\circ}C$ (conditions previously optimized via controlled experiments).

5.4.3. Morphological characterization

The morphology of nanocomposites was studied at room temperature through scanning and transmission electron microscopy (SEM and TEM) and atomic force microscopy (AFM). For SEM we used the high resolution Hitachi S-4700 microscope while for AFM we utilized the multimode Veeco scanning probe in tapping mode. Both SEM and AFM were done on ultramicrotomed surfaces of samples that were cut with a diamond knife at room temperature. SEM samples were coated with a vapor deposit of Pt for 25s. TEM was done on ultrathin sections of nanocomposites using a Hitachi HD-2000 microscope.

5.4.4. Rheological measurements

All the rheological measurements were carried out using a stress-controlled rheometer (CSM rheometer of Bohlin Instruments) equipped with a 25mm parallel plate geometry under nitrogen atmosphere. Prior to measurements, the compression molded samples were dried for a minimum of 4h at 120°C. The viscoelastic properties of nanocomposites were investigated in a broad range of temperature from 210°C up to 300°C. Small amplitude oscillatory shear (SAOS) frequency sweep tests were carried out between 0.06 and 200 rad/s in the linear viscoelastic regime. This regime was established in the standard way by measuring the modulus at constant frequency (10 rad/s) and increasing strain magnitude. Further, long time measurements (up to 3h) were conducted to investigate the thermal stability of the nanocomposite samples. We assumed that the particle sizes were sufficiently small compared to the gap; however, the absence of apparent slip at the wall has been ascertained by varying the gap from 0.5 to 1.5 mm. The differences were found to be insignificant, less than the reproducibility of the data estimated to be within 3.5% for all the frequency sweep tests conducted with the various nanotube loadings.

In addition, the effect of high shear on the microstructure of the nanocomposites was evaluated by subjecting each sample to different levels of constant shear stress for various periods of time. SAOS measurements were then performed without any rest time between the preconditioning step and the frequency sweep test.

5.4.5. Electrical resistivity measurements

The volume resistivity of the PC/MWCNT nanocomposite samples was determined by measuring the DC resistance across the thickness of compression molded disks using a Keithley electrometer model 6517 equipped with a two probe test fixture. We used a specific kind of test fixture firmly connected to the probes. All the connections were made using short wires to assure that the resistivity of the whole set up was negligible. The resistivity of the set up was measured each time before the tests to make sure that the system was working properly. This equipment allows resistivity measurements up to 10^{17} Ω. The level of applied voltage, adapted to the expected resistivity, was in the range of 1000 V for neat PC and samples containing up to 1wt% MWCNT and 100 V for samples with 2wt% and more MWCNT content. However, since for the more conductive samples, the accuracy of this equipment failed, samples with more than 2wt% MWCNT, were tested using the more adequate Keithley electrometer model 6220 connected to a

current source (Aligent 34401 A , 6 ½ Digit Multimeter). For each sample the *I-V* curve was obtained and the sample resistance was determined from the slope of the curve. The resistance was then converted to volume resistivity, ρ_v, ohm.cm, using the formula

$$\rho_v = AR_v / D \tag{5-1}$$

where *A* is the contact surface area, *D* is the thickness of the sample, and R_v is the measured resistance. The electrical conductivity (σ) of the nanocomposites is the inverse of volume resistivity. Prior to measurements all samples were dried for a minimum of 4h at 120°C.

5.4.6. Thermal conductivity measurements

The thermal conductivity of the nanocomposite samples was determined using a Thermo electron, Thermo-Haake instrument (Thermo Fisher Scientific), by means of a *Transient Line-Source Technique* according to the ASTM D5930. A line source of heat, localized at the center of the molten specimen being tested, is at a thermal equilibrium with the specimen which is at a constant initial temperature. During the course of the measurement, a known amount of heat produced by the line-source results in a heat wave propagating radially into the specimen. The rate of heat propagation is related to the thermal diffusivity of the polymer. The temperature rise of the line source varies linearly with the logarithm of time. When the temperature rise is plotted against the logarithm of time, the slope of the linear portion of the curve can be used directly to calculate the thermal conductivity of the sample using the following equation:

$$k = \frac{CQ}{4\pi\,Slope} \tag{5-2}$$

where *C* is the probe constant, *Q* is the heat output per unit length, W/m, and *k* is the thermal conductivity, W/m.K. Prior to measurements all samples were dried for a minimum of 4h at 120°C.

5.5.   Results

5.5.1. Morphology

The morphology of melt-mixed nanocomposites was examined in terms of the nanotube dispersion and distribution. In this context, the dispersion refers to how well the nanotubes are disaggregated and separated in the form of single tubes at the nanoscale. On the other hand, the nanotubes are well distributed if single nanotubes or sets of nanotubes like bundles are uniformly dispersed within the whole matrix, even though nanotube aggregates might be observed. For these reasons, TEM was used to study the dispersion, while the distribution was investigated using SEM and AFM. Figure 5.1 shows schematics of a single tube (Fig. 5.1a), a nanotube bundle (Fig. 5.1b) and aggregates (Figs. 5.1c-e). A nanotube bundle consists of many single tubes sticking together; it can be viewed as an equivalent tube with a larger diameter having a smaller effective aspect ratio. It is worthwhile to mention that both single tubes and tube bundles can participate in the formation of a network or aggregates. Aggregates could be formed by single tubes (Fig. 5.1c), tube bundles (Fig. 5.1d), or both of them (Fig. 5.1e).

(a)   **(b)**

(c)   **(d)**   **(e)**
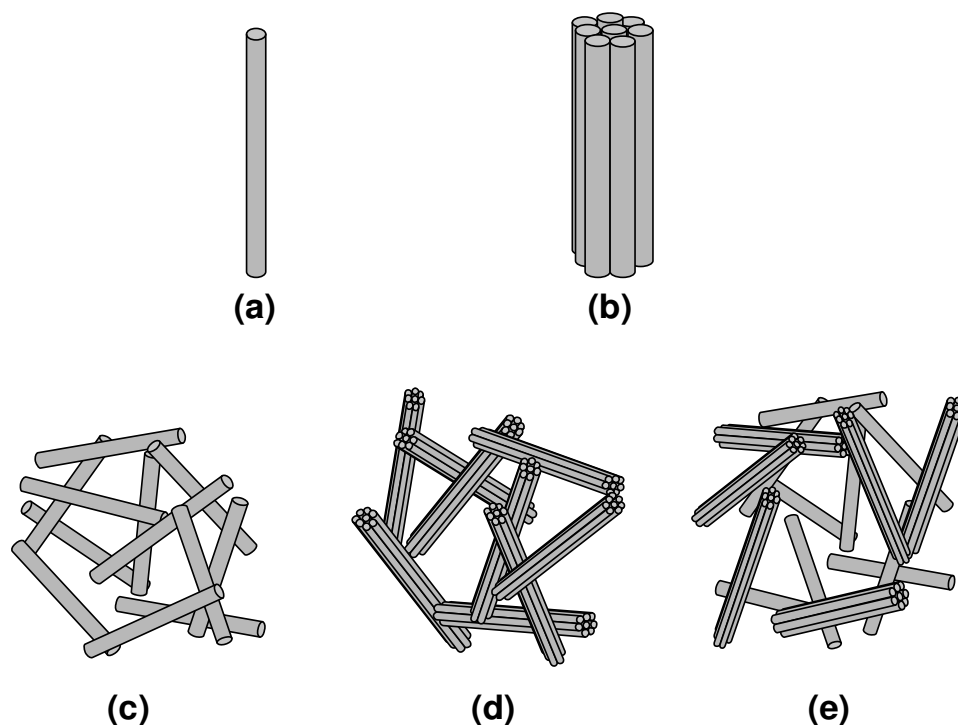
Figure 5.1: Schematic figure of (a) single tube, (b) nanotube bundle (c) aggregate of single tubes (d) aggregate of nanotube bundles (e) aggregate of single tube and nanotube bundles

Figure 5.2 shows SEM micrographs of melt-mixed nanocomposites prepared at 210°C and 250°C. It is observed that at 210°C the nanotubes are dispersed individually in the matrix (Fig. 5.2a) and the distribution at the micro level is quiet uniform. On the other hand, examination of the micrograph of samples prepared at 250°C (Fig. 5.2b) shows that the nanotube distribution at the micro level is not uniform. We observed for higher magnification that some bundles were pulled out from the matrix. These observations indicate that at 250°C some of the nanotube bundles (not single nanotubes) were individually distributed and the interactions between the nanotubes and the polymer matrix are somehow weak in this case.

a)   **b)**
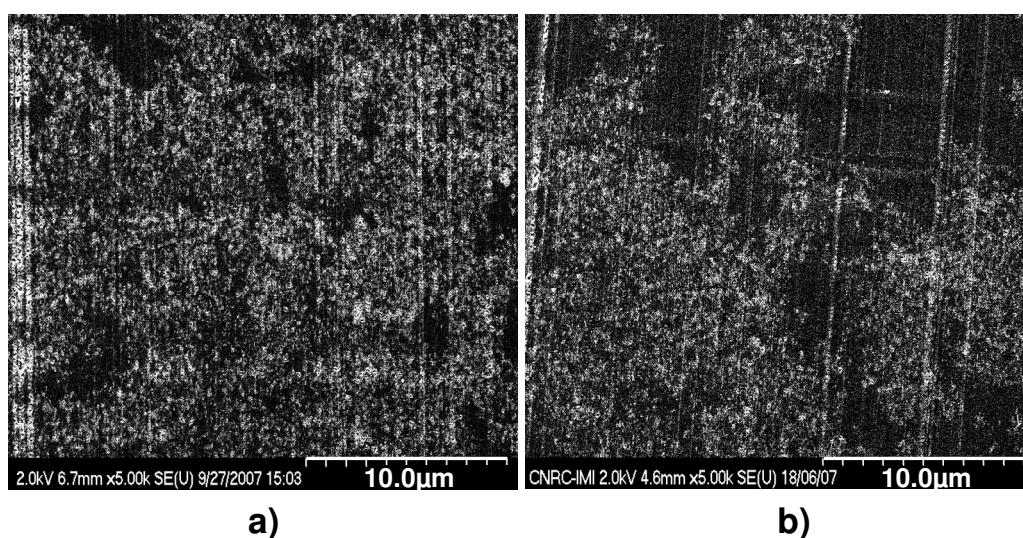
Figure 5.2: SEM micrographs of ultramicrotomed surfaces of PC / 5wt% MWCNT nanocomposites prepared at (a) 210 $^{\circ}$C and (b) 250 $^{\circ}$C

The quality of the dispersion is clearly seen in the TEM photomicrographs of Figure 5.3. For nanocomposites prepared at 210 $^{\circ}$C (Fig. 5.3a), the nanotubes are dispersed individually while at 250 $^{\circ}$C (Fig. 5.3b) there are aggregates formed in the system. These results are confirmed by AFM micrographs, shown in Figures 5.4a and 5.4b for samples compounded at 210 and 250 $^{\circ}$C, respectively. As both phase and height modes show clearly, the nanotubes for the suspensions prepared at 210 $^{\circ}$C are well distributed all over the matrix without any concentrated region. This is shown clearly in the micrographs with the higher resolution on the left side. However, for the suspensions prepared at 250 $^{\circ}$C the dispersion is not uniform: the nanotubes are concentrated in some area while there is a large region without any particles in it.
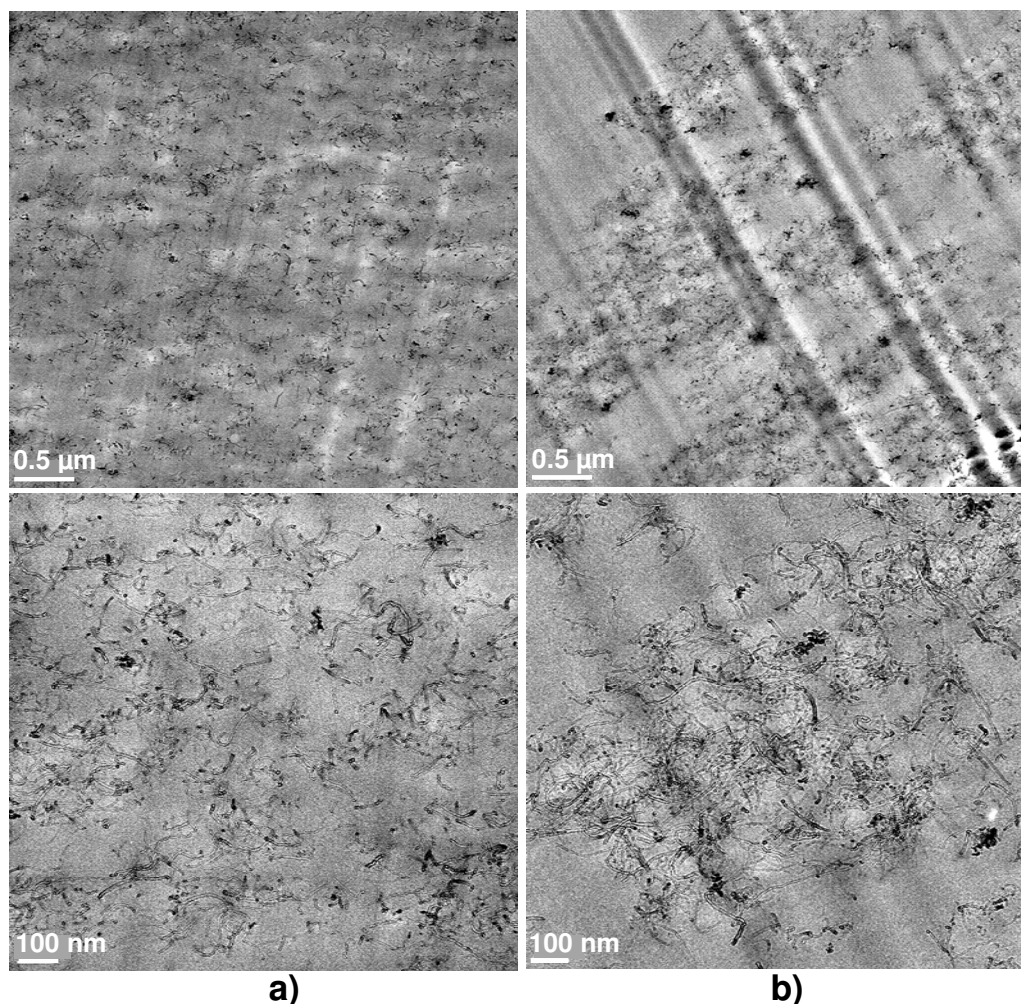
Figure 5.3: TEM micrographs of PC / 5wt% MWCNT nanocomposites prepared at (a) 210 $^{\circ}$C and (b) 250 $^{\circ}$C. The top and bottom micrographs are related to the low and high magnification, respectively

In summary, the quality of the dispersion was surprisingly better for samples prepared at 210°C. Normally, assuming that the dispersion of the nanoparticles is controlled by the diffusion, it is expected to have a better dispersion at higher temperature due to the lower viscosity of the polymer matrix. Apparently, in this case the shear stress plays a more important role than the viscosity of the matrix and the higher shear stress at the lower temperature results in a better dispersion and distribution. The main reason of this is still unclear and needs to be further investigated.

For further characterization we used the nanocomposites prepared at 210°C.

0   **Phase**   1.00 µm 0   **Height**   10.0 µm

a)

0   **Phase**   1.00 µm 0   **Height**   10.0 µm

b)
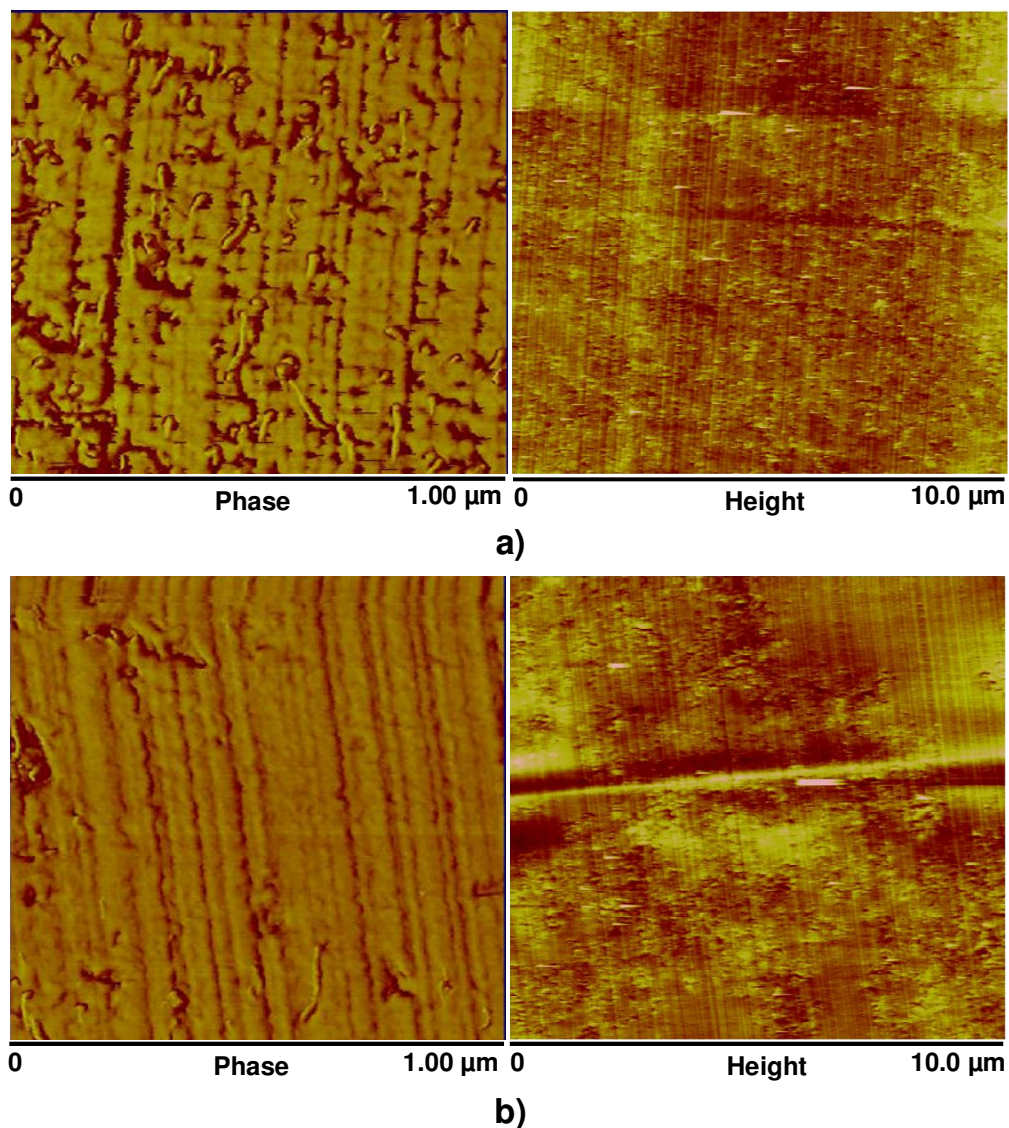
Figure 5.4: AFM micrographs of PC/5wt% MWCNT nanocomposites prepared at (a) 210 $^{\circ}$C and (b) 250 $^{\circ}$C. The micrographs on the left for the phase mode are shown for the higher magnification (scale bar of 1 µm)

5.5.2. Rheological properties

The complex viscosity ($\eta*$) and storage modulus (G') obtained from SAOS measurements at 230°C in absence of preshearing are reported in Figures 5.5 for the neat PC and all nanocomposites. At low frequencies the fully relaxed PC chains exhibit the typical Newtonian

viscosity plateau. The low frequency G' data for the neat PC were not accurate enough to verify the terminal zone, $G' \propto \omega^2$.
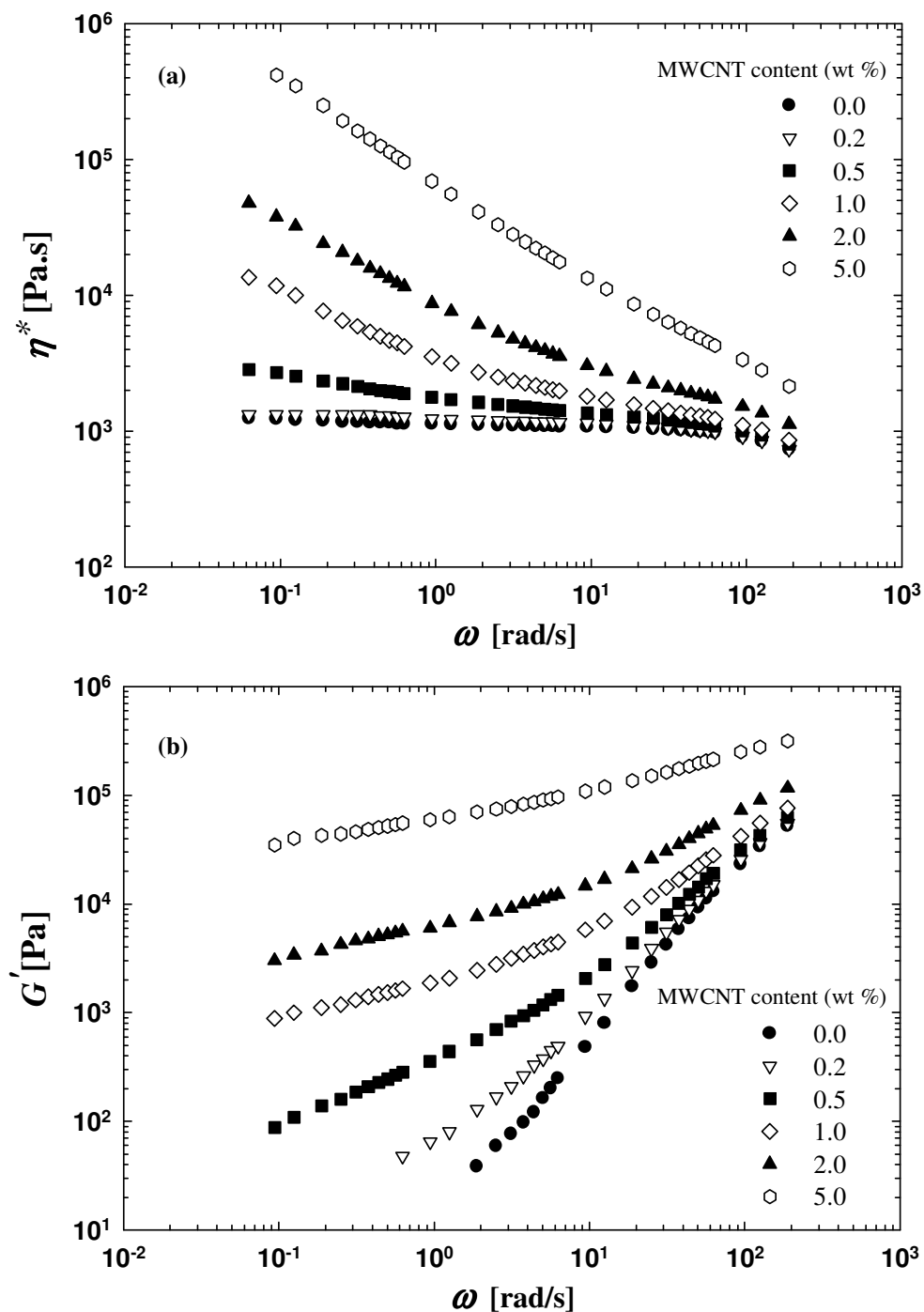
Figure 5.5: (a) Complex viscosity and (b) storage moduli of polycarbonate/MWCNT as a function of frequency at 230 ^{o}C

As can be seen in Figure 5.5, with the addition of MWCNT, the low frequency complex viscosity significantly increases, particularly at high loading, indicating that the long polymer chain relaxation in the nanocomposites is effectively restrained by the presence of the nanotubes. Thus, the Newtonian plateau for the viscosity disappears progressively and a remarkable shear-thinning behavior is exhibited. The terminal behavior for the storage modulus also disappears gradually and the dependence of G' on ω at low frequencies becomes very weak. For MWCNT loadings of 1 wt % and above, significant jumps in the low-frequency rheological properties are observed indicating a transition from viscoelastic liquid- to solid-like behavior. In other words, with increasing filler content, nanotube-nanotube interactions begin to dominate, leading eventually to a percolation network, which restrains the long-range motion of the polymer chains. Similar rheological behavior has been observed for other polymer nanocomposites containing clays or carbon nanotubes (Du et al. 2004; Thostenson et al. 2005; Hu et al. 2006; Zhang et al. 2006; Xiao et al. 2007).
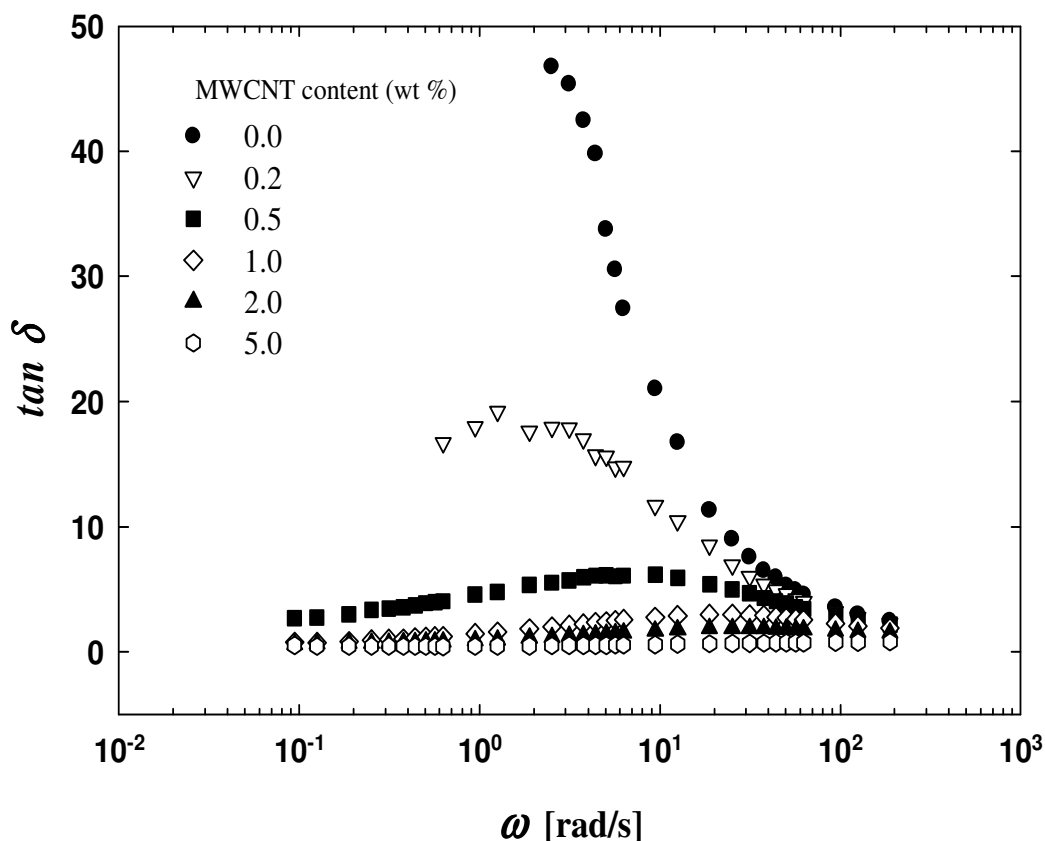
Figure 5.6: *tan δ* of polycarbonate/MWCNT as functions of the frequency at 230 °C

As expected, the loss tangent, *tanδ*, where *δ* is the phase angle, is shown in Figure 5.6 to be very sensitive to the structural change of the materials. In this figure, the peaks occur at the frequency of about 1 rad/s and disappear with increasing nanotube content, showing that the material becomes more elastic. This is also the characteristic of a viscoelastic material experiencing a fluid–solid transition. At the transition point, *tanδ* is expected to be independent of frequency.

It is also well known that an interconnected structure of anisometric filler in a polymeric matrix results in an apparent yield stress (Utracki 1986; Feldman 1988; Dealy and Wissbrun 1999; Shenoy 1999). While this effect is visible in dynamic measurements of *G′* and *G″* versus frequency by the presence of a plateau at low frequency, it is more obvious if we plot the complex viscosity versus the complex modulus. As Figure 5.7 reveals, above 1.0 %t of MWCNT an apparent yield stress is observed suggested by the rapidly increasing complex viscosity as the complex modulus is decreasing.
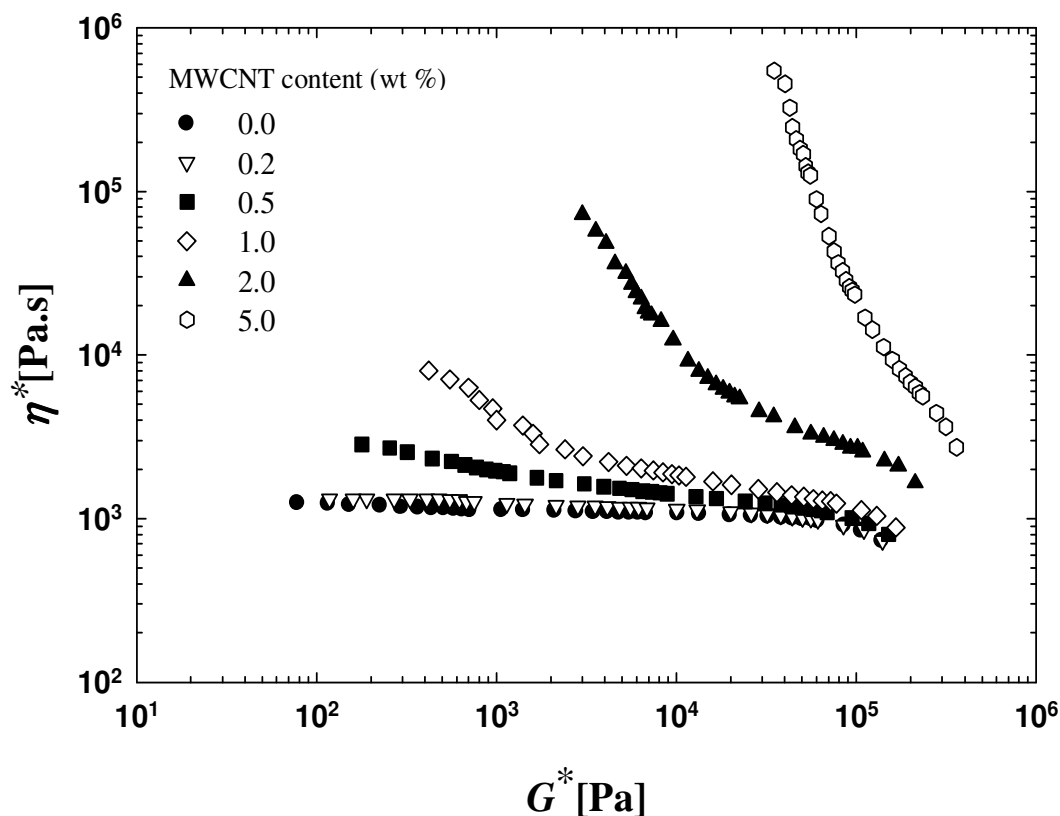
Figure 5.7: Plots of *η** versus *G** for the apparent yield stress in polycarbonate/MWCNT nanocomposites at 230 ^{o}C

The rheological percolation threshold was determined by using the low frequency G' data as a function of MWCNT loadings as reported in Figure 5.8.
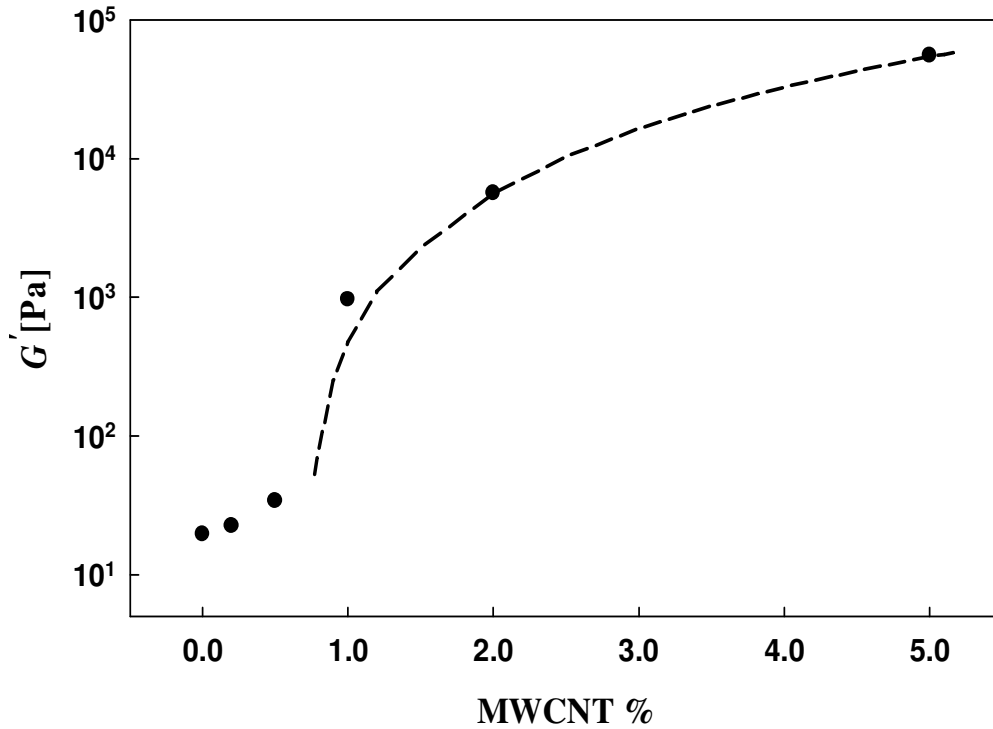
Figure 5.8: Storage modulus, G', of the polycarbonate/MWCNT nanocomposite as a function of the nanotube loading at 230 ^{o}C (1 rad/s data). The line is a fit with the power-law expression (Eq. 5-3)

As the MWCNT loading is increased up to about 1 wt %, the low frequency G' of the nanocomposite increases by almost two orders of magnitude compared with that of the polycarbonate matrix. It can be assumed that the viscoelastic properties of the nanocomposites at low MWCNT loadings ($\leq$ 0.5 wt %) are still dominated by the polycarbonate matrix. With increasing MWCNT loading, the nanocomposites experience a transition from liquid-like behavior to solid-like one, and the results suggest that the rheological percolation threshold for this system is between 0.5 and 1 wt%. The percolation threshold is defined as the value of the solid content above which the rheological properties increase in an exponential way. This value can be determined by applying a power-law function to the G' versus nanotube loading according to the following equation (Du et al. 2004; Moniruzzaman and Winey 2006):

$$G' = \beta_{cG}\left(\frac{m - m_{cG}}{m_{cG}}\right)^n \qquad \text{for } m > m_{cG} \qquad (5\text{-}3)$$

where β_{cG} and n are power-law constants, m is nanotube loading (wt%) and m_{cG} is the percolation threshold (wt%). The description of the data by Eq. 5-3 is shown in Figure 5.8 to be very good after the percolation point (as the definition of the equation suggests it can fit only the data beyond the percolation threshold) .The left limit of the dashed line corresponds to the percolation threshold value of 0.66 wt% at 230 ^{o}C.

Temperature effect

The results presented above are for measurements carried out at 230°C. Although the same behavior was observed for all temperatures studied, the effect of MWCNT loading was significantly different. The differences in the viscoelastic behavior as a function of temperature are better observed by using the so called Cole-Cole plots (Friedrich and Braun 1992; Ivanov et al. 2001). In fact, analogous to Cole-Cole plots used in dielectric spectroscopy (Cole and Cole 1941; Havriliak 1997), the real and imaginary components of viscoelastic properties are plotted against each other in such a representation. A regular semi-arc is obtained if the deformation behavior of the material can be described by a single relaxation time or a narrow distribution; however, in complex polymeric systems, processes with more than one relaxation time take place leading to the distortion of the arc or to the appearance of a second arc. Such plots were used to investigate the microstructure or molecular architecture of homopolymers, or materials with a wide relaxation time distribution such as heterogeneous polymeric systems like block copolymers and polymer blends (Harrell and Nakajima 1984; Chopra et al. 2002). In this study we used Cole-Cole plots to investigate temperature induced changes in the microstructure of nanocomposites and the results are reported in Figure 5.9 for two different temperatures, 210 and 300 ^{o}C, which are the two limits of our measurement temperature range. It can be observed clearly that at 210 ^{o}C (Fig. 5.9a), the neat polycarbonate and the nanocomposites containing low MWCNT loading present a single relaxation arc. This indicates that the presence of the MWCNT has almost no influence on the relaxation behavior of the PC and the rheological characteristics of the matrix dominate the behavior of the composites. However, at contents of 0.5 wt% and above, all plots are partitioned into two regions: a semi-curved arc at low viscosities corresponding to the local dynamics of polycarbonate chains and a linear or rigid end at higher viscosity related to the long-term relaxation of nanotubes-polymer or nanotube-nanotube networks . At higher MWCNT

loadings the first region progressively disappears and the linear region dominates the plots suggesting that the long-range motion of polymer chains is drastically restrained.
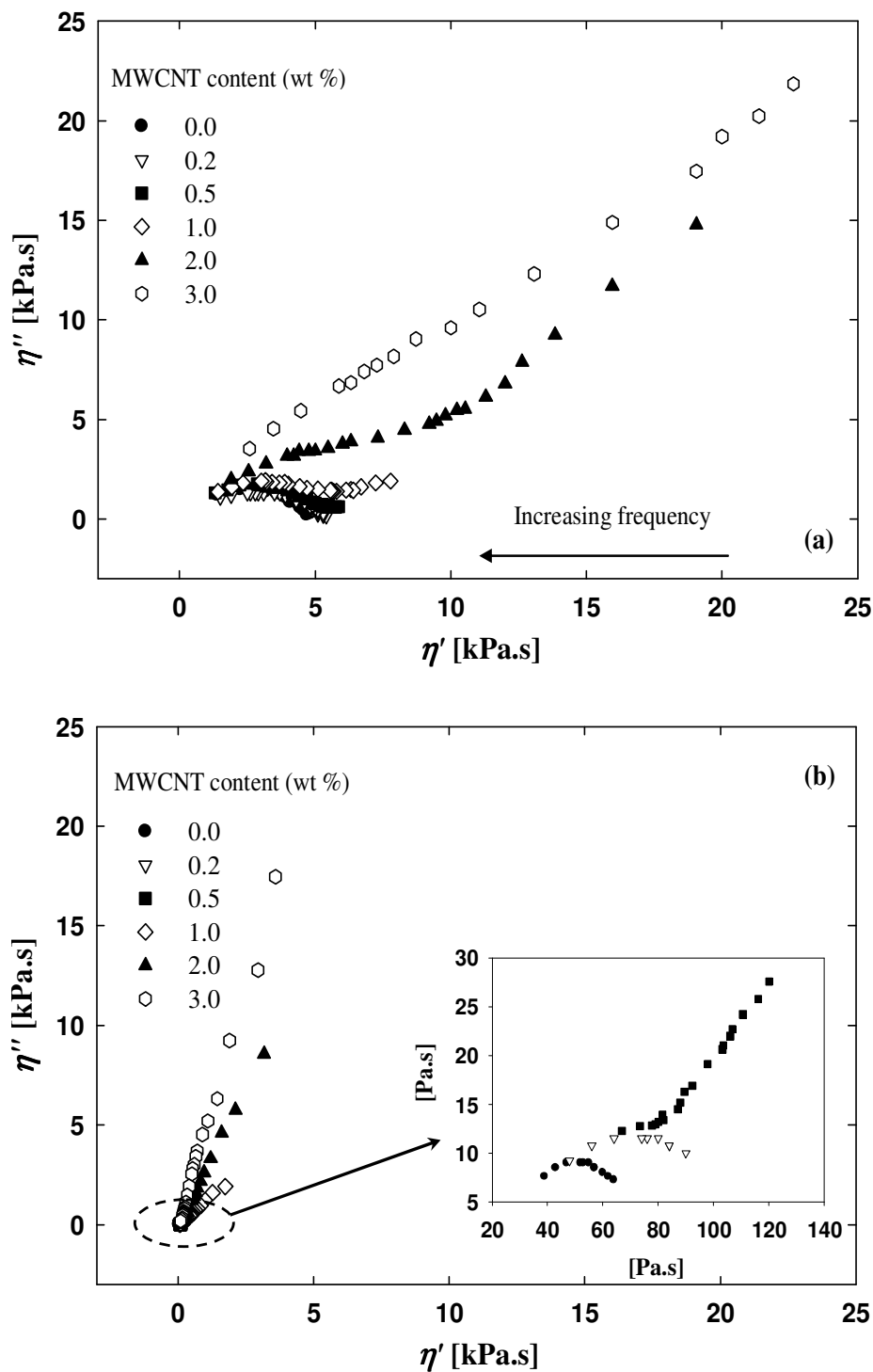
Figure 5.9: Cole-Cole plots of imaginary viscosity (η'') versus real viscosity (η') for polycarbonate/ MWCNT nanocomposites at (a) 210 ^{o}C (b) 300 ^{o}C

At 300 ^{o}C (Fig. 5.9b), however, these changes are more significant. To illustrate the effects for the low concentration nanocomposites an insert for the low viscosity values is presented inside Figure 5.9b. Even for the 0.2 wt% nanocomposite the Cole-Cole plot deviates from that of homogeneous polymeric materials suggesting that at higher temperature nanotube networks might be formed at a very low loading. The slopes of the linear or rigid ends of the plots are also significantly steeper, which reveals that the effect of nanotubes on the nanocomposite structure and properties is considerably enhanced at higher temperature.

To investigate the effect of temperature in more details, the rheological percolation thresholds of the nanocomposites (calculated from low frequency (1 rad/s) G' versus MWCNT loading and Eq. 5-3) are plotted versus the measurement temperature in Figure 5.10.
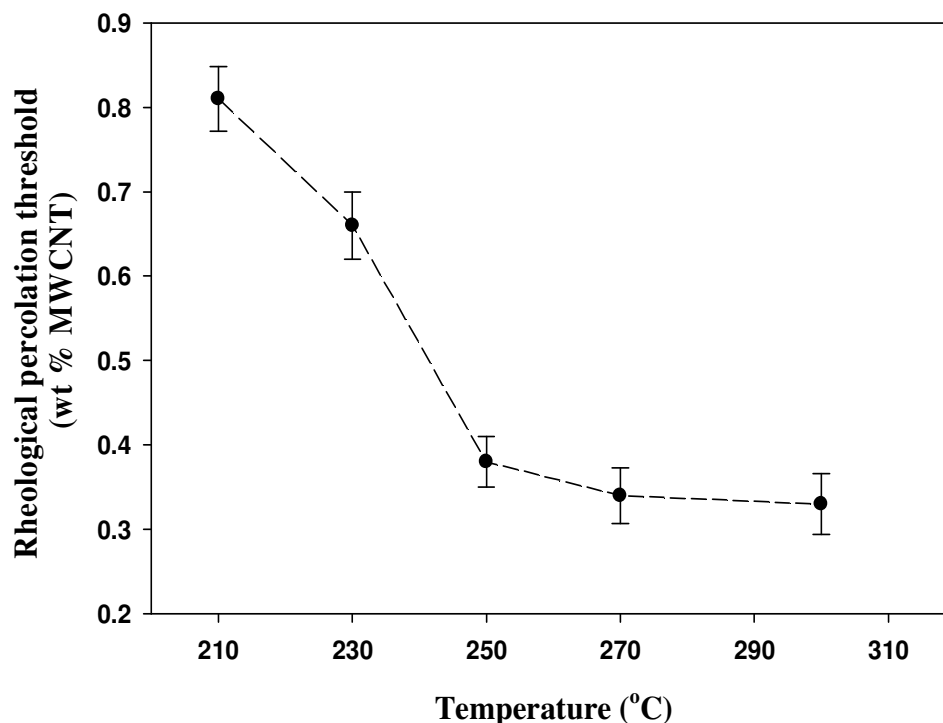
Figure 5.10: Effect of temperature on the rheological percolation threshold of polycarbonate/MWCNT nanocomposites

As this graph shows clearly the percolation threshold is very sensitive to temperature, decreasing considerably as the temperature rises; however, when the measurement temperature is high enough the percolation threshold tends to reach a plateau. Such a temperature dependency of the rheological percolation threshold has been established before in the literature (Abdel-Goad et

al. 2004; Wu et al. 2007) and it is in agreement with the trend shown by the Cole-Cole plots of Figure 5.9.

Figure 5.11 shows the effect of temperature on the reduced complex viscosity of the nanocomposites as a function of loading for different temperatures. By dividing the complex viscosity of the nanocomposites by that of the matrix at the same temperature, the reduced data show clearly the effect of temperature on the particle-particle interactions. Of great interest is the significant increases of the reduced viscosity of the nanocomposites as the temperature rises, the effect being more pronounced at larger MWCNT content. Therefore, contrarily to expectations, nanotube-nanotube interactions increase significantly with temperature particularly at larger MWCNT content. This could also suggest that the wettability of PC by the carbon nanotubes decreases as the temperature increases, resulting in the formation of large aggregates.
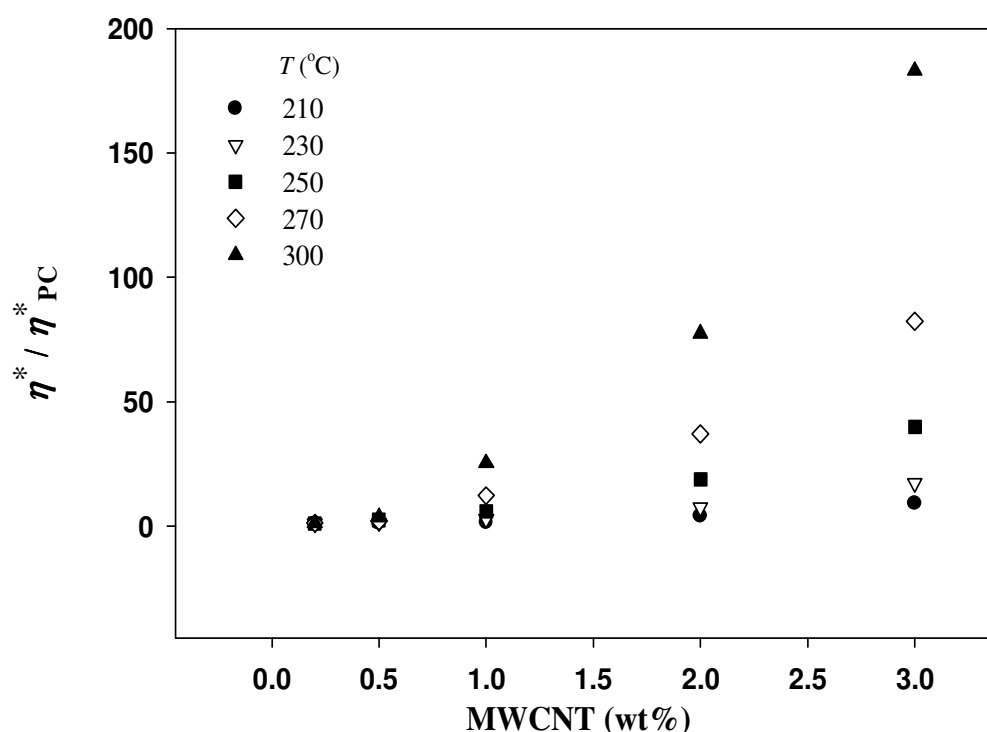
Figure 5.11:   Effect of temperature on reduced viscosity of polycarbonate/MWCNT nanocomposites (1 rad/s data)

The nanotube network can be considered to be an elastic structure and the strength of such a network can be related to the cohesion energy, which is the work required to break up the elastic structure (Bossard et al. 2007; Chougnet et al. 2007). The cohesive energy per volume unit, E_C, can be defined by

$$E_C = 0.5\gamma_C^2 G'$$ (5-4)

where γ_C is the critical deformation amplitude for the limit of the linear domain. Figure 5.12 reports the storage modulus of the nanocomposite containing 3 wt% MWCNT as a function of the strain amplitude for temperatures ranging from 210 to 300 °C.
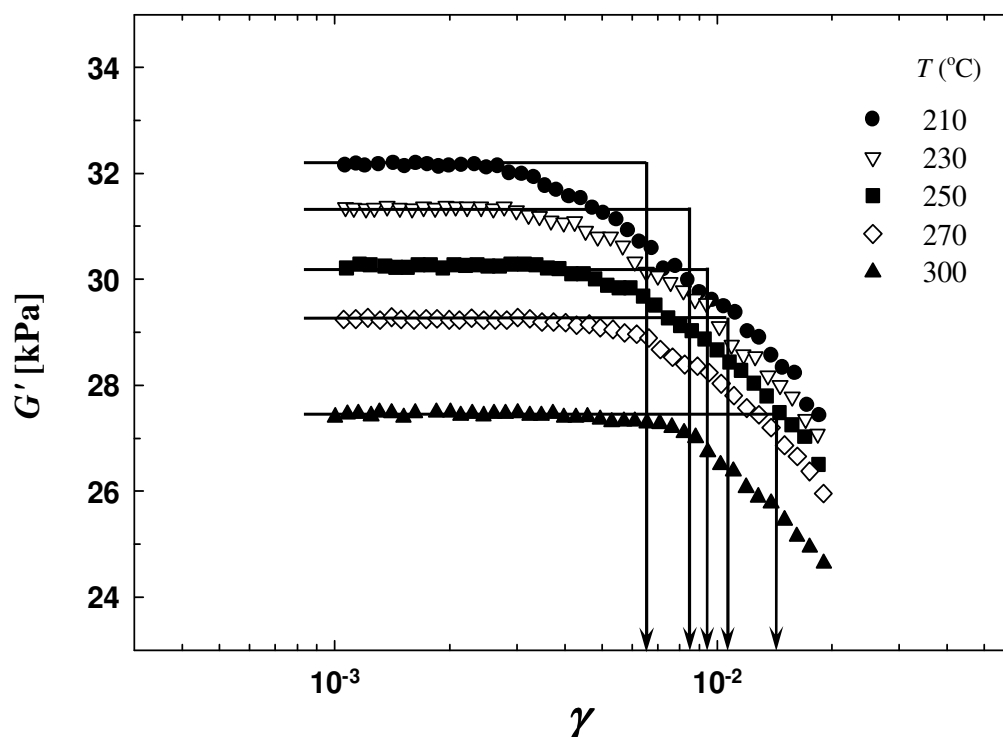
Figure 5.12: Storage modulus of PC / 3wt% MWCNT nanocomposites as a function of the strain amplitude

Basically, the linear domain is limited to very low deformation, where the storage modulus G' is constant. The linear domain for the loss modulus (data not shown) is much wider. In this work γ_C is taken as the value for which the storage modulus is equal to 95% of the plateau value. Table 5.1a reports the γ_C values for different temperatures of the nanocomposites containing 3wt% MWCNT. The values for G' and G'' in the linear regime at 1Hz, a characteristic elastic time λ and the cohesion energy can be also found in this table. As we expected, the cohesion energy increases with temperature. The cohesive energy is representative of the network strength and accordingly its increase is a direct consequence of the enhancement of nanotube-nanotube interactions (and stronger networks) at higher temperature. The effect of nanotube concentration

was also examined in the same manner. The key characteristics of the nanocomposites with different nanotube loadings at temperature of 270°C are reported in Table 5.1b. The cohesion energy increases with nanotube content indicating that the nanotube interactions (and networks) are stronger at higher loading level.

Table 5.1. Key characteristics of nanocomposites (G' and G'' data for $\omega = 6.28$ rad/s, $\gamma < \gamma_C$, the elastic characteristic time λ, and the cohesion energy E_C). (a) nanocomposite PC/3wt % MWCNT at different temperatures (b) nanocomposites PC/MWCNT with different nanotube contents at 270°C

T	G'	G''	$\lambda = G'/G''\omega$	γ_C	$E_C = 0.5\,\gamma_C^2 G'$
(°C)	(kPa)	(kPa)	(s)		(mJ/m^3)
210	30.4	53.6	0.090	0.0067	0.67
270	27.6	12.2	0.359	0.0119	1.95
300	25.1	8.8	0.457	0.0161	3.26

(a)

MWCNT content (wt%)	G' (kPa)	G'' (kPa)	$\lambda = G'/G''\omega$ (s)	γ_C	$E_C = 0.5\,\gamma_C^2 G'$ (mJ/m^3)
0.20	79	1659	0.008	0.0318	0.04
1.0	1875	2997	0.100	0.0150	0.21
3.0	27569	12223	0.359	0.0119	1.95

(b)

Orientation effect

It is widely accepted that shearing tends to align the particles in the flow direction, reducing markedly the particle-particle interactions and leading to a remarkable change of viscoelastic behavior (Fan and Advani 2007). It was observed that rod-like nanotubes are oriented easily along the shear direction and that the percolation network of nanotubes is quite sensitive to steady shear flow (Wu et al. 2007). In order to investigate the effect of orientation on the PC/MWCNT rheological behavior, we measured the percolation thresholds in SAOS after

applying different levels of stresses as preshearing steps. We first determined the shear stresses for which the nanocomposite response changes from solid- to liquid-like using plots of the steady shear stress versus shear rate of Figure 5.13. These values are indicated by the arrows in the figure. However, these critical points are not clear for the low nanotube content suspensions and should not be interpreted as apparent yield stress values.

For each concentration, the samples were presheared at two levels of shear stresses: the maximum allowable stress of the CSM rheometer (2400 Pa) as the high stress level and the stress value corresponding to the transition shown in Figure 5.13 as the low stress value. Note that preshearing at lower stresses than the minimum values shown in the figure did not affect subsequent SAOS measurements.
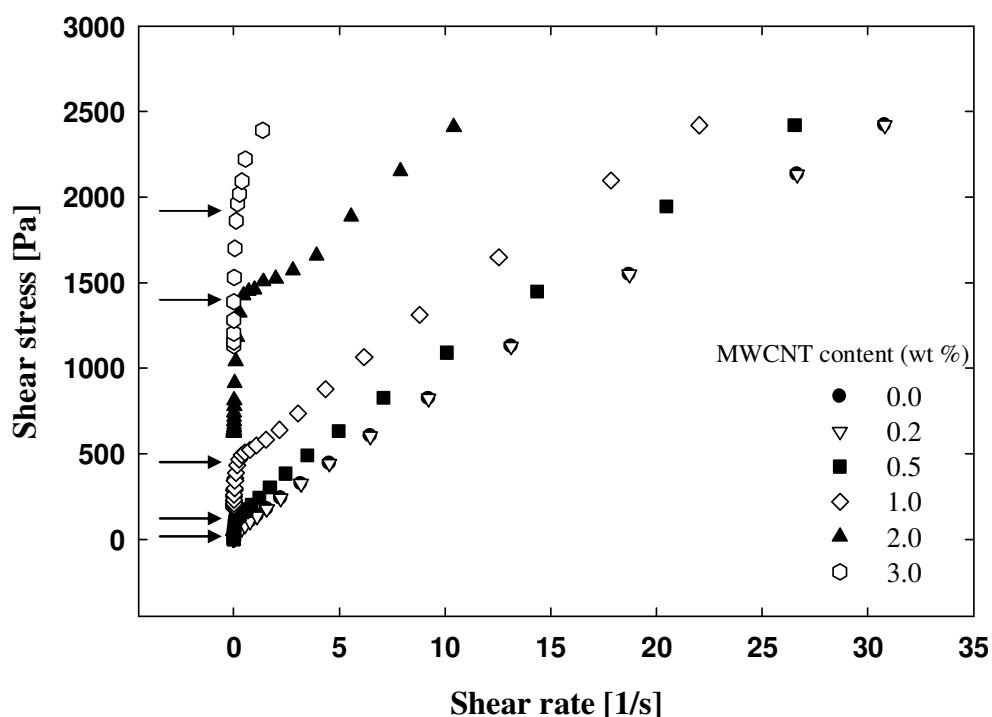
Figure 5.13: Steady shear stress versus shear rate of PC/MWCNT nanocomposites at 300 $^{\circ}$C. The arrows show the apparent yield stress of the nanocomposites

As soon as the preshearing step was completed (i.e. the shear viscosity has reached steady state), SAOS tests were conducted without any rest time. The preshearing conditions are summarized in Table 5.2.

Table 5.2. Preshearing conditions applied before SAOS measurements

NT %	Preshearing time at low stress level (s)	Preshearing time at high stress level (s)
0.2	2500	2000
0.5	2500	1500
1	2300	1200
2	2000	1000
3	1800	800

Figure 5.14 shows the effect of preshearing on the complex viscosity of the neat polycarbonate and nanocomposites containing 0.2 and 3 wt% of MWCNT at 300 °C.
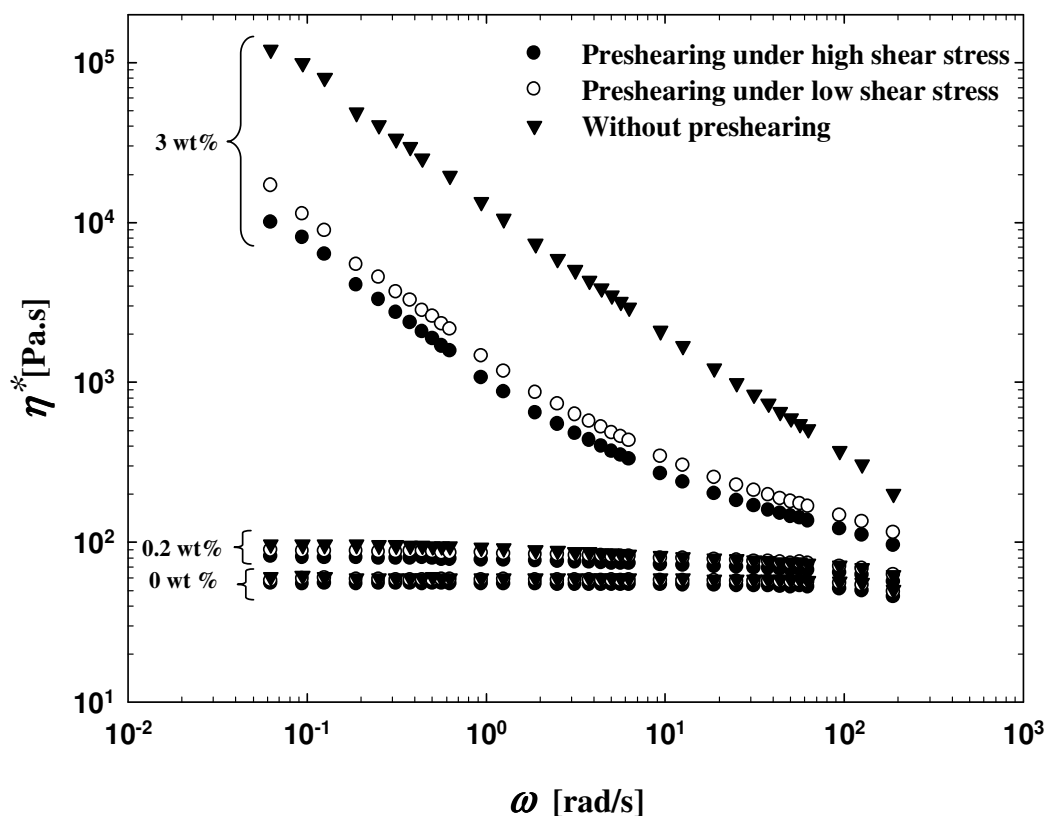
Figure 5.14: Effect of preshearing (without rest time) on the complex viscosity at 300 °C of nanocomposites with various nanotube loadings

Obviously, for the neat polycarbonate and the 0.2 wt% nanocomposites the effect of preshearing is negligible, which indicates that the viscoelastic behavior is dominated by the polymer matrix. However, for nanocomposites with high nanotube loadings the effect of preshearing becomes quite significant. Applying a shear flow prior to SAOS measurements, even at the low stress level, aligns the nanotubes in the flow direction and results in a lower complex viscosity.
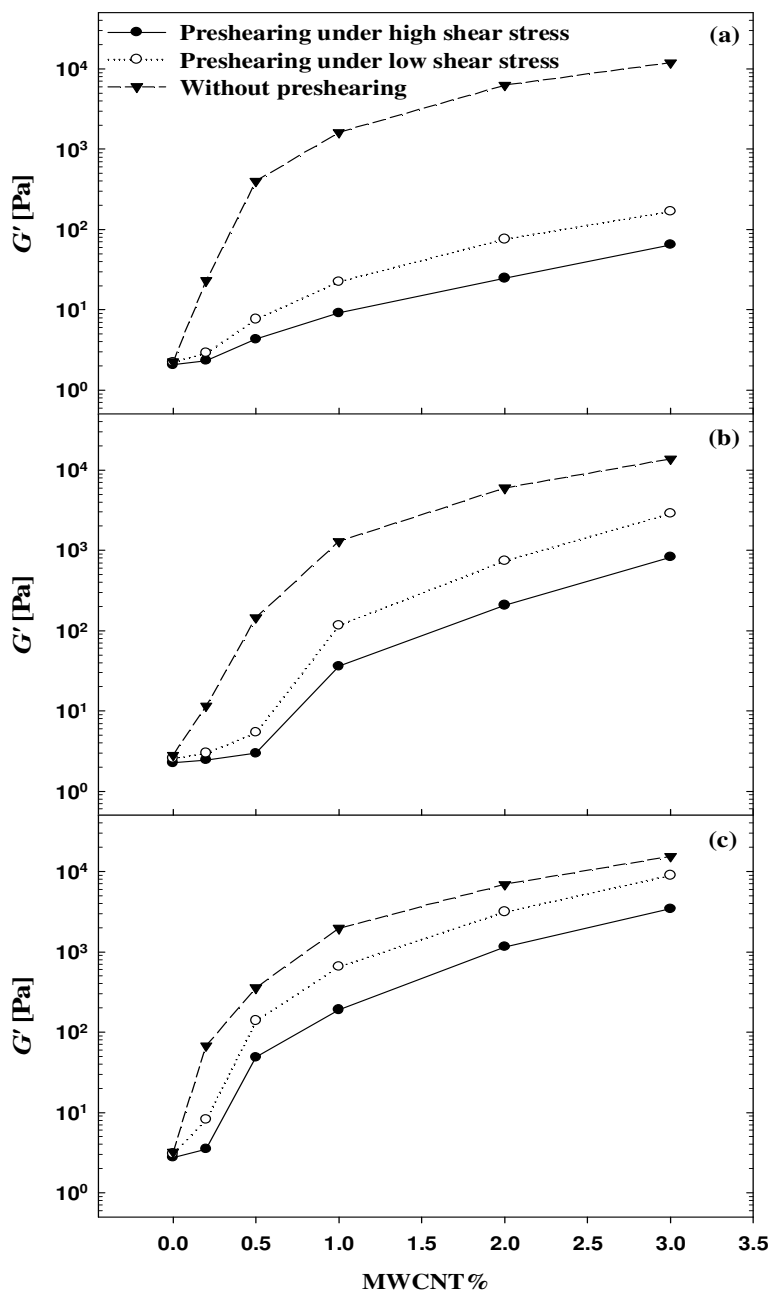
Figure 5.15: Effect of preshearing (without rest time) on G' data (1 rad/s): (a) 300 $^{\circ}$C, (b) 270 $^{\circ}$C, (c) 250 $^{\circ}$C

Consequently, the nanotubes interconnect minimally leading to a remarkable increase in the percolation threshold as one can deduce from Figure 5.15 that reports the elastic modulus data as a function of nanotube content for different shear levels or no preshearing. Furthermore, this figure reveals that the storage modulus at 300 $^{\circ}$C increases very little with nanotubes concentration after preshearing under both low and high stresses, suggesting that we do not have a percolated network anymore, even at high nanotubes content. Interestingly, Figures 5.15b & c show that at lower temperature the decrease of the storage modulus is much less sensitive to preshearing; at 250°C we still have percolated networks even after applying high levels of stress. The results of Figure 5.15 suggest that the nanotubes become more rigid (strengthened out) and align more easily in a shear flow as the temperature is increased.

Discussion

To our knowledge, no rheological model exists to predict the strong temperature dependency of the particle interactions as observed in this work. In this section, we consider the nanocomposite system as a viscous suspension of a rod-like filler to get at least a qualitative explanation of our experimental findings, although further experiments and theoretical consideration on the interactions between nanotubes and polymer chains as well as between the nanotubes themselves are still needed.

The viscosity of a suspension of solid particles is generally determined by the nature of interactions between the particles, which depends mainly on the filler concentration. In the case of rod-like particles the aspect ratio is another important factor affecting the viscosity of the suspension. For a particle of length L and diameter D, the aspect ratio is defined as $P=L/D$. For suspensions of such rod-like particles, depending on the rod dimensions, three concentration regimes are considered (Shaqfeh and Fredrickson, 1990):

1. Dilute regime where $\qquad \phi << (D/4L)^2$
2. Semi-dilute regime where $\quad (D/4L)^2 << \phi << (D/4L)$
3. Concentrated regime where $\quad (D/4L) << \phi$

where ϕ is the volume fraction.

In the dilute regime the particles interactions are almost negligible. In the semi-dilute regime the particles interact mostly through long-range hydrodynamic interaction. If additional non-hydrodynamic interactions become important then we have a concentrated suspension.

The particles in our system are MWCNT with a diameter ranging from 15 to 50 nm and the lengths between 1 and10 μm. The nanotube concentrations in the nanocomposites are between 0.2 to 3 wt%, which correspond to the volume fractions of about 0.14 to 2 vol% of MWCNT, considering the density of nanotubes to be 1.75 g/mL (Potschke et al. 2002). The density of polycarbonate was evaluated at the appropriate temperature to convert the mass fraction of nanotubes to the corresponding volume fraction. Subsequently, this concentration range corresponds to semi-dilute suspensions.

The intrinsic viscosity $[\eta]$ is one of the key characteristics to measure the contribution of the individual particles to the viscosity of a suspension and can provide considerable physical insights. It is defined by the following expression (Carreau et al. 1997):

$$[\eta] = \lim_{\phi \to 0} \frac{\eta_r - 1}{\phi} = \lim_{\phi \to 0} \frac{\eta_{sp}}{\phi} \qquad (5\text{-}5)$$

where the relative viscosity, η_r is the ratio of the suspension viscosity to the medium viscosity and η_{sp} is the specific viscosity. In our case, however, instead of using the suspension shear viscosity, we considered the complex viscosity and the intrinsic viscosity was then determined at each temperature by extrapolating the values of the specific complex viscosity/volume fraction to zero concentration as shown in Figure 5.16.
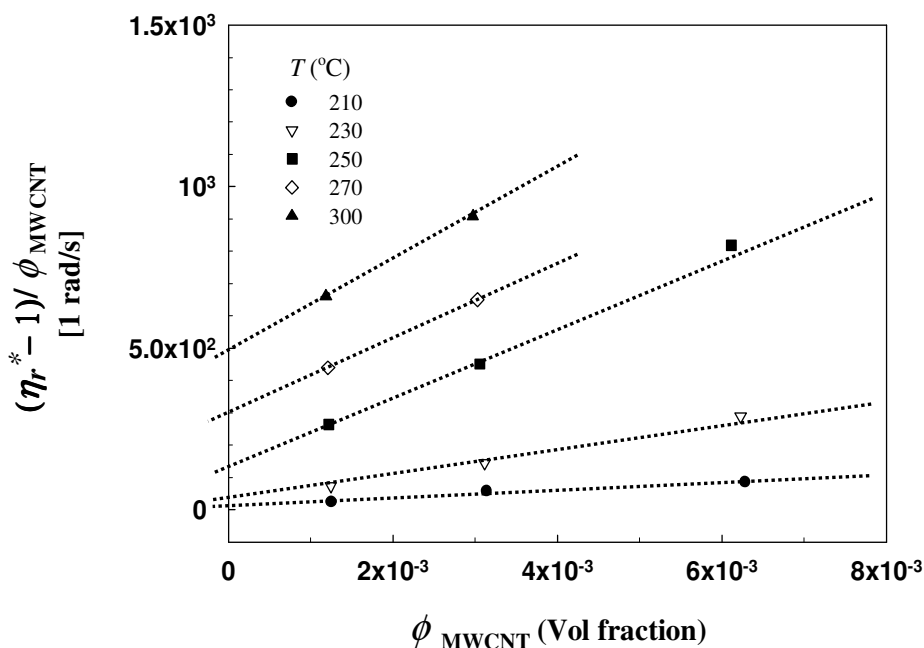
Figure 5.16: Specific viscosity/volume fraction of the nanocomposites as a function of volume fraction at different temperatures

The extrapolation is done assuming a linear behavior at the lowest concentrations and only two data could be used for the higher temperature measurements. The intrinsic viscosity values are listed in Table 5.3 for several temperatures. Interestingly the intrinsic viscosity value increases from 15 at 210 $^{\circ}$C to 180 at 300 $^{\circ}$C. These values are rationalized in the following paragraphs.

Table 5.3. Intrinsic viscosity of the nanocomposites and effective aspect ratio of nanotubes at different temperatures

T ($^{\circ}$C)	210	270	300
[η]	15±2	300±7	500±9
P_{eff}	25	151	205

It is well established that the intrinsic viscosity is strongly dependent on the particle asymmetry. For rod particles the intrinsic viscosity is related to the aspect ratio as (Barnes et al. 1989):

$$[\eta] = 7P^{5/3}/100 \tag{5-6}$$

Equation 5-6 was used to calculate the aspect ratios corresponding to the different temperature measurements and the results are reported in Table 5.3. We call this an effective aspect ratio, P_{eff}, since the suspensions probably form bundles of nanotubes as suggested by the low values reported in Table 5.3 for low temperature (the nominal aspect of the individual nanotubes should be between 20 and 666). P_{eff} is shown to increase from 25 for the lowest temperature measurements to 205 for 300 $^{\circ}$C indicating that at higher temperatures the bundles are more likely to be dispersed into individual nanotubes. As Figure 5.1 reveals the aspect ratio of an individual nanotube is much higher than that of a bundle. Lower percolation threshold and stronger nanotube networks at higher temperature are probably due to this effect of temperature on the effective aspect ratio of nanotubes.

On the other hand, it is well established that the intrinsic viscosity is proportional to the hydrodynamic volume of the filler. For a highly dilute suspension of hard spheres the specific viscosity can be predicted by the Einstein equation (Larson 1998):

$$\eta_{sp} = 2.5 \frac{N_B V_\eta}{V} \tag{5-7}$$

where N_B is the number of particles , V_η is the hydrodynamic volume of each particle and V is total volume. According to Eq. 5-5, the limiting value of the specific viscosity at very low concentration is equal to $[\eta]\phi$. Obviously for rod-like particles the proportionality constant would be different, but the increasing intrinsic viscosity with temperature could be assigned to an increase of the hydrodynamic volume of the nanotubes. In other words, the end-to-end distance of the nanotubes increases significantly with temperature suggesting that as discussed previously the nanotubes become more rigid (strengthened out) and align more easily in a shear flow compared to nanotubes that are more flexible at lower temperature.

Finally, to understand why the effect of temperature on the rheological properties is more pronounced at higher nanotube loading, as it was shown previously, we made use of the Andrade-Eyring equation defined for the complex viscosity as (Mendelson 1968):

$$\eta^* = B\exp(E_a/RT) \tag{5-8}$$

where E_a is the flow activation energy and R is the universal gas constant. In the case of nanocomposites, E_a can be related to the interactions between polymer chains and nanotubes. The value of E_a thus depends on the ease with which the nanotubes move through the polymer chains. To estimate the activation energy of the nanocomposites, we have plotted the values of ln η^* (determined at 1 rad/s) as a function of $1/RT$. The activation energy is then given by the slope of this curve. Table 5.4 reports the values of E_a for different nanotube loadings.

Table 5.4. Activation energy of the network formation at different nanotube loadings

MWCNT (wt%)	0.2	1	3
E_a(kJ/mol)	74.43	20.88	16.99

For the neat PC, the flow activation energy was found to be 83.9 kJ/mol in agreement with values of the literature (VanKrevelen 1990). The rapid decrease of the activation energy with increasing nanotube loading suggests that at higher nanotube loadings the nanotubes are less restricted and have less interaction with the polymer chains, hence, less wettability with the

polymer matrix and more particle-particle interactions (including all the interactions in the system between either individual nanotubes or nanotube bundles (Fig. 5.1)). A somewhat related idea was previously proposed by Dionne et al. (2006) who showed that the increasing energetic interaction between the polymer matrix and the filler with temperature increased the rate of the attachment (wetting) of the filler to the polymer according to the Arrhenius law, in which the activation energy was proportional to the a polymer-nanoparticle interaction parameter.

5.5.3. Conductivity measurements

In the case of conductive fillers, electrical measurements are useful to understand the relationship between the rheological behavior and the nanocomposites microstructure. Figure 5.17 presents the effect of the nanotube loading on the conductivity of the nanocomposites. The electrical percolation threshold is between 2 and 3 wt% of MWCNT in PC. The conductivity changes by more than 10 decades in this range of concentration and the nanocomposites with nanotube contents larger than 3wt% can be considered as electrically conductive. As for the rheological percolation threshold, the electrical percolation threshold can be found by applying a similar power-law expression to the electrical conductivity data (Hu et al. 2006):

$$\sigma = \beta_{c,\sigma} \left(\frac{m - m_{c,\sigma}}{m_{c,\sigma}} \right)^{n} \quad \text{for } m \geq m_{c,\sigma} \tag{5-9}$$

where $\beta_{c,\sigma}$ and n are power-law constants, and $m_{c,\sigma}$ is the electrical percolation threshold (wt%). Again this power-law expression is found to describe very well the data of Figure 5.17 (after the percolation points) with an electrical percolation threshold of about 2.55 wt%. It is worthwhile to note that rheological percolation threshold (0.66 wt %) is considerably smaller. This difference can be described in terms of the shorter tube–tube distance required for electrical conductivity as compared to that required to impede polymer mobility, so that more nanotubes are needed to reach the electrical percolation threshold. Furthermore, all the nanotubes cannot participate in the formation of an electrically conductive path. Only metallic and semiconducting nanotubes can contribute in the electrical conductivity. Nonmetallic tubes do not have a significant contribution in electrical conductivity, although they can restrict the polymer motion.

Finally, it is well known that carbon nanotubes are thermally conductive. Hence, there must be another type of percolated structure in the nanocomposites due to formation of a thermally

conductive network. Assuming that all nanotubes are thermally conductive, the thermal conductivity percolation threshold ought to be smaller than the electrical threshold. However, the tube–tube distance required for thermal conductivity is still smaller than that required to impede polymer mobility, so that the thermal conductivity percolation threshold is expected to be higher than the rheological threshold. In addition to electrical conductivity, Figure 5.17 reports the thermal conductivity of the nanocomposites as a function of MWCNT loading for a wide range of temperatures.
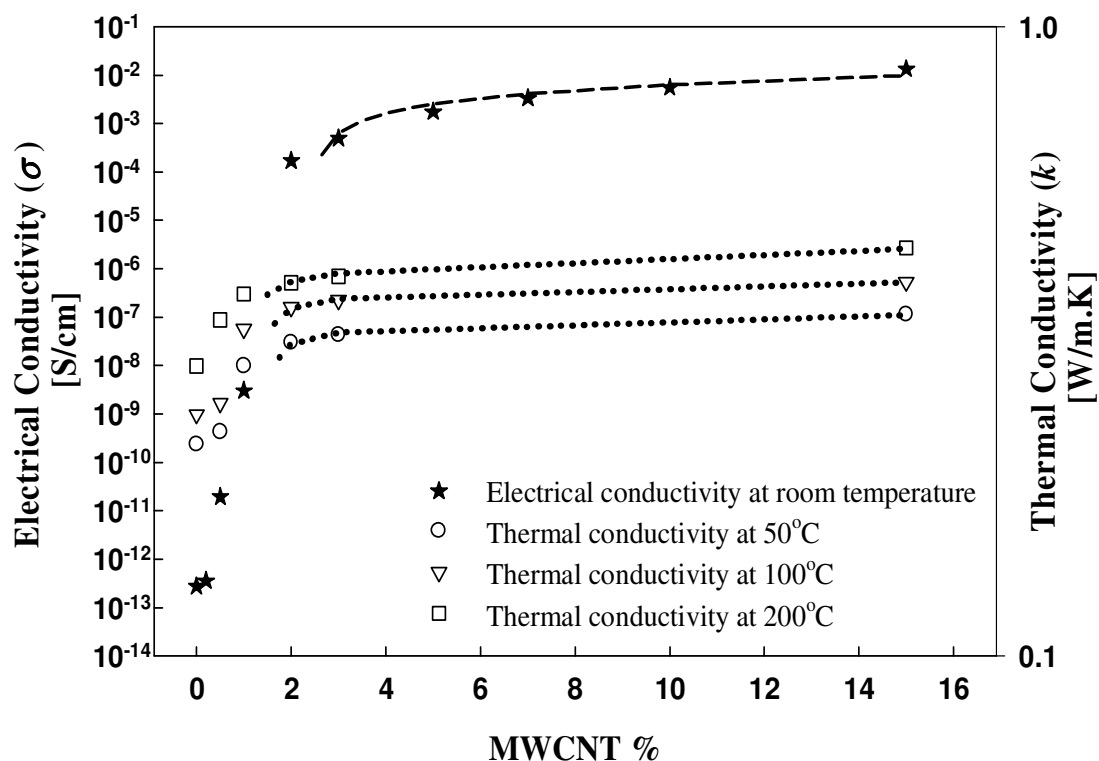
Figure 5.17: Electrical conductivity (σ) and thermal conductivity (k) of the polycarbonate/MWCNT nanocomposite as a function of the nanotube loading at room temperature. The lines are the best fits using Eq. 5-9

At very low concentration of nanotubes, the thermal conductivity gradually increases with increasing nanotube content. However, at a nanotube concentration between 1 to 2wt%, a remarkable jump in the thermal conductivity is observed. Even though the thermal conductivity values are still much less than the corresponding values in thermally conductive materials, this stepwise change in conductivity might be due to the formation of an interconnected structure of MWCNTs and can be regarded as a thermal percolation threshold. The values of the thermal percolation threshold can be found by using the same power-law expression as for the electrical

conductivity (Eq. 5-9). The fits are shown in Figure 5.17 and the thermal conductivity percolation values are about 1.7, 1.6 and 1.47 at 50, 100 and 200 $^{\circ}$C, respectively. As we expected the thermal percolation threshold has a value between the rheological and the electrical percolation thresholds

5.6. Concluding remarks

In this work we have examined the effects of temperature and nanotube loading on the rheological behavior of PC/MWCNT nanocomposites. A masterbatch was diluted to prepare the nanocomposites, and a reasonably good dispersion of nanotubes within the polymer matrix was confirmed using SEM, TEM and AFM.

Rheological measurements show that the percolation threshold and the strength of nanotube networks are significantly dependent upon the measurement temperature. Assuming that the nanotube network forms an elastic structure within the matrix, the strength of this network could be related to the cohesion energy, which is the work required to break it up. Thus, the increase of the cohesion energy with temperature is a direct consequence of the enhancement of nanotube-nanotube interactions and a stronger network at higher temperature.

The intrinsic viscosity was found to increase with temperature and the effective aspect ratio of the nanotubes was larger at elevated temperature. This suggests that the bundle size decreases with temperature and at higher temperature more nanotubes are dispersed individually and this also explains the lower percolation threshold and stronger nanotube networks at higher temperature. The increase of the intrinsic viscosity with temperature could be also due to the expansion of the nanotubes hydrodynamic volume. In other words, the end-to-end distance of the nanotubes increases significantly with temperature and results in more rigid nanotubes that align more easily under shear flow as evidenced by preshearing effects on the elastic modulus.

It was also shown that the effect of temperature is more pronounced at higher nanotube loading and can be described in terms of the activation energy of the nanocomposites. The decreasing of the activation energy with nanotube contents indicates that at higher level of loading the interactions between the nanotubes and the polymer chains decrease. Accordingly the nanotubes are less restricted and their motion and interactions are more affected by temperature.

Furthermore, electrical and thermal conductivity measurements were carried out and it was found that the formation of a conductive network above a certain content of nanotube results in

an obvious jump in the conductivity (thermal and electrical) of the nanocomposites. The thermal percolation threshold was found to be between the rheological and electrical threshold.

5.7. References

Abdel-Goad M, Potschke P (2005) Rheological characterization of melt processed polycarbonate-multiwalled carbon nanotube composites. J Non-Newton Fluid Mech 128(1): 2-6.

Abdel-Goad M, Potschke P, Alig I, Dudkin S, Lellinger D (2004) Rheological and dielectrical characterization of melt mixed polycarbonate-multiwalled carbon nanotube composites. Polymer 45(26): 8863-70.

Barnes H A, Hutton J F, Walters K (1989) An Introduction to Rheology. Elsevier, Amsterdam

Bossard F, Moan M, Aubry T (2007) Linear and nonlinear viscoelastic behavior of very concentrated plate-like kaolin suspensions. J Rheol 51(6): 1253-1270.

Breuer O, Sundararaj U (2004) Big returns from small fibers: A review of polymer/carbon nanotube composites. Polym Compos 25(6): 630-645.

Carreau P J, De Kee D C R, Chhabra R P (1997) Rheology Of Polymeric Systems Principles and Applications. Hanser , New York.

Chopra D, Kontopoulou M, Viassopoulos D, Hatzikiriakos S G (2002) Effect of maleic anhydride content on the rheology and phase behavior of poly(styrene-co-maleic anhydride)/ poly(methyl methacrylate) blends. Rheol Acta 41(1): 10-24.

Chougnet A, Audibert A, Moan M (2007) Linear and non-linear rheological behaviour of cement and silica suspensions. Effect of polymer addition. Rheol Acta 46(6): 793-802.

Cole K S, Cole R H (1941) Dispersion and Absorption in Dielectrics I. Alternating Current Characteristics. J Chem Phys 9(4): 341-351.

Dealy J M, Wissbrun K F (1990) Melt Rheology and its role in Plastics Processing: Theory and Applications. Van Nostrand Reinhold, New York.

Ding, W, Eitan A, Fisher F T, Chen X, Dikin D A, Andrews R, Brinson L C, Shadler L S, Ruoff R S (2003) Direct Observation of Polymer Sheathing in Carbon Nanotube-Polycarbonate Composites. Nano Lett 3(11): 1593-1597.

Dionne P J, Picu C R, Ozisik R (2006) Adsorption and Desorption Dynamics of Linear Polymer Chains to Spherical Nanoparticles: A Monte Carlo Investigation. Macromolecules 39(8): 3089-3092.

Du F, Scogna R C, Brand S, Fischer J E, Winey K I (2004) Nanotube networks in polymer nanocomposites: Rheology and electrical conductivity. Macromolecules 37(24): 9048-9055.

Fan Z, Advani S G (2007) Rheology of multiwall carbon nanotube suspensions. J Rheol 51(4): 585-604.

Feldman D (1988) Current topics in polymer science, vol. II, R. M. Ottenbrite, L. A. Utracki, and S. Inoue, Eds., C. Hanser Publishers, Munich, Vienna, New York, 1987, 358 pp. J Polym Sci C 26(5): 241-242.

Friedrich C, Braun H (1992) Generalized Cole-Cole behavior and its rheological relevance. Rheol Acta 31(4): 309-322.

Harrell E R, Nakajima N (1984) J Appl Polym Sci 29(3): 995-1010.

Havriliak J S (1997) Dielectric and mechanical relaxation in materials: analysis, interpretation and application to polymers. Hanser, Munich.

Hone J (2004) Carbon Nanotubes: Thermal Properties. Dekker Encyclopedia of Nanoscience and Nanotechnology: 603 - 610.

Hong J S, Kim C (2007) Extension-induced dispersion of multi-walled carbon nanotube in non-Newtonian fluid. J Rheol **51**(5): 833-850.

Hu G, Zhao C, Zhang S, Yang M, Wang Z (2006) Low percolation thresholds of electrical conductivity and rheology in poly(ethylene terephthalate) through the networks of multi-walled carbon nanotubes. Polymer 47(1): 480-488.

Iijima S (1991) Helical microtubules of graphitic carbon. Nature 354:56-58.

Iijima S, Ichihashi T (1993) Single-shell carbon nanotubes of 1-nm diameter. Nature 363(6430): 603-15.

Ivanov I, Muke S, Kao N, Bhattacharya S N (2001) Morphological and rheological study of polypropylene blends with a commercial modifier based on hydrogenated oligo (cyclopentadiene). Polymer 42(24): 9809-9817.

Kharchenko S B, Migler K B, Douglas J F, Obrzut J, Grulke EA (2004). Rheology, processing and electrical properties of multiwall carbon nanotube/polypropylene nanocomposites. ANTEC 2004:1877-1881.

Larson R G (1998) The Structure and Rheology of Complex Fluids. Oxford University Press, New York.

Ma W K A, Chinesta F, Ammar A (2008). Rheological modeling of carbon nanotube aggregate suspensions. J Rheol 52(6): 1311-1330.

Meincke O, Kaempfer D, Weickmann H, Friedrich C, Vathauer M, Waeth H (2004). Mechanical properties and electrical conductivity of carbon-nanotube filled polyamide-6 and its blends with acrylonitrile/butadiene/styrene. Polymer 45(3): 739-748.

Mendelson R A (1968) Prediction of melt viscosity flow curves at various temperatures for some olefin polymers and copolymers. Polym Eng Sci 8(3): 235-240.

Meyyappan M (2005) Carbon nanotubes : science and applications. CRC Press ,Boca Raton.

Moniruzzaman M, Winey K I (2006) Polymer nanocomposites containing carbon nanotubes. Macromolecules 39(16): 5194-5205.

Pham G T, Park Y -B, Wang S, Liang Z, Wang B, Zhang C, Funchess P, Kramer L(2008) Mechanical and electrical properties of polycarbonate nanotube buckypaper composite sheets. Nanotechnology 19(32): 325705. doi:10.1088/0957-4484/19/32/325705.

Potschke P, Abdel-Goad M, Alig I, Dudkin S, Lellinger D (2004) Rheological and dielectric characterization of melt mixed polycarbonate-multiwalled carbon nanotube composites. Polymer 45(26): 8863-8870.

Potschke P, Bhattacharyya A R, Janke A (2004). Carbon nanotube-filled polycarbonate composites produced by melt mixing and their use in blends with polyethylene. carbon (42):965-969.

Potschke P, Fornes T D, Paul D R (2002) Rheological behavior of multiwalled carbon nanotube/polycarbonate composites. Polymer 43(11): 3247-3255.

Rahatekar S S, Koziol K K K, Butler S A, Elliott J A, Shaffer M S P, Mackley M R, Windle A H. (2006). Optical microstructure and viscosity enhancement for an epoxy resin matrix containing multiwall carbon nanotubes. J Rheol 50(5): 599-610.

Singh S, Pei Y, Miller R, Sundararajan P R (2003). Long-Range, Entangled Carbon Nanotube Networks in Polycarbonate. Adv Functional Mater 13(11): 868-872.

Salvetat J P, Bonard J M, Thomson N H, Kulik A J, Forro L, Benoit W, Zuppiroli L (1999) Mechanical properties of carbon nanotubes. Appl Phys A 69(3): 255-260.

Shaqfeh E S G, Fredrickson G H (1990) The hydrodynamic stress in a suspension of rods. Phys Fluids A 2: 7–24.

Shenoy A V (1999) Rheology of Filled Polymer Systems. Springer,Verlag.

Sung Y T, Han M S, Song K H, Jung J W, Lee H S, Kum C K, Joo J, Kim W N (2006) Rheological and electrical properties of polycarbonate/multi-walled carbon nanotube composites. Polymer 47(12): 4434-4439.

Thostenson E T, Li C, Chou T -W (2005) Nanocomposites in context. Compos Sci Technol 65(3-4): 491-516.

Utracki L A (1986). Flow and flow orientation of composites containing anisometric particles. Polym Compos 7(5): 274-282.

Van Krevelen D W(1990) Properties of polymers. Elsevier Sci, Amsterdam.

Wu D, Liang W, Ming Z (2007) Rheology of multi-walled carbon nanotube/poly(butylene terephthalate) composites. J Polym Sci B 45(16): 2239-2251.

Wu D, Liang W, Yurong S, Ming Z (2007) Rheological properties and crystallization behavior of multi-walled carbon nanotube/poly(ε -caprolactone) composites. J Polym Sci B 45(23): 3137-3147.

Xiao K Q, Zhang L C, Zarudi L (2007) Mechanical and rheological properties of carbon nanotube-reinforced polyethylene composites. Compos Sci Technol 67(2): 177-182.

Xie X -L, Mai Y -W, Zhou X -P (2005).Dispersion and alignment of carbon nanotubes in polymer matrix: A review. Mater Sci Eng R: Rep 49(4): 89-112.

Xinfeng S, Hudson J L, Spicer P P, Tour J M, Krishnamoorti R, Mikos A G (2005) Rheological behaviour and mechanical characterization of injectable poly(propylene fumarate)/single-walled carbon nanotube composites for bone tissue engineering. Nanotechnology 16(7): 531-538.

Yu M -F, Lourie O, Dyer M J, Moloni K, Kelly T F, Ruoff R S (2000) Strength and breaking mechanism of multiwalled carbon nanotubes under tensile load. Science 287(5453): 637-640.

Zhang Q, Rastogi S, Chen D, Lippits D, Lemstra P J (2006) Low percolation threshold in single-walled carbon nanotube/high density polyethylene composites prepared by melt processing technique. Carbon 44(4): 778-785.

Chapter 6

Flow Induced Orientation of Multiwalled Carbon Nanotubes in Polycarbonate Nanocomposites: Rheology, Conductivity and Mechanical properties[*]

6.1. Presentation of the article

Followed by the first step and the rheological characterization of the nanotube structure, in this paper we studied the effect of nanotube alignment on both rheological and electrical conductivity percolation thresholds with the aim of finding a correlation between the rheological and electrical properties of the PC/MWCNT nanocomposites. Most specifically the influence of high shear conditions on the properties of the nanocomposites with a special focus on the electrical conductivity and structural changes in the nanotube networks was investigated. To this end, we systematically studied the percolation behavior as a function of nanotube orientation, varied from random to highly aligned by shearing the nanocomposites through different processing methods. The nanotube alignments were then studied through a variety of methods including SEM, TEM, Raman spectroscopy and rheological measurements. The results of this study showed that the nanotubes are preferentially aligned in the flow direction, particularly at large deformation rates. High degrees of nanotube alignment resulted in a significant increase in the rheological and electrical percolation threshold. The mechanical properties of the nanocomposites were also shown to depend on the processing conditions. Finally, we used a power-law type equation to correlate the percolation behavior and the nanotube alignment.

---

[*] ***Polymer.*** Submitted October 2009.

Flow Induced Orientation of Multiwalled Carbon Nanotubes in Polycarbonate Nanocomposites: Rheology, Conductivity and Mechanical properties

Samaneh Abbasi [1], *Pierre J. Carreau* [1], *Abdessalem Derdouri* [2]

1) CREPEC, Department of Chemical Engineering, Ecole Polytechnique Montreal, P.O.Box 6079, Station Centre-Ville Montreal QC, Canada

2) CREPEC, Industrial Materials Institute, National Research Council Canada, 75 de Mortagne, Boucherville, QC, Canada

6.2. Abstract

We investigated the effect of flow field and deformation rate on the nanotube alignment and on the properties of PC/multiwalled carbon nanotube nanocomposites. Samples of various MWCNT loadings were prepared by diluting a commercial masterbatch containing 15 wt % nanotubes using optimized melt-mixing conditions. Different processing conditions were then used to systematically change the degree of nanotube alignment, from random orientation to highly aligned. Morphological studies and Raman spectroscopy analysis revealed that the nanotubes are preferentially aligned in the flow direction, particularly at large injection or compression rates. Rheological measurements corresponding to high shear rate conditions showed drastic changes in the viscoelastic behavior. The complex viscosity significantly decreased and percolation threshold notably rose. High degrees of nanotube alignment also resulted in a significant increase in the electrical percolation threshold. The mechanical properties of the nanocomposites for different nanotube loadings were also shown to depend on the processing conditions, and somehow improved when the material was processed at higher rates. Finally, we used a power-law type equation to correlate the percolation behavior and the nanotube alignment. The estimated percolation threshold and the power index *n*, significantly increase with the degree of nanotube alignment as determined by Raman analysis.

Keywords: Multiwalled carbon nanotube, polycarbonate, alignment, morphology, Raman spectroscopy, rheological percolation, electrical percolation

6.3. Introduction

For the last two decades, carbon nanotubes (CNTs) have attracted a strong interest due to their unique electronic structure and extraordinary properties [1]. An extensive research effort has been devoted to the CNTs fabrication, characterization and development of applications. Their intrinsic structure, size scale and aspect ratio suggest a variety of applications in nanoelectronics, sensors and field emission as well as high performance nanocomposites.

Recently, considerable attention has been devoted to carbon nanotube / polymer composites from both processing and application points of view. Besides the individual properties of carbon nanotubes, numerous potential benefits are expected when they are employed as reinforcing agents in polymers. However, the efficiency of nanotubes to live up to their theoretical potential depends on a good dispersion within the host polymer. Three methods are commonly used to incorporate nanotubes into a polymer: solution mixing and film casting of suspensions of nanotubes in dissolved polymers, in-situ polymerization of nanotube-polymer monomer mixture and finally mixing of nanotubes in molten polymers. Melt mixing is the industrially preferred method in many cases because of its environmentally benign character, its versatility and its compatibility with current polymer processing techniques.

The intense interest in carbon nanotubes incorporated into polymeric materials stems from their potential to reach thermal, electrical and rheological percolations at relatively small concentrations [2-10]. At the percolation point, the formation of a filler network or interconnecting structure creates additional and large contributions to the nanocomposites properties. For sphere and ellipsoids fillers the percolation behavior is well understood [11], while the onset of percolation in the case of high aspect ratio fillers such as nanotubes strongly depends on their alignment. When the nanotubes are aligned in the polymer matrix the probability of tube-tube contacts decreases and consequently the percolation threshold raises [2, 12-14]. Accordingly, the full exploitation of the nanotube properties in polymer composite applications will require an exceptional control of the nanotube alignment in macroscopic parts.

It is well known that the microstructure of plastic parts is the result of complex changes imposed to the base polymer by the special processing conditions. Typical thermoplastic processing involves pellet melting, plastication, melt flow and pressurization and finally solidification from the molten state, either by crystallization or vitrification. A consequence of such processing methods is the stresses induced by combination of shear and elongational flow

field and cooling [15]. The complex thermo-mechanical history imposed on the polymer during processing leads to substantial spatial variations of chain orientation and the formation of a superstructure influenced by the local dynamics of the process. These effects result in anisotropy of the final physical properties particularly if the polymer is filled with solid particles of various shapes (glass or carbon fibers, clay or mica platelets, and carbon nanotubes or nanofibrils, etc.). The use of carbon nanotube based nanocomposites for commercial applications, thus, needs an understanding of how the processing conditions influence the nanotube networks and subsequently the nanocomposites properties.

Although considerable research has been conducted regarding the physical properties of carbon nanotube filled nanocomposites, including mechanical properties, electrical conductivity and rheological properties, only a few investigations have focused on the practical applications of nanocomposites in various industrial fields [13, 16-20].

Polycarbonate (PC), a typical amorphous polymer, is an important commercially available engineering thermoplastic for injection molding applications because of its excellent mechanical properties and processability. Recently, carbon nanotubes have been used as special filler to be incorporated into PC for stiffness reinforcement as well as thermal and electrical conductivities enhancement purposes [21-25].

It is the aim of this study to investigate the influence of high shear conditions on the properties of PC/ MWCNT nanocomposites with a special focus on the electrical conductivity and structural changes in the nanotube networks. To this end, we systematically studied the percolation behavior as a function of nanotube orientation, varied from random to highly aligned by shearing the nanocomposites through different processing methods.

It is still unclear how to truly and conveniently characterize the nanotube alignment in nanocomposites. Microscopic techniques are widely used to qualitatively determine filler alignment in the polymer matrix. X-ray diffraction (XRD) is also generally used to ascertain the degree of orientation. The orientation of the crystalline phase is well detected by using the X-ray method; however, DSC and XRD measurements showed that even after long time annealing there was no crystallization induced in the parts. Moreover, more than 50 wt% of MWCNT was required to attain the intensity to detect nanotube alignment [26]. Consequently, we used Laser Raman spectroscopy as an alternative method to quantitatively measure the degree of alignment. Laser Raman analysis is largely used for determining the degree of structural ordering in

molecules or the presence of defects in graphitic-like materials. This non-destructive technique also provides information on the microstructure of crystalline materials such as vibration of crystal lattices, electron structure and integrity of the crystal structure, etc. [27]. Polarized Raman spectroscopy was previously used on aligned MWCNTs to show that the observed relative intensities of the Raman *D* and *G* bands are sensitive to the orientation of the nanotubes [33]. In polymer nanocomposites, Raman spectroscopy was applied in order to get information of the MWNT orientation, alignment and crystallinity [13, 17].

With the aim of finding a correlation between the rheological and electrical properties of the PC/MWCNT nanocomposites, we studied the effect of nanotube alignment on both rheological and electrical conductivity percolation thresholds. Furthermore, we characterized the mechanical properties of the microinjected parts to have an idea on how polymer processing affects the mechanical structure of the nanocomposites. We optimized the nanocomposite preparation using various characterization methods. As nanotubes intertwine into agglomerates that are difficult to disperse we used a polymer/carbon nanotube masterbatch and diluted it to the required concentrations by adding the neat polycarbonate. This insured consistent and reproducible results.

6.4. Experimental

6.4.1. Materials

A masterbatch of 15 wt% MWCNT in PC was purchased from Hyperion Catalysis International, Cambridge, MA. According to the supplier, the carbon nanotubes are vapor grown and typically consist of 8-15 graphite layers wrapped around a hollow 5 nm core [10]. The diameter range was stated to vary from 15 to 50 nm and the length range of 1-10 μm as was confirmed by TEM characterization. The masterbatch was diluted with a polycarbonate (Calibre 1080) supplied by Dow Chemical to prepare nanocomposite samples of various loadings. This PC is not necessarily the same as the polycarbonate found in the masterbatch. Considering the small quantity of masterbatch used to prepare the nanocomposites, the original PC of the masterbatch is only a small fraction of the nanocomposites and does not significantly affect the results.

6.4.2. Nanocomposite preparation and molding

The composites were produced by melt mixing the masterbatch with the neat PC. Prior to mixing, all materials were dried for a minimum of 4h at 120 ^{o}C. Eight different composites with MWCNT contents between 0.5 and 15 wt% MWCNT were prepared using a 18 mm diameter twin-screw extruder, Leistritz ZSE 18HP, operating at 100 rpm and 210 ^{o}C under vacuum. Compression molding, conventional injection molding, microinjection molding and microinjection-compression molding were then employed to apply different levels of shear or deformation rate on the nanocomposites. Prior to each processing, the materials were dried under the conditions previously mentioned. Compression molding of dried nanocomposites were done using a Carver laboratory press, model 3912, operated manually at 270 ^{o}C. The disk shaped molded samples of 60mm diameter and 1.5 mm thickness were then cooled down to room temperature. For the conventional injection molding we used a Sumitomo SE50S electrical 50 ton injection molding machine to mold standard dog-bone shaped tensile test specimens of 150 mm in total length, with a gage section 10 mm wide by 4 mm thick by 80 mm long. Injection was done at an average barrel temperature of 300 ^{o}C under a pressure of approximately 100 MPa while injection speed was constant at 400 mm/s. The mold temperature was kept constant at 80 ^{o}C and cooling time was set to 10 s. Microinjection molding was done using a Battenfeld Microsystem 50 micromolding machine operating at the same processing conditions as the conventional one. To investigate the effect of mold geometry, two different mold cavities were used: one having a dog-bone shape of 15 mm long, with the center section of 1 mm wide by 0.78 mm thick by 4.3 mm long, gated at one end, and the other a disk shape of 25 mm in diameter and 1mm thick, gated at the centre. To examine the effect of the injection speed two additional injection speeds were also used in the case of the dog-bone samples: 200 and 800 mm/s. Finally, microinjection-compression molding was employed to evaluate the effect of applying a compression step at the end of the injection phase on the part properties, using the centrally gated disk cavity with the same dimensions as described before. The process consisted of injecting the melt into the cavity, while the mold was not totally closed. This leads to an initial cavity filling under a lower pressure than if the mold was closed, as in conventional injection molding. After the injection stage, the mold was closed to compress the melt and to completely fill the cavity. The operating conditions in this case are the same as microinjection molding using only 400

mm/s for the injection speed. The gap between the mold plates was about 1.2 mm and the mold closing speed used in this experiment was 1.5 mm/s.

6.4.3. Morphological characterization

The morphology of nanocomposites was studied through scanning and transmission electron microscopy (SEM and TEM) and atomic force microscopy (AFM). For SEM we used a high resolution Hitachi S-4700 microscope while for AFM we utilized a multimode Veeco scanning probe in tapping mode. Both SEM and AFM were done on ultramicrotomed surfaces of samples that were cut with a diamond knife at room temperature. SEM samples were coated with a vapor deposit of platinum for 25 s. TEM was done on ultrathin sections of nanocomposites using a Hitachi HD-2000 microscope. For injection molded samples, the specimens were cut both parallel and perpendicular to the flow direction.

6.4.4. Raman spectroscopy

Raman spectra were collected using a Renishaw spectrometer equipped with an inVia Raman microscope fitted with a 20x objective. The samples were excited using a NIR laser (785 nm) with a grating of 1200 g/mm in a regular mode. Measurements were carried out at two different orientations of the incident laser beam with respect to the flow direction in the samples and the polarization direction (Fig. 6.1). In the first configuration (Fig. 6.1a), the flow direction was parallel (0°) to the direction of the polarized beam; in the second one (Fig. 6.1b), it was perpendicular (90°). The MWCNT alignment in the composite was determined by comparing the spectra for parallel and perpendicular directions.
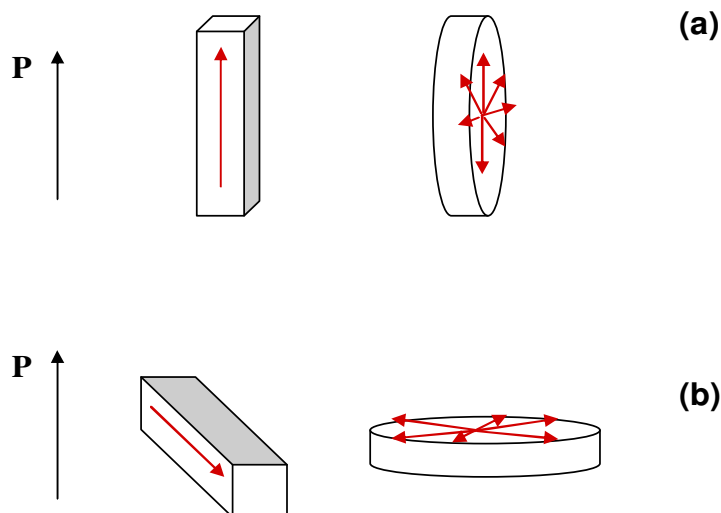
Figure 6.1: Schematic for Raman spectroscopy. Characteristic scattering configurations for the Raman spectroscopic measurements: (a) Parallel position of specimen, corresponding to 0° angle between polarization direction(P) and flow direction (red arrow); (b) Perpendicular position of specimen, corresponding to 90° angle between polarization direction(P) and flow direction (red arrows)

6.4.5. Rheological measurements

All the rheological measurements were carried out using a stress-controlled rheometer (CSM rheometer of Bohlin Instruments) equipped with a 25mm parallel plate geometry under nitrogen atmosphere. Prior to measurements, the samples were dried for a minimum of 4 h at 120 °C. To investigate the viscoelastic properties of the nanocomposites after processing, molded disks by compression, microinjection-compression and microinjection were used. They were put in the rheometer with precaution to avoid the formation of any bubbles or surface defects. Small amplitude oscillatory shear (SAOS) tests were carried out between 0.06 and 200 rad/s in the linear viscoelastic regime. This regime was established in the standard way by measuring the modulus at constant frequency (10 rad/s) and increasing strain magnitude. Further, long time measurements (up to 3h) were conducted to investigate the thermal stability of the nanocomposite samples. We assumed that the particle sizes were sufficiently small compared to the gap; however, the absence of apparent slip at the wall has been ascertained by varying the gap from 0.5 to 1.5 mm. The differences were found to be insignificant, less than the reproducibility of the data estimated to be within 3.5% for all the frequency sweep tests conducted with the various nanotube loadings.

In addition, the effect of high shear on the microstructure of the nanocomposites was evaluated by subjecting each sample to a high shear stress for various periods of time at 300 $^\circ$C (injection temperature). SAOS measurements were then performed without any rest time between the preconditioning step and the SAOS test.

Finally a capillary rheometer (Rosand) with a capillary of 32mm length and 1mm diameter was used to determine the steady-state viscosity as a function of shear rate for the neat polymer and nanocomposites.

6.4.6. Electrical conductivity measurements

The volume resistivity of the PC/MWCNT nanocomposite samples was determined by measuring the DC resistance across the thickness of compression molded disks using a Keithley electrometer model 6517 equipped with a two probe test fixture. This equipment allows resistance measurements up to 10^{17} Ω. The level of applied voltage, adapted to the expected resistance, was in the range of 1000 V for the neat PC and samples containing up to 1 wt% MWCNT and 100 V for samples with 2 wt% and more MWCNT. However, since for the more conductive samples, the accuracy of this equipment failed, samples with more than 2wt% MWCNT, were tested using the more adequate Keithley electrometer model 6220 connected to a current source (Aligent 34401 A , 6 ½ Digit Multimeter). This electrometer can be used only for semi-conductive materials. For each sample the *I-V* curve was obtained and the sample resistance was determined from the slope of the curve. The resistance was then converted to volume resistivity, ρ_v, using the formula

$$\rho_v = AR_v / D \tag{6-1}$$

where *A* is the contact surface area, *D* is the thickness of the sample, and R_v is the measured resistance. The electrical conductivity (σ) of the nanocomposites is the inverse of volume resistivity. Prior to measurements all samples were dried for a minimum of 4 h at 120 $^\circ$C.

6.4.7. Mechanical properties

An Instron Micro Tester model 5548 was used to measure the tensile strength, modulus and elongation at break of nanocomposites using microinjected tensile bars having a gage length of 4.3 mm. The tests were performed at room temperature using a crosshead speed of 50 mm/min, based on ASTM D638, and data acquisition rate of 13 points per second. The tensile strength and

elongation at break could be directly obtained from the stress-strain curves. To obtain the elastic modulus, a linear regression technique was utilized to define the slope of the stress-strain curve in the initial region before yield. All the reported values were calculated as average over six specimens for each composition and each condition with a maximum deviation of ±8%.

6.5. Effective shear rate estimation

Polymer processing proceeds generally under a complex flow field, which is a combination of elongational and shear flows. Injection molding is one of the most complex nanisothermal processes with a combination of different flow fields. The conditions are more complex in the case of microinjection molding particularly microinjection of disk shaped samples where the effect of elongational flow is more pronounced. Another complexity arises from the behavior of polymer melt at the relatively high shear rate of these processes and at different planes from the surface to the core of the sample. Since the accurate modeling of the processes is not the main idea of this study we made some simple assumptions to estimate the effective shear rates encountered in the processes used in this work and to have a better understanding of the effect of the flow field on the nanocomposite properties. Although the elongational flow could play an important role and affect the nanotubes alignment and polymer chains orientation especially for viscoelastic materials, the following estimates are based on the assumption that for these flows the fluid is purely viscous.

The flow geometries in compression molding, conventional injection molding, microinjection molding and microinjection-compression molding are illustrated in Figure 6.2. In principle, these problems should be solved using nonisothermal viscoelastic models, but this would result in rather complicated flow problems requiring the use of sophisticated software packages. Useful approximations, however, are obtained by considering isothermal Newtonian or power-law models and assuming the same orientation profile from the surface to the core of the samples.
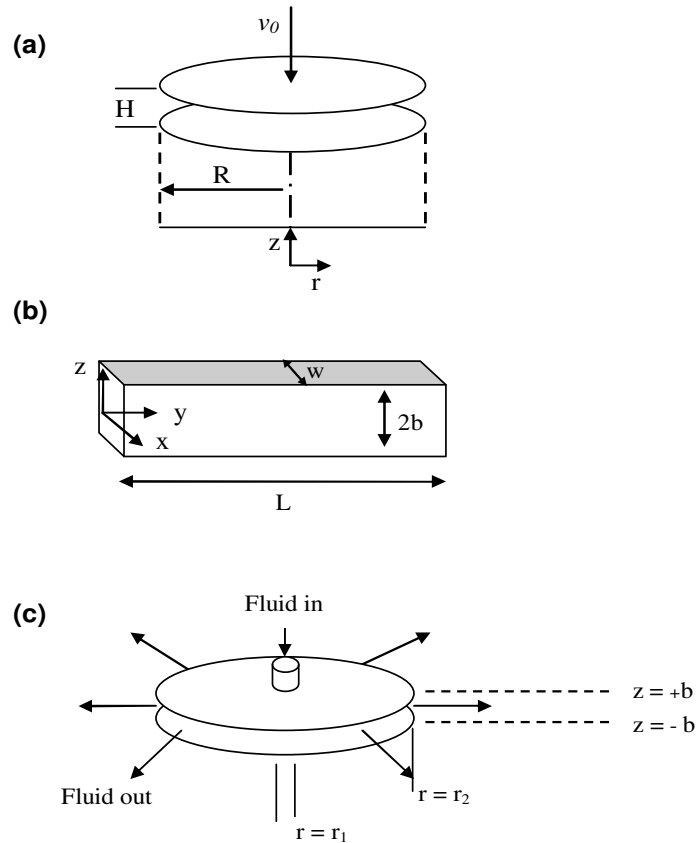
Figure 6.2: (a) Squeezing flow in compression molding between two parallel disks (b) longitudinal flow of conventional and microinjection molding of tensile bar (c) radial flow of microinjection molding of disk shaped sample

The calculations are provided for the 5 wt % MWCNT/PC nanocomposites that obey the following expression:

$$\eta = m|\dot{\gamma}|^{n-1} + \eta_\infty \qquad (6\text{-}2)$$

where m and n are the power-law parameters and η_∞ is the limiting viscosity at high shear rate. This expression contains two terms: the first term is a power-law viscosity and the second term is a Newtonian viscosity. At low shear rate the viscosity obeys a power-law behavior whereas at high shear rate the viscosity tends towards a constant value.
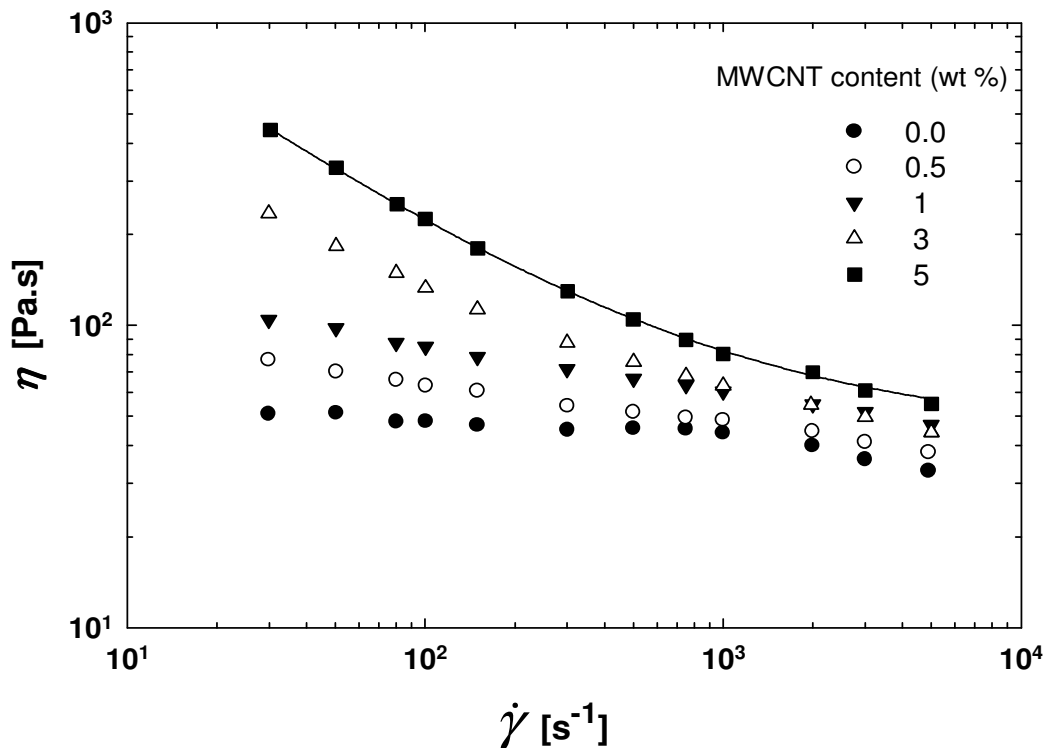
Figure 6.3: Viscosity versus shear rate for PC/MWCNT nanocomposites at 300 $^{\circ}$C. The line shows the best fit using Eq. 6-2

In a recent article, Abbasi et al. [34] investigated the effect of pre-shearing on the viscoelastic properties of PC/MWCNT nanocomposite samples, at high and low stresses. They pointed out that a high degree of nanotube alignment is obtained when high nanotube loadings are used. Due to the nanotubes alignment, the Cox-Merz rule could not be applied to the dynamic viscosity measurements to determine the power-law parameters of equation 6-2. Steady shear viscosity measurements were therefore carried out for various nanotube loadings at 300 $^{\circ}$C (injection temperature) using the capillary rheometer and the results are shown in Figure 6.3. As observed for the complex viscosity data reported in [34], the viscosity increases markedly with nanotube loading and the suspensions become more shear-thinning. However, the shear viscosity values of Figure 6.3 are considerably smaller than those reported in [34] for the complex viscosity due to nanotube alignment in shear flow as shown below. The 5 wt % nanocomposite data was fitted using the power-law equation above, resulting in the following parameters values: $m = 3.77 \times 10^{3}$ Pa.s^{n}, $n = 0.34$ and $\eta_{\infty} = 40$ Pa.s. The fit is shown to be excellent.

6.5.1. Compression molding

In compression molding (Fig. 6.2a) a blank of polymeric material is assumed to fill completely the region between two circular parts of the disk shaped mold of radius R and it can only flow on squeezing along the r direction. The bottom disk is fixed and the upper disk is made to approach the lower one very slowly with a constant speed of v_0 starting from an initial height of H. A simple form of the velocity profile for this problem is given by [35]:

$$v_r = \frac{1}{2\eta_e}\left(\frac{dp}{dr}\right)z(z-H)$$

(6-3)

where η_e is the effective viscosity. The pressure profile is as follows:

$$p = p_{atm} + \frac{3\eta_e v_0 R^2}{H^3}\left[1-\left(\frac{r}{R}\right)^2\right]$$

(6-4)

The effective rate of deformation can be calculated from the velocity profile:

$$\dot{\gamma} = \sqrt{2\left(\frac{\partial v_r}{\partial r}\right)^2 + 2\left(\frac{v_r}{r}\right)^2 + \frac{1}{2}\left(\frac{\partial v_r}{\partial z}\right)^2}$$

(6-5)

Combining Eqs. 6-3, 6-4 and 6-5, the following expression for the effective rate of deformation is obtained:

$$\dot{\gamma} = \frac{3v_0}{H^3}\sqrt{4z^2(z-H)^2 + \frac{r^2}{2}(2z-H)^2}$$

(6-6)

For a power-law fluid the velocity profile is as follows [36]:

$$v_r = \frac{H^{1+1/n}}{1+1/n}\left(-\frac{1}{mr^n}\frac{dp}{dr}\right)^{1/n}\left[1-\left(\frac{z}{H}\right)^{1+1/n}\right]r$$

(6-7)

with the pressure profile as:

$$p = p_{atm} + \frac{v_0^n}{H^{2n+1}}\left(\frac{2n+1}{2n}\right)^n\left(\frac{mR^{n+1}}{n+1}\right)\left[1-\left(\frac{r}{R}\right)^{n+1}\right]$$

(6-8)

The effective rate of deformation can then be obtained using Eq. 6-5.

The press can operate at speeds between 4 and 34 mm/s. Assuming H = 1.5 mm and R = 15 mm, the $\dot{\gamma}_e$ values at $z = H/4$ and $r = R/2$ as a typical point is obtained for the whole range of operating velocity (Table 6.1).

6.5.2. Injection molding

Conventional injection and microinjection molding of tensile bar

We consider the flow of polymer melt into thin rectangular cavities as illustrated in Figure 6.2b. The velocity profile for a Newtonian fluid is [37]:

$$v_y = \frac{b^2 \Delta p}{2l\eta_e}\left[1-\left(\frac{z}{b}\right)^2\right]$$

(6-9)

where Δp is the pressure difference between p_0, the pressure at $y = 0$ or injection pressure, and p_{atm}. The shear rate is obtained from the velocity profile as follow:

$$\dot{\gamma} = \left|\frac{\partial v_y}{\partial z}\right|$$

(6-10)

The effective shear rate is then calculated using the following equation for a Newtonian fluid of η_e:

$$\dot{\gamma}_e = \frac{\Delta p}{l\eta_e}z$$

(6-11)

For a power-law fluid the effective shear rate can be obtained from the following equation:

$$\dot{\gamma}_e = \left|\left(\frac{\Delta p}{ml}z\right)^{1/n}\right|$$

(6-12)

For the conventional injection molding case, we use p_0 = 100 MPa, b = 2 mm and L = 80 mm to calculate the effective shear rate at $l=L/2$ and $z = b/4$ for the 5 wt % MWCNT/PC nanocomposites. For microinjection molding, an estimated effective shear rate can be obtained taking p_0 = 100 MPa, b = 0.39 mm and L =4.3 mm, $l=L/2$ and $z = b/4$. The values are reported in Table 6.1.

Microinjection and microinjection-compression molding of disk

The radial flow of the polymeric melt between two disks is considered in this section (Fig. 6.2c). For a Newtonian melt, the velocity profile in this case is as follows [35, 37]:

$$v_r = \frac{\Delta p b^2}{2\eta_e r \ln(r_2/r_1)} \left[1 - \left(\frac{z}{b}\right)^2 \right] \tag{6-13}$$

Using Eq. 6-5, the effective shear rate is estimated from the following equation:

$$\dot{\gamma}_e = \frac{\Delta p b^2}{2\eta_e r \ln(r_2/r_1)} \sqrt{\frac{2}{r^2}\left[1-\left(\frac{z}{b}\right)^2\right]^2 + \frac{2}{b^2}\left(\frac{z}{b}\right)^2} \tag{6-14}$$

For a power-law fluid there is no analytical solution for this case. Neglecting the contribution of the elongational component of the flow, the following simplified expression is obtained [38]:

$$v_r = \frac{1}{r}\left(\frac{n}{n+1}\right)\left[\frac{(1-n)\Delta p}{(r_2^{1-n}-r_1^{1-n})}\frac{b^{n+1}}{m}\right]^{1/n}\left[1-\left(\frac{z}{b}\right)^{(n+1)/n}\right] \tag{6-15}$$

The effective shear rate is then obtained using Eq. 6-5. For $p_0 = 100\text{MPa}$, $2b = 1$ mm, $r_1 = 0.75$ mm and $r_2 = 12.5$ mm the $\dot{\gamma}_e$ values of microinjection molding of disk at $z = b/2$ and $r = (r_2-r_1)/2$ are reported in Table 6.1.

In microinjection-compression, each phase (injection and compression phases) features a specific shear rate. However, the applied shear rate in the second phase (compression) is almost negligible due to very low closing speed. The effective shear rate in injection phase can be calculated using Eqs. 6-13 &6-14. The only difference with microinjection of the disk is the injection pressure that is about 15 MPa in this case. The $\dot{\gamma}_e$ values at $z = b/2$ and $r = (r_2-r_1)/2$ of the disk are then obtained (Table 6.1).

Table 6.1. Effective shear rates encountered in the processes and Raman intensity ratios parallel/perpendicular to the flow direction

	Effective shear rate $\dot{\gamma}_e$ (s^{-1})		Raman intensity ratio parallel/ perpendicular		
	Newtonian model	Power-law model	$D_{\Pi}/D_{\perp}$	$G_{\Pi}/G_{\perp}$	$(D/G)_{\Pi}/(D/G)_{\perp}$
Compression molding (disk)	14.5-122	1.8-20	1.03	1	1.03
Microinjection- compression molding (disk)	4×10^3	1.2×10^5	1.33	1.2	1.08
Microinjection molding (disk)	2.7×10^4	3.2×10^7	1.52	1.37	1.1
Conventional injection molding (dog-bone)	3.1×10^4	2.6×10^7	1.71	1.55	1.1
Microinjection molding (dog-bone)	1.1×10^5	1.8×10^9	1.95	1.75	1.11

We note that the effective rate calculated for the different processes varies from a very low value of 1.8 s^{-1} for compression molding to 1.8×10^9 s^{-1} for microinjection of dog-bone samples. However, the values of $\dot{\gamma}_e$ calculated for the last three injection processes using the power-law expression are way excessive. Referring to Figure 6.3, the shear viscosity of the 5 wt % nanocomposite reaches the high shear plateau, η_{∞}, for $\dot{\gamma}\approx10^4$ s^{-1}. Hence, the calculations based on the Newtonian model with $\eta_e = \eta_{\infty} = 40$ Pa.s are more reasonable except possibly for the compression molding for which the shear rate in more in the power-range. The Raman intensity values of Table 6.1 are discussed below in light of the effective shear rate.

6.6. Experimental results

6.6.1. Morphology

SEM micrographs, taken at the surface of a compression molded sample (the part produced under the lowest shear rate) and a microinjected sample (the part produced under the highest shear rate), are shown in Figure 6.4 for 5 wt % nanocomposites.
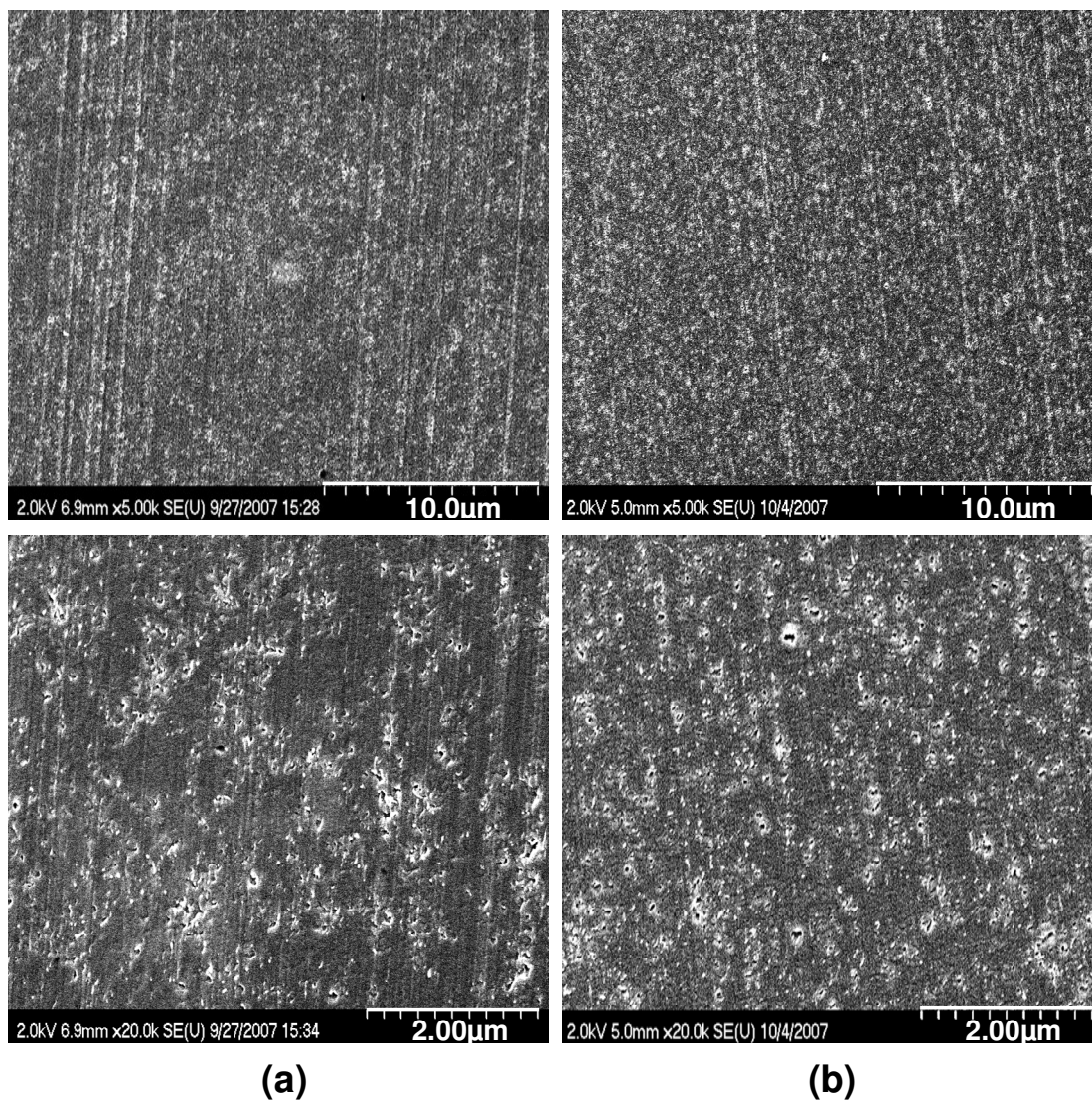
Figure 6.4: SEM micrographs of crayon surfaces of PC / 5wt% MWCNT nanocomposites processed in (a) compression molding and (b) microinjection molding. The top and the bottom micrographs are related to the low and high magnification, respectively

It can be seen that there is no preferred orientation within the nanocomposite in the compression molded sample (Fig. 6.4a). However, in the microinjected sample (Fig. 6.4b), only the ends of the nanotubes, as bright spots, can be observed in the micrographs. Since the injected specimens in this case were cut perpendicularly to the flow direction, seeing only the end of the nanotubes is an indication that the nanotube orientation is in the shear flow direction.

(a)

(b)
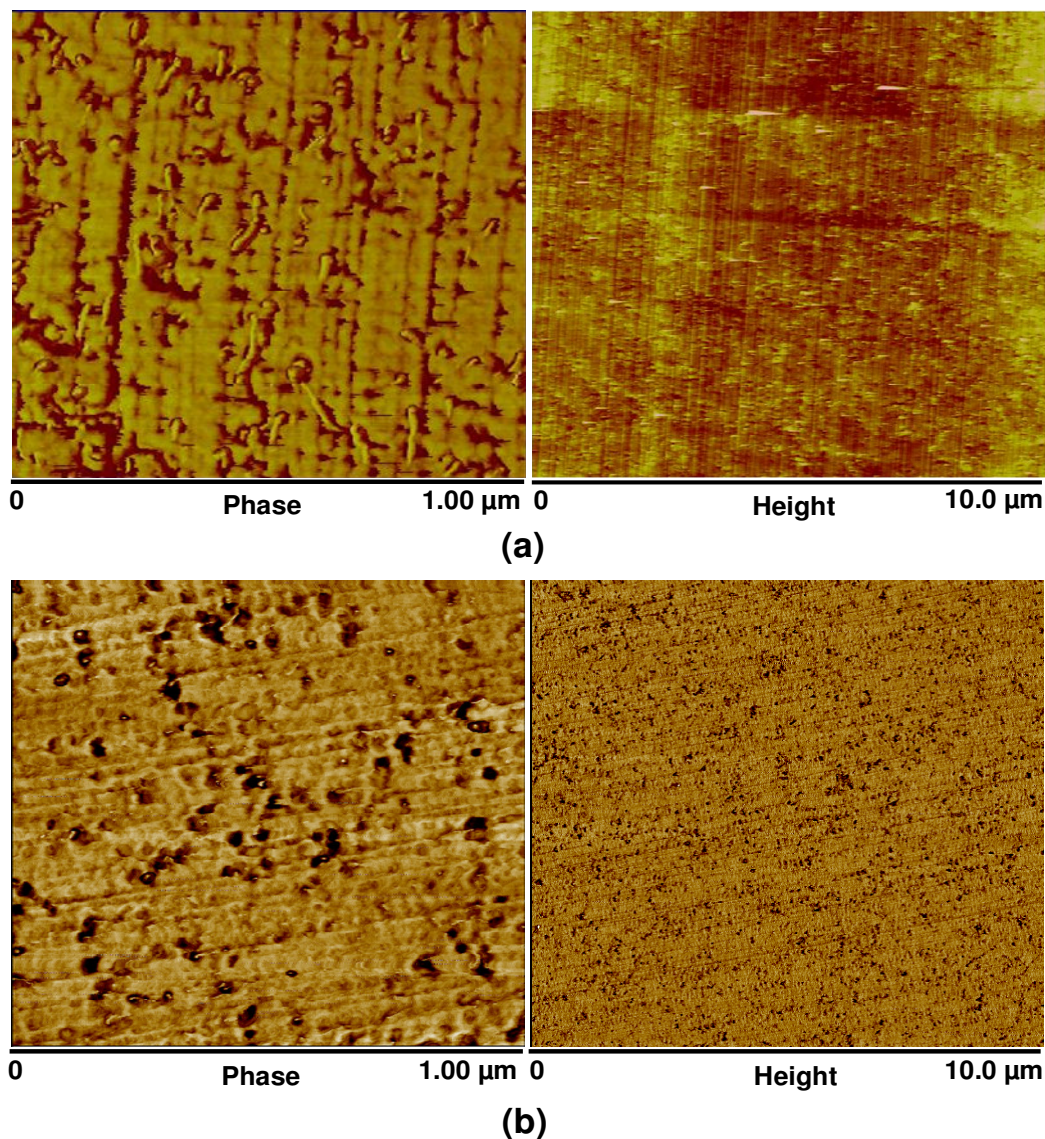
Figure 6.5: AFM micrographs of crayon surfaces of PC / 5wt% MWCNT nanocomposites processed in (a) compression molding and (b) microinjection molding. The left and the right micrographs are related to the phase and height modes, respectively

The nanotube orientation can be seen more clearly in AFM micrographs. For the compression molded sample (Fig. 6.5a) segments of length of some nanotubes can be observed in the phase mode image, while for the microinjected sample (Fig. 6.5b), cut perpendicularly to the flow direction, only black spots, representing the nanotube ends, are seen. The SEM and AFM micrographs show not only differences in orientation of the nanotubes between the samples made by the two molding processes, but they also indicate that their dispersion within the PC matrix is quite good, particularly in the case of the microinjected samples. The drastically high deformation rates encountered in microinjection molding contribute strongly not only to the nanotubes alignment but also to their distribution within the polymer matrix. The nanotubes diameter derived from the scale of the AFM micrographs is about 15 nm, remarkably within the range of the information given by the masterbatch supplier, indicating that the nanotubes are most probably individually dispersed.

To help understand more the effect of the shear flow on the nanotube alignment, TEM micrographs of samples prepared using different processing methods are shown in Figure 6.6. In the case of the injected samples, the images were all taken from thin sections cut along the flow direction. For the compression molded sample (Fig. 6.6a) the micrograph does not indicate any preferential orientation. On the other hand, the nanotubes are somehow oriented in the case of the microinjection-compression molded samples (Fig. 6.6b); however, it is still far from a perfect orientation and we can see isotropy in the system. Figure 6.6c shows the micrograph of a sample prepared by conventional injection molding; a clear orientation of the nanotubes along the length axis can be seen. The highest degree of orientation is obtained for microinjection molding where the nanotubes are well aligned and most of them are perfectly stretched along their length axis (Fig. 6.6d). Considering the fact that the nanotubes are often strongly entangled, a few nanotubes remain oriented transversely (perpendicular to the flow direction) after injection.
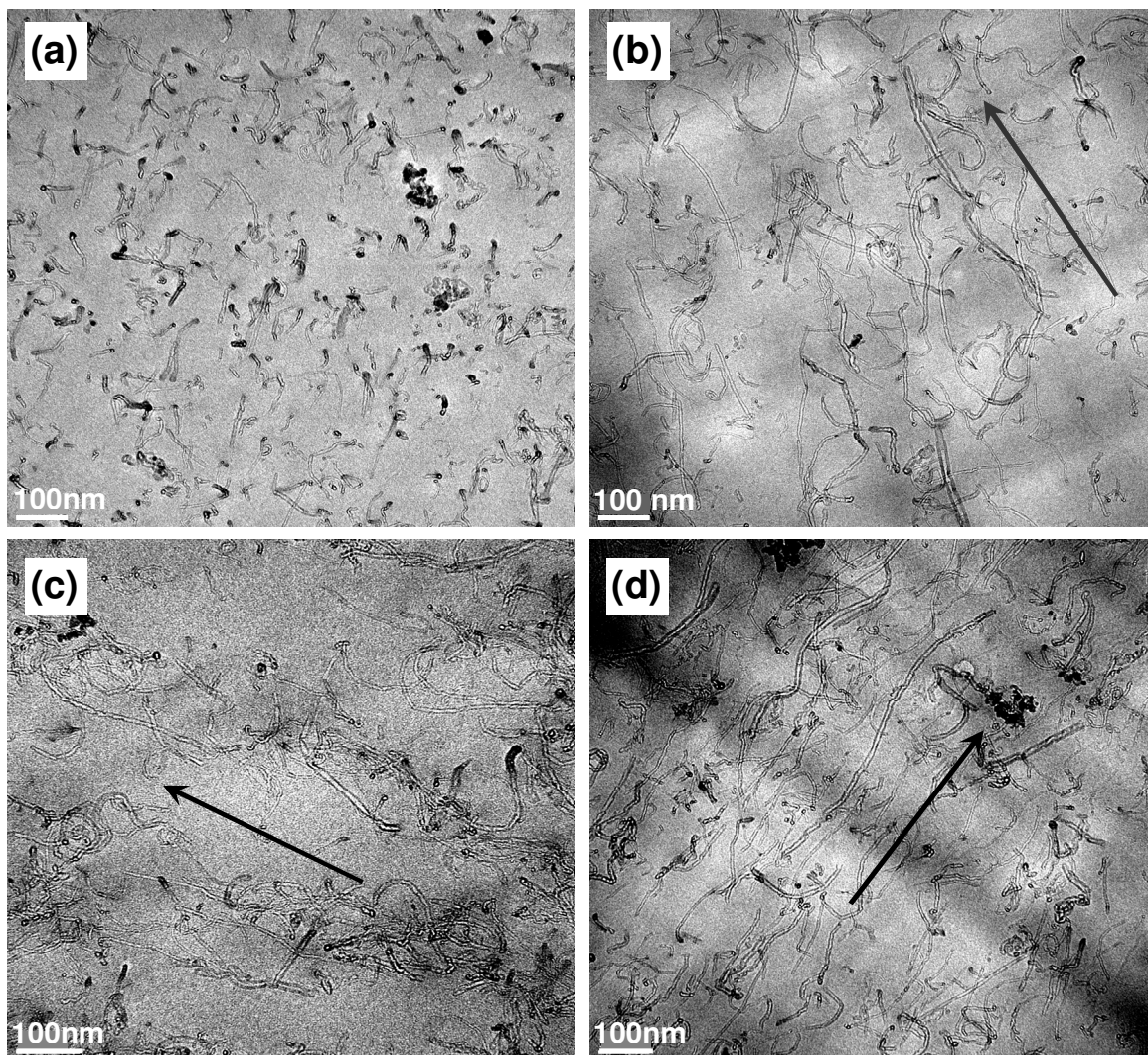
Figure 6.6: TEM micrographs of thin sections of PC / 5wt% MWCNT nanocomposites prepared along the flow direction. Samples were (a) compression molded, (b) microinjection-compression molded (c) conventional injection molded (d) microinjection molded. Arrows indicate the flow direction

The histograms of the nanotube length distribution are reported in Figures 6.7a-d. By nanotube length we mean the end-to-end distance of each segment of nanotube as it can be observed in the micrographs. Since the samples shown in Figure 6.6 were cut along the flow direction using a very sharp diamond knife, most nanotubes that are randomly located in the samples are sectioned. However, well flow oriented nanotubes were parallel to the cutting direction and therefore a large part of their full length is observed in the micrographs. For compression molded samples (Fig. 6.7a) most of the nanotubes have lengths less than 100 nm.

For compression microinjected samples (Fig. 6.7b) the observed nanotube length is longer and there are some exceeding 200 nm. For conventional injection (Fig. 6.7c) most of the nanotubes have lengths in the range of 200-400 nm and in the case of microinjection molding (Fig. 6.7d) the nanotubes length is in the range of 200-500 nm and in some cases reaches 700 nm. Although these values are still well below the initial length of nanotubes (1-10 μm, as specified in the material section) these values are a good indication of a high degree of nanotube alignment in microinjected parts.
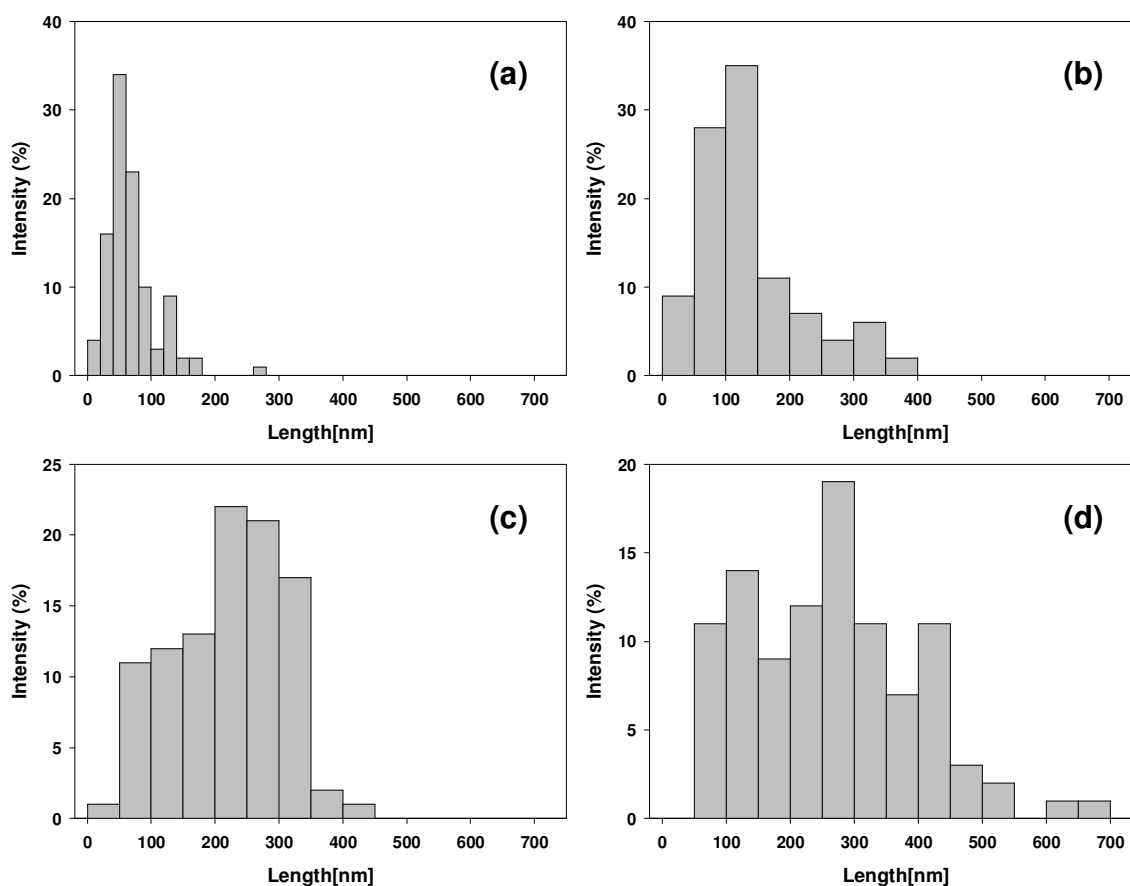
Figure 6.7: Histogram of nanotube length distribution for samples prepared in (a) compression molding (b) microinjection-compression molding (c) conventional injection molding (d) microinjection molding

6.6.2. Raman spectroscopy

Raman spectroscopy was used to further investigate the MWCNT alignment within the polycarbonate matrix. This is a non-destructive spectroscopy technique, which relies on the inelastic scattering of infrared light by molecules upon returning to their lower energy level after excitation. Depending on the frequency of the light used, Raman bands with different intensities are produced by vibration of various active groups within the polymer chains. The vibrational characteristics of these groups can then be used to determine and identify the polymer structure [28]. Carbon nanotubes show resonance-enhanced Raman scattering effects when a visible or near infrared laser is used as the excitation source. Both single walled carbon nanotubes (SWCNTs) and MWCNTs feature bands located in the higher wavenumber region over 500 cm^{-1}; however, Raman bands appearing in the low wavenumber region between 100 and 400 cm^{-1} (known as radial breathing modes or RBM) are a unique characteristic of SWCNTs [29] and are not generally observed for MWCNTs. The Raman spectra of the as-extruded neat polycarbonate and 5 wt% PC/MWCNT nanocomposites are shown in Figure 6.8. As it can be observed, the most important Raman bands of polycarbonate are located in the range of $500\text{-}1800 \text{ cm}^{-1}$ as assigned by Lee et al. [30]. Contrary to carbon nanotubes, most polymers including polycarbonate do not show a resonance enhancement effect [27]. In fact, the large differences between the intensity of the nanotube peaks and those arising from a polymeric matrix make the Raman spectroscopy an ideal technique for the study of nanotubes orientation.

As Figure 6.8 shows clearly, the Raman bands of polycarbonate almost vanish by incorporation of nanotubes into the matrix. Two important features in the Raman spectrum of MWCNTs are the *D* band (disorder band), located between $1330\text{-}1360 \text{ cm}^{-1}$ and the *G* band (graphite band or TM-tangential mode) located around 1580 cm^{-1}. These bands are clearly observed in the spectrum of PC/MWCNT of Figure 6.8. The *D* band originates from the sp^2 hybridized (graphite-like carbon atoms) disorder in the graphitic structure, and is the most sensitive Raman peak to the nanotube alignment. The *G* band, assigned to the in-plane vibration of the graphitic wall, is less sensitive to orientation [31]. Another Raman band in the spectrum of carbon nanotubes, named *G'*, is located at $\sim 2700 \text{ cm}^{-1}$ and is also not sensitive to the nanotube alignment [32].
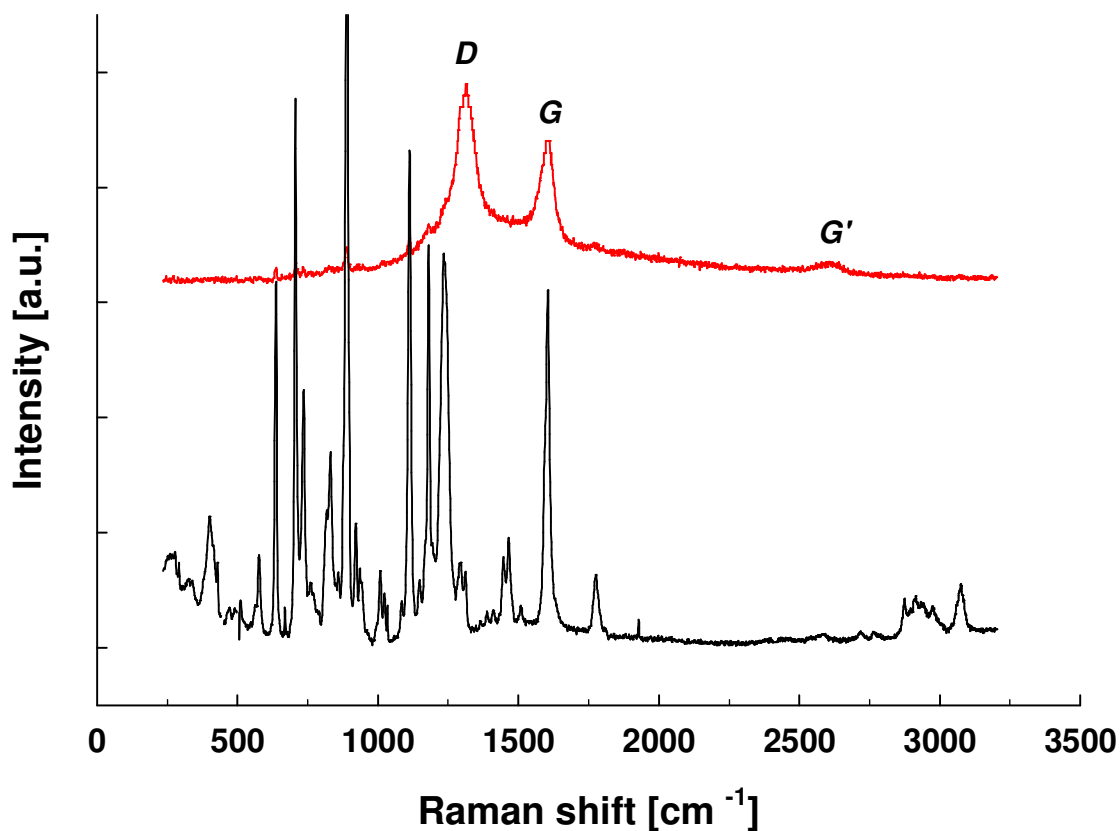
Figure 6.8: Raman spectra of neat polycarbonate (black) and PC / 5wt% MWCNT (red)

The intensity ratios $D_{\Pi}/D_{\perp}$ and $G_{\Pi}/G_{\perp}$ parallel/perpendicular to the flow direction were used to assess the degree of nanotube alignment. Raman spectra of PC/5wt% MWCNT are shown in Figure 6.9 for compression molded samples or samples produced under the lowest shear or deformation rate (Figs. 6.9a and b) and dog-bone shaped microinjected samples or the samples produced under the highest shear rate (Figs. 6.9c and d).
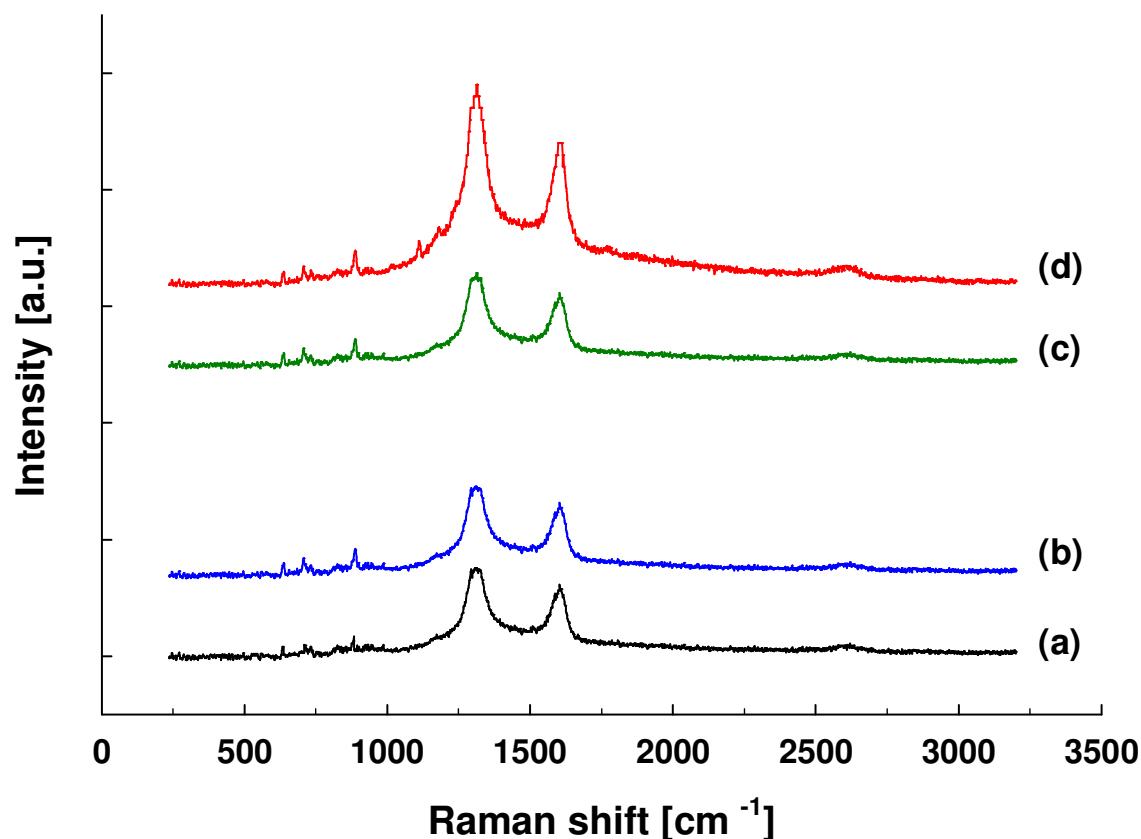
Figure 6.9: Raman spectra of PC / 5wt% MWCNT nanocomposites: bottom two; compression molded samples, top two, microinjected samples; (a) and (c) perpendicular, (b) and (d) parallel arrangements

For the compression molded samples, parallel (Fig. 6.9b) and perpendicular (Fig. 6.9a) spectra are almost the same and there are no significant differences between the intensities of the peaks. The $D_{\Pi}/D_{\perp}$ and $G_{\Pi}/G_{\perp}$ parallel/ perpendicular intensity values are therefore close to unity indicating that there is no preferential nanotube alignment in the polycarbonate matrix[10,39]. For microinjected samples, however, there are significant differences between the parallel (Fig. 6.9d) and perpendicular (Fig. 6.9c) Raman spectra. The intensities of both bands, D and G, are much larger in the parallel spectra.

The results obtained from the Raman spectra of the nanocomposites prepared under various levels of deformation rate (i.e. for different polymer processing conditions) are summarized in Table 6.1. From top to bottom, both ratios increase, demonstrating that the lowest nanotube alignment is found in the compression molded samples and the highest one in the dog-bone

shaped microinjected samples. These results are completely in agreement with the morphological analysis and clearly show that the different levels of shear rate applied to the nanocomposites result in significant differences in the nanotube alignment (Table 6.1). It is shown that when using microinjection molding, the applied shear rate is much larger than in conventional injection molding (Table 6.1), for the same injection speed and cavity shape. Therefore, nanotubes are well aligned in the longitudinal flow field of the microinjection mold of dog-bone shaped (tensile bar) and consequently the highest intensity ratios for both *D* and *G* bands are achieved in this case. In conventional injection molding, the lower level of shear rate results in a lower nanotube alignment even in the longitudinal flow field of the dog-bone shaped cavity and, accordingly, lower intensity ratios of Raman *D* and *G* bands are obtained. On the other hand, the nanotubes alignment decreases noticeably in the case of radial flow of the disk shaped cavity with respect to the longitudinal flow of the tensile bar cavity. Although the applied shear rate for this process is relatively the same as that in conventional injection, the nanotube alignment in this case is lower than for conventional injected tensile bars. This is due to the cavity being centrally gated, elongational flow is dominant at the gate (divergent flow) causing the nanotubes to first orient transversely (perpendicular to the main radial flow direction) in the core zone. Near the wall, shear flow dominates and tends to orient the nanotubes in the radial main flow direction. For dog-bone samples, nanotubes are mostly subjected to shear deformation and then are oriented in the flow direction.

Microinjection-compression molding proceeds in two phases, one with a high shear rate during injection and one with low shear rate during compression. Due to the high level of shear rate, the nanotubes are well aligned at the end of the first step or injection phase. However, during the compression phase, which can be assimilated to a squeeze flow, elongational flow perpendicular to the radial direction can be significant and diminish the effects of the first step (injection) on the nanotube alignment. As a result, a more isotropic structure is formed. Consequently, microinjection compression molding produces parts with the lower intensity ratios for the Raman *D* and *G* bands.

Finally the lowest level of nanotube alignment is obtained when a circular disk is produced using manual compression molding for which of the radial flow proceeds at extremely low deformation rate.

It is worthy to mention that the highest values of $D_\Pi/D_\perp$ for carbon nanotube are normally reported for nano or microfibers. In the case of melt spun PC nanofibers this ratio was found to be around 2.1 for PC/MWCNT [10] and around 2.6 for PC/SWCNT nanofibers [17]. Accordingly, the values found in this study for highly aligned nanotubes are somehow close to those related to spun fibers indicating that the alignment due to microinjection can be very high.

The *D/G* ratio is often used as a diagnostic tool for checking the degree of perfection of MWCNTs [32] or the degree of crystallinity in the nanotube structure [13]. A constant value of *D/G,* in both parallel and perpendicular geometries, then means that there is no change in the nanotube structure [40]. To check the induced changes in the crystalline structure of MWCNTs, we used the ratio of $(D/G)_\Pi/(D/G)_\perp$. If the nanotubes do not go through structural changes the *D/G* values is constant and $(D/G)_\Pi/(D/G)_\perp$ ratio should be equal to 1. As one can deduce from Table 6.1 this ratio is between 1.03-1.11 for all processes indicating that the crystalline structure of individual nanotubes is more or less stable.

6.6.3. Rheological properties

It is widely accepted that shear flow reduces markedly the particle-particle interactions and leads to a remarkable change of the viscoelastic behavior [41]. The percolation network of nanotubes is therefore quite sensitive to steady shear flow [42]. In order to investigate the effect of shear flow during polymer processing on the PC/MWCNT post-molding viscoelastic properties, SAOS rheological tests were conducted on compression, microinjection-compression and microinjected molded disk shaped samples at 300 ^{o}C, the average barrel temperature used in our processes. Figure 6.10 shows the effect of the different processing methods on the complex viscosity of the neat polycarbonate and the nanocomposites containing 5 wt% of MWCNTs. Obviously, for the neat polycarbonate the effect of processing conditions is negligible. However, for the 5 wt% nanocomposite this effect becomes quite large. The complex viscosity decreases by about two orders of magnitude for the sample made by microinjection molding, the process which features the highest levels of shear rate. Even the lower effective shear rate of microinjection-compression molding significantly shifts the complex viscosity to lower values. Note that the shear-thinning behavior of the nanocomposites is also affected by the processing method. Figure 6.10 reveals that for the 5 wt% nanocomposite the viscosity tends towards a plateau at high frequency. This is more striking for high shear rate processes. A similar trend was

observed in our last work when preshearing a 3% MWCNT/PC nanocomposite at 300 $^{\circ}$C [34]. The drastic reduction in viscosity and change in the shear-thinning behavior shown in Fig. 6.10 could be explained by the idea that carbon nanotubes tend to behave like macromolecules in solution. Under such high shear rates and shear stresses encountered in micro-injection molding, the nanotubes no longer ``stick`` together and are subjected to flow-induced disentanglement and alignment exhibiting shear thinning effect just like entangled polymer chains would in high shear flow conditions [43-45].
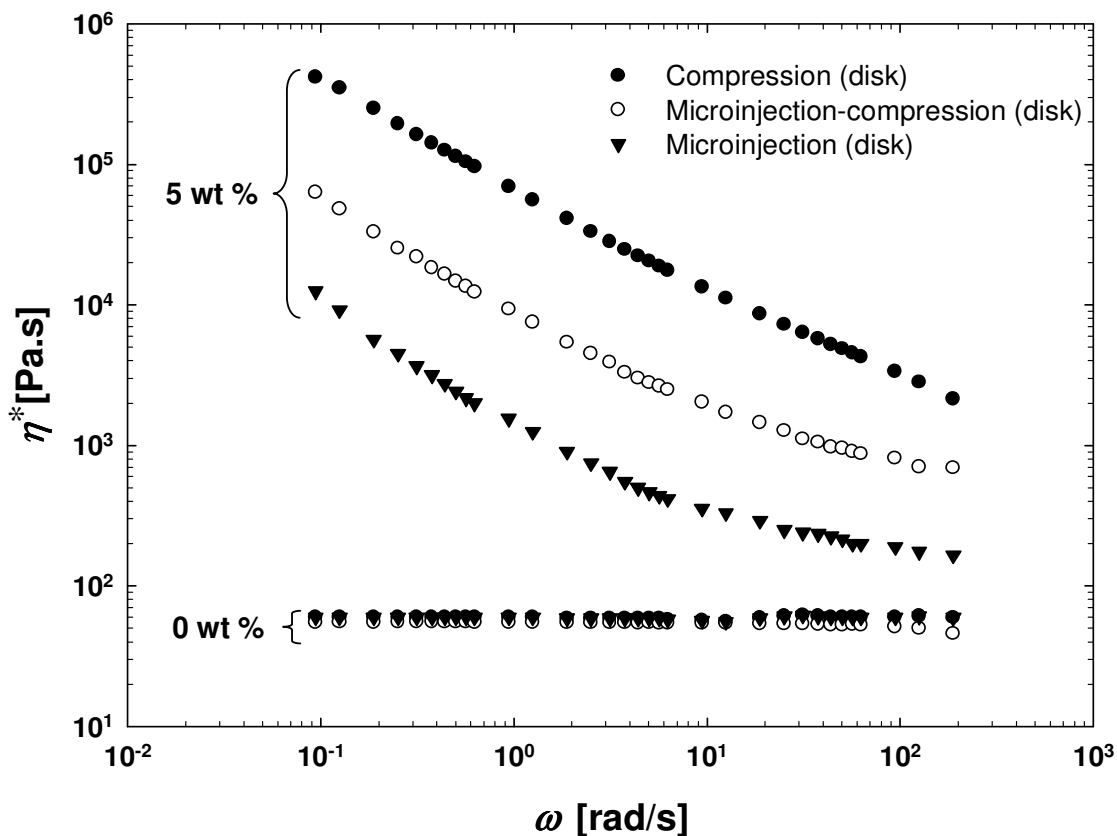
Figure 6.10: Complex viscosity at 300°C of neat polycarbonate and PC / 5wt% MWCNT nanocomposites for different processing methods

The rheological percolation threshold is also affected by the processing method. The percolation threshold is often defined as the value of the solid content above which the rheological properties increase in an exponential way. Figure 6.11 shows the storage modulus data reported as a function of nanotube content. The percolation threshold can be determined by applying a power-law function to G′ versus nanotube loading according to the following equation [6, 12, 46-48]:

$$G' = \beta_{c,G}\left(\frac{m - m_{c,G}}{m_{c,G}}\right)^{q} \qquad \text{for } m > m_{c,G} \tag{6-16}$$

where $\beta_{c,G}$ and q are parameters, m is nanotube loading (wt%) and $m_{c,G}$ is the percolation threshold (wt%). The description of the data by Eq. 6-16 is shown in Figure 6.11 to be excellent and the left limit of the dashed line corresponds to the percolation threshold value. The figure clearly shows that the percolation threshold is shifted towards larger nanotube content when the processing is carried out under higher effective shear rates and large stress for the presheared sample in the rheometer.
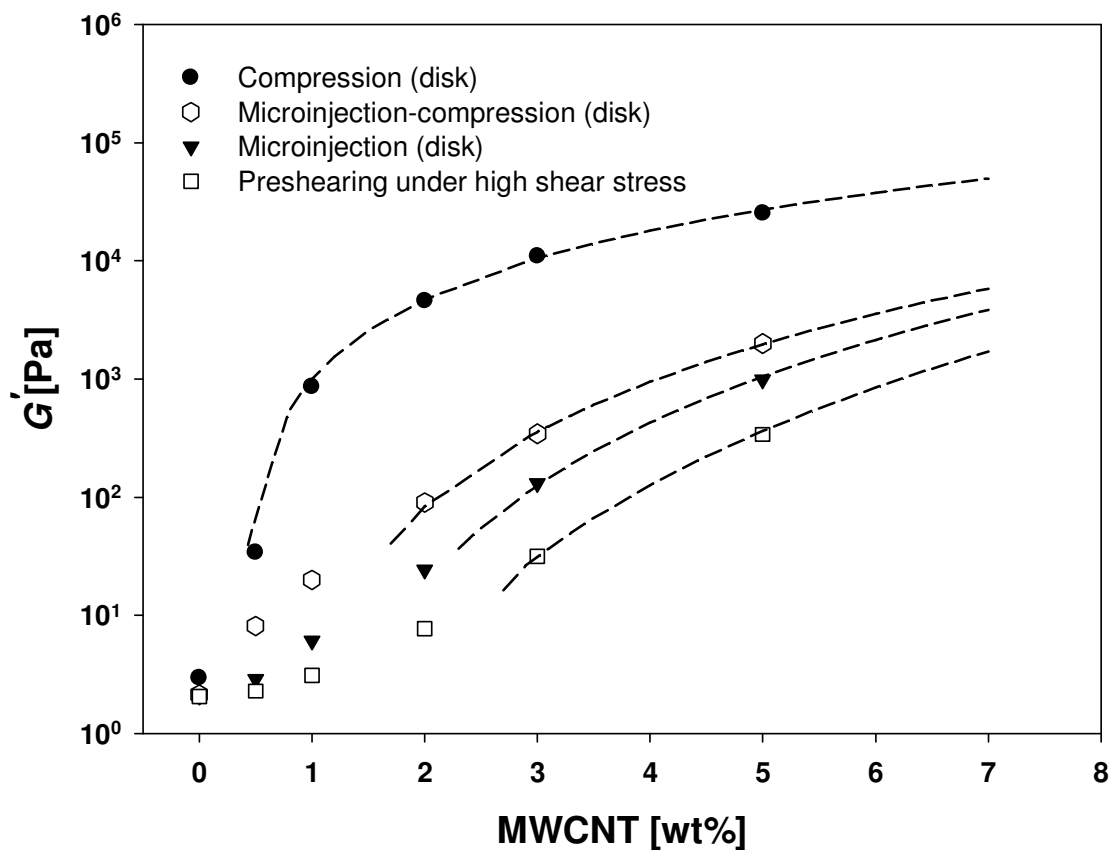
Figure 6.11: Effect of processing conditions and preshearing at 2400 Pa (without rest time) on G' data (1 rad/s) at 300 $^{\circ}$C

We also measured the percolation threshold in SAOS after applying a preshearing stress corresponding to the maximum allowable value for the CSM rheometer (2400 Pa) [34]. As soon as the preshearing step was completed (i.e. the shear viscosity has reached steady state), SAOS

tests were conducted without any rest time. As we expected, the effect of applying a high shear stress is more or less similar to the effect encountered in microinjection molding. In all cases the percolation threshold increases remarkably when the nanocomposites are subjected to high shear flow. As in the case of microinjected samples, we do not have a perfect or ideal percolated network in the presheared samples even at high nanotube loading as the storage modulus rises less markedly with nanotube concentration above the threshold.

6.6.4. Electrical conductivity

As the electrical conductivity of nanocomposites is one of the main properties of interest in this work, we investigated the effect of polymer processing on the electrical conductivity of the nanocomposites, particularly prepared by micromolding. Moreover, measurement of the electrical properties may be a useful tool to understand the relationship between the rheological behavior and the nanocomposites microstructure. Figure 6.12 presents the effect of nanotube loading on the electrical conductivity of the nanocomposites samples prepared by the same processing methods as previously.

Like the rheological percolation threshold, the electrical percolation threshold can be described by a similar power-law expression [6]:

$$\sigma = \beta_{c,\sigma} \left(\frac{m - m_{c,\sigma}}{m_{c,\sigma}} \right)^{q} \qquad \text{for } m > m_{c,\sigma} \tag{6-17}$$

where $\beta_{c,\sigma}$ and q are parameters, $m_{c,\sigma}$ is the electrical percolation threshold (wt%) and σ the electrical conductivity. Again this power-law expression is found to describe very well the data of Figure 6.12 where the left limit of the dashed line corresponds to the percolation threshold value in each case.
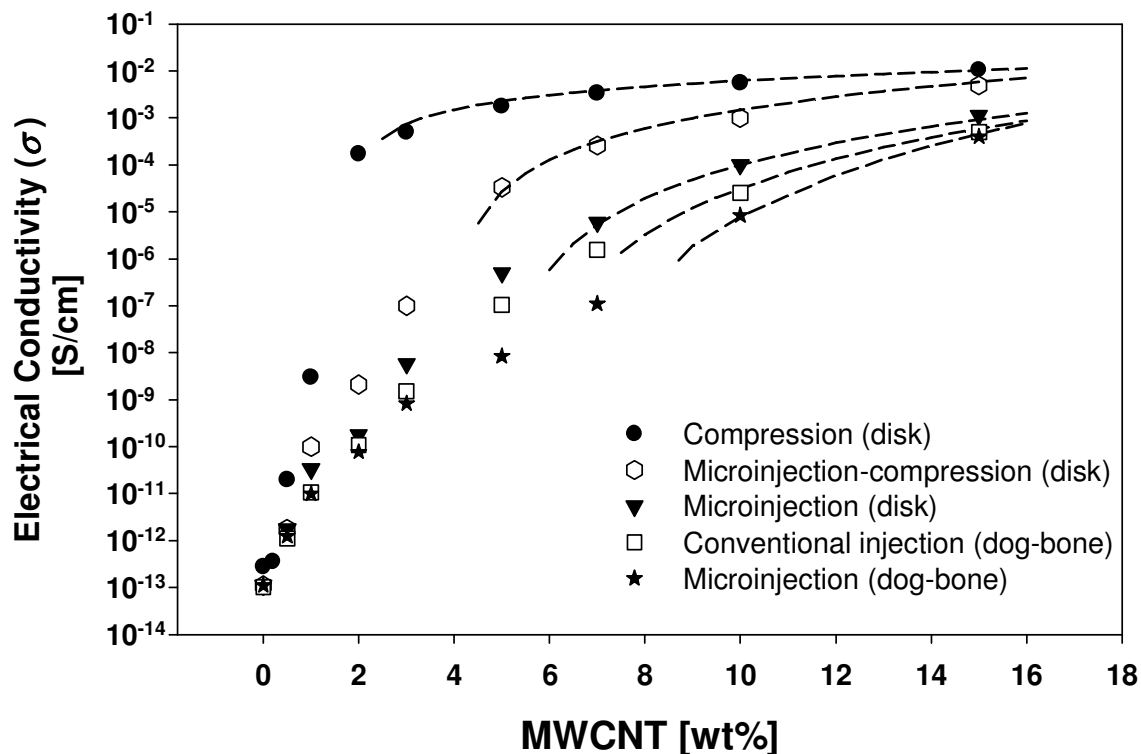
Figure 6.12: Effect of polymer processing conditions on the electrical conductivity and electrical percolation threshold of the nanocomposites

For compression molded samples the percolation threshold is found to be about 3 wt% nanotube content as the electrical conductivity rises suddenly by more than 10 decades. Above these concentrations, the conductivity increases slightly to eventually reach a plateau. This is typical of the percolation behavior usually observed for nanocomposites based on conductive fillers, and can be referred to as an ideal percolation behavior. Figure 6.12 shows that for samples made by a process involving an injection step, a rather monotonic increase of conductivity with loading is obtained. As stated previously, in injected samples the nanotubes are more or less well aligned in the flow direction depending on the level of shear rate, limiting the likelihood of close proximity and connection. A conductive pathway of nanotubes can then be formed only at high nanotube contents where the aligned nanotubes are close enough to allow for current passage. It is obvious that in such a condition, since there is no percolated network formed in the system anymore, the larger the nanotube loading is the shorter is the distance between the nanotubes and the higher is the conductivity level. Therefore, no sudden jump in electrical conductivity or percolation point is observed in Figure 6.12 for the injected samples, but rather a broad range of percolation over which electrical conductivity increases continuously. Microinjection molding

proceeds under extremely high levels of effective shear rate and almost completely aligns the nanotubes in the flow direction. Consequently, the percolation threshold estimated by Eq. 6-17 has larger values for parts produced by microinjection. The longitudinal flow in the dog-bone shaped cavity results in the highest value for the percolation threshold, about 9 wt% of nanotube loading.

Interestingly, the calculated percolation threshold is highly affected by the mold geometry. As Figure 6.12 reveals that for the disk shaped microinjected samples the percolation threshold is lower and the electrical conductivities are about one order of magnitude larger than that of dog-bone shaped samples. The radial (elongational) flow in the disk shape cavity reduces the effect of high shear rate and less nanotube alignment is achieved due to the elongational flow component, which orients the nanotubes transversely to the radial flow direction.This favors the formation of a percolated network. Both compression molding and microinjection-compression molding of disk shaped samples achieve similar levels of nanotube orientation in the transverse and radial flow directions. As a consequence, the electrical percolation threshold behavior pertaining to both processing methods are closely similar as can be seen from Figure 6.12.

6.6.5. Mechanical properties

The mechanical properties of dog-bone microinjected samples were analyzed and Figure 6.13 shows the influence of MWCNT concentration on the stress-strain behavior of microinjected tensile parts. Obviously the neat polycarbonate and the 0.5 wt% nanocomposite specimen show a strain hardening behavior and necking at high elongation. However, the nanocomposites with larger nanotube loadings show no strain hardening and become more brittle as the strain-to-failure decreases with nanotube concentration. All samples, with the exception of the largest concentration nanocomposite, show yielding before plastic flow.
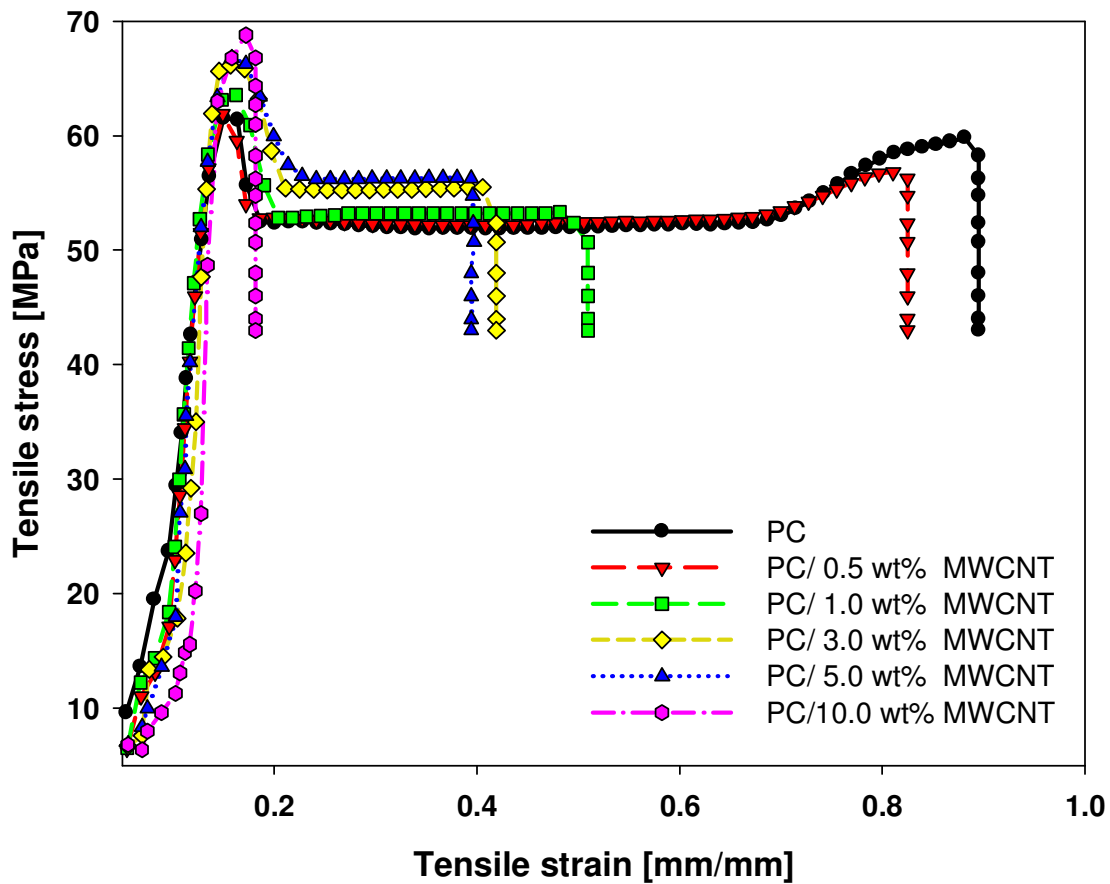
Figure 6.13: The effect of MWCNT content on the stress-strain behavior of dog-bone shaped microinjected nanocomposites

The values for the strength and the elongation at break of the nanocomposites of different nanotube loadings are summarized in Figure 6.14.
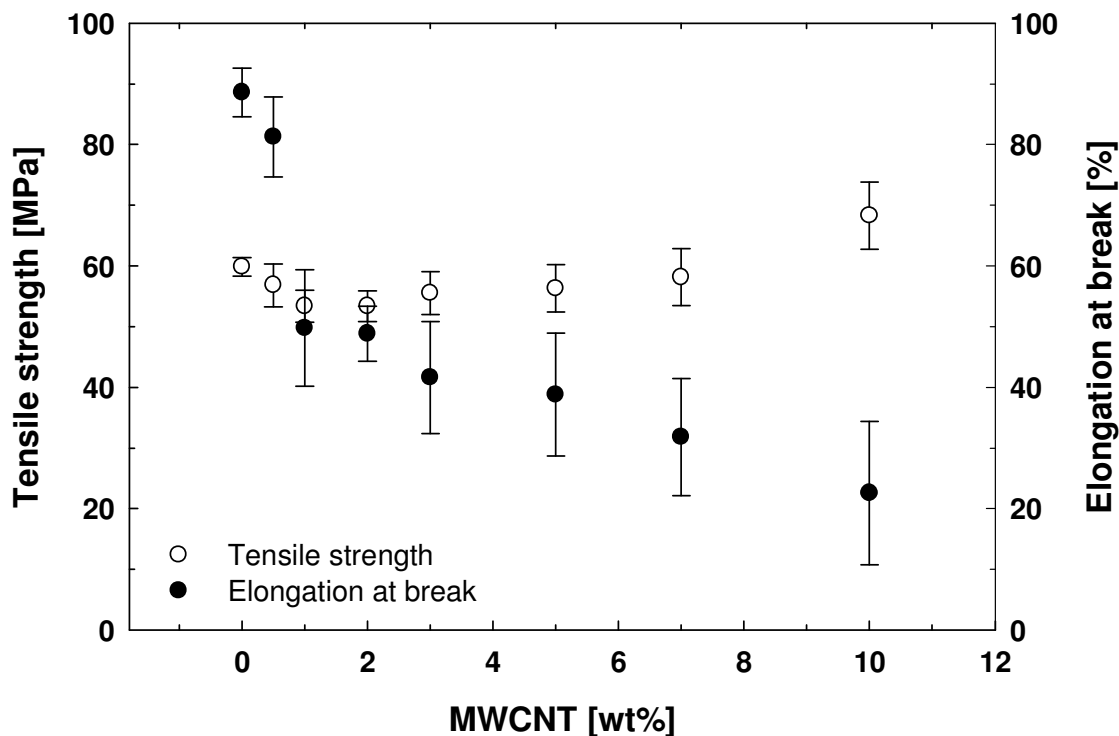
Figure 6.14: The effect of MWCNT content on the tensile strength and elongation at break of dog-bone shaped microinjected nanocomposites

We first observe a slight decrease in strength then an increase with MWCNT loading above 1% weight concentrations probably due to the formation of nanotube network at this level of loading. The effect of nanotube loading on the nanocomposite ultimate strength is not very significant and the overall tendency demonstrates only a modest increase with MWCNT concentration. This is probably due to the poor interaction between nanotubes and polymer chains so that the nanotubes could not achieve their theoretical potential as fillers with extremely high strength. Elongation at break is also strongly affected by nanotube loading, starting to decrease drastically for composites containing up to 1% of nanotubes. Beyond this concentration, ductility decreases at a lower rate until the samples become totally brittle at loadings of about 7-10 wt%. The structural change of the nanocomposite with increasing nanotube content is probably responsible for this phenomenon. Above 1 wt%, the formation of nanotubes aggregates or agglomerates could change the load transfer mechanism of the nanocomposites and result in a different trend in the mechanical properties.

The effect of MWCNT loading on the Young modulus of the nanocomposites, obtained from a closer view of the stress-strain curves (Fig. 6.13), is shown in Figure 6.15. The Young

modulus increases monotonically with loading and tends towards a plateau for large nanotube levels. The addition of 3 wt% of nanotubes results in a rise of the modulus by about 30%. Again, this is a weak effect of nanotube on the tensile modulus probably due to weak interactions between polymer chains and the filler.
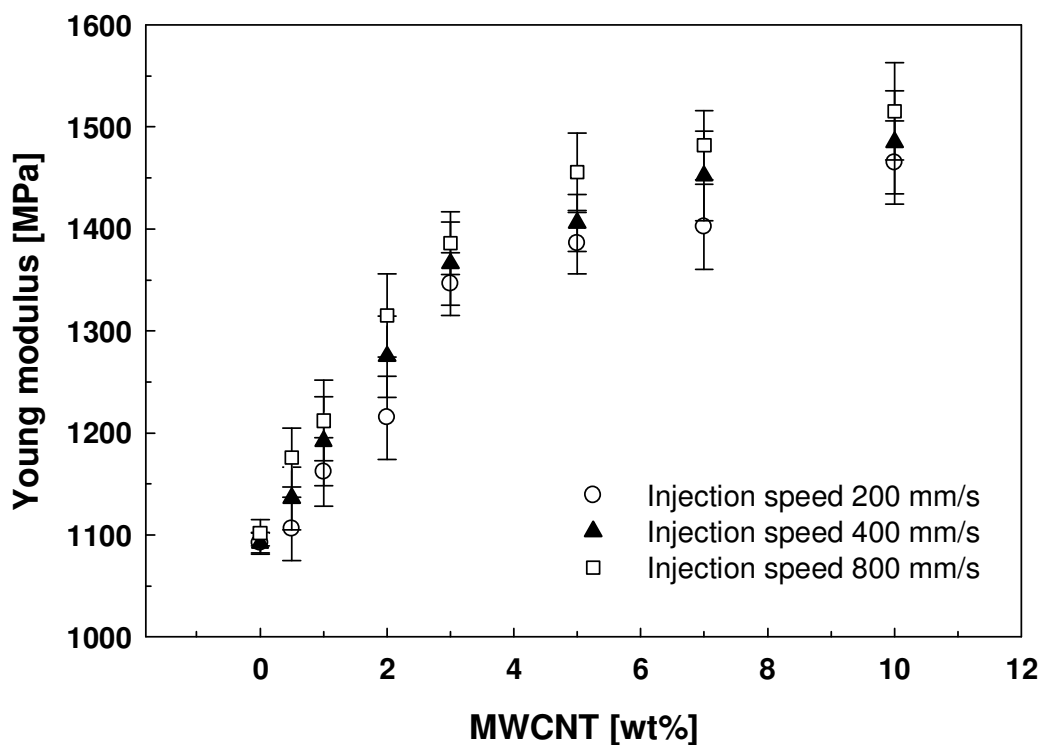
Figure 6.15:   Effect of microinjection speed on the Young modulus of the dog-bone shaped nanocomposites of different tube contents

Figure 6.15 also shows that the Young modulus is larger when the injection speed is the largest due to higher polymer chain orientation and larger degree of nanotube alignment. Although the effect is not highly significant, it is different from what reported previously in the case of conventional injection molding of polymer/long fiber composites like Kevlar [49]. They found that lower injection speeds create a thicker solidified layer and result in a higher shear flow field at the solid-melt interface. It is also shown that the polymer relaxation prior to solidification in the mold reduces the orientation in conventional injection [50]. Higher the injection speed increases the solidification time and results in a more relaxation. Consequently polymer chains are less oriented and fibers are less aligned in flow direction (along the length of the tensile bars).

In the case of microinjection molding, due to very small thickness of the sample the cooling time is very short. The whole sample solidifies rapidly and there is not enough time for the polymer chains to relax. Therefore, increasing the injection speed results in a higher orientation since the relaxation process is somehow ignorable in this process. It is worthwhile to note that the values obtained for the Young modulus of the microinjected parts, even for the neat polycarbonate, are considerably smaller than the typical values obtained for conventional or standard samples tested under the same test conditions (for the neat polycarbonate this value is about half of the standard values). It is still unclear to us why the microinjected parts have such low tensile modulus [51]. Our rheological measurements revealed that the degradation during this process was insignificant; the viscosity of the neat polycarbonate after processing was found to be similar to that before molding within the experimental error.

6.7. Discussion

It has been observed that the nanocomposites properties strongly depend on the processing conditions. Such dependency of the percolation threshold of nanotube based nanocomposites has been established qualitatively in the literature [13, 16] where the melt-processed films or fibers showed high electrical conductivity at low draw ratios but below the detection limit at high draw ratios. It seems that by changing the nanotube alignment in the nanocomposites we can control the nanocomposite properties. For instance, using a certain amount of nanotube loading, it would be possible to have conductive or resistive materials only by changing the flow type and the effective shear level. This interesting issue is discussed in this section. It is worthwhile to note that the rheological percolation threshold is considerably smaller than the electrical one for the same processing conditions. This difference can be described in terms of the shorter tube–tube distance required for electrical conductivity as compared to that required to impede polymer mobility, so that more nanotubes are required to reach the electrical percolation threshold. However, in spite of the fact that these percolating networks are due to different phenomena, their structures change in a similar way when they are subjected to a flow field. Clearly, if nanotubes start to be aligned in the flow direction, they interconnect minimally, as their orientations become less random, leading to a remarkable increase in the percolation threshold.

To investigate these aspects in more details, the electrical and rheological percolation thresholds are plotted against the $D_\Pi/D_\perp$ ratio, Raman intensity parallel/perpendicular to the

flow direction, in Figure 6.16. In the case of the rheological threshold, it was more convenient to use disk-shaped samples molded by compression, microinjection-compression and microinjection for the post-molding rheological properties measurements. The values of G' and σ obtained for the 5wt% MWCNT nanocomposites are also shown in the figure. As observed, the percolation threshold is quite low at low $D_{\Pi}/D_{\perp}$ ratio, which is an indication that the nanotubes networks are formed at very low concentrations when random orientation ($D_{\Pi}/D_{\perp}$ ~1) prevails.

The percolation thresholds significantly rise with $D_{\Pi}/D_{\perp}$ ratio (or nanotube alignment) so that in the highly aligned cases, like in microinjected samples where $D_{\Pi}/D_{\perp}$ is around 1.95, the electrical percolation threshold is about 9 wt% of MWCNT, which is quite high. More interestingly G' and σ decrease remarkably with increasing $D_{\Pi}/D_{\perp}$ ratio or nanotube alignment. We can therefore conclude that the $D_{\Pi}/D_{\perp}$ ratio is closely related to specific nanocomposites properties such as G' and σ.

In addition, the power-law type equations (Eqs. 6-16 &6-17) characterize well the post-percolation behavior and provide reasonably accurate values of the percolation thresholds. From the previous results of Figures 6.11 and 6.12, we observe that processing conditions that yield a nearly perfect percolation behavior tend to display a plateau immediately above the percolation threshold, indicating that further addition of nanotubes could not notably increase the related property of the nanocomposites. This is especially true for the compression molding parts where the shear stresses and shear rates are the lowest. In this situation, it is found that the best fit is achieved when the parameter q is ~1. Deviation from this value is indicative of an absence of a plateau or a perfect percolation behavior. In this case we see a broad range of percolation and the related properties keep increasing after percolation.
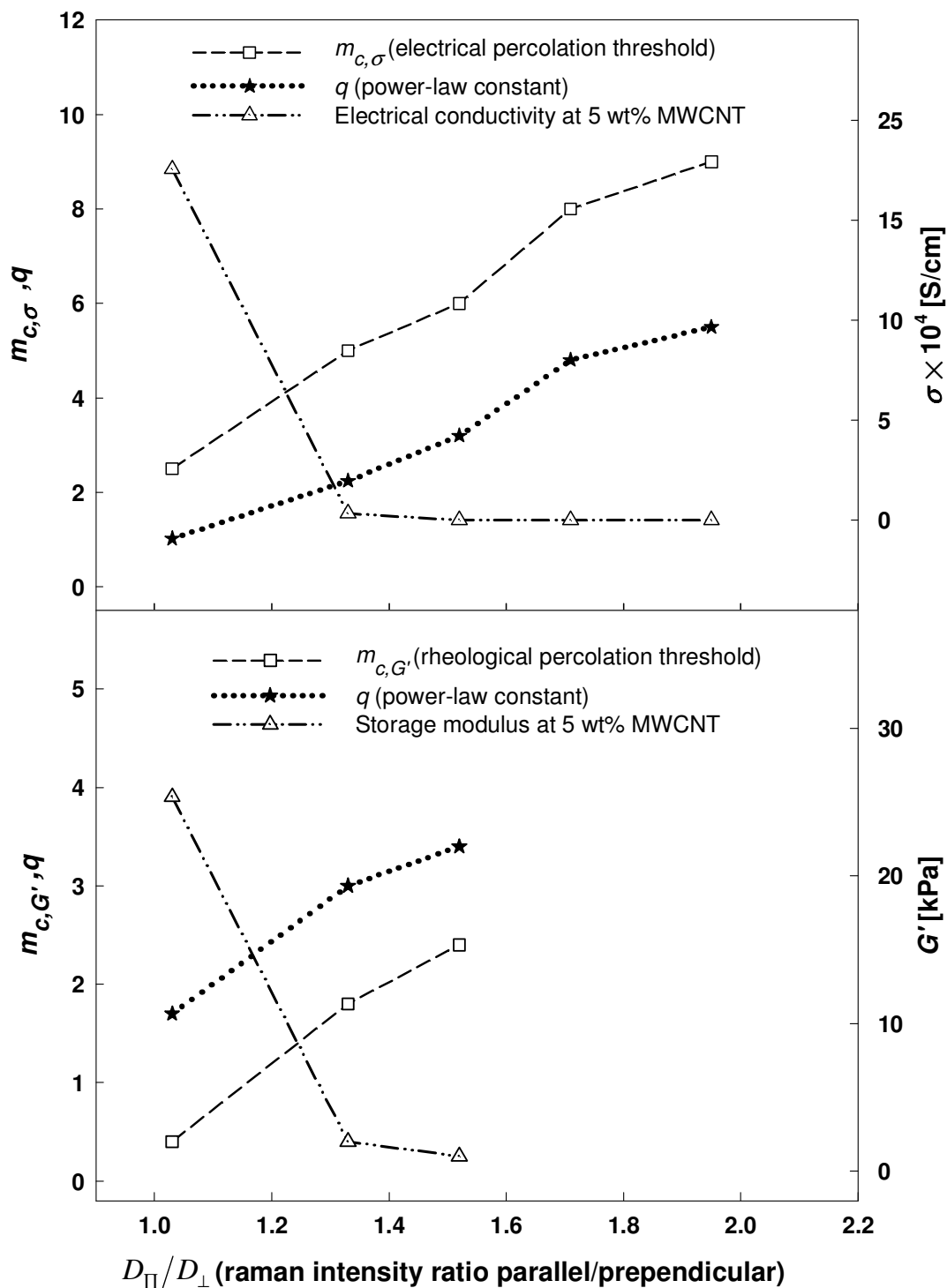
Figure 6.16: Effect of nanotube alignment on the rheological and electrical percolation thresholds of the nanocomposites, on the storage modulus and electrical conductivity of PC / 5wt% MWCNT nanocomposites and on the parameter q. $D_{\Pi}/D_{\perp}$ values are taken from Table 6.1

This is more applicable to the electrical percolation rather than the rheological percolation behavior, since in the former case complete tube-tube contacts are required to have a conductive network. The q values determined by fitting the respective power-law equations are shown in Figure 6.16 versus the $D_{\Pi}/D_{\perp}$ ratio. Of special interest is the significant increase in q as the nanotube alignment increases indicating that the percolation of highly aligned nanotubes is hardly possible.

6.8. Conclusions

In this work we have examined the effects of polymer processing conditions on the nanotube alignment and PC/MWCNT nanocomposites properties. A masterbatch was diluted to prepare nanocomposite samples at various concentrations and the nanocomposites were then subjected to different flow conditions in a controlled manner employing a variety of polymer processing methods. The morphological analysis, using SEM, TEM and AFM, showed that the nanotubes were randomly oriented in the plane of the compression molded samples, which were subjected to the lowest shear value, while they were well aligned in the longitudinal flow direction in the microinjected dog-bone samples, which featured very high shear values. Raman spectroscopy results indicate that the lowest values of $D_{\Pi}/D_{\perp}$ and $G_{\Pi}/G_{\perp}$ ratios were obtained for the compression molded samples while the highest values were related to the microinjected dog-bone samples. Interestingly, the nanotube alignment strongly affected the rheological properties and the electrical conductivity of the nanocomposites. The percolation thresholds rose significantly in both cases with increasing orientation level. Further analysis showed that for a given nanotube loading, the nanocomposite electrical conductivity level could be controlled by controlling the nanotube alignment. Moreover, by fitting a power-law equation to the storage modulus and electrical conductivity data we determined reasonably accurate values of percolation thresholds as well as the post-percolation behavior of the nanocomposites. The parameter, q, was found to be a very good indicator to investigate the percolation behavior of nanotube networks. It was found to increase with nanotube alignment, indicating that for highly sheared samples there is no perfect percolation behavior or ideal nanotube network. In these cases broad ranges of percolation were observed. The mechanical properties of the nanocomposites were also found to be sensitive to processing, albeit somehow improved by increasing the shear level.

6.9. References

[1]   Meyyappan M. Carbon nanotubes : science and applications. Boca Raton: CRC Press 2005.

[2]   Wu D, Liang W, Yurong S, Ming Z. Polym Sci B. 2007; 45(23): 3137-3147.

[3]   Abdel-Goad M, Potschke P. J Non-Newton Fluid Mech. 2005; 128(1):2-6.

[4]   Meincke O, Kaempfer D, Weickmann H, Friedrich C, Vathauer M, Warth H. Polymer. 2004; 45(3):739-48.

[5]   Moniruzzaman M, Winey KI. Macromolecules. 2006; 39(16):5194-205.

[6]   Hu G, Zhao C, Zhang S, Yang M, Wang Z. Polymer. 2006; 47(1):480-8.

[7]   Sung YT, Han MS, Song KH, Jung JW, Lee HS, Kum CK, Joo J, Kim WN. Polymer. 2006; 47(12):4434-9.

[8]   Shi X, Hudson JL, Spicer PP, Tour JM, Krishnamoorti R, Mikos AG. Nanotechnology. 2005; 16(7):531-8.

[9]   Kharchenko SB, Migler KB, Douglas JF, Obrzut J, Grulke EA. ANTEC 2004:1877-1881.

[10] Potschke P, Fornes TD, Paul DR. Polymer. 2002; 43(11):3247-55.

[11] Fangming D, Fischer JE, Winey KI. Phys Rev B. 2005; 72(12):121404-1.

[12] Du F, Scogna RC, Zhou W, Brand S, Fischer JE, Winey KI. Macromolecules. 2004; 37(24):9048-55.

[13] Potschke P, Brünig H, Janke A, Fischer D, Jehnichen D. Polymer. 2005; 46(23):10355-63.

[14] Kharchenko SB, Douglas JF, Obrzut J, Grulke EA, Migler KB. Nature Mater. 2004; 3(8):564-8.

[15] García Gutiérrez MC, Nogales A, Rueda DR, Domingo C, García-Ramos JV, Broza G, Roslaniec Z, Schulte K, Davies RJ, Ezquerra TA. Polymer. 2006; 47(1):341-5.

[16] Haggenmueller R, Gommans HH, Rinzler AG, Fischer JE, Winey KI. Chem. Phys. Lett. 2000; 330(3-4):219-25.

[17] Fornes TD, Baur JW, Sabba Y, Thomas EL. Polymer. 2006; 47(5):1704-14.

[18] Chae HG, Minus ML, Kumar S. Polymer. 2006; 47(10):3494-504.

[19] Sung JH, Kim HS, Jin H-J, Choi HJ, Chin I-J. Macromolecules. 2004; 37(26):9899-902.

[20] Liu LQ, Tasis D, Prato M, Wagner HD. Adv Mater. 2007; 19(9):1228-33.

[21] Potschke P, Bhattacharyya AR, Janke A. Carbon 2004; 42:965-969.

[22] Pham GT, Park YB, Wang S, Liang Z, Wang B, Zhang C, Funchess P, Kramer L. Nanotechnology. 2008; 19(32):325705.

[23] Ding W, Eitan A, Fisher FT, Chen X, Dikin DA, Andrews R, Brinson LC, Schadler LS, Ruoff RS. Nano Lett. 2003; 3(11):1593-7.

[24] Singh S, Pei Y, Miller R, Sundararajan PR. Adv Functional Mater. 2003; 13(11):868-72.

[25] Potschke P, Abdel-Goad M, Alig I, Dudkin S, Lellinger D. Polymer. 2004; 45(26):8863-70.

[26] Jin L, Bower C, Zhou O. Appl Phys Lett. 1998; 73(9):1197-9.

[27] Zhao Q, Wagner HD. Philos Transact A Math Phys Eng Sci. 2004; 362(1824):2407-24.

[28] Litchfield DW, Baird DG. Polymer. 2008; 49(23):5027-36.

[29] Jehng JM, Tung WC, Kuo CH. J Porous Mater. 2008; 15(1):43-51.

[30] Lee SN, Stolarski V, Letton A, Laane J. J Mol Struct. 2000; 521(1-3):19-24.

[31] Jorio A, Dresselhaus G, Dresselhaus MS. Carbon nanotubes: Advanced topics in the synthesis, structure, properties and applications. illustrated ed: Springer 2008.

[32] Bulusheva LG, Okotrub AV, Kinloch IA, Asanov IP, Kurenya AG, Kudashov AG, Chen X, Song H. phys status solidi (b). 2008; 245(10):1971-4.

[33] Rao AM, Jorio A, Pimenta MA, Dantas MSS, Saito R, Dresselhaus G, Dresselhaus MS. Phys Rev Lett. 2000; 84(8):1820-23.

[34] Abbasi S, Carreau P, Derdouri A, Moan M. Rheologica Acta.2009;48(9): 943-59

[35] Bird R B, Stewart W E, Lightfoot E N. Transport phenomena, 2nd ed. John Wiley & Sons 2007.

[36] Bird RB, Armstrong C, Hassager O. Dynamics of Polymeric liquids, vol.1. John Wiley & Sons 1924

[37] Baird DG, Collias DI. Polymer Processing Principle and Design. John Wiley & Sons 1998.

[38] Laurencena BR, Williams MC. J Rheol. 1974; 18(3): 331-355.

[39] Bliznyuk VN, Singamaneni S, Sanford RL, Chiappetta D, Crooker B, Shibaev PV. Polymer. 2006; 47(11):3915-21.

[40] Endo M, Kim YA, Fukai Y, Hayashi T, Terrones M, Terrones H, Dresselhaus MS. Appl Phys Lett. 2001; 79(10):1531-3.

[41] Fan Z, Advani SG. J Rheol. 2007;51(4):585-604.

[42] Defeng W, Liang W, Ming Z , Yalan Z . J Polym Sci B. 2007; 45(16):2239-51.

[43] Shafer MSP, Windle AH. Macromolecules, 1999; 32(20): 6864-66.

[44] Green MJ, Behabtu N, Pasquali M, Adams WW. Adams, Polymer. 2009; 50(21): 4979-97.

[45] Hobbie EK, Fry DJ. Physical Review Lett. 2006; 97, id. 036101.

[46] Xiao KQ, Zhang LC, Zarudi I. Compos Sci Technol. 2007;67(2):177-82.

[47] Zhang Q, Rastogi S, Chen D, Lippits D, Lemstra PJ. Carbon. 2006;44(4):778-85.

[48] Thostenson ET, Li C, Chou TW. Compos Sci Technol. 2005;65(3-4):491-516.

[49]   Yu Z, Ait-Kadi A, Brisson J. Polymer. 1994 ; 35(7): 1409-18

[50]   Tadmor Z. J. Applied Polym Sci. 1974; 18:1753-72

[51] Chu J, Kamal MR, Derdouri A, Hrymak A. ANTEC 2008: 2468-72.

Chapter 7

Properties of Microinjection Molding of Polymer Multiwalled Carbon Nanotube Conducting Composites[*]

7.1. Presentation of the article

Final properties of microinjected PC/MWCNT and PP/MWCNT were studied in this article. The effect of crystalline structure and polymer processing conditions on the morphology and properties of the nanocomposites was investigated in this paper. Followed by different types of micromolding in different processing conditions and using different cavity shapes, we employed a variety of characterization methods to discover the effect of process conditions on structure and properties of CNTs/polymer composites. The results of the morphological study revealed a large difference between the compatibility of MWCNT with polycarbonate as a polar amorphous polymer and with polypropylene as a non-polar polymer with high degree of crystallinity. It was also found that in microinjected samples the formed crystals were well oriented however the overall crystallinity was only slowly changed in such a high sheared conditions. The presence of crystalline structure improved the electrical conductivity of the nanocomposites; however, high degrees of nanotube alignment in microparts resulted in a significant increase in electrical percolation threshold. The mechanical properties of PP nanocomposites were also significantly affected by nanotube loading while the effect was weak in the case of PC nanocomposites.

Properties of Microinjection Molding of Polymer Multiwalled Carbon Nanotube Conducting Composites

Samaneh Abbasi [1], Abdessalem Derdouri [2], Pierre J. Carreau [1]

1) CREPEC, Department of Chemical Engineering, Ecole Polytechnique Montreal, P.O.Box 6079, Station Centre-Ville Montreal QC, Canada

2) CREPEC, Industrial Materials Institute, National Research Council Canada, 75 de Mortagne, Boucherville, QC, Canada

7.2. Abstract

The effects of processing conditions on the morphology, microstructure and properties of polypropylene/ multiwalled carbon nanotube (PP/MWCNT) and polycarbonate/ multiwalled carbon nanotube (PC/MWCNT) composites were studied. Samples of various MWCNT loadings were prepared by diluting commercial masterbatches of nanotubes using optimized melt-mixing conditions. A reasonably good dispersion and formation of nanotube networks within the polymer matrix were observed using SEM and TEM microscopy. Different processing conditions were used to systematically change the degree of nanotube alignment, from random to highly aligned orientation. Crystallinity and crystal orientation of compression molded and microinjected samples were determined by DSC and X-ray diffraction. The crystallinity of the PP/MWCNT nanocomposites was found to go through a maximum as a function of nanotube content while the overall rate of crystallization increased. We observed for the highly sheared microinjected PP/MWCNT samples the formation of well oriented crystals; however the overall crystallinity was only slightly affected by strain. Electrical conductivity of the nanocomposites was improved by the presence of the crystalline structure; although, high degrees of nanotube alignment in the microparts resulted in a significant increase in the electrical percolation threshold. The PP nanocomposites exhibited mechanical properties significantly enhanced by nanotube loading; this effect was small in the case of the PC nanocomposites.

Keywords: Multiwalled carbon nanotube, Polycarbonate, Polypropylene, Morphology, Crystallinity, Nanotube alignment, Electrical percolation

7.3. Introduction

After their discovery in 1991 by Iijima [1, 2] carbon nanotubes (CNTs) became attractive candidates for fundamental investigations due to their unique electronic structure and extraordinary properties. Since then, an extensive research effort has been devoted to the nanotube fabrication, characterization and development of applications [3]. Their intrinsic structure, size scale and aspect ratio suggest a variety of applications such as nanoelectronics, sensors and field emission as well as high performance nanocomposites.

Recently, considerable attention has been devoted to carbon nanotube / polymer composites from both processing and application points of view. Besides the individual properties of carbon nanotubes, numerous potential benefits are expected when they are employed as reinforcing agents in nanocomposites. One of the key interest in carbon nanotubes incorporated into polymeric materials stems from their potential to develop conductive polymer composites at relatively low concentrations [4-9].

High electrical conductivity in conductive particles based nanocomposites is explained in term of percolation i.e., the structure in which the particles touch one another, resulting in a continuous electrically conductive path. The filler concentration at which the electrical conductivity increases abruptly is known as the percolation threshold. It depends not only on the types of filler and polymer but also on the dispersion state of the filler and the morphology of the matrix [10-13].

The percolation threshold is found to be much higher in the case of thermoplastic matrices [8, 14-17] in comparison to thermoset filled systems [18]. In semi-crystalline matrices, additional complexity arises due to the crystallization induced phase separation and subsequent rejection of the nanotubes by the advancing crystalline phase [19, 20]. It is well known that carbon nanotubes are well dispersed in polar polymers such as poly (methyl methacrylate)(PMMA) [15] and polycarbonate (PC) [16]. However, in non-polar polymers such as polypropylene (PP), CNT dispersion remains a big challenge and might affect the percolation threshold as well.

Incorporation of carbon particles into incompatible polymer blends can provide them with electrical conductivity at very low filler content due to a double percolation phenomenon [21, 22]. Double percolation refers to the structure in which there are two types of percolation in the same composite material. The first one, which is typically observed in the reinforced composite materials, is associated with the electrical continuity of the conductive particles in the filler-rich

phase and the second one is associated with the continuity of this phase in the blend. The improvement in electrical conductivity will depend on the conductive particle concentration threshold in the filler-rich phase and on the volume fraction of the filler-rich phase required to induce co-continuity in the blend [22].

It is well known that the microstructure of plastic parts is the result of complex changes imposed to the base polymer by the special processing conditions [23]. Typical thermoplastic processing involves pellets melting, plastication, melt flow and pressurization and shaping and finally solidification from the molten state, either by crystallization or vitrification. The complex thermo-mechanical history imposed on the polymer during processing leads to substantial spatial variations of chain orientation under shear and elongational flows and to the formation of a superstructure controlled by the local dynamics of the process. These effects result in a large anisotropy of the final physical properties particularly if the polymer is semi-crystalline and is filled with solid particles of various shapes (glass or carbon fibers, clay or mica platelets, carbon nanotubes or nanofibrils, etc.). The use of carbon nanotube based nanocomposites for commercial applications, thus, the objective of this work is to develop a clear understanding of how processing conditions influence the nanotube networks and subsequently the nanocomposites properties.

With the recent trend towards product miniaturization, the rapid development of microsystem technologies has opened up new applications for polymer nanocomposites. Particularly, carbon nanotube based polymer composites are suitable candidates for the fabrication of microscale components where the nano size of the added particles is an advantage and only grams of materials are necessary to manufacture high-valued products. A number of processing technologies have been explored to produce polymer-based microdevices amongst which microinjection molding is one of the most suitable processes for producing microparts cheaply and with high precision.

As in the case of conventional injection molding, the properties of parts made by microinjection molding are strongly affected by the processing parameters. However, because of the exceptional characteristics of microinjection molding, these parameters and their effects are not necessarily the same as encountered in conventional molding. Microinjection molding features extreme injection pressures, very high shear and cooling rates as well as very short cycle times compared to the conventional processing. Significant reports on microinjection molding

appeared during this decade most of which were on neat polymers [21-25]. Some studies did consider polymer compounds containing fillers such as short glass fibers, glass particles and nanoceramic materials as illustrated by the work of Huang et al. [26, 27].

Another interesting processing alternative for producing microparts is microinjection-compression molding. This process is regarded as an extension of microinjection molding by incorporating a compression phase to compact the material inside the mold cavity. After injection of the melt into a semi-open mold, the polymer proceeds to the extremities of the cavity under relatively low pressure and stress [28] as the mold closes.

Polycarbonate, a typical amorphous polymer, is an important commercially available engineering thermoplastic for injection molding applications because of its excellent process ability and mechanical properties. Recently, carbon nanotubes have been used as a special filler to be incorporated into PC for stiffness reinforcement as well as thermal and electrical conductivity enhancement purposes [8, 14, 24-27].

Polypropylene is also one of the most commonly used polymers in the preparation of such nanocomposites owing to its well balanced physical and mechanical properties combined with benefits like low cost, low density, good processability and wide field of applications [28-31]. However, PP exhibits very poor compatibility and adhesion to other polymers and inorganic fillers owing to its non-polarity and crystallizability. It has been found that in PP/clay nanocomposites, crystallization of the PP matrix, led to the expulsion of clay platelets from the crystalline phase by thermodynamic forces [32].

It is the aim of this study to investigate the influence of crystalline structure, nanotube loading and microinjection molding conditions on the properties of polymer/MWCNT nanocomposites with a special focus on the electrical conductivity. To this end, we chose two polymers, a polar amorphous PC and an isotactic polypropylene (iPP) as a non-polar semi-crystalline polymer. Due to the high degree of crystallinity of polypropylene, the crystallization induced phase separation and the subsequent rejection of the nanotubes by the growing crystalline phase may result in a conductive nanotubes network at lower concentrations according to the concept of double percolation. We optimized the nanocomposites preparation to obtain the best possible nanotube dispersion as observed by transmission electron microscopy (TEM) and scanning electron microscopy (SEM). Thereafter, samples were prepared by compression molding and micromolding in different processing conditions and using different cavity shapes.

Finally, we employed a variety of characterization methods to investigate the effect of process conditions on structure and properties of the polymer/CNTs composites.

7.4. Experimental

7.4.1. Materials

Masterbatches of 20 wt% MWCNT in PP and 15 wt% MWCNT in PC were purchased from Hyperion Catalysis International, Cambridge, MA. According to the supplier, the carbon nanotubes are vapor grown and typically consist of 8-15 graphite layers wrapped around a hollow 5 nm core [33]. The diameter range was stated to vary from 15 to 50 nm and the length range between 1-10 μm as confirmed by TEM characterization. The masterbatches were then diluted with a polycarbonate (Calibre 1080) supplied by Dow Chemical and with an isotactic polypropylene (PP HD120) supplied by Borealis Co. to prepare nanocomposite samples of various loadings. The added polymer grades are not necessarily the same as the matrices used to make the masterbatches. Considering the small quantity of masterbatch used to prepare the nanocomposites, the original polymer of the masterbatch is only a small fraction of the nanocomposites and does not significantly affect the results. A polypropylene grafted maleic anhydride (PP-g-MA Polybond PB3150 with 0.5 wt% MA) was used as a compatibilizer to improve the dispersion in PP/MWCNT nanocomposites.

7.4.2. Nanocomposite preparation and molding

The composites were made by melt mixing the masterbatches with the neat polymers. The polycarbonate and PC/MWCNT masterbatches were dried for a minimum of 4 h at 120 $^{\circ}$C prior to mixing. The polypropylene, PP/MWCNT and PP-g-MA were also dried for 1 h at 90 $^{\circ}$C. Six samples with different MWCNT contents between 0.5 and 15 wt% MWCNT and 0.5 wt% PP-g-Ma were prepared using a lab-twin screw extruder, Leistritz ZSE 18HP, operating at 100 rpm and 210 $^{\circ}$C for the PC and at 250 rpm and 190 $^{\circ}$C for the PP nanocomposites (conditions previously optimized via a set of controlled experiments). Microinjection molding and microinjection-compression molding were then employed to produce microparts of different shapes and dimensions. Prior to each process, the nanocomposites were dried under the conditions previously mentioned. Compression molded disks were also prepared (Carver laboratory press, model 3912) to compare the nanocomposite properties before and after microinjection molding

more precisely. Microinjection molding was done using a Battenfeld Microsystem 50 micromolding machine. In the case of PC/MWCNT nanocomposites, injection was done at an average barrel temperature of 300 ^{o}C and under a pressure of approximately 100 MPa while the injection speed was constant at 400 mm/s. The mold temperature was kept constant at 80 ^{o}C and the cooling time was set to 10 s. For the PP/MWCNT nanocomposites, we used an average barrel temperature of 260 ^{o}C, a pressure of approximately 100 MPa and a constant injection speed of 400 mm/s. To reduce shrinkage the mold temperature was optimized and kept constant at 20 ^{o}C while the cooling time was set to 10 s. For mechanical tests, we used a mold with the dog-bone shape cavity of 15 mm long, with the center section of 1 mm wide by 0.78 mm thick by 4.3 mm long, gated at one end; while the electrical measurements were done using a disk shape mold of 25 mm in diameter and 1 mm thick, gated at the centre. Finally, microinjection-compression molding was employed to evaluate the effect of applying a compression step at the end of the injection phase on the part properties, using the centrally gated disk cavity with the same dimensions as described before. The process consisted of injecting the melt into the cavity, while the mold was not totally closed. This leads to an initial cavity filling under a lower pressure than if the mold was closed. After the injection stage, the mold was closed to compress the melt and to completely fill the cavity. The operating conditions in this case were the same as for microinjection molding in the injection phase, while during the compression phase, the mold closing speed and gap used in this experiment were set to 1.5 mm/s and 1.2 mm respectively.

7.4.3. Morphological characterization

The morphology of nanocomposites was studied through scanning and transmission electron microscopy (SEM, TEM). For SEM we used a high resolution SEM Hitachi S-4700 microscope. In the case of PC nanocomposite, SEM was done on ultramicrotomed surface of sample cut with a diamond knife at room temperature. The surface of the PP nanocomposite sample was etched using a potassium permanganate solution to eliminate the amorphous phase from the surface. The quality of the dispersion could be seen much better with this method rather than using ultramicrotomed surface. All SEM samples were then coated with a vapor deposit of platinum for 25 s. TEM was done on ultrathin nanocomposites cross sections for a better observation of the morphology, using a Hitachi HD-2000 microscope.

7.4.4. Crystallinity measurements

Differential scanning calorimetry (DSC) and X-ray diffraction (XRD) were used to study the crystallization behavior of PP/MWCNT nanocomposite. Non-isothermal crystallization analysis was performed using TA instrument Q-100 differential scanning calorimeter. Samples of about 5-10 mg were heated from 25 to 260 ^{o}C at a heating rate of 10 ^{o}C/min and then held for 5 min to eliminate thermal history of the materials. The samples were subsequently cooled to 25 ^{o}C at a cooling rate of 10 ^{o}C/min before starting a second heating at the same rate to the same final temperature. The degree of crystallinity was calculated using the following equation [34]:

$$X_c = \frac{\Delta H_f}{\Delta H_f^0 (1-w)} \times 100\% \tag{7-1}$$

In this equation, ΔH_f is the enthalpy of fusion of the samples and ΔH_f^0 (207J/g) is the enthalpy of fusion of the 100% crystalline polypropylene [35]. The weight percent of MWCNT, w, was introduced in this equation to correct for the effect of nanoparticles content. The compression and microinjection molded samples were also examined by wide angle X-ray diffraction (WAXD). The tests were carried out using a Bruker AXS X-Ray goniometer equipped with a Hi-STAR two-dimensional area detector. The generator voltage and current were 40 kV and 40 mA, respectively and the copper Cu Kα radiation (λ = 1.542 Å) was selected by a graphite crystal monochromator.

7.4.5. Electrical conductivity measurements

The volume resistivity of the nanocomposites were determined by measuring the DC resistance across the thickness of compression molded disks using a Keithley electrometer model 6517 equipped with a two probe test fixture. All the connections were made using short wires to insure that the resistivity of the whole set up was negligible. The resistivity of the set up was measured each time before the tests to make sure that the system was working properly. This equipment allows resistance measurements up to 10^{17} Ω. The level of applied voltage, adapted to the expected resistance, was in the range of 1000 V for the neat polymers and samples containing up to 1wt% MWCNT and 100 V for samples containing 2 wt% and more MWCNTs. However, since for the more conductive samples, the accuracy of this equipment failed, samples containing more than 1 wt% MWCNTs were tested using the more adequate Keithley electrometer model 6220 connected to a current source (Aligent 34401 A , 6 ½ Digit Multimeter). For each sample

the *I-V* curve was obtained and the sample resistance was determined from the slope of the curve. The resistance was then converted to volume resistivity, ρ_v, using the formula

$$\rho_v = AR_v / D \tag{7-2}$$

where A is the contact surface area, D is the thickness of the sample, and R_v is the measured resistance. The electrical conductivity (σ) of the nanocomposites is the inverse of volume resistivity. Prior to measurements all samples were dried under the conditions previously described.

7.4.6. Mechanical properties

An Instron Micro Tester model 5548 was used to measure the tensile strength, modulus and elongation at break of nanocomposites using microinjected tensile bars having a gage length of 4.3 mm. The tests were performed at room temperature using a crosshead speed of 50 mm/min, based on ASTM D638, and data acquisition rate of 13 data points per second. The tensile strength and elongation at break could be directly obtained from the stress-strain curves. To obtain the elastic modulus, a linear regression technique was utilized to define the slope of the stress-strain curve in the initial region before yield. All the reported values were averaged over six specimens for each composition with a maximum deviation of ±8%.

7.5. Results

7.5.1. Morphology

SEM micrographs of the surfaces of compression molded and microinjected samples for the nanocomposites of 3wt% MWCNTs in PP and 5wt% MWCNTs in PC are shown in Figure 7.1. It is worthy to mention that when the surface of the PP sample is chemically etched the presence of nanotubes can be observed more clearly. It is clear that for the polypropylene nanocomposites, nanotube aggregates are formed and the distribution is not uniform (Fig. 7.1a). However, the nanotubes are well dispersed in the polycarbonate matrix and the distribution at the micro level is quiet uniform (Fig 7.1b). As mentioned before the mixing conditions have been previously optimized. The presence of nanotube aggregates even after improving the mixing conditions and using PP-g-MA as a compatibilizer indicates that polypropylene is a difficult host, in the sense that the carbon nanotubes were not fully dispersed as individual entities. Although some small

aggregates were also seen in the PC/MWCNT nanocomposites nanotubes were dispersed almost individually even at the most unfavorable conditions.
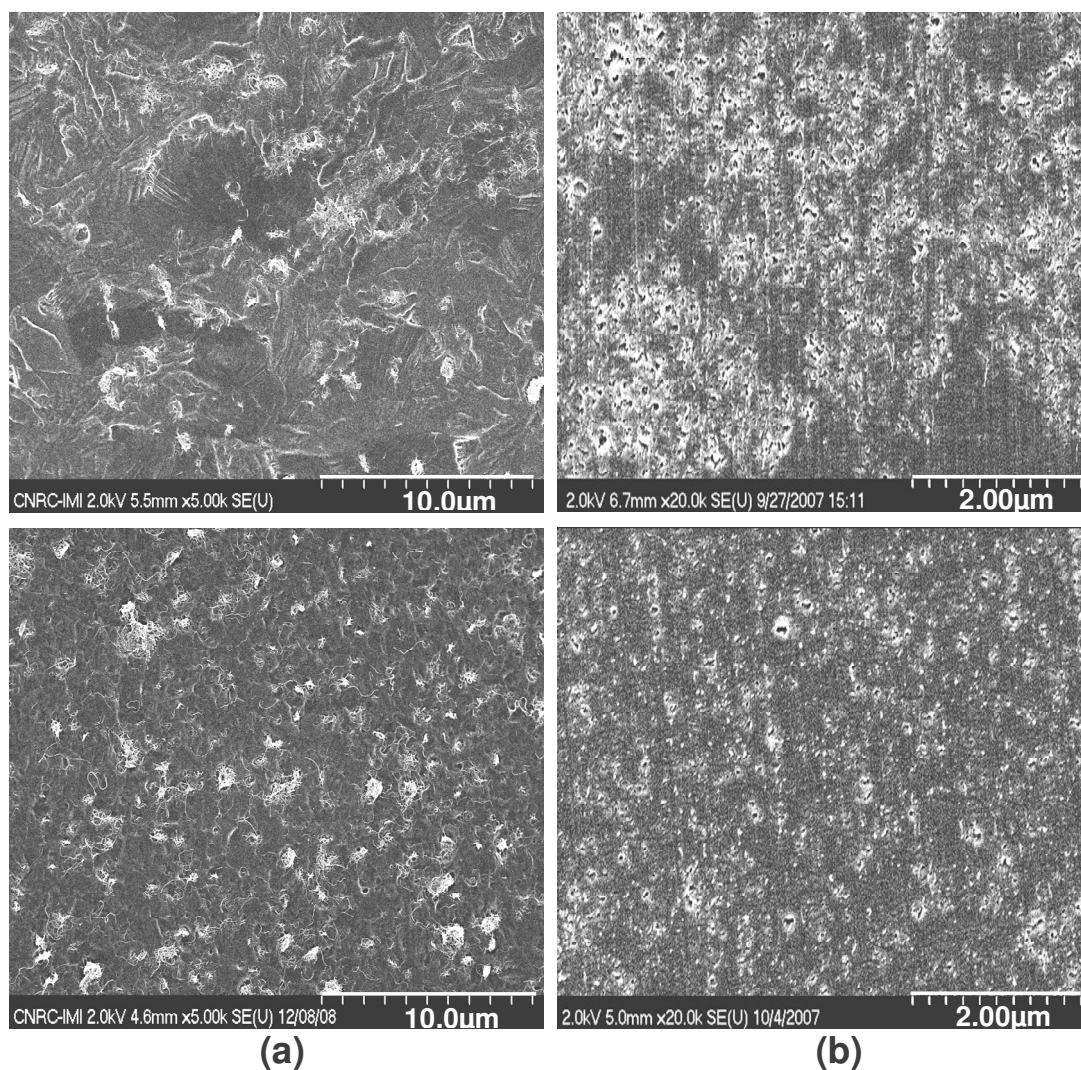
Figure 7.1: SEM micrographs of (a) etched surface of PP/ 3wt% MWCNT and (b) crayon surfaces of PC/ 5wt% MWCNT nanocomposites. The top and the bottom micrographs are related to the compression molded and microinjected samples, respectively

These results reveal clearly a large difference between the compatibility of MWCNTs with PC as a polar amorphous polymer and with PP as a non-polar polymer with a high degree of crystallinity. Due to the presence of strong polar-polar bonds, the nanotubes are better dispersed in PC without the formation of many aggregates; for polypropylene the lack of such polar bonds results in a poor dispersion of the nanotubes. In addition, the growth of the crystalline phase in

the later case may result in the expulsion of the nanotubes towards the amorphous phase and lead to the formation of large aggregates in the PP-based nanocomposites [20].

Figure 7.1 also indicates that the nanotubes are somehow better distributed in the case of the microinjected samples. The drastically high deformation rates in microinjection molding contribute strongly to the nanotube distribution within the polymer matrix. In the case of PP/MWCNT nanocomposites, the formation of smaller crystals in the microinjected samples may be considered as another cause for the better distribution of the nanotubes. However, aggregates are still observed in these samples. On the other hand, since the nanocomposite electrical conductivity is one of the main points of attention in this work, a well dispersed system may not be required for the formation of an electrically conductive network. As Figure 7.2 shows for both nanocomposites, in PP and in PC, an interconnected network of entangled MWCNTs exist forming a percolated network. This network seems to be even stronger and more efficient in the case of PP nanocomposites in spite of worse dispersion quality.

(a) **(b)**
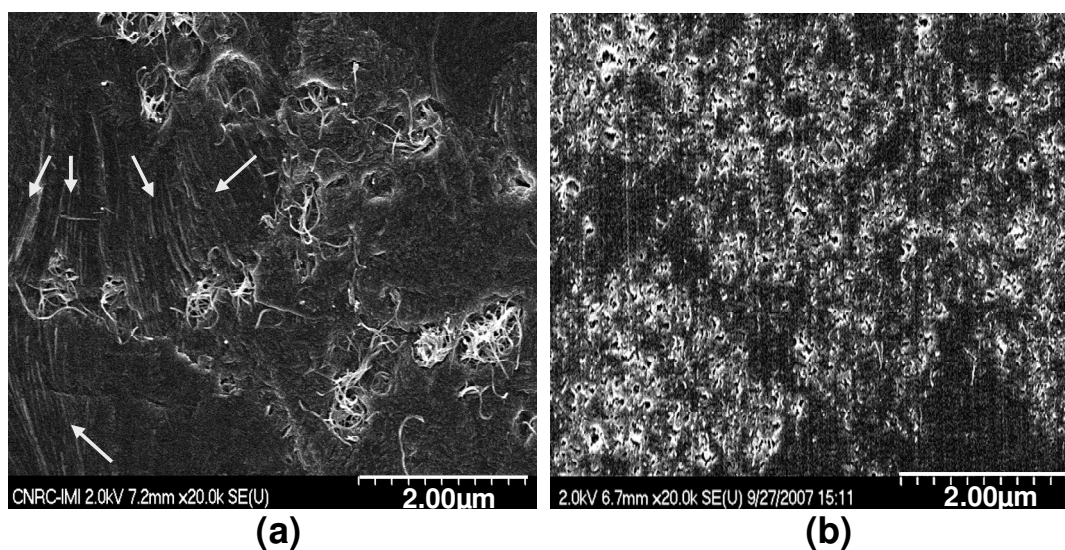
Figure 7.2: High resolution SEM micrographs of (a) etched surface of PP/ 3wt% MWCNT and (b) crayon surfaces of PC/ 5wt% MWCNT nanocomposites. The arrays indicate the lamellae of the formed spherulites of PP

The presence of a crystalline phase in the PP matrix creates a structure similar to a two-phase blend with one crystalline and the other amorphous [36]. From a thermodynamic point of view, fillers and other kinds of impurities can never exist in a crystal [32, 37, 38] and, therefore,

nanotubes are expected to be found only in amorphous phase. The white and somehow parallel strips seen in Figure 7.2a, indicated by the arrows, are the lamellae edge of crystal spherulites, which radiate from a nucleating center. The crystalline phase, distinguished by the presence of the lamellae, rejects the nanotubes in growing steps. Therefore, as the figure illustrates the nanotubes are located in the amorphous phase between the lamellae and form a continuous path in this blend-like structure. Consequently according to the concept of double percolation threshold strong nanotube networks are formed even at lower content compared to what is observed in PC/MWCNT nanocomposites. The overall percolation threshold in PP is equal to the threshold of the amorphous phase, which is only a fraction of the polymeric matrix and fewer nanotubes are needed to create a network in this part.

The formation of networks and the quality of the dispersion can be observed more clearly in TEM micrographs (Fig. 7.3). In the PP nanocomposites (Fig. 7.3a), in spite of non-uniform dispersion, a strong connection between the nanotubes and consequently a complete network formed in the nanocomposite provide a very suitable conductive pathway for the electrical current. In the PC nanocomposites (Fig. 7.3b), although nanotubes are well dispersed in whole samples, the nanotube networks seems to be not as strong as those formed in the PP nanocomposites.

(a)   **(b)**
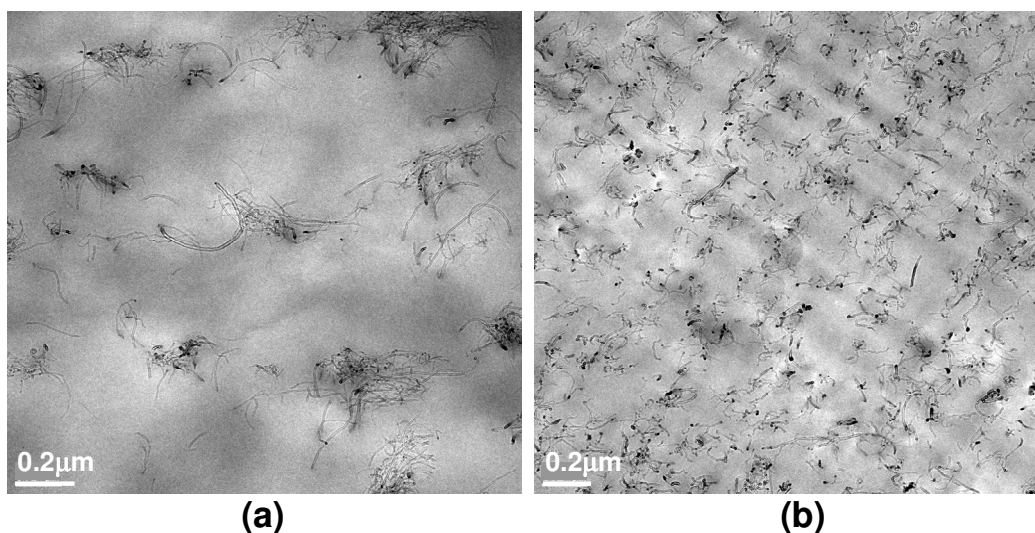
Figure 7.3: TEM micrographs of thin sections of (a) PP/ 3wt% MWCNT and (b) PC/ 5wt% MWCNT nanocomposites

7.5.2. Crystallization and crystalline structure

Carbon nanotubes are well known to impart profound changes to the crystallization behavior of semicrystalline polymers [39, 40]. The presence of nanotubes provides a tremendous amount of heterogeneous nucleation sites for crystallization as they act as effective nucleating agents [39, 41]. The overall crystallization process is therefore expected to be accelerated as a result of this heterogeneous nucleation process. The effects of nanotube loading on the crystallization and crystalline characteristics of PP/MWCNT nanocomposites were examined using DSC tests.
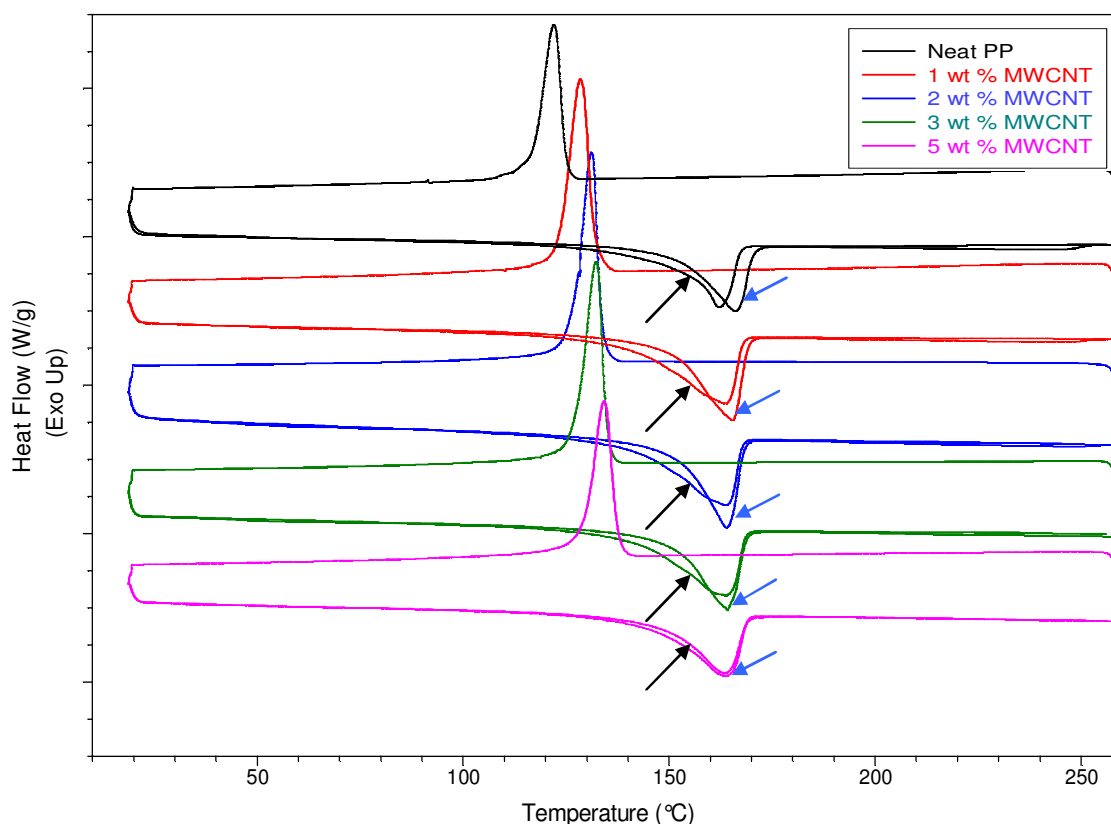
Figure 7.4: DSC micrograms for the PP nanocomposites of various nanotube loadings: first heating cycles for compression (black arrows) and microinjection (blue arrows) samples and cooling cycle

Figure 7.4 shows the DSC curves of the first heating and cooling cycles for compression and microinjection molding samples of various nanotube loadings. The second heating cycles for all samples are almost the same as the first heating cycle of the compression molded samples and, therefore, these cycles are not shown in the graph. From the cooling cycles it is obvious that the

crystallization onset and peak temperature (T_C values reported in Table 7.1) increase with nanotube concentration suggesting a high degree of crystal nucleation at the surface of the MWCNTs. The effect is more pronounced at lower MWCNT content. As it is increased, however, a saturation point in nucleating sites is reached and the accelerating effect disappears.

Table 7.1. Non-isothermal crystallization and melting parameter for various nanotube loadings for the PP samples prepared in compression (C), microinjection-compression (M-C) and microinjection (M) molding. The degree of crystallinity of compression molded samples obtained from XRD results is included

MWCNT (wt %)	T_C (°C)	Crystallinity (%) (DSC results)			Crystallinity (%) (XRD results)	T_m (°C)	
		C	M-C	M	C	C	M
0	122.0	38.6	47.8	44.4	39.9	162.1	166.0
0.5	124.4	43.7	50.9	47.6	49.7	162.3	165.9
1	128.4	52.2	57.6	54.6	51.3	163.5	165.2
2	131.0	53.7	59.6	56.2	52.2	163.6	163.9
3	132.1	52.8	57.3	53.8	50.0	163.7	163.8
5	134.1	43.2	45.8	44.7	47.5	163.7	163.7

The overall crystallization rate due to the combined effects of nucleation and growth is affected by the crystallization temperature. The degree of supercooling or the difference between T_m and T_c is then a good indication of crystallizability or crystallization rate. The smaller this difference, the higher the overall rate [42]. As Figure 7.4 and Table 7.1 show the T_c values significantly increase with nanotube loading, while the effect is not so pronounced in the case of T_m (values for the compression molded samples or samples before injection) and as a result the difference between T_m and T_c is lowering with nanotube loading. The half crystallization time ($t_{1/2}$), defined as the time required to reach 50% relative crystallinity, is usually reported to compare the rate of crystallization of different samples. It is calculated by using the following equation[43] :

$$X_r = \int_{T_0}^{T} Q dT \left/ \int_{T_0}^{T_\infty} Q dT \right. \tag{7-3}$$

where X_r is the relative crystallinity; Q is the heat flow at temperature T; T_0 and T_∞ are the initiation and termination crystallization temperature, respectively. The time related to each temperature can be calculated as follows:

$$t = (T_0 - T)/CR \tag{7-4}$$

where T_0 is onset temperature, T is current temperature and CR is the cooling rate ($10\ ^{\circ}$C/min in our case). The crystallization curves as a function of time during the cooling cycle are reported in Figure 7.5. As it is observed, the rate of crystallization increases with nanotube content even though the effect is somehow larger at low nanotube loading. From a thermodynamic point of view, higher temperature favors the movement of the polymer chains and accelerates the growth process. Accordingly the presence of the nanotubes shifts the crystallization temperature to higher temperatures and thermodynamically accelerates the crystallization process.
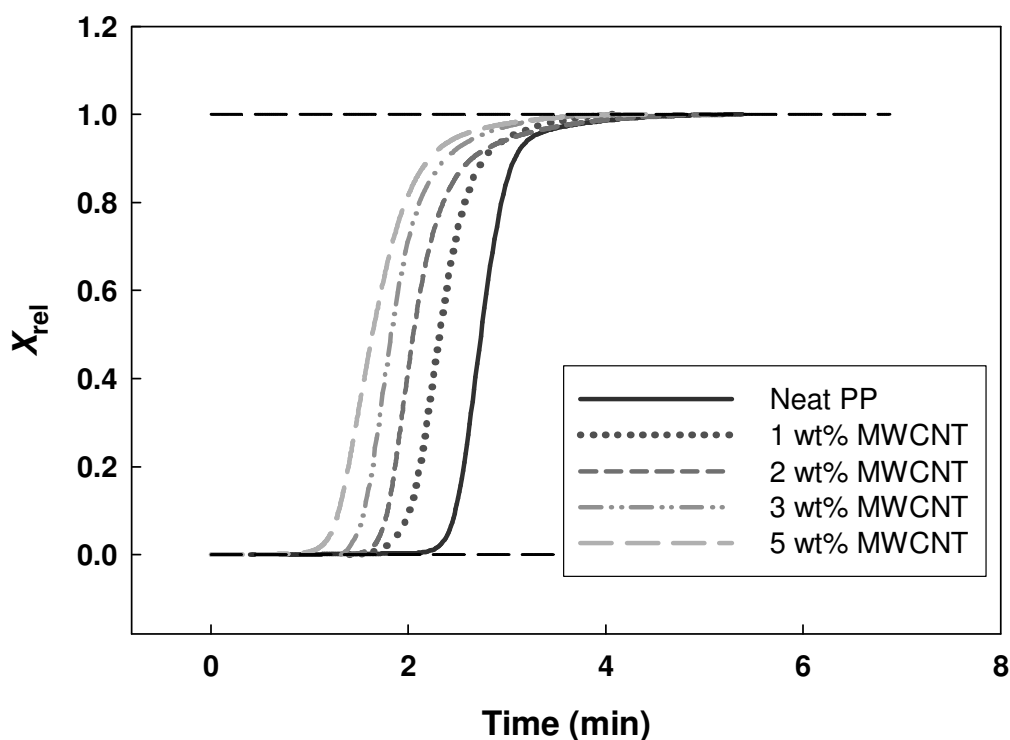
Figure 7.5: Relative crystallinity as a function of time at different carbon nanotube loading during cooling cycle

The degree of crystallinity of the nanocomposites of different nanotube content before injection (compression molded samples) and for microinjected and microinjection-compression molded samples are summarized in Table 7.1. In all cases, the results show first an increase then a decrease in the degree of crystallinity as a function of nanotube content. MWCNT content below 2 wt% causes an increase in crystallinity. At MWCNT content higher than 2%, a decrease in crystallinity is observed. It will be shown thereafter (electrical conductivity) that 2 wt% MWCNT is the critical amount of nanotube for a network formation and electrical percolation

threshold in PP nanocomposites. The process of polymer crystallization is controlled first by crystal nucleation and second by crystal growth. In this particular case, the addition of up to 2 wt% nanotubes to the PP matrix results in a rapid increase of the number of nucleating sites, an increase in the nucleation rate and the degree of crystallinity as well; above 2 wt% the rate of nucleation keeps increasing, albeit more slowly before leveling off. On the other hand, the formation of a nanotube network restricts the polymer chains motion and therefore the formed crystals can not grow properly and, consequently, the overall crystallization decreases.

The effects of microinjection and microinjection-compression processing are shown in Table 7.1. Clearly these processes do not dramatically influence the crystallinity of the nanocomposites. The extremely high shear rates of these processes during the injection phase are expected to orient the polymer chains in the flow direction and to result in higher crystallinity. However, since injection is very fast and the whole cycles take only few seconds, the chains do not have enough time to fully crystallize under the very high cooling rate. In microinjection-compression molding this effect is less pronounced as the cycle time is higher due to the compression phase and cooling rate is slower. This, combined with applying a certain level of pressure after injection, results in a relatively higher crystallinity. The results of T_m for compression (samples before injection) and microinjection samples are also shown in this table. It is well known that polymer chains are oriented under flow, and this results in a reduction of the entropy, S, of polymer melts. The equilibrium melting temperature is defined by [44]:

$$\Delta G = \Delta H - T_m^0 \Delta S = 0 \tag{7-5}$$

where ΔG is the free energy, ΔH and ΔS are the enthalpy and entropy of crystallization (or fusion), respectively. Considering that the enthalpy is not affected by flow, the equilibrium melting temperature must increase as a result of the entropy reduction [45]. In microinjection molding, in spite of short cycling time, the equilibrium melt temperature of the neat PP increases due to high deformation rate of the process, which results in highly oriented polymer chains. However, as shown in Table 7.1 there is no difference between the melting points for the 5 wt% nanocomposite before and after microinjection. Obviously, the presence of nanotubes hinders the polymer chain orientation. Accordingly, the effect of microinjection and microinjection-compression on the degree of crystallinity is decreased with nanotube loading.

The effect of microinjection process on crystallization and orientation of the crystalline phase was also considered using WAXD. The X-ray diffraction patterns obtained for the 5% PP/MWCNT composite are shown in Figures 7.6a and b.
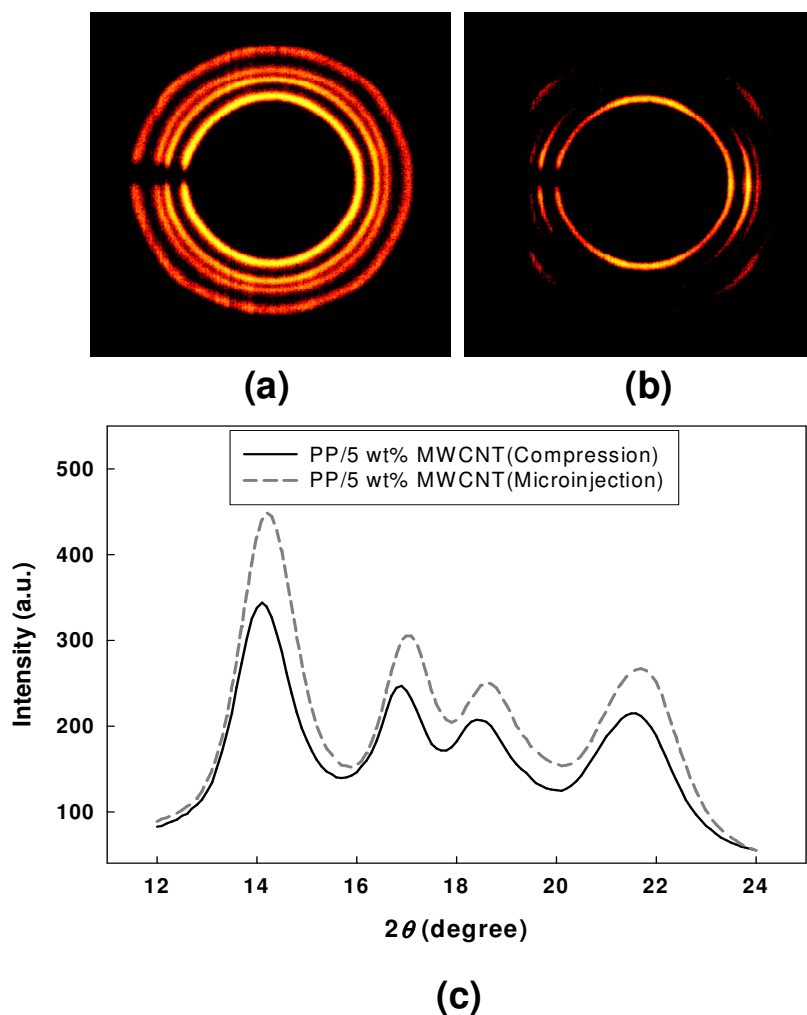
Figure 7.6: WAXD pattern of 5 wt% PP/MWCNT nanocomposites for (a) compression molded, (b) microinjected samples. (c) Diffraction spectrum with integration through the circles

For the compression molded samples whole rings are observed indicating random orientation. On the other hand, the diffraction patterns obtained from the microinjection sample exhibit distinct and bright asymmetric arcs, a clear indication of a relatively high level of orientation. The corresponding 2θ diffraction intensity curves are shown in Figure 7.6c. Both compression molded and microinjected samples show the same profile of the α-crystals of iPP and there is no effect of microinjection on the reflections indicating that the crystalline structure

of iPP did not change. After deconvolution of the peaks and from the area under the curves, the crystallinity was calculated and, similarly to DSC results, it was found that the degree of crystallinity increases up to 2 wt% nanotube loading and then decreases for larger loading; even though, the crystallinity obtained from WAXD was slightly different from that obtained using DSC (Table 7.1).

7.5.3. Electrical conductivity

One of the stated objectives of this work was to investigate the effect of the processing conditions on the electrical conductivity of nanocomposites based on carbon nanotubes. Microinjection molding was chosen because it imparts a high degree of shearing and orientation on the polymer chains and nanotubes as opposed to compression molding processing. Moreover, the electrical property data may be a useful to understand the relationship between the nanocomposite microstructure and the final properties of the microparts. Figure 7.7 presents the effect of the nanotube loading on the electrical conductivity of the disk shaped nanocomposites samples prepared by the same processing methods as previously.

The electrical conductivity above the threshold can be described by a power-law expression [6, 27]:

$$\sigma = \beta_{c,\sigma} \left(\frac{m - m_{c,\sigma}}{m_{c,\sigma}} \right)^q \qquad \text{for } m \geq m_{c,\sigma} \qquad (7\text{-}6)$$

where $\beta_{c,\sigma}$ and q are power-law constants, and $m_{c,\sigma}$ is the electrical percolation threshold (wt%). This power-law expression is found to describe very well the data of Figure 7.7 above the percolation threshold given by the left limit of the dashed line corresponds to the percolation threshold value in each case.

For compression molded samples the percolation threshold is found to be around 3 wt% of nanotubes for PC nanocomposites and around 1 wt% for PP nanocomposites. At these critical concentration levels, the electrical conductivity rises suddenly by more than 10 decades and the nanocomposites with nanotube contents larger than 1 and 3 wt% (in PP and PC nanocomposites, respectively) can be considered as electrically conductive. This sudden rise in the electrical conductivity is due to the formation of a network of connected nanotubes paths. Beyond this percolation threshold the electrical conductivity increases more gradually and asymptotically towards a plateau. This is a typical percolation behavior, which is usually observed in the

nanocomposites of conductive fillers and can be referred as an ideal percolation behavior [13, 46].
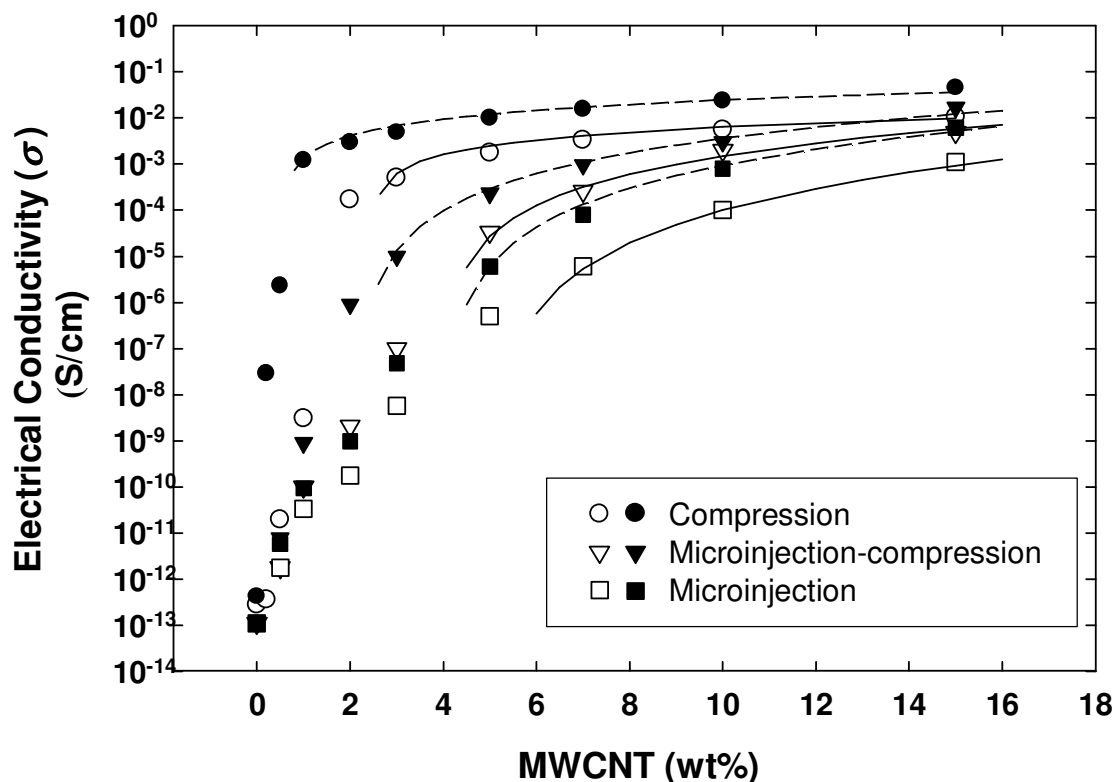
Figure 7.7: Effect of polymer processing conditions on electrical conductivity and percolation threshold of the PP/MWCNT (filled symbols) and PC/MWCNT (open symbols) nanocomposites. The lines shown are the best fits of Eq. 7-5

On the other hand, as can be seen from Figure 7.7, such a behavior is not obvious for the microinjection molded samples as no step-like increase in electrical conductivity is observed for both PP and PC based nanocomposites. In the microinjected samples the nanotubes are well aligned in the flow direction due to the very high shear rates of the process [27] and are less likely to interconnect. A conductive pathway resulting from a proximity effect would form only at high nanotube contents and consequently the percolation threshold is expected to rise. The percolation threshold of microinjected samples, as determined using equation 7-5, is higher at about 6 and 4 wt% of nanotubes loading in PC and PP nanocomposites, respectively. Our preliminary results (not presented here) revealed that for a dog-bone shaped mold cavity, where the flow is longitudinal, the percolation threshold is higher (about 9 wt%) and the electrical conductivities are about one order of magnitude lower than those of the disk shaped cavity

samples. The radial flow of the centrally gated cavity is largely elongational near the gate and near the flow front while shear flow is dominant near the cavity walls [47]. This results in a more complex orientation of the nanotubes: in the radial direction in the layers near the walls and in the transverse or azimutal direction in the core. This mixed orientation leads to a more random overall orientation and more interaction between the nanotubes resulting in a lower electrical percolation threshold.

The electrical threshold pertaining to microinjection-compression molded samples is found to be close to the one obtained in the compression molded samples. As described before, this process has two phases: an injection phase with a high shear rate-low pressure step and a compression phase with low shear rate-high pressure step. Due to the high level of shear rate, the nanotubes are well aligned near the cavity walls at the end of the first step or injection phase. However, the compression phase is similar to a squeeze flow, which forces the nanotubes to partially rearrange in the transverse direction and results in a somehow isotropic arrangement of the nanotubes. This is more favorable for the creation of nanotube networks. The effect of the presence of crystals on the electrical conductivity is also observed in Figure 7.7. Clearly for all processes, the electrical conductivity is about one order of magnitude larger and percolation threshold is somehow lower in the case of PP nanocomposite according to the concept of double percolation threshold. Polypropylene can be assumed as a two-phase blend whereas the nanotubes are mostly located in amorphous phase (as showed before in morphological study). Accordingly there are two types of percolation in the nanocomposite at the same time: continuity of the filler-rich phase or amorphous phase and percolation of nanotubes in this phase.

7.5.4. Mechanical properties

Typical stress-strain curves of both PP/MWCNT and PC/MWCNT nanocomposites with respect to nanotube content are shown in Figure 7.8. The neat PP presents the typical behavior of a ductile material with a very high elongation at break (700%). At about 250% of elongation strain hardening begins and then the tensile stress increases almost linearly with strain until fracture or break eventually occurs. In the case of nanocomposites with lower loading (0.5 and 1 wt% MWCNTs) the same ductile behavior is observed with necking and strain hardening but with significantly lower elongation at break. For the nanocomposites with higher nanotube contents (3 and 5 wt%), a brittle behavior is observed with breaking after the yield point.
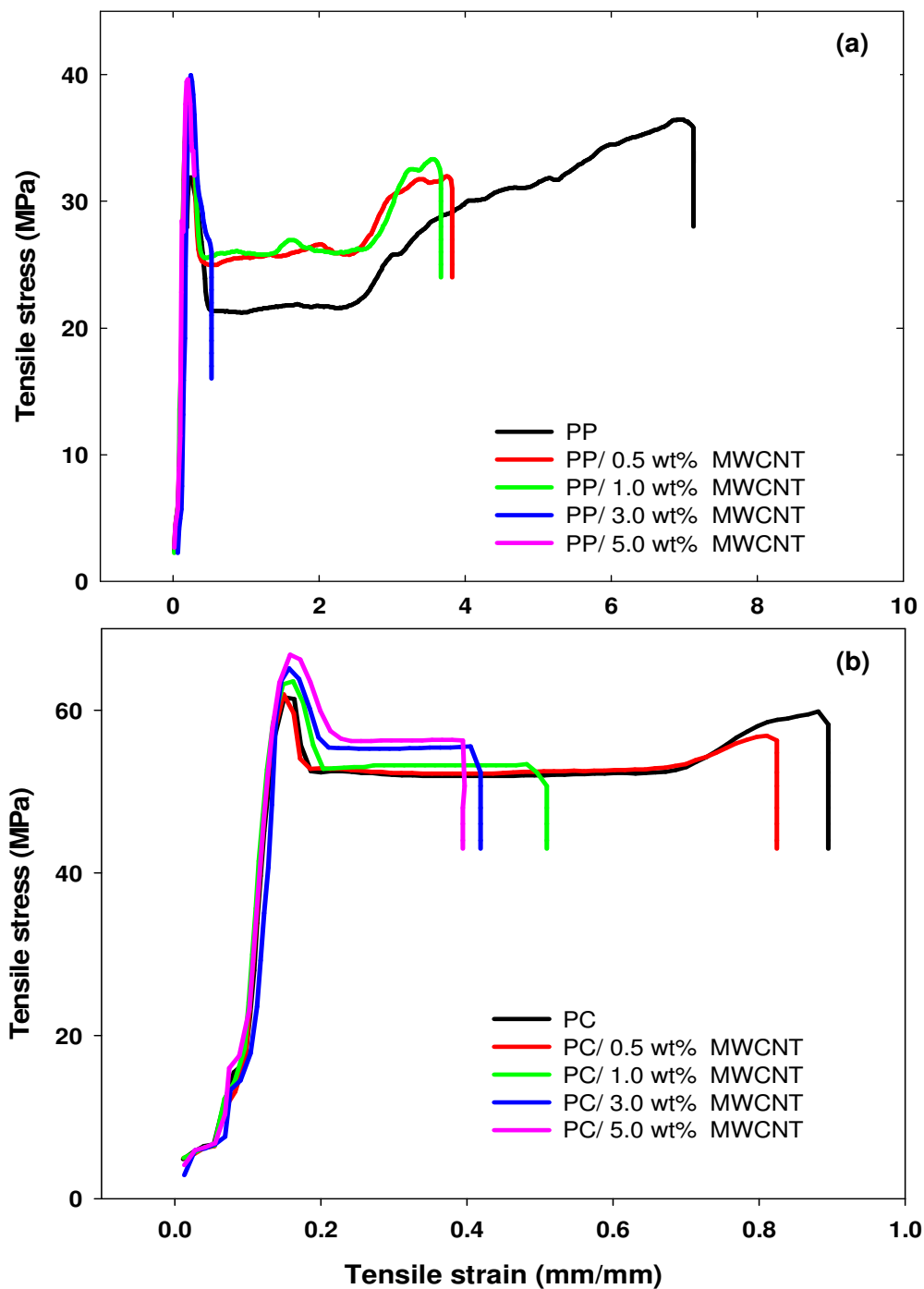
Figure 7.8: Tensile behavior: stress-strain diagrams of (a) PP/MWCNT and (b) PC/MWCNT

The neat PC shows the same ductile behavior with about 8 times lower elongation at break (90%). For the neat PC and the 0.5 wt% PC/ nanocomposite strain hardening and necking at high elongation are observed. However, the nanocomposites with higher nanotube loadings show no

strain hardening and become more brittle as the strain-to-failure decreases with nanotube concentration. All samples show yielding before exhibiting plastic flow.

As Figure 7.8 reveals, the elongation values at break for the PP/MWCNT nanocomposites are about 8 times larger than those of PC/MWCNT nanocomposites. However, in both cases, the values are strongly affected by nanotube loading, starting to decrease drastically beyond 1wt% of nanotubes loading. The structural change of the nanocomposites with increasing nanotube content is probably responsible for this phenomenon. At a critical concentration, the formation of nanotubes aggregates or agglomerates induces a change in the load transfer behavior of the nanocomposites and results in a different trend in the mechanical properties.
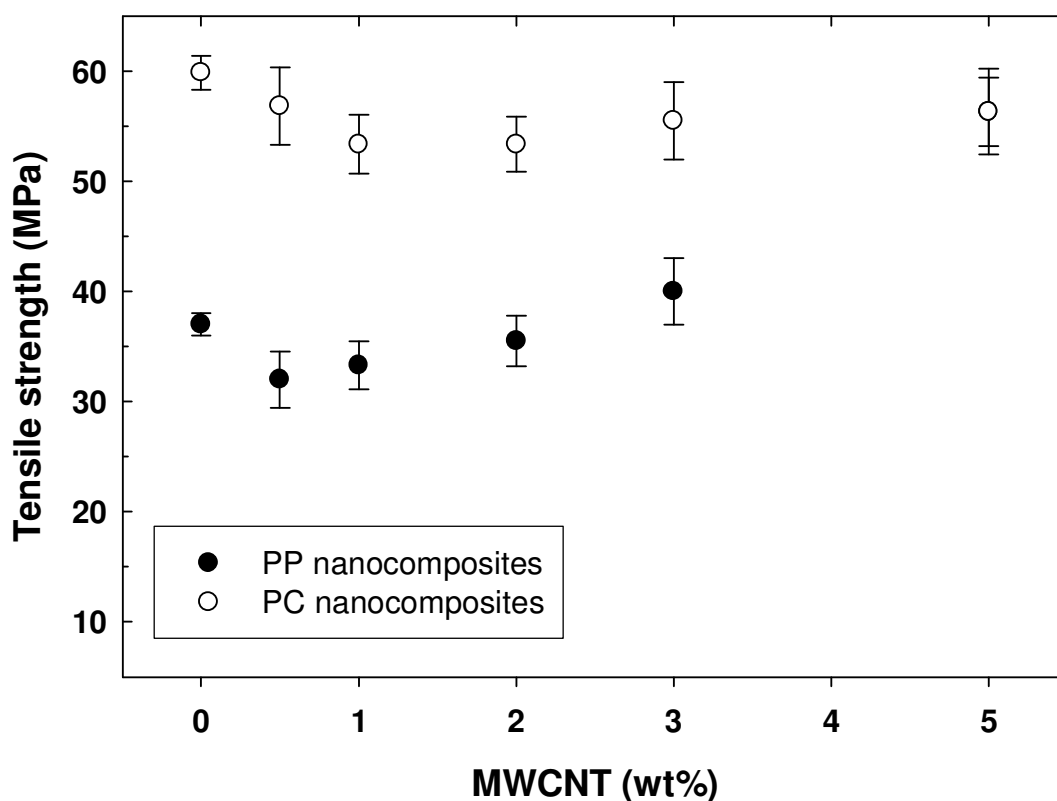
Figure 7.9: Tensile strength of dog-bone shaped microinjected PP/MWCNT and PC/MWCNT nanocomposites

The strength at break of the various nanocomposites is summarized in Figure 7.9 as a function of nanotube loading. As expected, the neat PC and its nanocomposites have larger strength than the PP and its nanocomposites. However, in both cases the effect of nanotube loading on the nanocomposite strength is not very significant and the overall tendency

demonstrates only a modest increase with MWCNT concentration. This could probably be due to the poor interaction between the nanotubes and polymer chains so that the nanotubes could not demonstrate their theoretical potential as very strong filler with extremely high strength [48]. We also observe first a slight decrease of the strength at break then an increase with MWCNT loading after 1 wt% in PC and after 2 wt% in PP, probably due to the formation of nanotube networks at these concentrations.
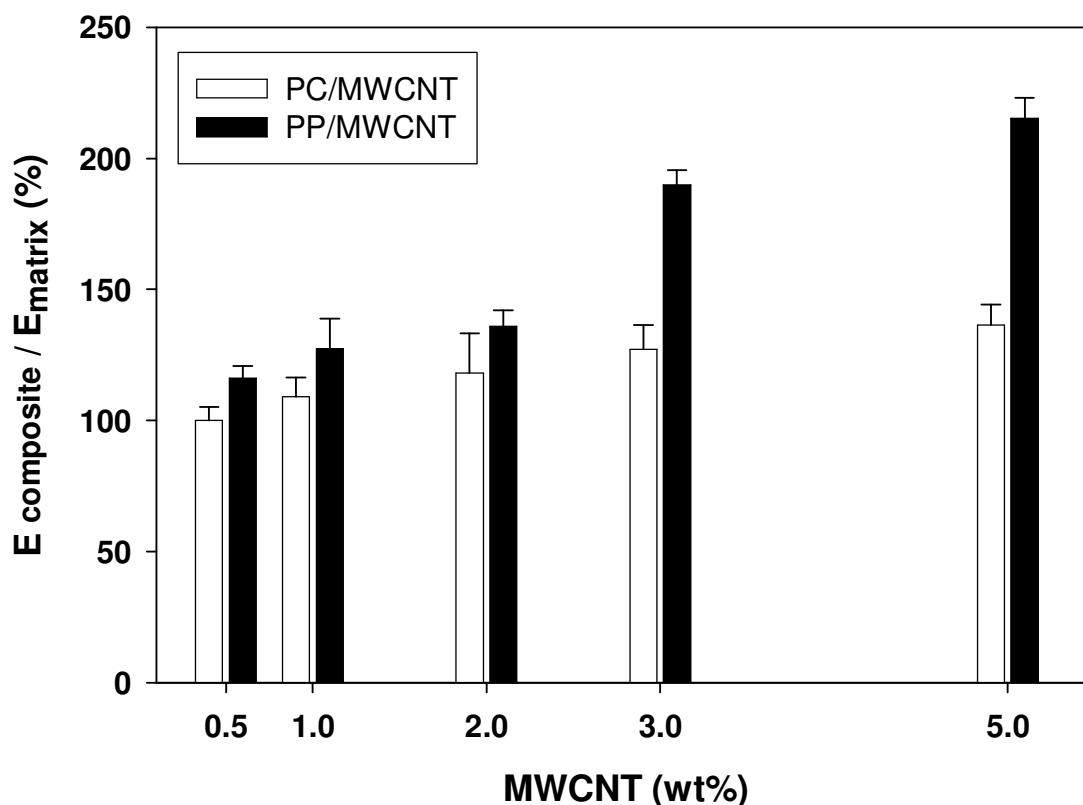
Figure 7.10: Relative Young modulus of PP/MWCNT and PC/MWCNT with respect to the neat polymers

The effect of MWCNT loading on the Young modulus of the nanocomposites is shown in Figure 7.10. In order to compare the effect of nanotubes on the modulus of PP and PC, the raw values are normalized with respect to the neat polymer modulus. It is observed that the addition of nanotubes significantly affects the Young modulus of PP while the effect is less significant in the case of PC/MWCNT nanocomposites. The modulus of PP increases by more than 90% with only 3 wt% of nanotubes largely due to the increased degree of crystallinity, while for PC the

amount of increase is considerably lower, about 30% for the same nanotube content. However, the rate of increase of the elastic modulus is more moderate for larger nanotube loadings.

7.6. Conclusions

In this work we have examined the effects of crystalline structure and polymer processing conditions on PP/MWCNT and PC/MWCNT nanocomposite properties. Related masterbatches were diluted to prepare the nanocomposites, and a reasonably good dispersion and formation of nanotube networks within the polymer matrices were confirmed using SEM and TEM. Prepared nanocomposites were then subjected to different shear values in a controlled manner employing a variety of polymer processing methods including compression molding, microinjection-compression molding and microinjection molding. The study of the crystalline behavior of PP/MWCNT nanocomposites using DSC and XRD methods revealed that the presence of the nanotubes provided a tremendous amount of sites for heterogeneous nucleating and as a result crystallization temperature increased. The rate of crystallization increased with nanotube content as well. The degree of crystallinity was also increased by the presence of nanotubes up to 2 wt %. For the nanotube loading of 3 wt% and higher, however, the crystallinity decreased due to the formation of nanotube networks, which restricted the polymer chains motion and slowed down the crystal growth. It was also found that the high shear values of microinjection molding only slightly changed the overall crystallinity because of very short cycle time of the process. However, the crystals were all oriented in the flow direction.

Interestingly, increasing the type of processing strongly affected the electrical conductivity of the nanocomposites. The percolation thresholds rose significantly in both PP and PC nanocomposites using processing involving larger shear rates. In these cases a broad range of percolation were observed. The presence of a crystalline structure was also found to improve the electrical conductivity of PP/nanocomposites according to the concept of double percolation threshold. Mechanical properties of the nanocomposites were also found to be significantly improved with the addition of nanotubes especially in case of the PP/MWCNT nano-composites.

7.7. References

1. S. Iijima, Nature, **354**, 6348(1991).

2. S. Iijima, T. Ichihashi, Nature, **363**, 6430(1993).

3. M. Meyyappan, *Carbon nanotubes : science and applications*. CRC Press, Boca Raton (2005).

4. O. Meincke, D. Kaempfer, H. Weickmann, C. Friedrich, M. Vathauer, H.O. Warth, Polymer, **45**,3(2004).

5. M. Moniruzzaman, K.I. Winey, Macromolecules, **39**, 16(2006).

6. G. Hu, C. Zhao, S. Zhang, M. Yang, Z.G. Wang, Polymer, **47**,1(2006).

7. Y.T. Sung, M.S. Han, K. H. Song, J.W. Jung, H.S. Lee, C.K. Kum, J. Joo, W.N. Kim, Polymer, **47**, 12(2006).

8. G.T. Pham, Y.B. Park, S. Wang, Z. Liang, B. Wang, C. Zhang, P. Funchess, L. Kramer, Nanotechnology, **19** ,32 (2008).

9. W.Y. Wang, G.H. Luo, F. Wei, J. Luo, Polym. Eng. Sci.(2009), In press.

10. L. Karasek, M. Sumita, J. Mater. Sci., **31**, 2 (1996).

11. M. Sumita, S. Asai, N. Miyadera, E. Jojima, K. Miyasaka, Colloid Polym. Sci., **264,** 3(1986).

12. M. Sumita, H. Abe, H. Kayaki, K. Miyasaka, J. Macromol. Sci. , Part B, **25,**1(1986).

13. D. Wu, L. Wu, W. Zhou, T. Yang, M. Zhang , Polym. Eng. Sci., **49**,9(2009).

14. P. Potschke, A.R. Bhattacharyya, A. Janke. Carbon, **42,**965(2004).

15. J. Zeng, B. Saltysiak, W.S. Johnson, D.A. Schiraldi, S. Kuma, Composites, Part B, **35**,2,(2004).

16. B. Lin , U. Sundararaj, P. Potschke, Macromol. Mater. Eng., **291,**3(2006).

17. F. Du, R.C. Scogna, W. Zhou, S. Brand, J.E. Fischer, K.I. Winey, Macromolecules, **37**,24(2004).

18. J.K.W. Sandler, J.E. Kirk, I.A. Kinloch, M.S.P. Shaffer, A.H. Windle, Polymer, **44**,19(2003).

19. K. Jeon , L. Lumata, T. Tokumoto, E. Steven, J. Brooks, R.G. Alamo, Polymer, **48**, 16(2007).

20. S.C. Tjong , G.D. Liang, S.P. Bao, Polym. Eng. Sci., **48**,1(2008).

21. M. Sumita, K. Sakata, S. Asai, K. Miyasaka, H. Nakagawa, Polymer Bulletin, **25**,2 (1991).

22. M. Sumita, K. Sakata, Y. Hayakawa, S. Asai, K. Miyasaka, M. Tanemura, Colloid Polym. Sci., **270,**2(1992).

23. V. Tan, M.R. Kamal, J. Appl. Polym. Sci. **22**,8(1978)

24. W. Ding, A. Eitan, F. T. Fisher, X. Chen, D. A. Dikin, R. Andrews, L. C. Brinson, L. S. Schadler, R. S. Ruoff, Nano Lett.,**3** ,11 (2003).

25. W. Ding, A. Eitan, F.T. Fisher, X. Chen, D.A. Dikin, R. Andrews, L.C. Brinson, L.S. Schadler, R.S. Ruoff, Nano Lett., **3**,11(2003).

26. P. Potschke, M. Abdel-Goad, I. Alig, S. Dudkin**,** D. Lellinger, Polymer, **45**,26(2004).

27. S. Abbasi, P. J. Carreau, A. Derdouri, M. Moan,Rheologica Acta **48**, 9(2009).

28. X. Chen, J. Hu, L. Zhou, W. Li, Z. Yang, Y. Wang, J. Mater. Sci. Technol. **24**, 2(2008).

29. T.E. Chang, L.R. Jensen, A. Kisliuk, R.B. Pipes, R. Pyrz**,** A.P. Sokolov, Polymer, **46**,2(2005).

30. A.A. Koval'chuk, A.N. Shchegolikhin, V.G. Shevchenko, P.M. Nedorezova, A.N. Klyamkina, A.M. Aladyshev, Macromolecules, **41**,9(2008).

31. K. Prashantha, J. Soulestin, M.F. Lacrampe, P. Krawczak, G. Dupin, M. Claes, Compos. Sci. Technol., **69**,11-12(2009).

32. H. G. Kilian, G. Lagaly, I. Chudacek, *Relationships of Polymeric Structure and Properties*. Progress in Colloid and Polymer Science. Vol. 78, Springer, Berlin / Heidelberg(1988).

33. P. Potschke, T.D. Fornes, D.R. Paul, Polymer, **43**,11(2002).

34. D.W. Litchfield, D.G. Baird, Polymer, **49**,23(2008).

35. G.W. Lee, S. Jagannathan, H.G. Chae, M. L. Minus, S. Kumar, Polymer, **49**,7(2008).

36. L. E. Nielsen , R. F. Landel, *Mechanical properties of polymers and composites*. 2nd ed. Marcel Dekker, New York (1993).

37. A. Sharples, *Introduction to polymer crystallization*. St. Martin's Press, New York (1966).

38. T. S. Nordmark, G.R. Ziegler, Carbohydrate Polym.,**49**,4(2002).

39. D. Wu, L. Wu, G. Yu, B. Xu, M. Zhang. Polym. Eng. Sci., **48**,6(2008).

40. J. Y. Kim., S.-I. Han, S. H. Kim , Polym. Eng. Sci., **47**,11(2007).

41. S.Y. Lin, E.C. Chen, K.Y. Liu, T.M. Wu, Polym. Eng. Sci. (2009), In press.

42. C.-F. Ou, M.-S. Chao, S.-L. Europ. Polym. J.**36**,12(2000).

43. Z. Li, G. Luo, F. Wei, Y. Huang, Compos. Sci. Technol., **66**,7-8(2006).

44. B. Monasse, B., J. Mater. Sci., **30**,19(1995).

45. T. W. Haas, B. Maxwell, Polym. Eng. Sci.,**9,**4(1969).

46. X. Feng, G. Liao, J. Du, L. Dong, K. Jin, X. Jian., Polym. Eng. Sci.,**48**,5(2008).

47. M. Vincent, E. Devilers, and J.F. Agassant, J Non-Newton Fluid Mech, **73**,3(1997).

48. F. Zhengping, W. Jianguo, G. Aijuan, Poly. Eng. Sci., **46**,5(2006).

Chapter 8

Carbon Nanotube Conductive Network in Crystalline and Amorphous Polymers and Polymer Blends[*]

The idea of the final part of the project was to improve the electrical conductivity of the nanocomposites based on the concept of "double percolation threshold". The results obtained in the last part showed that crystalline materials have higher electrical conductivity even at high shear conditions. In this paper the effect of crystalline phase on the nanotube alignment and on electrical conductivity was investigated in more details. The results confirmed that nanotubes are well aligned in sheared samples however the level of alignment is less in crystalline polymer. It was also shown that the orientation of crystalline phase slightly decreased with addition of nanotube in PP. The electrical conductivity of PP/CBT blend was also improved through a double percolation that is the basic requirement for the conductivity of the ternary nanocomposites. It was also found that the nanotubes affected the morphology of the blends resulted in a smaller and more elongated dispersed phase.

---

[*] ***Polymer.*** To be submitted.

8.1. Abstract

We investigated the electrical conductivity and percolation behavior of binary composites of PP/MWCNT and PC/MWCNT and ternary composites of PP/CBT (cyclic butylene terephthalate)/MWCNT. Samples of various MWCNT loadings were prepared by diluting commercial masterbatches of nanotubes using optimized melt-mixing conditions. SEM and TEM techniques were then used to examine the quality of dispersion and formation of nanotube networks within the polymer matrix. In binary composites TEM and Raman spectroscopy results showed that nanotubes are well aligned in sheared samples although the level of alignment is less in crystalline polymer. XRD result revealed that the crystal orientation decreased with incorporation of nanotubes into polypropylene. The conductivity properties were also significantly altered by nanotube alignment in both PP and PC nanocomposites; electrical conductivity decreased and percolation threshold rose in high sheared samples; however the presence of crystalline phase improved the conductivity even at high shear condition through the concept of double percolation threshold. The electrical conductivity of PP/CBT blend was also improved through a double percolation that is the basic requirement for the conductivity of the ternary nanocomposites. It is also found that the nanotubes affected the morphology of the blend resulted in a smaller and more elongated dispersed phase.

8.2. Introduction

Carbon nanotubes (CNTs) are ideal fillers for high performance nanocomposites due to their intrinsic structure, size scale and aspect ratio combined with unique electronic structure and outstanding properties (Dresselhaus, Dresselhaus et al. 1995; Meyyappan 2005). In recent years, carbon nanotube / polymer composites have spurred considerable interest because of their extraordinary properties from both processing and application points of view. One of the key interest in carbon nanotubes incorporated into polymeric materials stems from their potential to develop conductive polymer composites at relatively low concentrations (Meincke, Kaempfer et al. 2004; Hu, Zhao et al. 2006; Moniruzzaman and Winey 2006; Sung, Han et al. 2006; Pham, Park et al. 2008). Percolation theories are frequently applied to describe high electrical conductivity in composites made of conductive filler and an insulating matrix. It has been shown that the percolation threshold depends not only on the types of filler and polymer but also on the dispersion state of the filler and the morphology of the matrix (Sumita, Abe et al. 1986; Sumita, Asai et al. 1986; Karásek and Sumita 1996; Sandler, Kirk et al. 2003).

In the case of high aspect ratio fillers such as nanotubes the onset of percolation strongly depends on their alignment as well. When the nanotubes are aligned in the polymer matrix, the probability of tube-tube contacts decreases and consequently the percolation threshold raises (Abbasi, Carreau et al. ; Du, Scogna et al. 2004; Kharchenko, Douglas et al. 2004; Potschke, Brünig et al. 2005). Additional complexity arises in semi-crystalline matrices due to the crystallization induced phase separation and subsequent rejection of the nanotubes by the advancing crystalline phase (Jeon, Lumata et al. 2007; Tjong 2008). Moreover, carbon nanotubes are well dispersed in polar polymers such as poly (methylmethacrylate) (PMMA) (Zeng, Saltysiak et al. 2004) and polycarbonate (PC) (Lin 2006). However, in non-polar polymers such as polypropylene, CNT dispersion remains a big challenge and might affect the percolation threshold as well.

Incorporation of carbon particles into incompatible polymer blends can provide them with electrical conductivity at very low filler content due to a double percolation phenomenon (Sumita, Sakata et al. 1991; Sumita, Sakata et al. 1992). Double percolation refers to the structure in which there are two types of percolation in the same composite material. The first one, which is typically observed in the reinforced composite materials, is associated with the electrical continuity of the conductive particles in the filler-rich phase and the second one is associated with

the continuity of this phase in the blend. In a blend of two polymers the difference in affinity of added conductive particles to each polymer component of the ternary composite system results in a heterogeneous distribution of the conductive filler. The affinity of the conductive particles to the polymer components of the blend and consequently their distribution between them is directly controlled by their respective interfacial energies. For the attainment of high electrical conductivity, both types of percolation are required and the conductivity improvement will depend on the conductive particle concentration in the filler-rich phase and on the volume fraction of the filler-rich phase in the blend (Sumita, Sakata et al. 1992). Following this concept, the electrical resistivity of the blend of PC and polyethylene (PE) was significantly reduced when co-continuity was achieved at 70% PE volume faction using only 0.41 vol% of multi wall carbon nanotubes (MWCNTs) (Potschke, Bhattacharyya et al. 2004).

Polycarbonate (PC) and polypropylene (PP) are important commercially available thermoplastics because of their well balanced physical and mechanical properties. Recently, carbon nanotubes have been used as a special filler to be incorporated into these polymers for stiffness reinforcement as well as thermal and electrical conductivities enhancement purposes (Abbasi, Carreau et al. 2009 ; Potschke, Abdel-Goad et al. 2004; Potschke, Bhattacharyya et al. 2004; Chang, Jensen et al. 2005; Pham, Park et al. 2008). However, polypropylene exhibits very poor compatibility and adhesion towards other materials and inorganic fillers owing to its non-polarity and absence of functional groups. It has been found that in PP/clay nanocomposite, crystallization of the PP matrix, led to clay platelets expulsion from the crystalline phase by thermodynamic forces (Khunová 1988).

The idea of this study is to investigate the effect of crystalline structure on the nanotube alignment and consequently on the microstructure and electrical conductivity of the nanocomposites in high shear conditions. The attention is focused on two kinds of polymer: polycarbonate (PC) as a polar amorphous polymer and isotactic polypropylene (iPP) as a non-polar semi-crystalline polymer. Microscopic techniques were used to qualitatively analyze the formation of nanotube network and nanotube dispersion and alignment in the polymer matrix. X-ray diffraction was also used to ascertain the degree of orientation. By using the X-ray method normally the orientation of the crystalline phase is well detected. Consequently, we used an alternative method, Raman spectroscopy, to quantitatively measure the degree of alignment. Laser Raman analysis is one of the methods largely used for determining the degree of structural

ordering or the presence of defects in graphitic-like materials. This is a non-destructive spectroscopy technique which provides information of CNTs and CNFs such as vibration of crystal lattice, electron structure and integrity of crystal structure, etc (Zhao and Wagner 2004). It was previously shown that the high shear rates of polymer processing resulted in a high degree of nanotube alignment and consequently changed the behavior of nanotube networks (Abbasi, Carreau et al. 2009). The combination of all these techniques can provide us with complimentary information about how the presence of crystalline phase changed the shear induced properties of the nanocomposites. The nanocomposite preparation was optimized using various characterization methods including transmission electron microscopy (TEM) and scanning electron microscopy (SEM). As nanotubes intertwine into agglomerates that are difficult to disperse we used premixed polymer/carbon nanotube masterbatches and diluted them to the required concentrations by adding the base polymer. This insured consistent and reproducible results.

The effect of selective location of carbon nanotube and the double percolation phenomenon on the electrical conductivity of the nanocomposites was investigated on blends of cyclic butylene terephthalate (CBT) with PP/MWCNT nanocomposites with different nanotube loadings at various CBT blend compositions.

8.3. Experimental

8.3.1. Materials

Masterbatches of 20 wt% MWCNT in PP and of 15 wt% MWCNT in PC were purchased from Hyperion Catalysis International, Cambridge, MA. According to the supplier, the carbon nanotubes are vapor grown and typically consist of 8-15 graphite layers wrapped around a hollow 5 nm core (Potschke, Fornes et al. 2002). The diameter range was stated to vary from 15 to 50 nm and the length range between 1-10 μm as was confirmed by TEM characterization. The masterbatches were then diluted with isotactic polypropylene (PP HD120) supplied by Borealis Co. and with polycarbonate (Calibre 1080) supplied by Dow Chemical to prepare nanocomposite samples of various loadings. The added polymer grades are not necessarily the same as the matrices used to make the masterbatches. Considering the small quantity of masterbatch used to prepare the nanocomposites, the original polymer of the masterbatch is only a small fraction of the nanocomposites and does not significantly affect the results. Polypropylene grafted maleic

anhydride (PP-g-MA Polybond PB3150 with 0.5 wt% MA) was used as compatibilizer to try improving the dispersion in PP/MWCNT nanocomposites. Cyclic butylene terephthalate (CBT) supplied by Cyclics Co. was used to prepare the blend of PP/CBT at different CBT concentrations.

8.3.2. Nanocomposite preparation and molding

The composites were made by melt mixing the masterbatches with the neat polymers. Polycarbonate and PC/MWCNT masterbatch were dried for a minimum of 4h at 120°C prior to mixing. Polypropylene, PP/MWCNT and PP-g-MA were also dried for 1hr at 90°C. Eight different composites with MWCNT contents between 0.5 and 15 wt% MWCNT were prepared using a lab-twin screw extruder, Leistritz ZSE 18HP, operating at 100 rpm and 210°C in case of PC composites and at 250 rpm and 190°C in case of PP composites. Microinjection molding was then used to prepare dog-bone shaped tensile bars under high shear condition using a Battenfeld Microsystem 50 micromolding machine. Compression molded disks were also prepared (Carver laboratory press, model 3912) to compare the nanocomposite properties before and after microinjection molding more precisely.

Ternary nanocomposites of PP/CBT/MWCNT were produced by diluting the PP/MWCNT masterbatch with proper amount of PP and CBT. Thirty six composites with six different CBT contents between 0 and 40wt% and six nanotube loadings between 0.2-5wt% were prepared using the same twin screw operating at 185°C and 250 rpm. These conditions were required to minimize residence time and avoid the possible polymerization of CBT into poly (butylene terephthalate) at 185°C (according to rheological measurements carried out on CBT at 185°C, polymerization time is about 300s).

8.3.3. Morphological characterization

The morphology of nanocomposites was studied through scanning and transmission electron microscopy (SEM). High resolution Hitachi S-4700 microscope was used in this study. In the case of PC nanocomposites, SEM was done on ultramicrotomed surfaces of samples that were cut with a diamond knife at room temperature. The surfaces of the PP and PP/CBT nanocomposite samples were etched with potassium permanganate solution to eliminate the amorphous phase from the surface. The quality of the dispersion can be seen much better with this method rather than using ultramicrotomed surface. In the case of PP/CBT blend without

nanotube SEM was done on fracture surface in the liquid nitrogen. All SEM samples were then coated with a vapor deposit of Pt for 25s. Transmission electron microscopy (TEM) was also done on ultrathin nanocomposites cross sections for a better observation of the morphology at higher resolution, using a Hitachi HD-2000 microscope.

8.3.4. Nanotube alignment

Raman spectroscopy was used as the most accurate method for nanotube quantitative alignment measurements. Raman spectra were collected using a Renishaw spectrometer equipped with an inVia Raman microscope fitted with a 20x objective. The samples were excited using a NIR laser (785 nm) with a grating of 1200 g/mm in a regular mode. Measurements were carried out at two different orientations of the incident laser beam with respect to the flow direction in the samples and the polarization direction (Fig. 8.1).
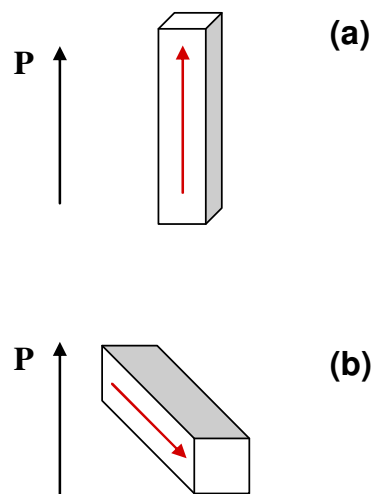
Figure 8.1: Schematic for Raman spectroscopy. Characteristic scattering configurations for the Raman spectroscopic measurements: (a) Parallel position of specimen, corresponding to 0° angle between polarization direction(P) and flow direction (red arrow); (b) Perpendicular position of specimen, corresponding to 90° angle between polarization direction(P) and flow direction (red arrows)

In the first configuration (Fig. 8.1a), the flow direction was parallel (0°) to the direction of the incident laser beam; in the second one (Fig. 8.1b), it was perpendicular (90°); The MWCNT alignment in the composite was determined by comparing the spectra for parallel and perpendicular directions.

8.3.5. Crystal orientation

Wide angle X-ray diffraction (WAXD) measurement was carried out using a Bruker AXS X-Ray goniometer accompanied with a Hi-STAR two-dimensional area detector. The generator voltage and current were 40 kV and 40 mA respectively and the copper Cu Kα radiation (λ = 1.542 Å) was selected by a graphite crystal monochromator. The method is based on the dissraction of a monochoromatic X-ray beam by the crystallographic planes of the polymer crystalline phase. The orientation factors from WAXD are mainly due to the crystalline part.

8.3.6. Electrical conductivity measurements

The volume resistivity of the PC/MWCNT nanocomposite samples was determined by measuring the DC resistance across the thickness of the samples using a Keithley electrometer model 6517 equipped with a two probe test fixture (ref to paper 2). This equipment allows resistance measurements up to 10^{17} Ω. The level of applied voltage, adapted to the expected resistance, was in the range of 1000 V for neat PC and samples containing up to 1wt% MWCNT and 100 V for samples with 2wt% and more MWCNT content. However, since for the more conductive samples, the accuracy of this equipment failed, samples with more than 2wt% MWCNT, were tested using the more adequate Keithley electrometer model 6220 connected to a current source (Aligent 34401 A , 6 ½ Digit Multimeter). For each sample the *I-V* curve was obtained and the sample resistance was determined from the slope of the curve. The resistance was then converted to volume resistivity, ρ_v, using the formula

$$\rho_v = AR_v / D \tag{8-1}$$

where A is the contact surface area, D is the thickness of the sample, and R_v is the measured resistance. The electrical conductivity (σ) of the nanocomposites is the inverse of volume resistivity. Prior to measurements all samples were dried in the conditions previously described.

8.3.7. Rheological measurements

The rheological measurements were carried out using a stress-controlled rheometer (CSM rheometer of Bohlin Instruments) equipped with a 25mm parallel plate geometry under nitrogen atmosphere. Prior to measurements, the samples were dried under the conditions previously described. Small amplitude oscillatory shear (SAOS) tests were carried out between 0.06 and 200

rad/s in the linear viscoelastic regime. This regime was established in the standard way by measuring the modulus at constant frequency (10 rad/s) and increasing strain magnitude. Further, long time measurements (up to 3h) were conducted to investigate the thermal stability of the nanocomposite samples. We assumed that the particle sizes were sufficiently small compared to the gap; however, the absence of apparent slip at the wall has been ascertained by varying the gap from 0.5 to 1.5 mm. The differences were found to be insignificant, less than the reproducibility of the data estimated to be within 3.5% for all the frequency sweep tests conducted with the various nanotube loadings.

8.4. Results

8.4.1. PP & PC nanocomposites

Morphology

As observed in the previous chapters nanotubes are dispersed almost individually in the polycarbonate and the distribution at the micro level is quiet uniform. For polypropylene, however, nanotube aggregates are formed and the distribution is not uniform. These results revealed clearly a large difference between the compatibility of MWCNT with polycarbonate as a polar amorphous polymer and with polypropylene as a non-polar polymer with a high degree of crystallinity. Formation of strong polar-polar bonds results in a better dispersion of the nanotubes in polycarbonate without the development of many aggregates; however, for polypropylene the lack of such polar bonds results in a poor dispersion of the nanotubes. In addition, the growth of the crystalline phase in the later case may result in the expulsion the nanotubes towards the amorphous phase and leads to the formation of large aggregates in the PP-based nanocomposites (Tjong 2008).

On the other hand, as previously mentioned, a well dispersed system may not be necessarily required for the formation of an electrically conductive network. It was shown that for both nanocomposites, PP and PC/MWCNT, an interconnected network of entangled MWCNTs exist forming a percolated network. This network seems to be even stronger and more efficient in the case of PP nanocomposites in spite of worse dispersion quality. The presence of a crystalline phase in the PP matrix creates a structure similar to a two-phase blend with one phase crystalline and the other amorphous(Nielsen and Landel 1993). Nanotubes are expected to be found only in

the amorphous phase since from the thermodynamic point of view fillers and other impurities can never exist in a crystal (Sharples 1966; Khunová 1988; Nordmark and Ziegler 2002). The crystalline phase, or the spherulitic structure, rejects the nanotubes as it grows. Thus the nanotubes end up being confined in the amorphous phase between spherulites and form a continuous path in this blend like structure. Consequently according to the concept of double percolation threshold the strong nanotube networks are formed even at lower content compared to what is observed in PC/MWCNT nanocomposites where there is crystalline phase. The overall percolation threshold in PP is equal to the threshold of the amorphous phase which is only a fraction of the polymeric matrix and fewer nanotubes are needed to create a conductive network in this case.

It has been shown that the nanotubes are well aligned when they are subjected to high shear rates (Abbasi, Carreau et al.). The nanotubes alignment in microinjected samples is shown in the TEM micrographs of Figure 8.2. The images were taken from thin sections cut along the flow direction.

(a) **(b)**
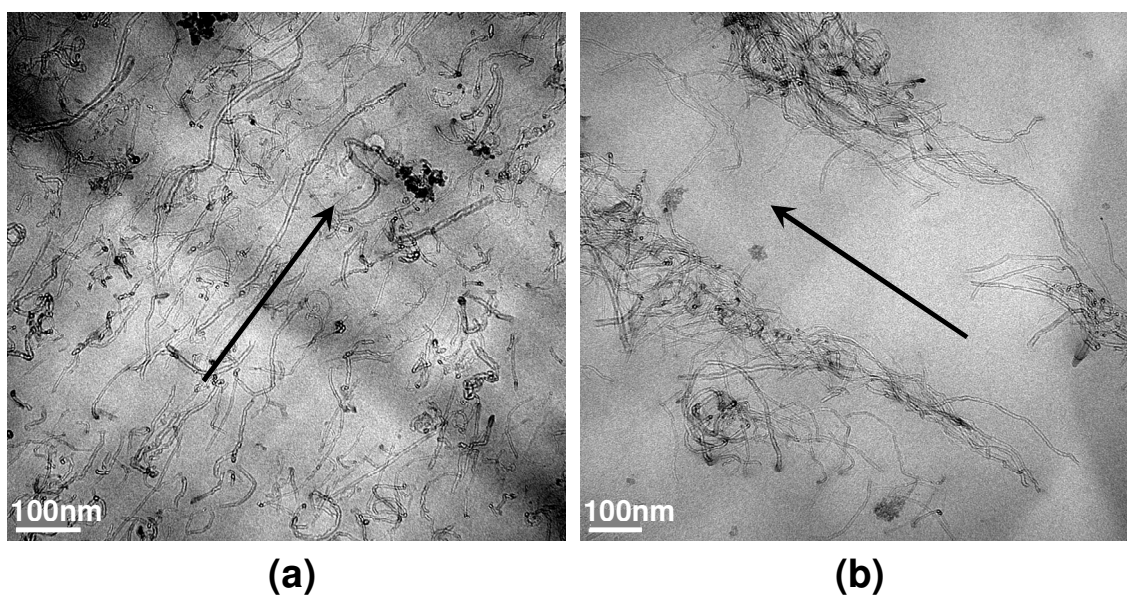
Figure 8.2: TEM micrographs of thin sections of (a) PC / 5wt% MWCNT and (b) PP/ 3wt% MWCNT nanocomposites

In the case of polycarbonate (Fig. 8.2a) the nanotubes are well aligned and most of them are perfectly stretched along their length axis. Considering the fact that the nanotubes are often strongly entangled, a few nanotubes remain oriented transversely (perpendicular to the flow

direction) after injection. In PP nanocomposite (Fig. 8.2b), however, we mostly observe nanotube aggregates overall orientation in the flow direction. Individual nanotubes are not well aligned and in some area there are bent nanotubes which connect the oriented aggregates together.

Nanotube alignment

Raman spectroscopy is used to further investigate MWCNT alignment within the polymeric matrices. This is a non-destructive spectroscopy technique, which relies on the inelastic scattering of infrared light by molecules upon returning to their lower energy level after excitation (Litchfield and Baird 2008). Carbon nanotubes show resonance-enhanced Raman scattering effects when a visible or near infrared laser is used as the excitation source. Both SWCNTs and MWCNTs feature bands located in the higher wavenumber region over 500 cm^{-1}; however, Raman bands appearing in the low wavenumber region between 100 and 400 cm^{-1} (known as radial breathing modes or RBM) are a unique characteristic of SWCNTs (Jehng, Tung et al. 2008) and are not generally observed for MWCNTs.

Contrary to carbon nanotubes, most polymers including polypropylene and polycarbonate do not show a resonance enhancement effect (Zhao and Wagner 2004). In fact, the large differences between the intensity of nanotube peaks and those arising from a polymeric matrix make the Raman spectroscopy an ideal technique for the orientation study of nanotubes.

As Figure 8.3 shows clearly, the Raman bands of neat polymers almost vanish after incorporation of nanotubes into them. Two important features in the Raman spectrum of multiwalled carbon nanotubes are the *D* band (disorder band), located between 1330-1360 cm^{-1} and *G* band (graphite band or TM-tangential mode) located around 1580 cm^{-1}. These bands are clearly observed in the spectrum of PP/MWCNT and PC/MWCNT of Figure 8.3. Another Raman band in the spectrum of carbon nanotubes, designated *G'*, is located at ~2700 cm^{-1} but is not sensitive to the nanotubes alignment (Bulusheva 2008).
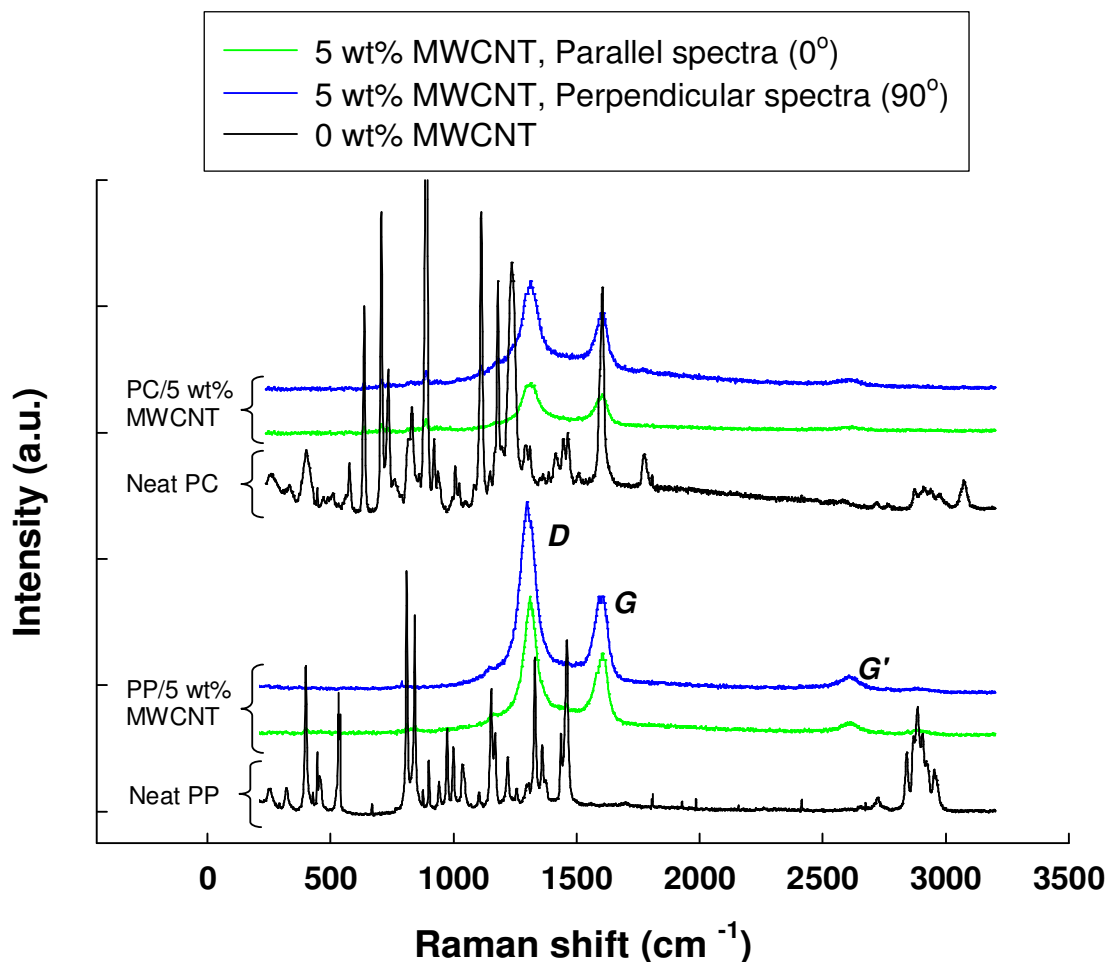
Figure 8.3: Raman spectra of neat polymers (black) and nanocomposites of 5wt% MWCNT: perpendicular (green) and parallel (blue) geometries

The intensity ratios $D_{\Pi}/D_{\perp}$ and $G_{\Pi}/G_{\perp}$ parallel/perpendicular to the flow direction are used to assess the degree of nanotube alignment. Raman spectra of PP/5wt% MWCNT and PC/5wt% MWCNT are shown in Figure 8.3 for microinjected samples.

As this figure reveals, the difference between the intensities of the peaks in parallel and perpendicular spectra is much more significant in PC/MWCNT nanocomposite, compared to what is observed in PP/MWCNT nanocomposites indicating that the nanotubes are more aligned in the former case. The intensity ratios $D_{\Pi}/D_{\perp}$ and $G_{\Pi}/G_{\perp}$ parallel/perpendicular to the flow direction are summarized in Table 8.1. Both ratios are much higher in the PC nanocomposite, demonstrating that the nanotubes are highly aligned in PC while the lower ratios obtained for the

PP nanocomposite indicate that the alignment is less in PP. These results are completely in agreement with the morphological analysis and clearly show the different level of alignment in the nanocomposites. The presence of the crystalline phase in PP significantly reduces the nanotube alignment.

Table 8.1. Intensity ratios parallel/perpendicular to the flow for direction

	Intensity ratio parallel/ perpendicular		
	$D_\Pi/D_\perp$	$G_\Pi/G_\perp$	$(D/G)_\Pi/(D/G)_\perp$
PC/5 wt% MWCNT	1.95	1.75	1.11
PP/5 wt% MWCNT	1.35	1.24	1.08

The *D/G* ratio is often used as a diagnostic tool for probing the perfection of MWCNTs (Bulusheva 2008) or degree of crystallinity in nanotube structure (Potschke, Brünig et al. 2005). A constant value of *D/G,* in both parallel and perpendicular geometries, then means that there is no change in the nanotube structure (Endo, Kim et al. 2001). To check the induced changes in the crystalline structure of MWCNTs, we used the ratio $(D/G)_\Pi/(D/G)_\perp$. When the nanotubes do not go through structural changes the *D/G* ratios are almost constant (Potschke, Brünig et al. 2005) and $(D/G)_\Pi/(D/G)_\perp$ should be close to unity. This is clearly the case for both the 5% MWCNT PC and PP nanocomposites as this ratio is about 1.11 and 1.08 respectively (see Table 8.1), indicating that the crystalline structure of individual nanotubes are more or less stable.

Crystal Orientation

WAXD was employed to study the orientation of the crystalline phases in the presence of nanotubes using microinjected PP parts.

The results obtained from two-dimensional WAXD analysis are shown in Figure 8.4. Within the compression molded or non-injected polypropylene samples (Fig. 8.4a) there is no preferred orientation and whole rings are observed indicating random orientation; microinjected PP samples (Fig. 8.4b), however, exhibit distinct and bright asymmetric arcs, a clear indication of a relatively high level of orientation. Figure 8.4c shows the effect of nanotube on the orientation

of PP phase in the nanocomposites. Although the bright arcs are still observed as an indication of crystal orientation, compared to what is presented in Figure 8.4b the arcs are fairly less sharp and more likely to whole ring indicating that the orientation decreases to some extent by adding nanotubes to the PP nanocomposites. This effect is analyzed later on in more details using tilt-angle XRD analysis.
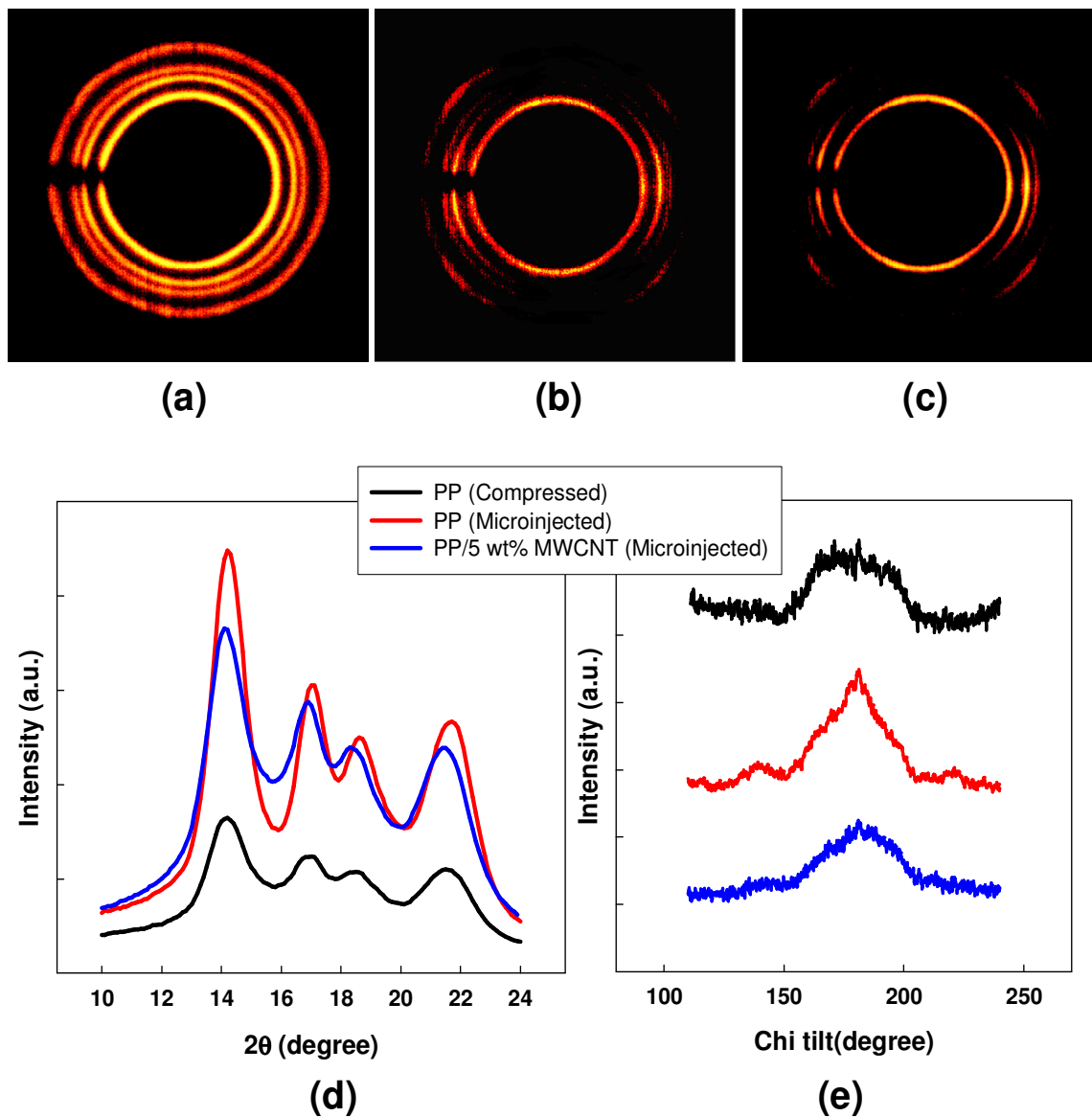
Figure 8.4: WAXD pattern of (a) compression molded PP (b) microinjected PP (c) microinjected nanocomposite of 5 wt% PP/MWCNT. (d) Diffraction spectrum with integration through the circles. (e) Tilt-angle spectrum with integration through 2θ

The 2θ diffraction intensity of the samples is shown in Figure 8.4d. Both compression molded and microinjected samples show the same profile of the α-crystals of iPP and there is no effect of microinjection on the reflections indicating that the crystalline structure of iPP did not change. The same profile can be also observed for the nanocomposites of PP/5wt% MWCNT suggesting that the nanotubes do not change the structure of α-crystals of iPP.

To support the WAXD results on orientation, the intensity is plotted as a function of the tilt (azimuthal) angle. The azimuthal angle,ϕ, is 0 or 180° along the perpendicular axis to flow direction or 90 or 270° along the axis parallel to flow direction. For each ϕ the average intensity was extracted from the 2D WAXD patterns and the result is shown in Figure 8.4e. Compression molded polypropylene sample gives a broad peak centered on an azimuth angle of 180° which is a good indication of random orientation; in the case of the microinjected PP sample the peak is rather sharp indicating that the PP crystals are oriented in the flow direction. Interestingly, by introducing nanotubes into PP (PP/5 wt% MWCNT) the peak at the same tilt angle is relatively broader than that observed in neat microinjected PP. This is an indication of slightly lower crystal orientation as it was previously concluded from the WAXD patterns.

Electrical conductivity

Electrical conductivity of the nanocomposites is one of our main interests in this work. Moreover, measurement of the electrical properties is a useful tool to understand the relationship between the nanocomposites microstructure and its final properties. Figure 8.5 presents the effect of nanotube loading on the electrical conductivity of the PP and PC nanocomposites. The electrical percolation threshold can be found by applying a power-law expression to the electrical conductivity data (Abbasi, Carreau et al.; Hu, Zhao et al. 2006):

$$\sigma = \beta_{c,\sigma} \left(\frac{m - m_{c,\sigma}}{m_{c,\sigma}} \right)^q \qquad \text{for } m \geq m_{c,\sigma} \tag{8-2}$$

where $\beta_{c,\sigma}$ and q are power-law constants, and $m_{c,\sigma}$ is the electrical percolation threshold (wt%). This power-law expression is found to describe very well the data of Figure 8.5 where the left limit of the dashed line corresponds to the percolation threshold value in each case.

For compression molded (non-processed) samples the percolation threshold is found to be around 3 wt% of nanotube for PC nanocomposites and around 1 wt% for PP nanocomposites.

These values show evidently the effect of crystalline structure on the electrical properties of the nanocomposites. In semi-crystalline polypropylene a nanotubes network is formed at a lower nanotube loading. In fact, the crystallization induced phase separation produces a blend of crystalline and amorphous phases. Most nanotubes are located in the amorphous phase, or continues phase, and create a conductive network at a lower concentration according to the concept of double percolation threshold, as discussed the morphology results section. As a consequence, the conductivity values after percolation are about one order of magnitude higher in the case of PP nanocomposite.
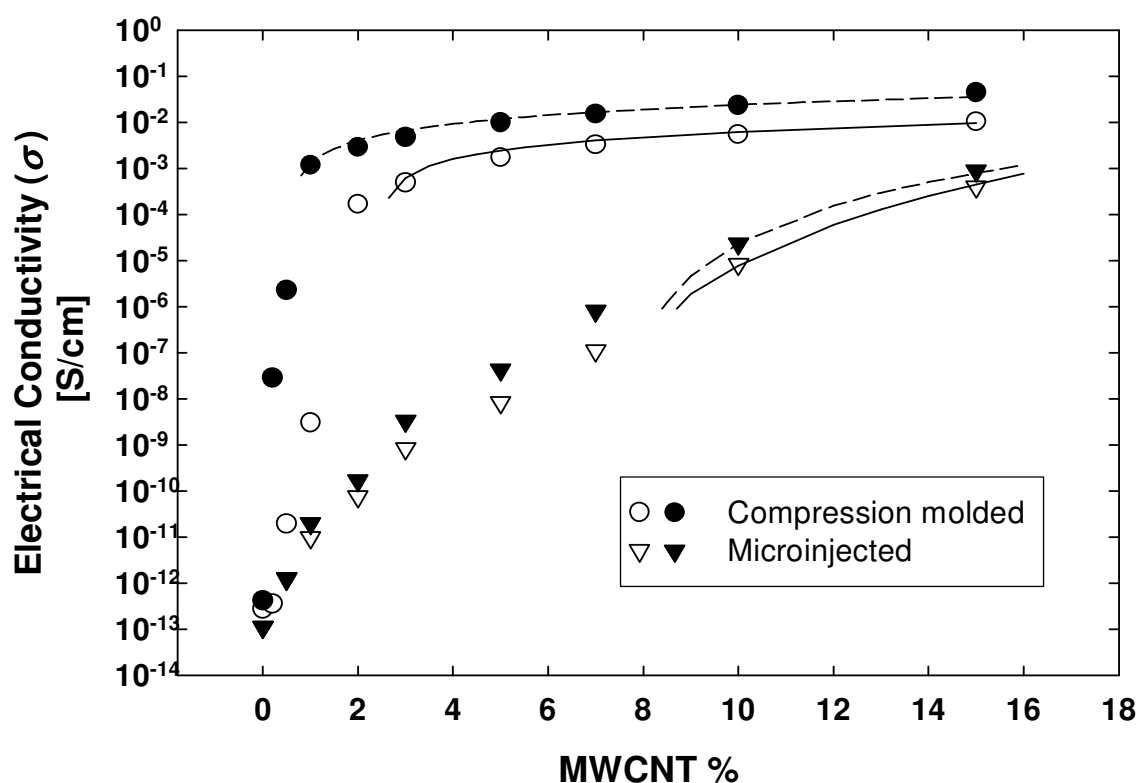
Figure 8.5: Electrical conductivity of compression molded and microinjected nanocomposites: PP/MWCNT (filled symbols) and PC/MWCNT nanocomposites (blank symbols)

As stated in the previous parts, in microinjected samples the nanotubes are well aligned in the flow direction and are less likely to be connected. To form a connected or percolated network in such a system, more nanotubes are required and consequently the percolation threshold rises. In other words, a conductive network of nanotubes can be formed only at high loadings where the aligned nanotubes are close enough to create a pathway for current transmission. It is seen from Figure 8.5 that that in such conditions where nanotubes alignment predominates, no stepwise

increase in electrical conductivity occurs at a percolation point as it can be observed in compression molded samples but rather a broad range of percolation over which electrical conductivity increases continuously.

Interestingly, a lower percolation threshold and a higher electrical conductivity level can be observed in the case of PP nanocomposites relative to PC nanocomposites. As discussed previously, the presence of a crystalline phase decreases the nanotubes alignment resulting in a more isotropic arrangement which is more favorable for the creation of nanotube networks.

Rheological properties

The complex viscosity ($\eta*$) obtained from SAOS measurements at 250°C are reported in Figures 8.6 for the PC (Fig. 8.6a) and PP (Fig. 8.6b) nanocomposites. At low frequencies the fully relaxed polymer chains exhibit the typical Newtonian viscosity plateau. As can be seen in Figure 8.6a, with the addition of MWCNT, the low frequency complex viscosity of PC significantly increases, particularly at high loading, indicating that the long polymer chain relaxation in the nanocomposites is effectively restrained by the presence of the nanotubes. Thus, the Newtonian plateau for the viscosity disappears progressively and a remarkable shear-thinning behavior is exhibited. Significant jumps in the low-frequency rheological properties are observed for MWCNT loadings of 0.5 wt % and above indicating a transition from viscoelastic liquid- to solid-like behavior. In other words, with increasing filler content, nanotube-nanotube interactions begin to dominate, leading eventually to a percolation network, which restrains the long-range motion of the polymer chains. Similar but to a lesser extent rheological behavior is observed for PP nanocomposites. In contrast to the electrical conductivity results the effect of nanotubes on the viscosity of polypropylene in significantly lower, while the percolation threshold is also higher, between 1-2 wt % nanotube loading. Although the viscosities of neat PP and its nanocomposites with low nanotube loadings are higher than those observed in neat PC and low loading PC nanocomposites, at higher nanotube loading (particularly after percolation point) the viscosity of PC nanocomposites is about 1 order of magnitude higher than that of PP nanocomposites. As we mentioned in last parts, the rejection of nanotubes by the crystalline phase during cooling and the existence of a double percolation threshold are the most important reasons of higher conductivity and lower percolation threshold in PP nanocomposites. During the rheological measurements, conducted in the molten state, no crystalline phase is present and

accordingly, the quality of dispersion comes to affect the rheological properties. In the PP nanocomposites, nanotubes are mostly dispersed in the form of aggregates rather than individual nanotubes. Consequently, the nanotubes are less effective in impeding the polymer chain motion and hence, the complex viscosity decreases and the rheological percolation threshold rises as higher loadings are needed to create nanotube networks and increase significantly the viscoelastic properties.
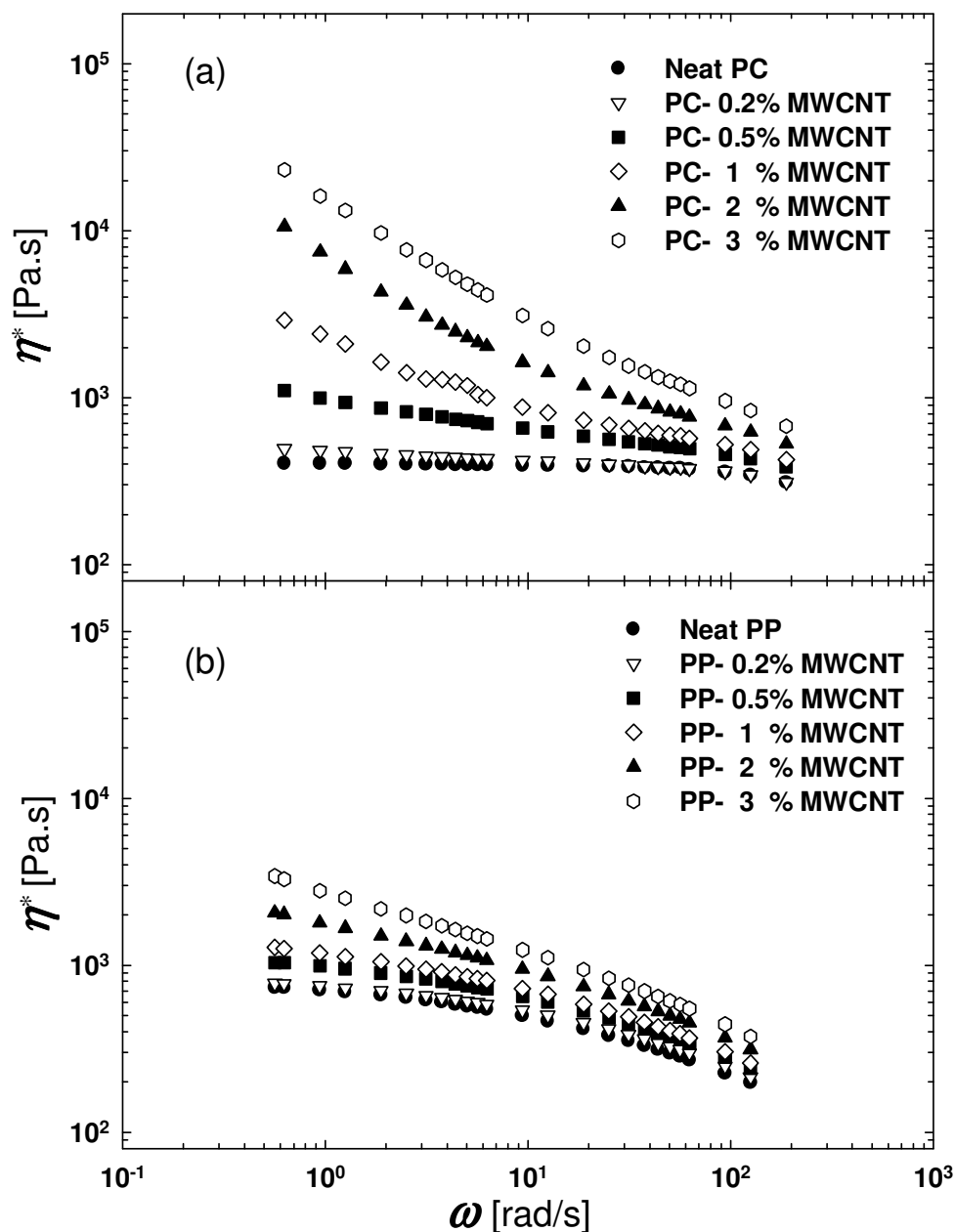
Figure 8.6: complex viscosity of (a) PC/MWCNT (b) PP/MWCNT nanocomposites at 250 $^{\circ}$C

8.4.2. PP/CBT blend nanocomposites

In this section, the morphology and electrical properties of MWCNT-filled PP/CBT blends are studied. The selective location of carbon nanotubes and the double percolation threshold of the nanocomposites are analyzed in detail.

Morphology

Figure 8.7 shows the SEM micrograph of an iPP/CBT (80/20) blend without nanotubes (Fig. 8.7a) and filled with 1 wt% MWCNT (Fig. 8.7b). The dark zones constitute the polypropylene matrix while the white domains form the minor CBT phase. As Figure 8.7b revealed the carbon nanotubes are preferentially located in or at the edge of the CBT phase due to their higher affinity to CBT.

As it can be observed in Figure 8.7a, the CBT phase forms the minor or dispersed phase which is in the shape of complete circle indicating that at this composition the blend is still far from co-continuous structure. Incorporation of nanotubes into the blend results in a completely different morphology (Fig. 8.7b). The nanotubes form a network of bridges between PP and CBT connecting these two phases together. Due to the significantly lower viscosity of CBT and also if we accept that the carbon nanotubes have a greater affinity with CBT (higher wettability) then the CNT strings we see in the right micrograph of Figure 8.7b try to link CBT domains (micrograph at left) between them across the PP phase. Rejection of the CNTs by PP helps in establishing this network of bridges between CBT domains and enhances the compatibility of two phases in the the blend. The smaller size of the CBT domains is also an enhancing factor as is the lower viscosity of CBT which allows for more mobility. It seems that the nanotubes act as compatibilizers trying to connect two phases or to make compatibility between them. The effect of these bridge or connecting structures on the electrical conductivity of the blends will be discussed later on.
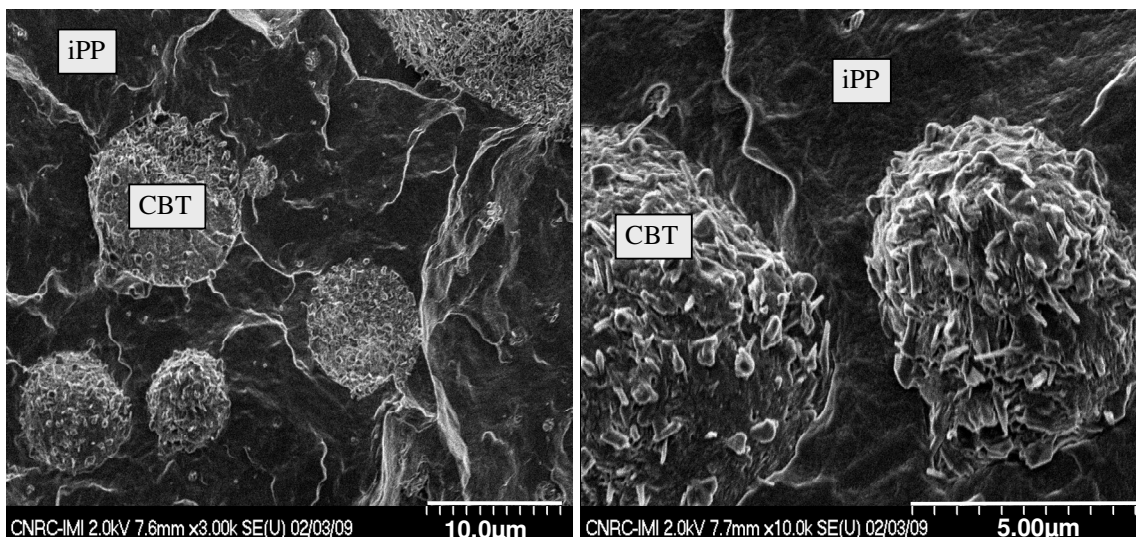
(a)
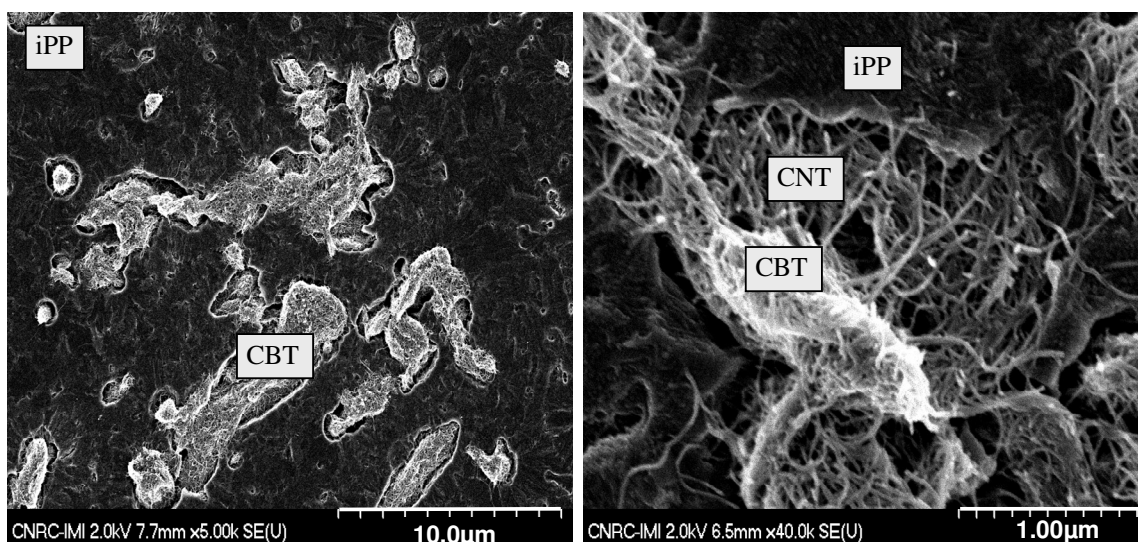
(b)

Figure 8.7: SEM micrograph of iPP/CBT (80/20) without nanotube (a) and filled with 1 wt% MWCNT (b). Images are taken at low (micrographs in the left) and high (micrographs in the right) magnification

Figure 8.7 also reveals that by incorporation of nanotubes into the blend, the minor CBT phase become completely elongated (Fig. 8.7b), changing from droplets into strips, and consequently the blend morphology changes to co-continuous structure. It is well known that the viscosity ratio of the two components of a blend is an important factor affecting the morphology of the blend. As this ratio is closer to 1, the minor phase becomes smaller and more irregular. The viscosity of PP is much larger than that of CBT. However, the nanotubes more likely increase the

CBT viscosity and result in a kind of compatibility between two phases. In fact, when the CBT viscosity increases, the kinetic of the phase coalescence is perturbed during the molding process (Gubbels, Jerome et al. 2002).

Electrical conductivity

As it was stated before, the electrical conductivity of polymer blends filled with nanotubes depends on two factors: the nanotube loading, which controls the first percolation or the percolation of nanotubes in the filler-rich phase, and the blend composition, which controls the second percolation or continuity of the filler-rich phase in the blend. Figure 8.8 shows the effect of these two parameters, MWCNT loading and CBT content, on the electrical conductivity of MWCNT-filled PP/CBT blends.
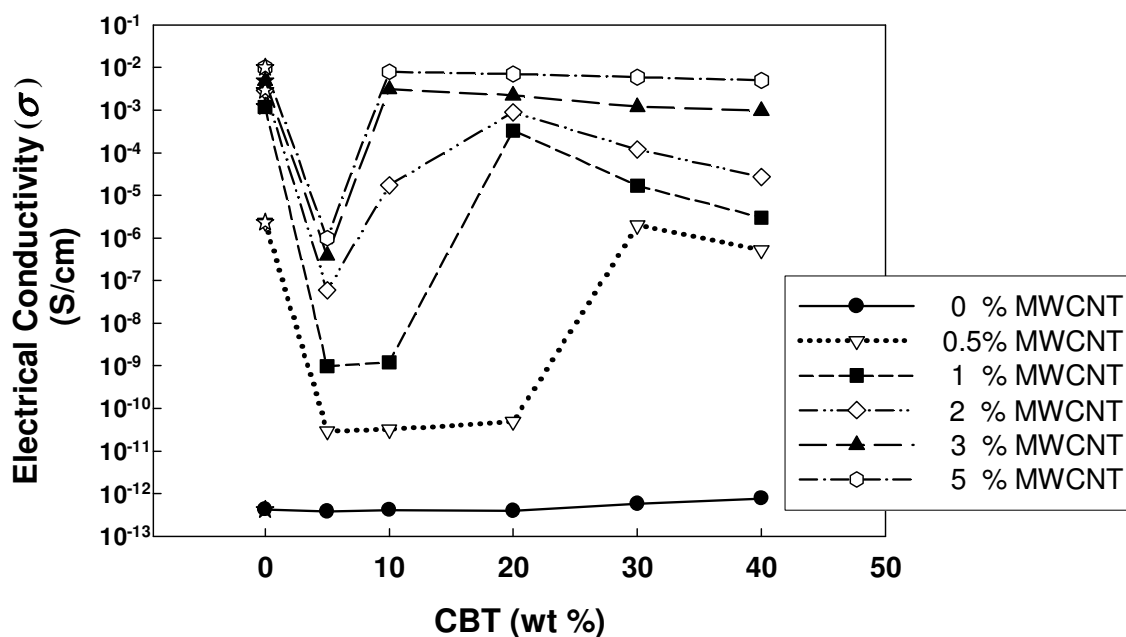
Figure 8.8: Dependence of electrical conductivity on CBT content at various nanotube loadings

As this figure shows clearly, incorporation of 5 wt% CBT into PP significantly decreases the electrical conductivity and therefore the nanotube percolation threshold rises. But the trend is not the same for all compositions of the blend. When the CBT content reaches to 30 wt% the blend becomes conductive with only 0.5 wt% nanotube loading. In fact, based on the concept of double percolation threshold, in order to get conductive blends, the filled phase or CBT phase should exhibit a continuous phase in a co-continuous blend. The electrical conductivity of such a blend

depends on two types of percolation: The first percolation is associated with the electrical continuity of the nanotubes in the filler-rich phase or CBT phase and the second one is associated with the continuity of this phase in the blend. The second percolation or the continuity of the CBT phase in blend of 30 wt% CBT filled with 0.5 wt% nanotube creates a conductive blend at a significantly low nanotube loading. However, at this nanotube loading the electrical conductivity decreases when increasing CBT content because the local concentration of nanotubes in the CBT phase decreases and 0.5wt% loading would not be sufficient to create conductive blends. Similarly, the 1 and 2wt% nanotube loadings are still too low to create conductive network at large CBT content and hence the electrical conductivity of these nanocomposites decreases after a certain level of CBT content; however, for nanotube loading of 3wt% and higher, a lower CBT percolation threshold is observed, beyond which the electrical conductivity increases and reaches a constant value irrespective of the CBT concentration.

As it is clearly observed the co-continuity composition (the composition in which the conductive blend is formed) strongly depends on the nanotube loading. For the samples containing more nanotubes the second percolation threshold (the CBT content needed to form a co-continuous structure) is shifted to lower CBT content due to the effect of nanotube on the morphology of the blend as shown previously. Figure 8.9 shows this effect in the composites of MWCNT-filled iPP/CBT (95/5) blend. Comparing Figure 8.9a (blend without nanotubes) with Figure 8.9b (nanocomposites of 0.5 wt% nanotube) we can see that by incorporation of only 0.5wt% nanotubes into the blend, the minor CBT phase becomes much smaller. When the nanotube concentration is increased to 2 wt% the CBT domains become more elongated (Fig. 8.9c), changing from droplets into strips, which are more favorable to form a continuous phase. According to conductivity results (Fig.8.8) the blend shown in Figure 8.9c is still far from a conductive one because the co-continuous structure has not formed in it yet. At nanotube loading of 2 wt% the conductive blend is formed when the CBT content reaches to 20 wt%.
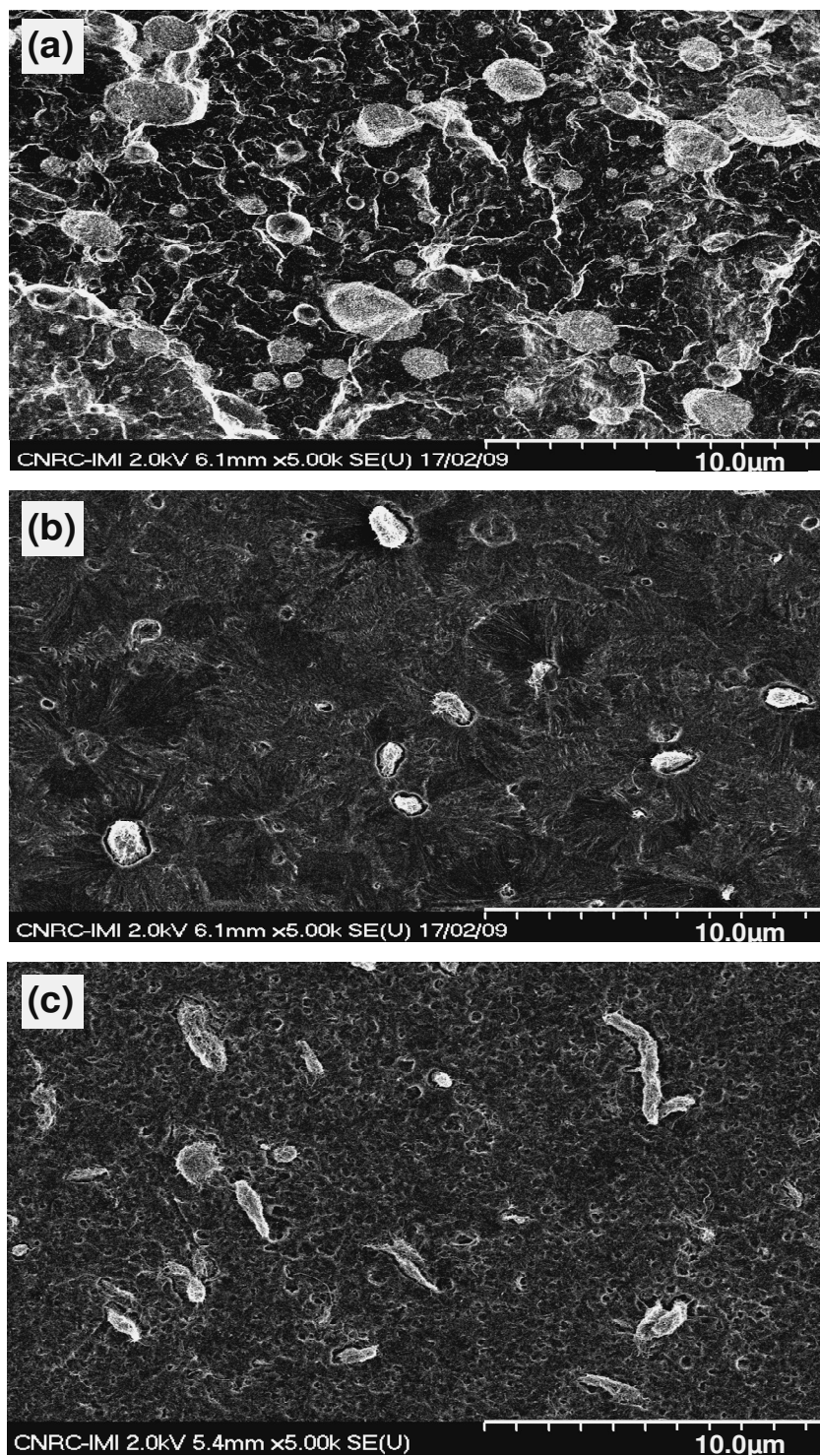
Figure 8.9: SEM micrographs of (a) iPP/CBT (95/5) blend (b) 0.5 wt% MWCNT filled iPP/CBT (95/5) blend (c) 2 wt% MWCNT filled iPP/CBT (95/5) blend

Another interesting observation in Figure 8.8 is related to the blend of 5% CBT which is far from co-continuous structure and second percolation threshold as it is confirmed by morphological studies (Fig. 8.9). The conductivity of this blend even with only 0.5 wt% nanotubes loading is about two orders of magnitude higher than that of observed in the blend without any nanotubes. Formation of bridge like structure or connection between CBT and PP phases by nanotubes is the main reason of this observation. These connections create local connection between dispersed areas through continues phase and a semi co-continuous structure is formed in the nanocomposites.

8.5.   Conclusions

In this work we have examined the effect of crystalline structure and nanotube alignment on electrical conductivity of PP/MWCNT and PC/MWCNT nanocomposites at high shear rates through the concept of double percolation threshold. Related masterbatches were diluted to prepare the nanocomposites, and the formation of nanotube networks within the polymer matrices and the alignment of nanotube in sheared conditions were observed using SEM and TEM respectively. Raman spectroscopy results of high sheared samples indicate that the values of $D_{\Pi}/D_{\perp}$ and $G_{\Pi}/G_{\perp}$ ratios decreased in the presence of crystalline phase in the nanocomposites. XRD result showed that addition of carbon nanotubes reduced the orientation of crystalline phase in the crystalline polymer (PP). Interestingly, the presence of crystalline phase and the nanotube alignment both affected the electrical conductivity of the nanocomposites. The percolation thresholds rose significantly with increasing orientation level; however the presence of a crystalline structure improved the electrical conductivity and decreased the percolation threshold according to the concept of double percolation threshold.

The effect of nanotube loading on the electrical conductivity of the PP/CBT blend was also considered and it was found that a double percolation is the basic requirement for the conductivity of this nanocomposite. Percolation of nanotubes in filler-riched phase and the continuity of this phase in the blend both affected the electrical conductivity of the nanocomposites. The nanotubes also affected the morphology of the blends by increasing the viscosity of the filler-rich phase. As a consequence, smaller and more elongated dispersed phase was achieved in the presence of nanotubes.

Chapter 9

General Discussion

It is well known that the microstructure of plastic parts is the result of complex changes imposed to the base polymer by the special processing conditions. A consequence of such processing methods is the stresses induced by combination of shear and elongational flow field and cooling. The complex thermo-mechanical history imposed on the polymer during processing leads to substantial spatial variations of chain orientation and the formation of a superstructure influenced by the local dynamics of the process. These effects result in a large anisotropy of the final physical properties particularly if the polymer is filled with solid particles of various shapes (glass or carbon fibers, clay or mica platelets, and carbon nanotubes or nanofibrils, etc.). The use of carbon nanotube based nanocomposites for commercial applications, thus, needs an understanding of how the processing conditions influence the nanotube networks and subsequently the nanocomposites properties. When the nanotubes are aligned in the polymer matrix, the probability of tube-tube contacts decreases and consequently the percolation threshold raises. Moreover, the efficiency of nanotubes to live up to their theoretical potential depends on a good dispersion within the host polymer. Accordingly, the full exploitation of the nanotube properties in polymer composite applications will require an exceptional control of the nanotube dispersion and alignment in macroscopic parts.

The rheological properties of polymer nanocomposites including viscoelastic (time or frequency-and temperature–dependent) behavior are of practical importance in relation to processing and characterizing the composite microstructure. The rheological behavior depends on the material microstructure, the state of the nanotubes dispersion, the aspect ratio and orientation of the nanotubes, the interaction between nanotubes and polymer chains as well as nanotube-nanotube interactions. The temperature influences the rheological properties of the matrix, but it also can affect the state of dispersion of the nanocomposites via changes in the particle-particle interactions and in the wettability of the nanotubes with the matrix.

In order to achieve the goals of this project, we first examined the rheological behavior of polycarbonate (PC)/ MWCNT nanocomposites in light of interactions between CNTs and polymer chains or between CNTs themselves. This is a quite complex and difficult system to study since the typical behavior of polymeric systems almost vanishes in the presence of a

nanotube network. For example, as soon as the nanotube network is formed the low frequency terminal zone observed for the neat polymer disappears. Furthermore, the high temperature behavior adds another complexity to this difficult system. Therefore the typical analysis methods used for conventional polymeric systems are not useful in this context and a more innovative investigation is required to establish the relationship between the rheological behavior and microstructure of such a system. The rheological measurements showed that the percolation threshold and the strength of nanotube networks are significantly dependent upon the measurement temperature. Assuming that the nanotube network forms an elastic structure within the matrix, the strength of this network could be related to the cohesion energy, which is the work required to break it up. Thus, the increase of the cohesion energy with temperature is a direct consequence of the enhancement of nanotube-nanotube interactions and a stronger network at higher temperature. The intrinsic viscosity was found to increase with temperature and the effective aspect ratio of the nanotubes was larger at elevated temperature. This suggests that the bundle size decreases with temperature and at higher temperature more nanotubes are dispersed individually. It can also explain the lower percolation threshold and stronger nanotube networks at higher temperature. The increase of the intrinsic viscosity with temperature could be also due to the expansion of the nanotubes hydrodynamic volume. In other words, the end-to-end distance of the nanotubes increases significantly with temperature and results in more rigid nanotubes that align more easily under shear flow as evidenced by preshearing effects on the elastic modulus. It was also shown that the effect of temperature is more pronounced at higher nanotube loading and can be described in terms of the activation energy of the nanocomposites. The decreasing of the activation energy with nanotube contents indicates that at higher level of loading the interactions between the nanotubes and the polymer chains decrease. Accordingly the nanotubes are less restricted and their motion and interactions are more affected by temperature. Furthermore, electrical and thermal conductivity measurements were carried out and the thermal percolation threshold was found to be between the rheological and electrical threshold.

In this work we aimed mainly to find a correlation between rheological properties and the final properties of microinjected parts. Therefore, at the next step we investigated the influence of high shear conditions on the properties of PC/ MWCNT nanocomposites with a special focus on the electrical conductivity and structural changes in the nanotube networks. To this end, we systematically studied the percolation behavior as a function of nanotube orientation, varied from

random to highly aligned by shearing the nanocomposites through different processing methods. The morphological analysis, using SEM, TEM and AFM, and Raman spectroscopy results showed that the nanotubes were randomly oriented for the compression molded samples, which were subjected to the lowest shear value, while they were well aligned in the longitudinal flow direction in the microinjected dog-bone samples, which featured very high shear values. Interestingly, the nanotube alignment strongly affected the rheological properties and the electrical conductivity of the nanocomposites. The percolation thresholds rose significantly in both cases with increasing orientation level. Further analysis showed that for a given nanotube loading, the nanocomposite electrical conductivity level could be controlled by nanotube alignment. Moreover, by fitting a power-law equation to the storage modulus and electrical conductivity data we determined reasonably accurate values of percolation thresholds as well as the post-percolation behavior of the nanocomposites. The power-law constant, q, was found to be a very good parameter to investigate the perfection of nanotube networks. This parameter was found to increase with nanotube alignment, indicating that for highly sheared samples we did not have a perfect percolation behavior or an ideal nanotube network. In these cases broad ranges of percolation were observed. The mechanical properties of the nanocomposites were also found to be sensitive to processing, albeit somehow improved by increasing the shear level.

As the electrical conductivity of nanocomposites is one of the main properties of interest in this work, we tried to improve the conductivity of the microparts by introducing crystalline phase in the nanocomposites. The effect of crystalline structure on the nanotube alignment and consequently on the microstructure and electrical conductivity of the nanocomposites in high shear conditions were therefore studied by processing the nanocomposites of MWCNT and isotactic polypropylene (iPP) as a non-polar semi-crystalline polymer. Comparing with the results previously found in the nanocomposites of polycarbonate (PC) as a polar amorphous polymer for which due to the formation of strong polar-polar bonds nanotubes were better dispersed in polycarbonate without the formation of many aggregates; however, for polypropylene the lack of such polar bonds resulted in a poor dispersion of the nanotubes. In addition, the growth of the crystalline phase in the later case might result in the expulsion the nanotubes towards the amorphous phase and led to the formation of large aggregates in the PP-based nanocomposites. In spite of the different levels of dispersion, in both nanocomposites the nanotubes were connected and a percolated network was formed. The study of the crystalline behavior of

PP/MWCNT nanocomposites using DSC and XRD methods revealed that the presence of the nanotubes provided a tremendous amount of sites for heterogeneous nucleating and as a result crystallization onset and peak temperature increased. As expected, the rate of crystallization also increased with nanotube content. The crystallinity was also increased with nanotube contents up to 2 wt %. For nanotube loadings of 3 wt% and higher, however, the crystallinity decreased due to the formation of nanotube networks, which restricted the polymer chains motion and slowed down the crystal growth. It was also found that the high shear values of microinjection molding only slightly changed the overall crystallinity because of very short cycle time of the process. However, the crystals were all oriented in the flow direction. The percolation thresholds rose significantly in both PP and PC nanocomposites with increasing shear values. However, the presence of a crystalline structure improved the electrical conductivity according to the concept of double percolation threshold. Morphological analysis and Raman spectroscopy results of high sheared samples indicate that the nanotube alignment decreased in the presence of crystalline phase in the nanocomposites. XRD result showed that the addition of carbon nanotubes reduced the orientation of crystalline phase in the crystalline polymer (PP). These results clearly revealed that the incorporation of nanotubes or the presence of a crystalline phase reduced the effect of shear rate in micromolding.

Mechanical properties of the nanocomposites were also found to be significantly improved with the addition of nanotubes in case of PP/MWCNT nanocomposites, although the effect was not significant in PC/MWCNT nanocomposites.

Finally the effect of carbon nanotubes on the morphology and electrical conductivity of ternary nanocomposites of PP/CBT/MWCNT were investigated and it was found that a double percolation threshold is the basic mechanism for the conductivity of such nanocomposites. The nanotubes also affected the morphology of the blends by increasing the viscosity of the filler-riched phase. As a consequence, smaller domains and a more elongated dispersed phase were achieved in the presence of nanotubes.

Chapter 10

Conclusions and Recommendations

10.1. Conclusions

In the frame of this thesis novel concepts for the shear induced alignment of nanotubes, characterization of MWCNT/polymer nanocomposites and fabrication of optimized nanocomposite based microinjected parts were presented. The following conclusions can be drawn from this work:

1.   The rheological percolation threshold and the strength of nanotube networks are significantly dependent upon the measurement temperature.

2.   The strength of the nanotube network could be related to the cohesion energy. The increase of the cohesion energy with temperature is a direct consequence of the enhancement of nanotube-nanotube interactions and a stronger network at higher temperature.

3.   Higher intrinsic viscosity of the nanocomposites and larger effective aspect ratio of the nanotubes at elevated temperature suggest that the bundle size decreases with temperature and at higher temperature more nanotubes are dispersed individually. This also explains the lower percolation threshold and stronger nanotube networks at higher temperature.

4.   The expansion of the nanotube hydrodynamic volume with temperature or higher end-to-end distance of the nanotubes at higher temperature result in more rigid nanotubes that align more easily under shear flow as evidenced by preshearing effects on the elastic modulus.

5.   The activation energy of the nanocomposites decreased with nanotube contents indicating that at higher level of loading the interactions between the nanotubes and the polymer chains decreased. Accordingly the nanotubes are less restricted and their motion and interactions are more affected by temperature.

6.   The formation of a conductive network above a certain content of nanotubes results in an obvious jump in the conductivity (thermal and electrical) of the nanocomposites. The thermal percolation threshold was found to be between the rheological and electrical threshold.

7.   The morphological analysis, using SEM, TEM and AFM, as well as Raman spectroscopy results showed that the nanotubes were randomly oriented for the compression molded samples, which were subjected to the lowest shear value, while they were well aligned in the longitudinal flow direction in the microinjected dog-bone samples, which featured very high shear values.

8.   The nanotube alignment strongly affected the rheological properties and the electrical conductivity of the nanocomposites. Consequently the percolation thresholds rose significantly in both cases with increasing orientation level. For highly sheared samples there was no perfect percolation behavior and broad ranges of percolation were observed.

9.   For a given nanotube loading, the nanocomposite electrical conductivity level could be controlled by controlling the nanotube alignment.

10.   The presence of the nanotubes provided a tremendous amount of sites for heterogeneous nucleating and as a result crystallization temperature and rate of crystallization increased.

11.   The degree of crystallinity increased by the presence of nanotubes up to 2 wt % and then decreased due to the formation of nanotube networks at higher loading

12.   The presence of a crystalline structure improved the electrical conductivity of PP/nanocomposites even at high sheared conditions according to the concept of double percolation threshold.

13.   The mechanical properties of the nanocomposites significantly improved with the addition of nanotubes especially in case of the PP/MWCNT nanocomposites.

14.   The incorporation of nanotubes or the presence of a crystalline phase reduced the effect of shear rate in micromolding. The nanotubes were less aligned in the crystalline material. The crystalline phase was also less oriented in the presence of nanotubes.

15.   In PP/CBT/MWCNT nanocomposite a double percolation is the basic mechanism for the conductivity improvement. Percolation of nanotubes in filler-riched phase (CBT) and the continuity of this phase in the blend both affected the electrical conductivity of the nanocomposites.

16.   Smaller domains and a more elongated dispersed phase were achieved in the presence of nanotubes due to increases of the viscosity of this phase.

10.2. Recommendations

For the future work, the following subjects are recommended:

1.   To develop and compare different methods for CNT dispersion in polymer/CNT nanocomposite particularly in the case of PP/MWCNT nanocomposites. These methods can include chemical modification, in-situ polymerization or other compatibilizing methods. These methods can be used along with different types of CNTs to compare their final properties.

2.   To investigate the effect of preshearing and annealing the samples in the rheometer on the rheological properties and electrical conductivity using a proper electrorheometer.

3.   To explore the effect of preshearing and rest time at different temperatures, different shear rates and different rest times on PP/MWCNT nanocomposites, which are more thermally stable and are less sensitive to temperature.

4.   To study the elongational viscosity of the nanocomposites under different conditions in order to enhance the understanding of the effect of polymer processing on the structure and properties of nanocomposites by combining the effect of shear and elongational flow.

5.   To describe the high temperature rheological properties of CNT-filled nanocomposite followed by modeling of microinjection molding of nanocomposites taking into account the most important controlling forces and phenomena occurring during microinjection molding.

6.   To study the rheological properties of PP/CBT/MWCNT nanocomposites and to investigate the effect of microinjection molding on the morphology and properties of the final parts. The obtained results in this part may be further used to improve the properties of microinjected parts by producing nanocomposites of MWCNT and different polymer blends.

REFERENCES

Abbasi S., Carreau P., Derdouri A., Moan M. (2009). "Rheological properties and percolation in suspensions of multiwalled carbon nanotubes in polycarbonate." Rheologica Acta **48**(9): 943-959.

Abdel-Goad M. ,Potschke P. (2005). "Rheological characterization of melt processed polycarbonate-multiwalled carbon nanotube composites." Journal of Non-Newtonian Fluid Mechanics **128**(1): 2-6.

Abdel-Goad M., Potschke P., Alig I., Dudkin S., Lellinger D. (2004). "Rheological and dielectrical characterization of melt mixed polycarbonate-multiwalled carbon nanotube composites." Polymer **45**(26): 8863-8870.

Ajayan P. M., Schadler L. S., Giannaris C., Rubio A. (2000). "Single-walled carbon nanotube-polymer composites: Strength and weakness." Advanced Materials **12**(10): 750-753.

Anand K. A., Agarwal U. S., Joseph R. (2006). "Carbon nanotubes induced crystallization of poly(ethylene terephthalate)." Polymer **47**(11): 3976-3980.

Barber A. H., Cohen S. R., Kenig S., Wagner H. D. (2004). "Interfacial fracture energy measurements for multi-walled carbon nanotubes pulled from a polymer matrix." Composites Science and Technology **64**(15 SPEC ISS): 2283-2289.

Bernholc J., Roland C., Yakobson B. I. (1997). "Nanotubes." Current Opinion in Solid State and Materials Science **2**(6): 706-715.

Blond D., Barron V., Ruether M., Ryan K. P., Nicolosi V., Blau W. J., Coleman J. N. (2006). "Enhancement of modulus, strength, and toughness in poly(methyl methacrylate)-based composites by the incorporation of poly(methyl methacrylate)-functionalized nanotubes." Advanced Functional Materials **16**(12): 1608-1614.

Breuer O. and U. Sundararaj (2004). "Big returns from small fibers: A review of polymer/carbon nanotube composites." Polymer Composites **25**(6): 630-645.

Bulusheva L. G., Okotrub A. V., Kinloch I. A., Asanov I. P., Kurenya A. G., Kudashov A. G., Chen X., Song H. (2008). "Effect of nitrogen doping on Raman spectra of multi-walled carbon nanotubes." physica status solidi (b) **245**(10): 1971-1974.

Chang T. E., Jensen L. R., Kisliuk A, Pipes R. B., Pyrz R, Sokolov A. P. (2005). "Microscopic mechanism of reinforcement in single-wall carbon nanotube/polypropylene nanocomposite." Polymer **46**(2): 439-444.

Chen L., Yu Z.-L., Pang X.-J., Qu M.-Z., Zhang Q.-t., Wang B.,Bai-Lan, Zhang B.-L. (2006). "Fabrication and characterization of polycarbonate/carbon nanotubes composites." Composites Part A (Applied Science and Manufacturing) **37**(9): 1485-1489.

Chen S. C., Chang J. A., Chang Y. J., Chau S. W. (2005). Micro injection molding of micro fluidic platform, Boston, MA, United States, Society of Plastics Engineers, Brookfield, CT 06804-0403, United States.

Chien R.-D. (2006). "Micromolding of biochip devices designed with microchannels." Sensors and Actuators, A: Physical **128**(2): 238-247.

Coleman J. N., Cadek M., Blake R., Nicolosi V., Ryan K. P., Belton C., Fonseca A., Nagy J. B., Gun'ko Y. K., Blau W. J. (2004). "High-performance nanotube-reinforced plastics: Understanding the mechanism of strength increase." Advanced Functional Materials **14**(8): 791-798.

Coleman J. N., Khan U., Blau W. J., Gun'ko Y. K. (2006). "Small but strong: A review of the mechanical properties of carbon nanotube-polymer composites." Carbon **44**(9): 1624-1652.

Coleman J. N., Khan U., Gun'ko Y. K. (2006). "Mechanical reinforcement of polymers using carbon nanotubes." Advanced Materials **18**(6): 689-706.

Dalmas F., Dendievel R., Chazeau L., Cavaille J.-Y., Gauthier C. (2006). "Carbon nanotube-filled polymer composites. Numerical simulation of electrical conductivity in three-dimensional entangled fibrous networks." Acta Materialia **54**(11): 2923-2931.

Dang Z.-M., Yao S.-H., Xu H.-P. (2007). "Effect of tensile strain on morphology and dielectric property in nanotube/polymer nanocomposites." Applied Physics Letters **90**(1): 012907.

Ding W., Eitan A., Fisher F.T., Chen X., Dikin D. A., Andrews R., Brinson L. C., Schadler L. S., Ruoff R. S. (2003). "Direct observation of polymer sheathing in carbon nanotube-polycarbonate composites." Nano Letters **3**(11): 1593-1597.

Dondero W. E., Gorga R. E. (2006). "Morphological and mechanical properties of carbon nanotube/polymer composites via melt compounding." Journal of Polymer Science, Part B: Polymer Physics **44**(5): 864-878.

Dresselhaus M. S., Dresselhaus G., Saito R. (1995). "Physics of carbon nanotubes." Carbon **33**(7): 883-891.

Du F., Fischer J. E., Winey K. I. (2003). "Coagulation method for preparing single-walled carbon nanotube/poly(methyl methacrylate) composites and their modulus, electrical conductivity, and thermal stability." Journal of Polymer Science, Part B: Polymer Physics **41**(24): 3333-3338.

Du F., Scogna R. C., Zhou W., Brand S., Fischer J. E., Winey K. I. (2004). "Nanotube networks in polymer nanocomposites: Rheology and electrical conductivity." Macromolecules **37**(24): 9048-9055.

Eitan A., Fisher F. T., Andrews R., Brinson L. C., Schadler L. S. (2006). "Reinforcement mechanisms in MWCNT-filled polycarbonate." Composites Science and Technology **66**(9): 1159-1170.

Endo M., Kim Y. A., Fukai Y., Hayashi T., Terrones M., Terrones H., Dresselhaus M. S. (2001). "Comparison study of semi-crystalline and highly crystalline multiwalled carbon nanotubes." Applied Physics Letters **79**(10): 1531-1533.

Fangming D., Fischer J. E., Winey K. I. (2005). "Effect of nanotube alignment on percolation conductivity in carbon nanotube/polymer composites." Physical Review B (Condensed Matter and Materials Physics) **72**(12): 121404(R).

Fisher F. T., Eitan A., Andrews R., Schadler L.S., Brinson L.C. (2004). "Spectral response and effective viscoelastic properties of MWNT-reinforced polycarbonate." Advanced Composites Letters **13**(2): 105-111.

Gubbels F., Jerome R., Teyssie P., Vanlathem E., Deltour R., Calderone A., Parente V., Bredas J. L. (2002). "Selective Localization of Carbon Black in Immiscible Polymer Blends: A Useful Tool To Design Electrical Conductive Composites." Macromolecules **27**(7): 1972-1974.

Garcia-Gutierrez M. C., Nogales A., Rueda D. R., Domingo C., Garcia-Ramos J. V., Broza G., Roslaniec Z., Schulte K., Davies R. J., Ezquerra T. A. (2006). "Templating of crystallization and shear-induced self- assembly of single-wall carbon nanotubes in a polymer-nanocomposite." Polymer **47**(1): 341-345.

Gorga R. E., Cohen R. E. (2004). "Toughness enhancements in poly(methyl methacrylate) by addition of oriented multiwall carbon nanotubes." Journal of Polymer Science, Part B: Polymer Physics **42**(14): 2690-2702.

Hone J., Llaguno M. C., Biercuk M. J., Johnson A. T., Batlogg B., Benes Z., Fischer J. E. (2002). "Thermal properties of carbon nanotubes and nanotube-based materials." Applied Physics A: Materials Science and Processing **74**(3): 339-343.

Hu G., Zhao C., Zhang S., Yang M., Wang Z. (2006). "Low percolation thresholds of electrical conductivity and rheology in poly(ethylene terephthalate) through the networks of multi-walled carbon nanotubes." Polymer **47**(1): 480-488.

Huang C. K. (2006). "Filling and wear behaviors of micro-molded parts made with nanomaterials." European Polymer Journal **42**(9): 2174-2184.

Huang C. K., Chen S. W., Yang C. T. (2005). "Accuracy and mechanical properties of multiparts produced in one mold in microinjection molding." Polymer Engineering and Science **45**(11): 1471-1478.

Huang C. K., Chiu S. W. (2005). "Formability and accuracy of micropolymer compound with added nanomaterials in microinjection molding." Journal of Applied Polymer Science **98**(5): 1865-1874.

Jehng J.-M., Tung W.-C., Kuo C.-H. (2008). "The formation mechanisms of multi-wall carbon nanotubes over the Ni modified MCM-41 catalysts." Journal of Porous Materials **15**(1): 43-51.

Jeon K., Lumata L., Tokumoto T., Steven E., Brooks J., Alamo R. G. (2007). "Low electrical conductivity threshold and crystalline morphology of single-walled carbon nanotubes - high density polyethylene nanocomposites characterized by SEM, Raman spectroscopy and AFM." Polymer **48**(16): 4751-4764.

Jia Z., Wang Z., Xu C., Liang J., Wei B., Wu D., Zhu S. (1999). "Study on poly(methyl methacrylate)/carbon nanotube composites." Materials Science and Engineering A **271**(1-2): 395-400.

Karásek L., Sumita M. (1996). "Characterization of dispersion state of filler and polymer-filler interactions in rubber-carbon black composites." Journal of Materials Science **31**(2): 281-289.

Kashiwagi T., Grulke E., Hilding J., Harris R., Awad W., Douglas J. (2002). "Thermal Degradation and Flammability Properties of Poly(propylene)/Carbon Nanotube Composites." Macromol. Rapid Commun. **23**(13): 761-765.

Kharchenko S. B., Douglas J. F., Obrzut J., Grulke E. A., Migler K. B. (2004). "Flow-induced properties of nanotube-filled polymer materials." Nature Materials **3**(8): 564-568.

Khunová V., Smatko V., Hudec I., Beniska J. (1988). Relationships of Polymeric Structure and Properties. Berlin / Heidelberg, Springer

Kim J. Y., Kim S. H. (2006). Effect of carbon nanotube on properties of poly(ethylene 2,6-naphthalate) nanocomposites, Charlotte, NC, United States, Society of Plastics Engineers, Brookfield, CT 06804-0403, United States.

Kim J. Y., Kim S. H. (2006). "Influence of multiwall carbon nanotube on physical properties of poly(ethylene 2,6-naphthalate) nanocomposites." Journal of Polymer Science, Part B: Polymer Physics **44**(7): 1062-1071.

Kim J. Y., Park H. S., Kim S. H. (2007). "Multiwall-carbon-nanotube-reinforced poly(ethylene terephthalate) nanocomposites by melt compounding." Journal of Applied Polymer Science **103**(3): 1450-1457.

Kim S., Kim J., Lee S., Park S., Kang K. (2006). "Thermophysical Properties of Multi-Walled Carbon Nanotube-Reinforced Polypropylene Composites." International Journal of Thermophysics **27**(1): 152-160.

Kinloch I. A., Roberts S. A., Windle A. H. (2002). "A rheological study of concentrated aqueous nanotube dispersions." Polymer **43**(26): 7483-7491.

Konishi Y., Cakmak M. (2005). "Structural hierarchy developed in injection molding of nylon 6/clay/carbon black nanocomposites." Polymer **46**(13): 4811-4826.

Kuan H.-C., Ma C.-C. M., Chang W.-P., Yuen S.-M., Wu H.-H., Lee T.-M. (2005). "Synthesis, thermal, mechanical and rheological properties of multiwall carbon nanotube/waterborne polyurethane nanocomposite." Composites Science and Technology **65**(11-12): 1703-1710.

Kukla C., Loibl H., Detter H., Hannenheim W. (1998). "Micro-injection moulding - the aims of a project partnership." Kunststoffe Plast Europe **88**(9): 6-7.

Kwiatkowska M., Broza G., Schulte K., Roslaniec Z. (2006). "The in-situ synthesis of polybutylene terephthalate/carbon nanotubes composites." Reviews on Advanced Materials Science **12**(2): 154-159.

Kymakis E., Amaratunga G. A. J. (2006). "Electrical properties of single-wall carbon nanotube-polymer composite films." Journal of Applied Physics **99**(8): 084302.

Lau K.-T., Gu C., Hui D. (2006). "A critical review on nanotube and nanotube/nanoclay related polymer composite materials." Composites Part B (Engineering) 37(6): 425-436.

Lee G.-W., Jagannathan S., Chae H. G., Minus M. L., Kumar S. (2008). "Carbon nanotube dispersion and exfoliation in polypropylene and structure and properties of the resulting composites." Polymer **49**(7): 1831-1840.

Lee H.-J., Oh S.-J., Choi J.-Y.,Kim J. W., Han, J.,TanL.-S., Baek J.-B. (2005). "In situ synthesis of poly(ethylene terephthalate) (PET) in ethylene glycol containing terephthalic acid and functionalized multiwalled carbon nanotubes (MWNTs) as an approach to MWNT/PET nanocomposites." Chemistry of Materials **17**(20): 5057-5064.

Leelapornpisit, W., Ton-That M.-T., Perrin-Sarazin F.,Cole K. C., Denault J, Simard B. (2005). "Effect of carbon nanotubes on the crystallization and properties of polypropylene." Journal of Polymer Science, Part B: Polymer Physics **43**(18): 2445-2453.

Li X., Huang Y.-D., Liu L, Li J. (2006). "Multi-walled carbon nanotubes-poly(p-phenylene-2,6-benzoxazole) nanocomposites prepared by in-situ polymerization process." Guti Huojian Jishu/Journal of Solid Rocket Technology **29**(3): 212-216.

Li X., Huang Y., Li J. (2006). "Study on synthesis and dispersion characteristics of MWNTs/PBO composites prepared by in-situ polymerization." Iranian Polymer Journal (English Edition) **15**(4): 317-322.

Li Z., Luo G., Wei F., Huang Y. (2006). "Microstructure of carbon nanotubes/PET conductive composites fibers and their properties." Composites Science and Technology **66**(7-8): 1022-1029.

Lin B., Sundararaj U., Potschke P. (2006). "Melt Mixing of Polycarbonate with Multi-Walled Carbon Nanotubes in Miniature Mixers." Macromolecular Materials and Engineering **291**(3): 227-238.

Lin T. S., Cheng L. Y., Hsiao C.-C., Yang A. C. M. (2005). "Percolated network of entangled multi-walled carbon nanotubes dispersed in polystyrene thin films through surface grafting polymerization." Materials Chemistry and Physics **94**(2-3): 438-443.

Liou A. C., Chen R. H. (2006). "Injection molding of polymer micro- and sub-micron structures with high-aspect ratios." International Journal of Advanced Manufacturing Technology **28**(11-12): 1097-1103.

Litchfield D. W., Baird D. G. (2008). "The role of nanoclay in the generation of poly(ethylene terephthalate) fibers with improved modulus and tenacity." Polymer **49**(23): 5027-5036.

Liu T., Phang I. Y., Shen L., Chow S. Y., Zhang W.-D. (2004). "Morphology and mechanical properties of multiwalled carbon nanotubes reinforced nylon-6 composites." Macromolecules **37**(19): 7214-7222.

López Manchado M.A., Valentini L., Biagiotti J. ,Kenny J.M. (2005). "Thermal and mechanical properties of single-walled carbon nanotubes-polypropylene composites prepared by melt processing." Carbon **43**(7): 1499-1505.

Lu X., Chao D., Zheng J., Chen J., Zhang W., Wei Y. (2006). "Preparation and characterization of polydiphenylamine/multi-walled carbon nanotube composites." Polymer International **55**(8): 945-950.

Mazinani S., Ajji A., Dubois C. (2009). "Morphology, structure and properties of conductive PS/CNT nanocomposite electrospun mat." Polymer **50**(14): 3329-3342.

Meincke O., Kaempfer D., Weickmann H., Friedrich C., Vathauer M., Warth H. (2004). "Mechanical properties and electrical conductivity of carbon-nanotube filled polyamide-6 and its blends with acrylonitrile/butadiene/styrene." Polymer **45**(3): 739-48.

Meyyappan M. (2005). Carbon nanotubes : science and applications. Boca Raton, CRC Press.

Moniruzzaman M., Du F., Romero N., Winey K. I. (2006). "Increased flexural modulus and strength in SWNT/epoxy composites by a new fabrication method." Polymer **47**(1): 293-298.

Moniruzzaman M., Winey K. I. (2006). "Polymer nanocomposites containing carbon nanotubes." Macromolecules **39**(16): 5194-5205.

Nielsen L. E., Landel R. F. (1993). Mechanical Properties of Polymers and Composites. 2nd ed. New York, Marcel Dekker.

Nordmark T. S., Ziegler G. R. (2002). "Spherulitic crystallization of gelatinized maize starch and its fractions." Carbohydrate Polymers **49**(4): 439-448.

Pham G. T., Park Y.-B., Wang S., Liang Z., Wang B., Zhang C., Funchess P., Kramer L. (2008). "Mechanical and electrical properties of polycarbonate nanotube buckypaper composite sheets." Nanotechnology **19**(32): 325705.

Phang I. Y., Ma J., Shen L., Liu T., Zhang W.-D. (2006). "Crystallization and melting behavior of multi-walled carbon nanotube-reinforced nylon-6 composites." Polymer International **55**(1): 71-79.

Potschke P., Abdel-Goad M., Alig I., Dudkin S., Lellinger D. (2004). "Rheological and dielectrical characterization of melt mixed polycarbonate-multiwalled carbon nanotube composites." Polymer **45**(26): 8863-8870.

Potschke P., Bhattacharyya A. R., Janke A. (2004). Carbon nanotube-filled polycarbonate composites produced by melt mixing and their use in blends with polyethylene, Strasbourg, France, Elsevier Ltd.

Potschke P., Bhattacharyya A. R., Janke A., Goering H. (2003). "Melt mixing of polycarbonate/multi-wall carbon nanotube composites." Composite Interfaces **10**(4-5): 389-404.

Potschke P., Brünig H., Janke A., Fischer D., Jehnichen D. (2005). "Orientation of multiwalled carbon nanotubes in composites with polycarbonate by melt spinning." Polymer **46**(23): 10355-10363.

Potschke P., Fornes T. D., Paul, D. R. (2002). "Rheological behavior of multiwalled carbon nanotube/polycarbonate composites." Polymer **43**(11): 3247-3255.

Putz K. W., Mitchell C. A., Krishnamoorti R., Green P. F.(2004). "Elastic modulus of single-walled carbon nanotube/poly(methyl methacrylate) nanocomposites." Journal of Polymer Science, Part B: Polymer Physics **42**(12): 2286-2293.

Qian D., Wagner G. J., Liu W. K.,Yu M.-F., Ruoff R. S. (2002). "Mechanics of carbon nanotubes." Applied Mechanics Reviews **55**(6): 495-532.

Ramasubramaniam R., Chen J., Liu H. (2003). "Homogeneous carbon nanotube/polymer composites for electrical applications." Applied Physics Letters **83**(14): 2928-2930.

Reich S., Thomsen C., Maultzsch J. (2004). <u>Carbon nanotubes : basic concepts and physical properties</u>. Weinheim, Germany, Wiley-VCH, Verlage GmbH & Co.KGaA,Weinheim.

Rich A., Collins P., Hagerstrom J. (2002) "Nanotubes for Conductive Plastics Move to the Next Performance Level." Hyperion Catalysis International: Paper No. 2002-01-1037.

Ruan S. L., Gao P., Yang X. G.,Yu T. X. (2003). "Toughening high performance ultrahigh molecular weight polyethylene using multiwalled carbon nanotubes." <u>Polymer</u> **44**(19): 5643-5654.

Safadi B., Andrews R., Grulke E.A. (2002). "Multiwalled carbon nanotube polymer composites: Synthesis and characterization of thin films." <u>Journal of Applied Polymer Science</u> **84**(14): 2660-2669.

Salvetat J. P., Bonard J. M., Thomson N. H., Kulik A. J., Forro L.,Benoit W., Zuppiroli L. (1999). "Mechanical properties of carbon nanotubes." <u>Applied Physics A: Materials Science and Processing</u> **69**(3): 255-260.

Sammalkorpi M., Krasheninnikov A., Kuronen A., Nordlund K., Kaski K. (2004). "Mechanical properties of carbon nanotubes with vacancies and related defects." <u>Physical Review B (Condensed Matter and Materials Physics)</u> **70**(24): 245416(R).

Sandler J. K. W., Kirk J. E., Kinloch I. A., Shaffer M. S. P., Windle A. H. (2003). "Ultra-low electrical percolation threshold in carbon-nanotube-epoxy composites." <u>Polymer</u> **44**(19): 5893-5899.

Satapathy,B. K., Weidisch R., Potschke P., Janke A. (2007). "Tough-to-brittle transition in multiwalled carbon nanotube (MWNT)/polycarbonate nanocomposites." <u>Composites Science and Technology</u> **67**(5): 867-879.

Sha B., Dimov S.S., Pham D.T., Griffiths C. A (2006). Study of Factors Affecting Aspect Ratios Achievable in Micro-injection Moulding. Cardiff, Manufacturing Engineering Centre, Cardiff University, Cardiff CF24 3AA, UK.

Sharples A. (1966). <u>Introduction to polymer crystallization</u>. New York, St. Martin's Press.

Shen Y. K., Chien H. W., Lin Y. (2004). "Optimization of the micro-injection molding process using grey relational analysis and MoldFlow analysis." Journal of Reinforced Plastics and Composites **23**(17): 1799-1814.

Shenogina N., Shenogin S., Xue L., Keblinski P. (2005). "On the lack of thermal percolation in carbon nanotube composites." Applied Physics Letters **87**(13): 133106.

Shenoy A. V., Saini D. R., Nadkarni V. M. (1983). "Rheograms of filled polymer melts from melt-flow index." Polymer Composites **4**(1): 53-63.

Shi X., Hudson J. L., Spicer P. P., Tour J. M., Krishnamoorti R.,Mikos A.G. (2006). "Injectable nanocomposites of single-walled carbon nanotubes and biodegradable polymers for bone tissue engineering." Biomacromolecules **7**(7): 2237-2242.

Shin D. H., Yoon K. H., Kwon O. H., Min B. G., Hwang C. I. (2006). "Surface resistivity and rheological behaviors of carboxylated multiwall carbon nanotube-filled PET composite film." Journal of Applied Polymer Science **99**(3): 900-904.

Su Y.-C., Shah J., Lin L. (2004). "Implementation and analysis of polymeric microstructure replication by micro injection molding." Journal of Micromechanics and Microengineering **14**(3): 415-422.

Sumita M., Abe H., Kayaki H., Miyasaka K. (1986). "Effect of melt viscosity and surface tension of polymers on the percolation threshold of conductive-particle-filled polymeric composites." Journal of Macromolecular Science, Part B **25**(1): 171-184.

Sumita M., Asai S., Miyadera N., Jojima E., Miyasaka K. (1986). "Electrical conductivity of carbon black filled ethylene-vinyl acetate copolymer as a function of vinyl acetate content." Colloid & Polymer Science **264**(3): 212-217.

Sumita M., Sakata K., Asai S., Miyasaka K., Nakagawa H. (1991). "Dispersion of fillers and the electrical conductivity of polymer blends filled with carbon black." Polymer Bulletin **25**(2): 265-271.

Sumita M., Sakata K., Hayakawa Y., Asai S., Miyasaka K., Tanemura M. (1992). "Double percolation effect on the electrical conductivity of conductive particles filled polymer blends." Colloid & Polymer Science **270**(2): 134-139.

Sung Y. T., Han M. S., et al. (2006). "Rheological and electrical properties of polycarbonate/multi-walled carbon nanotube composites." Polymer **47**(12): 4434-4439.

Sung Y. T., Kum C. K., Song K. H., Jung J. W., Lee H. S., Kum C. K., Joo J., Kim W. N. (2005). "Dynamic mechanical and morphological properties of polycarbonate/multi- walled carbon nanotube composites." Polymer **46**(15): 5656-5661.

Thostenson E. T., Li C., Chou T.-W. (2005). "Nanocomposites in context." Composites Science and Technology **65**(3-4): 491-516.

Thostenson E. T., Ren Z., Chou T. W. (2001). "Advances in the science and technology of carbon nanotubes and their." Composites Science and Technology **61**(13): 1899-1912.

Tjong S. C., Liang G. D., Bao S. P. (2008). "Effects of crystallization on dispersion of carbon nanofibers and electrical properties of polymer nanocomposites." Polymer Engineering & Science **48**(1): 177-183.

Velasco-Santos C., Martinez-Hernandez A. L., Fisher F. , Ruoff R. , Castano V. M. (2003). "Dynamical-mechanical and thermal analysis of carbon nanotube-methyl-ethyl methacrylate nanocomposites." Journal of Physics D: Applied Physics **36**(12): 1423-1428.

Ward I. M., Coates P. H., Dumoulin M. M. (2000). Solid Phase Processing of Polymers, Hanser Gardner.

Whiteside B. R., Martyn M. T., Coates P. D., Greenway G., Allen P., Hornsby P. (2004). "Micromoulding: Process measurements, product morphology and properties." Plastics, Rubber and Composites **33**(1): 11-17.

Winslow D. N., Cohen M. D., Bentz D. P., Snyder K. A., Garboczi E. J. (1994). "Percolation and pore structure in mortars and concrete." Cement and Concrete Research **24**(1): 25-37.

Wu C.-H., Liang W.-J. (2005). "Effects of geometry and injection-molding parameters on weld-line strength." Polymer Engineering and Science **45**(7): 1021-1030.

Wu F., He X., Zeng Y.,Cheng H. M. (2006). "Thermal transport enhancement of multi-walled carbon nanotubes/ high-density polyethylene composites." Applied Physics A: Materials Science and Processing **85**(1): 25-28.

Wu H.-L., Ma C.-C. M., Yang Y.-T., Kuan H.-C., Yang C.-C., Chiang C.-L. (2006). "Morphology, electrical resistance, electromagnetic interference shielding and mechanical properties of functionalized MWNT and poly(urea urethane) nanocomposites." Journal of Polymer Science, Part B: Polymer Physics **44**(7): 1096-1105.

Xiao K. Q., Zhang L. C., Zarudi I. (2007). "Mechanical and rheological properties of carbon nanotube-reinforced polyethylene composites." Composites Science and Technology **67**(2): 177-182.

Xie X.-L., Mai Y.-W., Zhou X.-P. (2005). "Dispersion and alignment of carbon nanotubes in polymer matrix: A review." Materials Science and Engineering R: Reports **49**(4): 23.

Xinfeng S., Hudson J. L., Spicer P. P., Tour J. M., Krishnamoorti R., Mikos, A. G. (2005). "Rheological behaviour and mechanical characterization of injectable poly(propylene fumarate)/single-walled carbon nanotube composites for bone tissue engineering." Nanotechnology **16**(7): 531-538.

Xu G., Yu L., Lee L. J., Koelling K. W. (2005). "Experimental and numerical studies of injection molding with microfeatures." Polymer Engineering and Science **45**(6): 866-875.

Yang Y.-K. (2006). "Optimization of injection molding process for mechanical properties of short glass fiber and polytetrafluoroethylene reinforced polycarbonate composites: A case study." Journal of Reinforced Plastics and Composites **25**(12): 1279-1290.

Yao D., Kim B. (2004). "Scaling issues in miniaturization of injection molded parts." Journal of Manufacturing Science and Engineering, Transactions of the ASME **126**(4): 733-739.

Yu M.-F., Lourie O., Dyer M. J., Moloni K., Kelly T. F., Ruoff R. S. (2000). "Strength and breaking mechanism of multiwalled carbon nanotubes under tensile load." <u>Science</u> **287**(5453): 637-640.

Zeng H., Gao C., Wang Y., Watts P. C. P., Kong H., Cui X., Yan D. (2006). "In situ polymerization approach to multiwalled carbon nanotubes-reinforced nylon 1010 composites: Mechanical properties and crystallization behavior." <u>Polymer</u> **47**(1): 113-122.

Zeng J., Saltysiak B., Johnson W. S., Schiraldi D. A., Kumar S. (2004). "Processing and properties of poly(methyl methacrylate)/carbon nano fiber composites." <u>Composites Part B: Engineering</u> **35**(2): 173-178.

Zhang D., Kandadai M. A., Cech J., Roth S., Curran S. A. (2006). "Poly(L-lactide) (PLLA)/multiwalled carbon nanotube (MWCNT) composite: Characterization and biocompatibility evaluation." <u>Journal of Physical Chemistry B</u> **110**(26): 12910-12915.

Zhang Z., Zhang J., Chen P., Zhang B., He J., Hu G.-H. (2006). "Enhanced interactions between multi-walled carbon nanotubes and polystyrene induced by melt mixing." <u>Carbon</u> **44**(4): 692-698.

Zhao J., Mayes R. H., Chen G., Xie H., Chan P. S., (2003). "Effects of Process Parameters on the Micro Molding Process." <u>Polymer Engineering and Science</u> **43**(9): 1542-1554.

Zhao Q., Wagner H. D. (2004). "Raman spectroscopy of carbon-nanotube-based composites." <u>Philosophical Transactions of the Royal Society A: Mathematical, Physical and Engineering Sciences</u> **362**(1824): 2407-2424.